

# Sheffield Hallam University

*Fatigue in C/Si/Mn steels.*

MORTON, Kenneth.

Available from the Sheffield Hallam University Research Archive (SHURA) at:

<http://shura.shu.ac.uk/20087/>

## A Sheffield Hallam University thesis

This thesis is protected by copyright which belongs to the author.

The content must not be changed in any way or sold commercially in any format or medium without the formal permission of the author.

When referring to this work, full bibliographic details including the author, title, awarding institution and date of the thesis must be given.

Please visit <http://shura.shu.ac.uk/20087/> and <http://shura.shu.ac.uk/information.html> for further details about copyright and re-use permissions.

POND STREET  
SHEFFIELD S1 1WB

6873

7903631012



14.2.96 20.35

613 16-15  
23 DEC 2003 5pm

2514

60M

REFERENCE ONLY

ProQuest Number: 10697394

All rights reserved

INFORMATION TO ALL USERS

The quality of this reproduction is dependent upon the quality of the copy submitted.

In the unlikely event that the author did not send a complete manuscript and there are missing pages, these will be noted. Also, if material had to be removed, a note will indicate the deletion.



ProQuest 10697394

Published by ProQuest LLC (2017). Copyright of the Dissertation is held by the Author.

All rights reserved.

This work is protected against unauthorized copying under Title 17, United States Code  
Microform Edition © ProQuest LLC.

ProQuest LLC.  
789 East Eisenhower Parkway  
P.O. Box 1346  
Ann Arbor, MI 48106 – 1346

FATIGUE IN C/Si/Mn STEELS

by

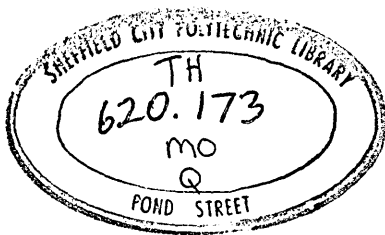
KENNETH MORTON, A.C.T.

A research project submitted in partial fulfilment  
for the degree of Doctor of Philosophy  
of the Council for National  
Academic Awards

Sponsoring Establishment : Sheffield City Polytechnic

Collaborating Establishment : British Railways

October, 1979



790363101

# CONTENTS

	Page No
Abstract	(i)
Acknowledgements	(ii)
Nomenclature	(iii)
1. <u>INTRODUCTION</u>	1
1.1. The problem	1
1.2. Project approach	3
2. <u>LITERATURE REVIEW</u>	6
2.1. Prediction of fatigue life	6
2.1.1. Description of service environment	6
2.1.2. Cycle counting	8
2.1.3. Description of material response to loading	10
2.1.4. Fatigue life curves	13
2.1.5. Fatigue damage calculations	18
2.2. Metallurgical aspects of fatigue	19
2.2.1. Microstructural characteristics of cyclic deformation	19
2.2.2. Surface damage, crack initiation and stage II cracks	30
2.2.3. Composition, microstructure - property relationships	36
3. <u>PROJECT DETAILS</u>	
3.1. Project plan	41
3.2. Project design	41
3.3. Experimental procedure	43
3.3.1. Materials	43
3.3.2. Heat treatments	44
3.3.3. Quantitative microscopy	44
3.3.4. Fatigue testing procedure	45
3.3.5. Monotonic testing procedure	45
3.3.6. Production of cyclic stress-strain curves	47
4. <u>FATIGUE, MECHANICAL PROPERTY AND MATERIAL RELATIONSHIPS</u>	50
4.1. Introduction	50
4.2. Constant amplitude fatigue data	50
4.2.1. Experimental design	50
4.2.2. Materials	50
4.2.3. Results	51
4.2.3.1. Results of fatigue tests	51
4.2.3.2. Composition - fatigue property relationships	52
4.2.3.3. Microstructure - fatigue property relationships	54
4.2.4. Discussion	55

	Page No
4.3. Fatigue parameter – mechanical property relationships	57
4.3.1. Experimental design	57
4.3.2. Results and discussion	57
4.3.2.1. Monotonic test results	57
4.3.2.2. Cyclic test results	58
4.3.2.3. Fatigue – mechanical property relationships	59
4.4. Fatigue parameter – material relationships	63
4.4.1. Experimental design	63
4.4.2. Results	63
4.4.2.1. Microstructural considerations	64
4.4.2.2. Metallurgical variables – mechanical property relationships	66
4.4.3. Discussion	69
5. <u>CHARACTERISTICS OF FATIGUE DAMAGE AND FRACTURE IN C/Si/Mn STEELS</u>	77
5.1. Introduction	77
5.2. Surface damage and microcracks	77
5.3. Stage I fracture characteristics	79
5.4. Stage II fracture characteristics	80
6. <u>FATIGUE RESISTANCE OF C/Si/Mn STEELS IN VARIABLE LOAD ENVIRONMENTS</u>	83
6.1. Introduction	83
6.2. The SAE test programme	83
6.3. The life prediction programme	85
6.3.1. Programme description	85
6.3.2. Evaluation of programme	86
6.3.3. Evaluation of the Masing hypothesis for C/Si/Mn steels	87
6.4. A comparison of C/Si/Mn steels subjected to random load histories	89
6.4.1. Procedure	89
6.4.2. Life prediction results	91
6.4.3. Discussion of results	92
7. <u>CONCLUDING REMARKS</u>	96
8. <u>CONCLUSIONS</u>	108–110
9. <u>RECOMMENDATIONS FOR FUTURE WORK</u>	111
10. <u>REFERENCES</u>	112
11. <u>STATEMENT OF POST GRADUATE STUDY</u>	137

ABSTRACT

British Railways is a major material user. It has high maintenance costs due partly to the premature withdrawal of components from service caused by metal fatigue. The main interest in fatigue, in terms of greater component efficiency, lies in the successful prediction of life for different, variable amplitude loading conditions. This requires extensive knowledge of both the service load environment and the response of metals to variable cyclic loads. This thesis presents the results of an investigation into the cyclic behaviour of ferrite-pearlite, C/Si/Mn steels.

An analytical, computer based method for predicting fatigue life, forms the basis of the approach used. The materials data required in the analysis is obtained for a series of steels containing a wide range of compositions and microstructures. This data is assessed in terms of more easily obtained mechanical properties and also in terms of the metallurgical variables. Certain assumptions in the model regarding material behaviour are also evaluated using the data. Finally, the data is used to assess the importance of material changes in variable amplitude fatigue situations.

Observations of surface fatigue damage and fracture surfaces have also been carried out. This work is used to develop a theory for the formation and development of cracks in ferrite-pearlite structures.

To conclude, the results of the various investigations are used to consider the future development of fatigue resistant materials.

(ii) ACKNOWLEDGEMENTS

This research project was carried out at the Research and Development Division of British Railways under the supervision of Dr P. Watson. I greatly appreciate the encouragement and guidance which I have received from Dr Watson. I also wish to thank my college supervisor Mr P. Warin and my college assessor Dr F.B. Pickering for helpful and stimulating discussions.

Research carried out in an industrial organisation inevitably involves the assistance of many workers and I am indebted to a great number of my colleagues. In particular I would like to thank Mr B. Dabell, Mr R. Rebbeck, Mr P. Cheesewright and Dr J.B. Lupton for providing immensely useful computer programmes and Mr J. Chelu who assisted greatly with the mechanical testing programme.

In addition I would like to thank the staff of the drawing office, the typing bureau, typist Mrs I.R.Lloyd-Jones, and the reprographic section who have assisted in the compilation of the thesis.

I am also indebted to GKN Technological Centre for allowing me to use their fatigue life prediction programme and to the British Railways Board for enabling this thesis to be submitted for a further degree.

Finally, I wish to acknowledge the help and understanding shown by my wife Janet and two sons Glen and Ian throughout the difficult "writing up" period.

(iii) NOMENCLATURE

- S = nominal stress amplitude
- $\Delta S$  = nominal stress range
- $\sigma_o$  = local stress amplitude
- $\Delta\sigma$  = local stress range
- $\sigma_o$  = mean stress
- $\sigma_{max}$  = maximum stress
- $\sigma_y$  = monotonic lower yield stress
- $\sigma_y'$  = cyclic yield stress
- $\delta\sigma_y'$  = Yield range increment
- $\sigma_u$  = ultimate tensile stress
- $\sigma_f$  = monotonic true fracture stress
- $\sigma_f'$  = fatigue strength coefficient
- $\sigma_a$  = strength parameter in ferritic steel
- $\sigma_p$  = strength parameter in pearlitic steel
- $\sigma_{ap}$  = strength parameter in ferrite-pearlite steel
- P = load
- $P_f$  = load at fracture
- A = Cross-sectional area of test specimen gargle length
- $A_0$  = original cross-sectional area of test specimen
- $A_f$  = final cross-sectional area of test specimen
- e = nominal strain amplitude
- $\Delta e$  = nominal strain range
- $\epsilon_e$  = elastic strain amplitude
- $\epsilon_p$  = plastic strain amplitude
- $\epsilon_t$  = total strain amplitude
- $\Delta\epsilon_e$  = elastic strain range
- $\Delta\epsilon_p$  = plastic strain range
- $\Delta\epsilon_t$  = total strain range

$\epsilon_f$  = monotonic true fracture strain  
 $\epsilon_f'$  = fatigue ductility coefficient  
 $L$  = instantaneous gauge length  
 $L_0$  = original gauge length  
 $E$  = Young's modulus  
 $K_\sigma$  = actual stress concentration factor  
 $K_\epsilon$  = actual strain concentration factor  
 $K_t$  = theoretical elastic stress concentration factor  
 $K$  = monotonic strength coefficient  
 $n$  = monotonic strain hardening exponent  
 $K'$  = cyclic strength coefficient  
 $n'$  = cyclic strain hardening exponent  
 $N_f$  = cycles to failure  
 $N_{f_i}$  = number of cycles to failure at the stress level (i)  
 $n_i$  = number of cycles at a given stress level  
 $2N_f$  = reversals to failure  
 $D$  = fatigue damage  
 $c$  = fatigue ductility exponent  
 $b$  = fatigue strength exponent  
 $f_a$  = volume fraction of ferrite  
 $d_a$  = average grain diameter of ferrite  
 $\bar{\lambda}_a$  = mean free ferrite path  
 $f_p$  = volume fraction of pearlite  
 $S^0$  = interlamellar spacing of pearlite  
 $\Delta W$  = plastic strain energy per cycle  
 $\Delta K$  = stress intensity factor  
 $T$  = time  
 $d_\gamma$  = prior austenite grain size  
 $G$  = growth rate of transformed product  
 $\gamma_{temp}$  = austenitising temperature  
 $I.T.T.$  = isothermal transformation temperature

## 1. INTRODUCTION

### 1.1. The Problem

Fatigue failures in metallic structures have been a cause for concern ever since machinery which subjected its component parts to repeated loading was produced. In spite of the extensive research in fatigue it is still responsible for the majority of service failures today (1). In a major industry like British Railways which uses vast quantities of materials, it is inevitable that many components fail by fatigue. The following are examples of the problems found in "bulk railway products" made from simple C/Si/Mn steels.

Fig.1 (a and b) is an example of one of the most dangerous problems in rails. The failure (known as star cracking) is initiated by the development of a fatigue crack at one of the rail end bolt holes. Brittle fracture results when the critical fatigue crack size is reached, (typically 2-3 mm, see fig.1b).

This type of failure is particularly dangerous for several reasons,

- a) if a section of the rail head becomes detached, as is clearly possible, there is a high probability of a train derailment.
- b) the critical bolt hole fatigue crack is shielded from view by the fishplates connecting the abutting rails; detection is therefore difficult,
- and c) Only a small percentage of rail ends develop these defects and the associated track characteristics are difficult to quantify. It is therefore virtually impossible to predict the vulnerable rails.

Fig.2 is an example of a fractured wheel. In this figure, which shows a fracture face, it can be seen that the origin of the failure is a threaded bolt hole in the wheel web (marked A). Fatigue cracks have grown from each side of the bolt hole and extend to the web circumference in one direction and for about 4 cm in the other.

This example again represents a very dangerous situation for similar reasons given for the star cracked rail failure. In this case the growing fatigue crack was also not detected because it was shielded by a cover plate bolted on to the wheel web. However, an additional problem highlighted by this failure is the unpredictability of service loads. Two generations of identical wheels had previously performed satisfactorily on the same fleet of vehicles operating on the same track. Therefore, in recent years an unexpected and undetected deterioration in the track has occurred which has resulted in the application of greater, and for the first time, fatigue damaging loads on the wheels.

When studying problems of this type it is worth considering some of the design philosophies behind the production of such components. The early fatigue research workers established through "simulation" tests a working relationship between the level of applied load and the number of repetitions required to produce a fatigue crack. Additionally, a material dependent stress parameter (fatigue limit) was noted for iron based alloys, below which fatigue cracks could not grow (2-5). Utilising this information, an engineering design approach was conceived based on the complete prevention of failure. This approach requires that each load bearing component be designed such that the operating stresses are all below the fatigue limit of the material and hence can be tolerated indefinitely. Components designed to these principles can be excessively large and inefficient when high factors of safety are employed.

In many industries, efficiency has been increased by the adoption of finite life design methods which utilise techniques for predicting fatigue life. Operating stresses are occasionally allowed to reach levels in certain critical regions, where plastic deformation will occur. This will lead to a finite life because cyclic, irreversible plasticity is an essential feature in the formation of fatigue cracks. Initial designs are usually produced by a combination of prior experience with similar components, empirical

rules from design codes and fatigue data from simple tests. In certain circumstances these preliminary designs may be modified due to the results of prototype tests. At British Rail for example, development of the "Advanced Passenger Train" (APT) has included extensive trials with prototype units.

Whichever design philosophy is adopted, a successful method relies on the precise knowledge of the relationship between operating stresses and material response to cyclic loads. It is perhaps surprising therefore that designers rarely obtain an accurate pre-assessment of either aspect. This situation will only improve when current research workers produce a satisfactory method of estimating fatigue life and when the pertinent data on both service loadings and material properties are available.

### 1.2. Project Approach

When initiating fatigue research programmes, the service components to which the research is aimed needs to be clearly defined. In this respect, the ability of a component to tolerate fatigue cracks is a major consideration because this strongly influences the approach to be used. In response to the drive for more efficient designs, crack tolerant structures have become more widespread. This has resulted in a major change of emphasis in the study of fatigue. In recent years the majority of fatigue research work in the U.K. has concentrated on developing and applying the principles of linear elastic fracture mechanics. This approach assumes that the initiation of a crack represents only a small fraction of life due to inherent crack-like defects present in some components (welded structures for example). The rate of crack propagation and the ability of a material to tolerate cracks (fracture toughness) have been adjudged by the workers in the field as the most important features of the fracture formation process. The relationship between these two properties and either stress parameters or material variables has been extensively studied for a wide

range of situations. The approach is particularly useful when applied to low stressed components, manufactured from fracture tough materials that contain crack-like defects. If supported by extensive inspection procedures both safe and efficient components can result.

In the railway industry however, the approach has only limited applicability for the following reasons:-

(i) many of the materials used (high carbon steels, cast irons) are relatively brittle and are not able to tolerate large cracks.

(ii) critical areas in components are not usually known.

(iii) inspection of critical areas is usually difficult and in some cases impossible, for both technical and economic reasons.

(iv) service loadings are not usually known and in any case are unpredictable on a long term basis.

The fatigue failures previously discussed highlight some of these points. It is clear therefore, that many important railway products cannot tolerate fatigue cracks and hence the early design philosophy of total prevention of failure is more pertinent. In order to maximise efficiency with this approach fatigue research should concentrate on the study of crack initiation phenomena and the development of methods for predicting the lives of short cracks.

A very promising method for relating materials data to engineering fatigue problems, especially if initiation or early crack growth are important, is the "local stress-strain" approach developed by Morrow and Topper and their co-workers (6,7). This approach has received a good deal of attention in recent years and has been adopted by many workers as the basis for life prediction procedures.

A major feature of the "local stress-strain" approach to fatigue is its dependence on the cyclic behaviour of materials. This includes a detailed understanding of the complex relationships between stress and strain from

the commencement of loading and the effect of cyclic loads on life. The development has led to a better appreciation of the fatigue process in materials and several "fatigue parameters" which encompass the entire life range have now been proposed. Useful metallurgical research is therefore possible because the effect of composition and microstructure in fatigue can be evaluated in terms of such fatigue parameters. The objectives of the current research project are to study the cyclic deformation and fatigue behaviour of C/Si/Mn steels with ferrite-pearlite microstructures. The work is aimed at producing cyclic data for incorporation into fatigue life prediction procedures. In addition the micromechanisms responsible for fatigue crack formation and the effect of metallurgical variables in variable loading situations is studied. The data obtained is intended to form the basis of material selection and future material development programmes.

## 2. LITERATURE REVIEW

### 2.1. Prediction of fatigue life using local stress-strain approach

Since fatigue failures invariably initiate at critical regions in a component such as holes, notches and fillets it is obvious that the fatigue process is a highly localised event. A philosophy which is intimately concerned with local occurrences is therefore essential for the basis of a life prediction procedure. In recent years the "local stress-strain" approach has been developed for this purpose. The objective of this philosophy, is an analysis suitable for predicting the fatigue behaviour of a notched component subjected to variable loads. The technique relates the behaviour of a small element of material at a critical location in a component to that of small, smooth, laboratory specimens.

The procedure combines the information from three major areas:-

- a) The loading characteristics in service.
- b) Material response to cyclic loading.
- c) Fatigue damage accumulation.

A block diagram, incorporating the major individual features and outlining the overall approach is shown in fig.3.

#### 2.1.1. Description of Service Environment

##### Service strains - local conditions

In the majority of cases the service loading at a critical location is extremely complex, usually variable in nature and rarely known in practice. Unfortunately an accurate knowledge of local stress-strain conditions is essential for any realistic estimate of service performance. Localised stress-strain information can be obtained either by measurement or calculation but in the majority of cases it is both difficult and expensive. The first stage in obtaining this information is to locate the critical regions in a component. An indication can be obtained by the use of brittle lacquers. These are usually sprayed onto components prior to

static loading in a laboratory rig although they can be used much more profitably on components in situ. Under loading, cracks will appear in the brittle coating at the most highly stressed regions which are the critical locations in most components. The direction of cracks in the brittle lacquer will also indicate the direction of maximum strain which can then be used to position strain gauges accurately for subsequent measurement of strains.

The use of strain gauges is now a well established strain evaluation technique for many service situations. In most cases the signals are "captured" and stored on magnetic tapes for subsequent interpretation and analysis. Unfortunately in some service situations the local strains cannot be measured. This is usually due to the physical inability of getting leads to and from the strain gauges or because the critical location is between contacting surfaces (wheels on rails for example). For many such cases it is possible to use a combination of nominal strain measurements and finite element analysis to calculate the local conditions.

If local strains cannot be measured directly, then assessments should be made as close as possible to the critical location. From this information (nominal) it is possible to calculate the local conditions from a knowledge of the stress concentration factor. An analysis used to relate nominal and local conditions was proposed by Neuber (8). He showed that:-

$$K_t^2 = K_\sigma \cdot K_\epsilon \quad (1)$$

where  $K_t$  = theoretical elastic stress concentration factor

$K_\sigma$  = actual stress concentration factor

$K_\epsilon$  = actual strain concentration factor

This relationship was originally derived for a shear strained prismatic body with a specific stress-strain relationship but it was extended to direct stress situations in many materials (9,10).

Equation (1) has been interpreted and developed by Topper et al (11) and written in the following forms:-

$$\frac{\Delta\sigma \cdot \Delta\epsilon_t}{\Delta S \cdot \Delta e} = K_t^2 \quad (2)$$

or

$$K_t \cdot (\Delta S \cdot \Delta e)^{1/2} = (\Delta\sigma \cdot \Delta\epsilon)^{1/2} \quad (3)$$

where  $\Delta S$  = nominal stress range  
 $\Delta e$  = nominal strain range  
 $\Delta\sigma$  = local stress range  
 $\Delta\epsilon_t$  = local total strain range

In most cases the nominal conditions are elastic, so that:-

$$K_t \cdot \Delta S = (\Delta\sigma \Delta\epsilon_t E)^{1/2} \quad (4)$$

or

$$K_t \cdot \Delta e = (\Delta\sigma \Delta\epsilon_t)^{1/2} / E^{1/2} \quad (5)$$

where  $E$  = Young's modulus

These equations define the unknown terms (local) with respect to the known terms (nominal). The theoretical elastic stress concentration factor  $K_t$  can usually be obtained for specific geometries from standard texts such as that prepared by Peterson (12).

### 2.1.2. Cycle Counting

In order to utilise the information obtained from service strain measurements or calculation, the load or strain history obtained needs to be combined with material response information. This is usually in the form of stress or strain-life curves which have been produced from constant amplitude tests. The method of combination requires the variable service signal to be reduced to the individual cycles with their respective range and mean level. This process is referred to as cycle counting.

There are two main cycle counting methods used at present, range-mean analysis and rainflow analysis. Dabell and Watson (13) have shown that the range-mean analysis is very sensitive to small cycles within the signal

which tend to reduce the damaging effect of the large reversals. As a result of this work specific guidelines have been suggested for use with this method. This involves repeating the analysis several times using different gate levels. An alternative approach is the rainflow counting method developed by Matsuishi and Endo specifically for the purpose of considering fatigue damage (14). This method needs no gating and every range is included. It is now generally considered to be the most suitable method of cycle counting (13). The main features of the method are as follows:-

Consider the variable strain-time history shown in fig.4 with the time axis in the vertical direction. Consider raindrops beginning to flow from position A; the start of the record. The rain will flow down the "roof" until it reaches the edge (B); it will then drip down until it reaches the larger roof (C) when it will again flow away from the zero time position. This will continue until the largest roof has been crossed except for two conditions:-

(i) The rain will stop when it meets another flow of rain.

An example of this is from 1 to B'.

and (ii) The rain stops when it comes opposite a maximum more positive than the maximum from which it started (or a minimum more negative than the minimum from which it started). In the diagram, the minimum at (2) is more negative than the initial minimum at A, thus the original flow is halted opposite (2).

Each new flow of rain starts from the inside of a peak. For example, the second flow will originate from the inside of the second peak (B) and proceed to (1). It will be halted when it is opposite the next maximum (C).

Using this set of rules a variable amplitude signal can be reduced to a series of reversals whose maximum and minimum values and hence range and

mean levels are obtained. The complex process is usually carried out by a computer. An important feature of rainflow cycle counting is that the results represent actual material behaviour. The stress-strain hysteresis loops shown in fig.4 correspond to the rainflow cycle counting output for the signal above and also to material response to that signal.

### 2.1.3. Description of Material Response to loading

#### Monotonic stress-strain relationship

When a material is loaded in either tension or compression there are two distinct characteristics for the relationship between true stress and true strain:-

- (1) Up to the yield stress, stress amplitude ( $\sigma_a$ ) is linearly related to elastic strain ( $\epsilon_e$ ), (Hooke's Law)

$$\sigma_a = \epsilon_e \cdot E \quad (6)$$

- (2) Beyond the yield stress, the stress-strain relationship usually obeys a logarithmic law,

$$\sigma_a = K \cdot (\epsilon_p)^n \quad (7)$$

where  $\epsilon_p$  = plastic strain  
K = monotonic strength coefficient  
n = monotonic strain hardening exponent.

This is referred to as the Ludwig (15) or Ramberg-Osgood (16) expression.

For metal fatigue to occur, applications of load that take the material beyond the cyclic yield stress are needed, ie, cyclic plasticity is a pre-requisite for metal fatigue. The relationship between stress and strain under cyclic conditions is often different to the monotonic relationship and is obviously more pertinent to fatigue studies.

### Cyclic stress-strain relationship

This curve can again be separated into two distinct regions:-

$$(1) \quad \sigma_a = \epsilon_a \cdot E \quad \text{up to yield} \quad (8)$$

$$\text{and (2)} \quad \sigma_a = K' (\epsilon_p)^{n'} \quad \text{beyond yield} \quad (9)$$

where  $K'$  = cyclic strength coefficient

$n'$  = cyclic strain hardening exponent.

The cyclic strain hardening exponent ( $n'$ ) is the slope of a graph between log cyclic stress amplitude and log cyclic plastic strain amplitude. It is analogous to the strain hardening exponent obtained from the monotonic stress-strain curve.

A cyclic stress-strain curve can be produced in a number of ways; the two most common methods being the multiple specimen method and the Incremental Step Test method (17). The curve itself is defined as the locus of the tips of stable cyclic stress-strain hysteresis loops produced at various strain amplitudes. The first method requires several specimens to be tested at different, constant amplitude strain levels. However, an Incremental Step Test can be used to produce the curve from just one specimen. In this test a specimen is subjected to a variable strain input of gradually decreasing and then increasing strain amplitudes, as shown in fig.5. The material responds to this input, stabilises, and then repeatable stress-strain data is produced. From this data (stress and strain hysteresis loop maxima and minima) the cyclic stress-strain curve can be obtained. This is also shown in fig.5.

Transient material behaviour, ie, the changes that occur in going from the monotonic to the cyclically stabilised state, can be affected by such variables as prior history, temperature, frequency of cycling and waveform. The most important consideration however is the initial

condition of the material (annealed, hardened, cold worked etc). As a general rule hardened materials tend to cyclically soften whereas annealed material usually harden. The terms "cyclic softening and hardening" refer to the stress response of a material which is subjected to constant amplitude strain cycling. If the stress maxima at a hysteresis loop tip decreases during cycling then the material is said to have "softened" and visa-versa. The overall effect can lead to such phenomena as cyclic mean stress relaxation and cyclic creep (18).

### Stress-Strain Hysteresis

When a material is subjected to cyclic loads the relationship between stress and strain usually takes the form of a hysteresis loop. These loops usually exhibit the following major features:-

1. Both the loading and unloading part of the loop begins with a linear relationship between stress and strain. The constant in the relationship is approximately equal to Young's modulus although there is evidence to suggest that the modulus is affected by strain amplitude (19). Deviation from linearity occurs at a level lower than that anticipated from the monotonic yield stress, and is dependent in some materials on the previous history (18,19,20).
2. The inelastic portion of the curves are related by a logarithmic relationship similar to the Ramberg-Osgood expression.
3. In most materials the stress-strain curves can be considered symmetrical in tension and compression.

Masing (21) hypothesised that the shape of the two sides of a stable hysteresis loop was equal to that of a monotonic stress-strain curve multiplied by two. Morrow and Halford (22,23) have improved this approximation for many materials by replacing the monotonic curve in this

hypothesis, by the cyclic  $\sigma-\epsilon$  curve. This approximation should be used with caution however, for not all materials exhibit these characteristics as highlighted recently by Jhansale (18,19). Materials which do show this correlation between hysteresis loop shape and the cyclic  $\sigma-\epsilon$  curve, are referred to as Masing materials and conversely non-Masing materials do not show the relationship.

For materials that have symmetrical loops the general relationship between stress and strain for each side is given by:-

$$\Delta\sigma = E\Delta\epsilon_t - 2^{1-n'} K' (\Delta\epsilon_t - 2\epsilon_e)^{n'} \quad (10)$$

where  $\Delta\sigma$  = stress range  
 $\epsilon_e$  = elastic strain amplitude

Under variable amplitude loading the stress-strain relationship for each reversal of load will follow the stable hysteresis loop shape, but a feature referred to as material "memory" can alter the anticipated loop shape. This is illustrated in fig.6. On re-loading from point "A" to "B" the material is subjected to a small reversal "CD". On re-loading from "D" the material does not take the path of the hysteresis loop (dotted line) but reverts to its original path at point "C". This is an extremely significant material characteristic which must be considered in any material model that is adopted for a fatigue life prediction procedure.

#### 2.1.4. Fatigue life curves

Engineers and metallurgists have been producing "fatigue life curves" for well over a century starting with the famous work by Wöhler (2-5). The early curves were usually plots of applied nominal stress against cycles to failure but several investigators were also interested in the strain response during cycling (24,25).

The first mathematical description of fatigue life characteristics was produced by Basquin in 1910 (26). He noted that the logarithm of applied nominal stress was linearly related to the logarithm of cycles to failure.

Mathematically this can be expressed by:-

$$\sigma_o = \text{constant} \cdot (N_f)^b \quad (11)$$

where the constant and "b" are the intercept and slope of the graph respectively. This relationship forms the basis of many modern engineering design codes.

In the 1940s, Hanstock attempted to relate fatigue life to damping capacity which he defined as the capacity of a solid to convert vibrational energy to some other form (27). This he regarded as the ratio of the total plastic strain per cycle to the maximum elastic strain. Working with two Aluminium - Magnesium alloys he derived the following equation:-

$$(\Delta\epsilon_p - B) \cdot N_f = \text{Constant} \cdot (A) \quad (12)$$

where

B = slope of  $N_f \cdot \Delta\epsilon_p - N_f$  plot

A = intercept of  $N_f \cdot \Delta\epsilon_p - N_f$  plot

This relationship was not substantiated by other workers but it lead the way to the development of relationships between plastic strain and fatigue life.

In the early 1950's two investigators (Manson and Coffin) established that fatigue life was dependent on plastic strain in the following way:-

$$\Delta\epsilon_p = \text{constant} \cdot (2N_f)^c \quad (13)$$

where the constant and "c" are the intercept and slope respectively of a plot of log plastic strain and log cycles to failure.

Manson (28) was searching for an equation that he could use to compare materials subjected to thermal stresses. He eventually obtained the above relationship by re-analysing data produced by Sachs et al (29) working with 24S-T Aluminium alloy. This was one of the few studies made at the time, which had measured plastic strain in tests that were carried out under constant total strain range control. Coffin was also studying the effect of thermal stresses on fatigue life but in his case he was concerned with the development of stainless steels for nuclear reactor components (30). Based on his own precise experimental data he noted an excellent relationship between total plastic strain and cycles to failure and he also suggested that the constant was equivalent to the true fracture ductility in simple tension.

The Coffin/Manson equation has now been verified for many materials and therefore has become a well established method of presenting fatigue data. Since its inception considerable effort has been expended in trying to quantify and understand the two constants in the expression. Initially the coefficient was studied in great detail, with most workers taking the Coffin approach in trying to relate it to the energy required to cause fracture in a tensile test (31-35). This has resulted in several different expressions for the coefficient in terms of the monotonic fracture ductility. These will be discussed in a later section of the work. The exponent (c) on the other hand has usually been studied with respect to the cyclic strain hardening exponent (n'). Morrow (36,37) has shown through an energy argument that c is related to n' by the following expression:-

$$c = \frac{-1}{1 + 5n'} \quad (14)$$

In this work Morrow pointed out that there is a precise relationship between c, n' and b (the Basquin exponent from the stress-life curve) if

it is assumed that  $K'$  and  $n'$  are constant up to the fracture strain.

This relationship is:-

$$n' = \frac{b}{c} \quad (15)$$

This leads to:-

$$b = \frac{-n'}{1 + 5n'} \quad (16)$$

Summarising the previous work and considering fatigue life in terms of total strain, Morrow presented the following equation and introduced the "fatigue parameter" concept.

$$\Delta\epsilon_{t/2} = \Delta\epsilon_e/2 + \Delta\epsilon_p/2 = \sigma_1'/E.(2N_f)^b + \epsilon_f'(2N_f)^c \quad (17)$$

where:-

$\epsilon_f'$	= Fatigue ductility coefficient	}	From Coffin/ Manson expression
$c$	= Fatigue ductility exponent		
$\sigma_1'$	= Fatigue strength coefficient	}	From Basquin expression
$b$	= Fatigue strength exponent		

Fig.7 is an illustration of this relationship from which it can be seen that fatigue data can be presented in the form of total strain - life curves which are a combination of the Coffin/Manson and Basquin relationships. This method of presentation is now preferred for results produced from tests in which the strain range was the controlled parameter.

The total strain-life expression quoted, only applies to fully reversed loading situations in which mean stress is zero. For realistic fatigue life predictions some modification is necessary.

#### Mean stress considerations

It has been known for many years that a tensile mean stress will cause a reduction in life and a compressive mean stress will reduce fatigue damage and hence prolong life. Gerber in 1874 (38) and Goodman in 1899 (39) were the first to establish empirical methods for predicting the effect

of mean stress. Both these workers studied only the effect of tensile mean stress on the fatigue limit.

Morrow has shown that mean stress effects can be readily assessed within the total strain approach (37).

$$\Delta\epsilon_{t/2} = \left( \frac{\sigma_f' - \sigma_o}{E} \right) \cdot (2N_f)^b + \epsilon_f' (2N_f)^c \quad (18)$$

where  $\sigma_o = \text{mean stress}$

More recently Smith, Watson and Topper (40) have demonstrated that a combined stress-strain damage parameter can account for mean stress effects. The parameter, which is the product of the maximum stress in a reversal ( $\sigma_{\max}$ ) and the strain amplitude, has been shown to apply to a wide range of materials (41,42). The fatigue life relation can be written:-

$$\sigma_{\max} \cdot \epsilon_t = \sigma_f (2N_f)^b \left[ \left( \frac{\sigma_f'}{E} \right) (2N_f)^b + \epsilon_f' (2N_f)^c \right] \quad (19)$$

This relationship is similar in form to that between  $\epsilon_t$  and  $2N_f$ .

A log-log plot of  $\sigma_{\max} \cdot \epsilon_t - 2N_f$  can be constructed for any material from the strain-life curve or more precisely from a knowledge of

$\sigma_f'$ ,  $\epsilon_f'$ ,  $b$  and  $c$ . The resultant curve can be used in association with the Palmgren-Miner rule to calculate fatigue damage for the variable amplitude, variable mean stress signals which are normal in many service situations.

Another important factor to be considered when calculating fatigue life is the effect of periodic or initial overloads...

#### Overload considerations

In the past there has been considerable research effort aimed at understanding the effects of overloads on fatigue behaviour. Workers have reported both beneficial (43,44) and detrimental effects (45-48).

Much of the confusion, particularly in block programme or step tests, probably results from the different mean stresses that can exist due to transfer effects in high-low loading sequences. If the low strain level is established following the maximum high stress level in compression then a tensile mean stress will result. However, if the low strain follows a tensile stress then a compressive mean stress is produced. For apparently identical loading conditions, the latter case will give a longer life.

Watson et al (49) studied the effect of periodic overloads produced in railway track vehicles travelling over points and crossings. This study concluded that in the absence of residual stresses, periodic overloads made a significant contribution to fatigue damage. The decrease in fatigue life was due mainly to a decrease in the number of cycles required to produce a small crack. The overall effect is greater in the long life régime than in the low cycle region, which is to be expected if the development of a small crack is accelerated.

To account for this effect in a life prediction model, a fatigue life curve is required that has been suitably modified. This can be produced by subjecting all test specimens to overloads prior to the onset of testing at the required lower level (47).

#### 2.1.5. Fatigue Damage Calculations

Fatigue damage caused by repeated plastic straining of a material is usually predicted by using a cumulative damage summation rule. The rule first proposed by Palmgren (50) and later adopted by Miner (51) defines damage per cycle as the inverse of the number of cycles to failure at any given stress level. Damage accumulates on a linear basis and failure of the specimen is normally taken when the summation is equal to unity, ie,

$$\sum \frac{n_i}{N_{fi}} = D = 1 \text{ at failure} \quad (20)$$

where  $n_i$  = number of cycles at a given stress level  
 $N_{fi}$  = number of cycles to failure at the same stress level.  
 $D$  = Damage.

In the absence of a better method of assessing the accumulation of fatigue damage and final failure, this approach is usually adopted in life prediction procedures.

## 2.2. Metallurgical aspects of fatigue

### Introduction

The aim of this part of the review is to gain an appreciation of the important metallurgical factors that influence the formation of an engineering fatigue crack (typically 1 mm long). The following topics are included with particular emphasis on steels:-

- (i) Microstructural aspects of cyclic deformation.
- (ii) Metallurgical aspects of crack initiation and propagation.
- (iii) Composition, microstructure - property relationships.

### 2.2.1. Microstructural Characteristics of cyclic deformation

#### Transient Behaviour

The characteristics of cyclic deformation have been studied for a very long time. Bauschinger, as long ago as 1886 (52) discovered that the yield stress during the reverse flow of deformed steel was lower than the flow stress in the original deformation direction. More recently, the transient phenomena, cyclic softening and cyclic hardening have been identified. These characteristics relate to the progressive change in material behaviour that occurs during cycling. Depending on the initial material condition, prior loading history and strain amplitude, a metal can either harden or soften. For constant strain amplitude tests, the maximum stress level in each cycle can either increase (cyclic hardening)

or decrease (cyclic softening) during a test. A plot of stress amplitude against cycles shows that in many metals the change in stress is most marked during the first few percent of life and then reaches a constant value which is indicative of stability in the material. Several workers have shown that rapid material stability occurs in steels similar to the ones used in this investigation (53,54,55). The major iron based alloys which do not exhibit these characteristics are austenitic steels which tend to work harden throughout a fatigue test.

In order to appreciate the dislocation mechanisms responsible for these cyclic characteristics in steels, the dislocation patterns produced during monotonic loading must first be considered. In polycrystalline iron that contains a dispersion of second phase particles (ferrite-pearlite steels), grain boundaries and cementite particles will act as barriers to dislocation motion. New dislocations, generated from sessile sources (Frank-Read type for example), pile-up behind each other at a barrier producing back stresses. These microscopic, internal back stresses reduce the efficiency of dislocation generation from a source and hence a greater applied stress is required to maintain deformation. This is the dislocation mechanism responsible for work hardening in these steels. It also indicates that parameters such as yield stress are microstructure dependent, ie, the smaller the interbarrier spacing the greater the applied stress required for deformation.

However, when a load reversal occurs, the back stress developed as a result of dislocation pile-ups will aid the movement of dislocations in the opposite direction. In addition, dislocations of opposite sign will be created from the source. Since screw dislocations of opposite sign attract and annihilate each other, the net effect will be a reduction in the dislocation density and hence a softening in the lattice. Thus a lower stress will be required to produce yield in the reversed loading direction (Bauschinger effect)

The effect of subsequent cycles is dependent on the initial material condition. Heavily cold worked materials usually soften with cycling whereas annealed metals tend to harden (37). In the first case, the prior deformation produces a high dislocation density, which will be in a cellular configuration for high stacking fault energy metals (56). On cycling, the dislocation structure will be modified by a series of processes which include the initial unpinning of trapped dislocations, followed by partial annihilation of screw dislocations. (These processes are discussed more fully in the next section). Hence softening will result. In the second case, the dislocation density will increase with deformation until the stabilised pattern characteristic of the strain amplitude, has been attained. Therefore, hardening will occur.

Whichever mechanism is prevalent in a material, the changes are usually progressive. James and Sleeswyk (57) have studied the microscopic behaviour that occurs in a number of materials; aluminium, copper, nickel,  $\alpha$ -brass and some stainless steels. They found that the original dislocation pattern never completely broke down in any of these materials following a single load reversal.

#### Formation of stable structures

##### (i) Single Crystals and single phase polycrystals

The stable dislocation structure produced during cycling is strongly dependent on strain amplitude and stacking fault energy (58-62). For a high stacking fault energy material the structure at low strain amplitudes is characterised by clusters of dipoles and dislocation loops which are produced by random encounters between dislocations. It has been found that a high proportion of the original dislocations do not lie on slip planes (sessile dislocations) and these quickly trap the few glide dislocations. As the stress is increased, these sessile dislocations can act as sources which readily generate new dislocations. During deformation, screw dislocations can mutually annihilate through cross-slip

and edge dislocations form very stable dipolar groupings which preferentially form on planes perpendicular to the primary slip direction. The clusters of dislocation loops are usually separated by channels and the combination takes on a veined appearance.

At higher strain levels intense bands can form which are now commonly referred to as persistent slip bands. These are often softer than the surrounding material and usually contain a cellular dislocation substructure. The formation of the cellular structure begins with a local breakdown of a vein which results in the rapid formation of new glide dislocations. Screw dislocations will again mutually annihilate each other whereas the edge dislocation components will produce tilt walls by the polygonisation process. The phenomenon is the result of encounters between edge dislocations having the same burgers vector, moving on parallel slip planes. This situation usually produces repulsion between the two dislocations, but if one becomes trapped at an obstacle, they may be forced to pass near to each other. This results in the two dislocations taking up very stable positions almost on top of each other. Large long range stresses accompany the dislocation couple which restricts the movement of dislocations on neighbouring planes and leads to a build up of edge dislocation arrays (tilt walls).

The final stage in the evolution of dislocation structures in high stacking fault energy materials, is that of homogeneous cell formation which occurs at high strain amplitudes. Cell formation is triggered by the onset of multiple glide which requires the presence of a sufficiently strong local surplus of dislocations of one type and sign. Sufficiently large quantities of edge dislocations in the cell walls of the persistent slip bands or screw dislocations in the channels, will produce non-primary slip which leads to cell formation (62).

### Accommodation of Strain After Stabilisation

The accommodation of strain after stabilisation has not received much attention. However, Laird (60) has recently discussed some work of Finney (63) who studied the role of persistent slip bands in the cyclic deformation of copper single crystals. He established that in plastic strain controlled tests the strain is always concentrated in the slip bands (see also 64, 65) and during a fatigue test the number of slip bands increase. Fox (66) obtained similar results when studying the surface damage characteristics of low carbon steels tested under load controlled conditions, (lives  $\approx 10^6$ ) cycles. However, at lower loads the area of surface that was damaged did not increase during the test.

Cyclic deformation will initially occur in those grains most favourably oriented for slip and least constrained by the surrounding grains. At stress levels that produce a stable structure consisting of veins of dislocation dipoles, the imposed strain is accommodated in the channels between the veins. No spread of deformation is required and an equilibrium situation develops.

At higher stresses, favourably oriented grains cyclically harden until the stage is reached when dislocation movement becomes easier in adjacent grains. Some of the strain is therefore transferred and eventually many grains may be involved in accommodating the imposed strain. In the grains that contain persistent slip bands or a complete cellular network, deformation is achieved by the movement of dislocations from one cell boundary to another. A balance is reached between the number of dislocations released from one side of the cell in part of the loading cycle, to the number deposited on the opposite cell wall following a load reversal (62).

The ease by which materials are able to transfer strain to other grains is an important material characteristic because such de-localisation

will result in a less severe notch-peak topography at the surface.

Another interesting observation is that the imposed strain is accommodated by a continually increasing number of grains, even after stabilisation. This is an indication of the degree of slip irreversibility that occurs particularly at the specimen surface (62).

#### Effect of Stacking Fault Energy

In most alloy systems an increase in the alloy content will cause a reduction in stacking fault energy. One of the effects resulting from such changes is that the material will have a reduced tendency to cross-slip. An associated effect is that the flow stress of the material will be increased (58).

Much work has been carried out to establish stacking fault energy - cross-slip - fatigue life characteristics in many materials (67,68). However, this has been difficult to achieve due to the inseparable effects resulting from changes in some of the other mechanical properties. Plumbridge and Ryder (58) however have quoted work on copper alloyed with either aluminium or nickel (69). Both these elements produce similar changes in most mechanical properties but aluminium has the greatest effect on stacking fault energy. It was found that the copper-aluminium alloy had superior fatigue properties to the copper-nickel alloy, indicating the beneficial effects resulting from a suppression of a material's ability to cross-slip.

From a microstructural viewpoint, it has been found that as stacking fault energy is decreased, the cyclic deformation character changes from wavy to planar slip. Dislocation substructures also reflect this change in slip character, planar arrays of dislocations being observed rather than the cell or vein structure (61).

### Cyclic Deformation Characteristics in Iron

Pure iron has a high stacking fault energy and therefore deformation is usually characterised by wavy slip patterns as slip normally occurs on the (110), (112), and (123) planes. The stabilised dislocation structure is dependent on the applied strain range in a similar way to most other metals. At high strains the familiar cellular structure is produced (67,70) whereas at lower levels workers have observed veins containing dipoles and multipoles (65).

Feltner and Laird (61) have demonstrated that the stabilised cyclic stress-strain curve for iron is unique, being independent of previous strain history. Abdel-Raouf and Plumtree (56) extended this work by seeking the actual prior strain condition whereby no change in the mechanical properties takes place on subsequent cycling. They found that cycling both annealed and heavily cold worked iron at a strain amplitude of 0.015 produced a cellular dislocation structure with an average cell diameter of 1.5  $\mu$  metres. Specimens loaded in tension to an equivalent strain (12%) also contained a cell size of 1.5  $\mu$  metres which remained unaltered by cycling.

### Cyclic Deformation Characteristics in Iron containing Solute Elements

In most alloy systems the addition of a solute element to a metal produces an increase in strength. Solid solution strengthening occurs if the initial movement of glide dislocations is affected by the solute atoms or if the mobility is made more difficult as a result of higher friction on the glide planes. During the last twenty five years many theories have been published on both "dislocation locking" mechanisms and the friction associated with deformation processes in alloys (71-79). The difficulty now is to establish which theories (mechanisms) are important in any given alloy system. In the current work a knowledge of the precise mechanism is not considered to be important. It is well established

that both silicon and manganese produce an increase in strength when alloyed to iron. The atomic size difference between these two elements and iron is similar and the magnitude of the effects tend to be similar. This is despite the fact that manganese additions slightly increase the iron lattice spacing whereas silicon additions reduce it.

The effect of alloying on the surface slip characteristics has only been studied extensively in one of these systems; Fe-Si. One of the earliest studies to show the marked effect of silicon additions on deformation behaviour was that of Barrett, Ansel and Mehl (80). They showed that alloying progressively reduced the wavy nature of the slip lines. This is due to the reduced stacking fault energy in silicon irons which suppresses cross-slip activity and changes the slip characteristics from wavy to planar.

Boettner and McEvily (67) made a detailed study and comparison of fatigue slip bands in iron and iron-silicon alloys produced as single crystals. In pure iron the slip bands were ill-defined, had a very irregular notch-peak topography and in only a few grains were ribbon-like extrusions observed. With increases in silicon content the slip bands became more regular, homogeneous and in all cases aligned to the (110) plane. A very uniform notch-peak topography was observed in these materials. They also found that fatigue cracks in the silicon irons were usually nucleated at pits or non-metallic inclusions located at the base of the re-entrant angles of the surface extrusions.

Golland and James (81) carried out a similar exercise on iron and iron-silicon alloys. Their work on the silicon irons supported that of McEvily and Boettner, but they also established that the slip band depth was much greater in these materials and therefore more likely to develop into cracks than the diffuse, shallow slip bands found in pure iron. This theory however, is not borne out by their fatigue results, which indicate a superiority in the iron-silicon alloys.

## (ii) Characteristics in Multiphase Materials

### General Comments

Multiphase materials can be divided into two principal classes:-

- a) Those in which phases are intentionally introduced for strengthening purposes. These include precipitation hardened, dispersion strengthened and eutectic alloys.
- b) Those in which impurity phases are present as a by-product from the material processing. The major impurities that have a significant effect on fatigue life are the numerous non-metallic inclusions that are inherent in commercially produced metals.

The steels studied in this project fall into both these categories.

They are dispersion strengthened steels with cementite particles present in the microstructure, and they contain non-metallic inclusions.

### Iron Containing Cementite

Additions of carbon to iron produce cementite ( $\text{Fe}_3\text{C}$ ) as a second phase which can exist in many different forms. The commercially important range of ferrite-pearlite microstructures are of interest in this study. Deformation characteristics in alloys containing pearlite were studied by Jenkins et al in 1942 (82). Steels varying in carbon from 0.40 to 1.14% were examined and they established that slip was confined to the ferrite regions in the pearlite colonies. It was also favoured in those colonies containing cementite plates oriented in a direction parallel to the maximum shear stress.

McGrath and Bratina (83) carried out a detailed electron microscopy study of steels containing a significant pearlite content ( $\approx 10\%$ ). In this grade of steel they established that slip was favoured in the polygonal grains of ferrite and only a limited number of clusters of tangled dislocations were formed at the ferrite/cementite interfaces. Cycling,

even at high stresses, produced only minor modifications to the dislocation structure in the pearlitic ferrite. The dislocation structures generated in the polygonal grains of ferrite had many similarities to those found previously in pure iron specimens, i.e. veins, persistent slip bands or a cellular network were observed, depending on the level of applied stress. This was also found by Klesnil et al (70) working with a 0.11% carbon steel.

Taylor (84) has recently completed an extensive metallographic study of the cyclic deformation characteristics in fully pearlitic steels. He supported the earlier work of Jenkins et al regarding the location and orientation dependency of slip in lamellar structures. Transmission electron microscopy of specimens tested at low strains revealed patches of high dislocation density in the ferrite, which increased in size during cycling. The ferrite/cementite interface was considered to be the source of the dislocations and their movement was favoured in the ferrite phase. The cementite lamellae had little effect on the growth characteristics of the patches.

These observations support the theory of Ashby (85) for the existence of "geometrically necessary" dislocations at such interfaces. Ashby proposed that when strong hard particles are distributed in a soft matrix the deformation is non-linear with no slip occurring in the second phase particles. Such particles therefore, introduce microscopic strain gradients throughout the structure. Ashby calculated the displacements to produce compatible deformation which are required to maintain material integrity and argued geometrically that dislocations are necessary at the interfaces, to produce these displacements.

Calabrese and Laird (86) have observed that in "lamellar" microstructures virtually no surface slip band structure is formed. This was confirmed

by Taylor's work (84) on three eutectoid steels with different cementite morphologies. He found that the maximum height of "extrusions" in a coarse lamellar pearlite and a steel with spheroidal cementite particles was about 0.5  $\mu$ metres. In a fine lamellar pearlite, no distinguishable notch-peak topography was observed in fatigue specimens tested at a full range of strain amplitudes. Calabrese and Laird postulated that in such structures, the slip distance was so short and the dislocation motion so reversible that no significant slip offset was produced.

#### Iron Containing Non-Metallic Inclusions

It has been known for many years that non-metallic inclusions are associated with fatigue mechanisms in steel. It is now generally accepted that the fatigue limit is reduced as the total volume fraction of oxide inclusions increases. It is interesting to note that manganese sulphide inclusions are never associated with crack initiation (87-93). The observations related to oxides has been explained in statistical terms, i.e., as the inclusion content increases there is a higher probability of one existing at the critically stressed location in the specimen (93). This suggests that the main effect of non-metallic inclusions is to accelerate the crack initiation process by acting as a geometric stress raiser.

Lankford (94) recently carried out a microstructural investigation to characterise the initiation and very early stages of crack growth in AISI 4340 steel. This is a 0.4% carbon, low alloy steel which was tested in the oil quenched and tempered condition. In such a steel, tempered to produce a yield stress of 890 N/mm<sup>2</sup>, he made some very interesting observations of the inclusion related crack initiation process. He found that many oxide inclusions had debonded after the first loading cycle even at loads below the fatigue limit and microcracks had formed in slip bands on either side of the inclusions. With subsequent cycling the cracks initially grew around the inclusion prior

to growing along the surface to eventually link with other growing cracks. In specimens with lives less than  $10^6$  cycles, inclusion debonding and crack initiation occurred within a few thousand cycles of each other, but the crack continued to be influenced by the inclusion until a major portion of the lifetime was completed.

Fatigue life is affected by the stress-strain field in the metal matrix around the inclusion. This local stress concentration is due to:-

- a) The creation of tessellated stresses due to the variation in thermal characteristics of the inclusion and the metal. These are usually tensile for most oxide inclusions (95,96),  
and
- b) The creation of inhomogeneous strains due to variations in the stress-strain relationships of the inclusion and metal (95,99,100).

The observations suggest that non-metallic inclusions are a dominant microstructural feature in most crack initiation processes. The effect is dependent on some of their physical and mechanical properties. The most important factors in assessing the influence of inclusions on crack initiation is their chemistry, size, location and morphology. Alumina and calcium aluminates are the most detrimental oxide types in steels and they become more damaging as their size increases (97,98).

### 2.2.2. Surface Phenomena, Crack Initiation, and Stage II Cracks

#### General Comments

The previous discussion has described some of the important microstructural changes that occur in a cyclically loaded material. It has been established that the slip process is not homogeneous and dislocation concentrations can occur in veins, persistent slip bands, cell walls and at the interfaces between second phase particles and the matrix. At the surface these inhomogeneous displacements are revealed as slip lines

or bands and in some metals extreme surface irregularities which are referred to as extrusions and intrusions are formed.

Many of the dislocation configurations which have been described develop throughout the specimen, but they do not appear to weaken the metal. This conclusion is based on many experiments that have involved cycling, surface removal, and then further cycling. Early work of this type showed that removing the effects of surface damage by electropolishing could prolong life indefinitely (101). More recently, work by Grosskreutz (102), in which he re-tested the two halves of a broken fatigue specimen, showed the same effect. In this case comparable lives were found in all three specimens.

The inhibition of surface slip markings also results in an increased fatigue resistance for a material. Alden and Backofen (103) showed that anodising aluminium significantly increases crack initiation life. Similarly, work on orientation effects in single crystals has shown that surface damage and crack initiation tendencies are reduced if the glide plane is oriented parallel to the specimen surface (104). Hard, high modulus surface coatings can also be effective in suppressing surface slip (105).

Cracks propagating into a material are usually divided into two types; stage I near the surface and stage II for the remainder of the crack. In stage I the crack runs along the slip planes that are most favourably oriented in terms of the maximum shear stress (about  $45^{\circ}$  to the direction of the applied load) and usually extend for only a few grains. Cracking in stage I, which is crystallographic in nature, accounts for the majority of the fatigue life in smooth specimens tested at low strain levels, yet has still not been extensively studied in many commercial materials.

## The Characteristics of Stage I Cracks

The dependence of fatigue crack initiation on plastic deformation and surface slip is now an accepted principle. The crack initiation process requires plastic deformation to create surface damage. This may be enhanced by local microstructural notches such as grain boundaries or non-metallic inclusions but cracks can form without such irregularities. For this latter case the generation of extrusions can produce a crack source in many materials, although it must be noted that microcracks do not normally exist at every extrusion. Crack initiation from extrusions has been extensively studied in many materials and several theories, all based on a cross-slip mechanism, have been proposed (106-112). However, extrusion formation is not typical of the surface deformation characteristics of ferrite, although they have been shown to exist, in a non-classical form, to a limited degree (113). Slip band formation in which the notch-peak height is very short, is a much more common feature in this material.

Fox (66) has shown that crack initiation from such bands is the dominant crack initiation mechanism for a number of steels up to 0.41% carbon. In the 0.41% carbon steel, which contained about 40% pearlite, the creation of surface damage occurred preferentially in the polygonal ferrite grains in the microstructure. Fatigue crack initiation was never observed in the pearlite colonies.

The development of a slip band into a growing fatigue crack has been observed in pure iron (102). Initially the notch peak topography is generated due to the irreversibility of slip in tension and compression in this material. The irregular surface results in inhomogeneous deformation with strain being concentrated at the notches. Continued cycling eventually leads to the formation of cracks at these locations.

Neumann (114) has proposed a model for crack formation in slip bands, based on alternating slip in two essentially perpendicular slip planes. With reference to fig.8, stress concentration initially occurs at the coarse slip step produced by deformation along slip plane (1). This concentration of stress causes slip to be activated along slip plane (2) during the tensile part of the cycle, (8b and c). Reversal of load into compression initially activates plane (1), followed by plane (2) to produce the microcrack shown in fig.8d. The next tensile portion causes slip on plane (3) which is parallel to slip plane (1). The process continues through stages (f), (g) and (h) until an extensive crack is formed. This is an idealised model but it demonstrates that cracks can be formed by a simple slip mechanism if certain conditions apply. It has been verified for the case of fully reversed loading of copper single crystals (114).

#### The Characteristics of Stage II Cracks

Stage II cracks have a general (macroscopic) propagation direction at right angles to the direction of the applied load along the plane of principal stress. However, on a microscale, the crack grows on many differently oriented planes and in numerous directions, depending on the microstructure and the properties of the material. A common feature of this stage are fatigue "striations", which are a series of peak and valleys in a furrow-like configuration, running perpendicular to the direction of crack propagation. The following list outlines some of the major observations made of them.

- i) They represent the growth of the crack in one cycle.
- ii) The separation of the striation peaks is a variable dependent on the rate of crack propagation through the specimen.

- iii) Striation patterns may cover the entire fracture surface, as in many of the aluminium alloys or they may be discontinuous as in steels.
- iv) Inclusions and second phase particles change locally the direction of striations, (115-119).
- v) At relatively long crack lengths, striations are often accompanied by secondary cracks (120).
- vi) Striations do not occur in materials tested in vacuum (121,122).
- vii) They do not appear below a certain value of stress.

An additional feature of stage II growth found in some materials are "brittle striations". These are identified as steps or ridges that develop in the same direction as the growing crack. They are encountered most frequently in high strength, dispersion hardened materials and therefore are a common feature in steels (123).

Many observations have been made on the fracture characteristics of ferrite-pearlite steels and in general similar features have been reported (124-129). Both normal and brittle striations appear on the fracture surfaces, but the normal type tend to be very irregular and varied in their arrangement. They do not form over the entire surface and as the pearlite content increases they become less frequent. The inter-striation spacing reflects the crack growth rate through the material, i.e., striations become more widely separated as the growth rate increases.

Several models have been proposed for the formation of striations; the most common one being that of Laird and Smith (130). In this model see fig.9, which was established for pure aluminium, it was proposed that crack extension occurs only during the tensile part of a cycle. This

action produces deformation at the crack tip resulting in an increased plastic zone size in that region which then causes the crack to become blunt and to stop growing. During the compressive part of the cycle the crack tip again becomes sharp, due to the effect of slip in the opposite direction, and in addition two "ears" form; one on each side of the crack. These "ears" lead to the peak and valley topography typical of striations as the above process is repeated with every subsequent cycle.

Other workers have commented on the crystallographic nature of striations. Matting and Jacoby (131), postulated that cracking occurs generally on the principle slip plane which is at an angle of between  $30^{\circ}$  and  $50^{\circ}$  to the applied load. Pelloux and co-workers, on the other hand, have proposed that in f.c.c. metals, growth occurs on the (100) and (110) planes as a result of decohesion on the (111) planes, (121,122,132).

Kocanda (127) and Bowles and Broek (133) have suggested mechanisms of striation formation based on the observation that striations do not form in aluminium alloys tested under vacuum. Essentially, they state that striations form due to an irreversible slip process caused by oxidation at the crack tip, i.e., when oxidation occurs the crack cannot completely close during the compression part of the cycle. Kocanda has also suggested (127) that striations form as a result of plastic strain ahead of the crack tip and dislocation models involving cross-slip have been proposed. On this same theme, Forsyth and Ryder (134) developed a mechanism involving the generation of microvoids at inclusions or second phase particles ahead of the crack tip.

It is evident from the examples quoted that the mechanism of striation formation is complex and variable. It is probably affected by the local crack tip strain level (plastic zone size) and how this influences

the degree of strain hardening on the principal slip planes. The extent of secondary cracking, and the size and volume fraction of second phase particles in the microstructure are also important.

### 2.2.3. Composition, microstructure - property relationships

#### Monotonic Properties

The relationships in steels between chemical composition and mechanical properties were first studied about a century ago (135-139). By the beginning of this century there was so much information available that researchers of the time were able to embark on extensive reviews. For example, Stead was able to assess the influence of most of the major alloying elements in iron in 1916 (140). However, McWilliam in 1918 (141) was the first to use regression analysis in an attempt to assess the combined effects of C, Si and Mn in iron. His equation for the ultimate tensile strength ( $\sigma_u$ ) was:-

$$\sigma_u = 262 + 496 (\% \text{ C}) + 83 (\% \text{ Si}) + 42 (\% \text{ Mn}) + 689 (\% \text{ P}) \text{ N/mm}^2 \quad (21)$$

This equation was derived from tests on steels containing only low levels of silicon and manganese and high levels of phosphorus. It therefore has only limited applicability.

The first major attempt at developing joint composition, and microstructure - property relationships was carried out by Gensamer and co-workers about 1940 (142-146). In order to study solid solution hardening effects they produced alloy steels which were subsequently completed decarburised by heat treatment. They found that every element they added to carbon free ferrite produced an increase in strength of varying magnitude. To evaluate the effect of adding more than one element to iron they developed the concept of "Equivalent Nickel Concentration". Nickel, which is soluble in iron over a wide range of concentrations was found to have only a moderate effect on strength.

To obtain the nickel equivalent of another element they calculated the concentration of nickel that would increase the strength by the same amount as 1% of the alloying element in question. Simple addition of nickel equivalents produced the overall strength contribution of a complex alloy system.

From their very extensive microstructure - property studies they developed the following criterion which applies to both pearlites and bainites.

"The resistance to deformation of a metallic aggregate, consisting of a hard phase dispersed in a soft matrix, is proportional to the logarithm of the mean straight path through the continuous phase".

This rule was derived using two other observations that were available to these workers:-

(i) Dislocation movement, which is responsible for deformation, is halted by hard particles and therefore the mean path through the soft matrix represents the average distance travelled by dislocations.

(ii) The rate of dislocation generation is semilogarithmically related to the applied stress because the logarithm of the rate of flow ( $d\epsilon/dT$ ) plots as a straight line against stress.

The use of this second observation is in my view invalid as the rate of dislocation generation is not relevant. However, the empirically produced logarithmic rule was first questioned seriously by Hall (147) and Petch (148). Using mild steel, ingot iron and spectrographic iron they both found that a strength parameter, ie, yield (147), fracture (148) was inversely related to the square root of the grain diameter. The theories of other workers (149) which considered the relationship between a strength parameter and the internal stresses created by an array of dislocations piled up at a grain boundary, were used to explain the observation.

Most of the recent theoretical work on the deformation of two phase structures supports the Hall/Petch model. Ashby (85) for example in his work on plate-like precipitates in a soft matrix produced an expression for the number of geometrically necessary dislocations required in his model and incorporated the expression into the relationship between flow stress and dislocation density produced by Nabarro et al (150). The final result indicates an inverse relationship between flow stress and the square root of the plate spacing. Embury and Fisher (151) studied the deformation characteristics of drawn coarse and fine pearlite using transmission electron microscopy. Their observations indicated that a cellular dislocation substructure was produced in which the mean cell diameter decreased with increasing strain. They produced a relationship between yield stress and the reciprocal of the square root of the mean dislocation spacing in the undrawn wire. This conclusion was also substantiated by Langford (152).

The next major effort to produce composition, structure, property relationships in steels was carried out by Irvine and co-workers starting in the late 1950's. They have now completed their studies for steels varying in pearlite content from zero to 100% (153-157). In most of their work they have used multiple regression analysis techniques to analyse the results. With this method a pre-conceived model is required incorporating the known or the most probable metallurgical relationship between the structural parameters and properties. For example, when considering a range of steels with varying ferrite/pearlite ratio's, an equation is required that will weight the importance of parameters associated with pearlite according to some function of the volume fraction of pearlite. The equation that they adopted in (157) was:-

$$\sigma_{ap} = f_a^m \cdot \sigma_a + (1 - f_a^m) \cdot \sigma_p \quad (22)$$

where  $\sigma_{ap}$  = strength parameters in the ferrite/pearlite steel  
 $\sigma_a$  = the same strength parameters in ferrite only  
 $\sigma_p$  = the same strength parameters in pearlite only  
 $f_a$  = volume fraction of ferrite  
 $m$  = an index used when the strength parameter does not vary linearly with pearlite content.

In this work they came to the following conclusions regarding the structure, composition, property relationships of ferrite-pearlite steels:-

- (a) The ferrite grain size has a dominant effect on the strength of steels containing appreciable ferrite content, whereas in fully pearlitic steels the interlamellar spacing is the important microstructural feature. For both types of steel the Hall/Petch relationship was found to apply.
- (b) Silicon has a similar solid solution hardening effect in both ferrite and pearlite.
- (c) The solid solution hardening effect due to manganese is only significant in steels with a high ferrite content.

### Cyclic Properties

Compared to the large efforts made in studying monotonic data, the work relating metallurgical variables to cyclic properties is quite small. Until quite recently the only "fatigue parameter" was the fatigue or endurance limit which was usually related to other, more easily obtained mechanical properties rather than to metallurgical variables. The most successful correlation was between fatigue limit and ultimate tensile strength but substantial scatter has been found even in this relationship. In the early 1960's, Rowe (1,158) considered an alternative relationship between fatigue limit and monotonic work hardening parameters:-

$$\text{Fatigue limit} = (A)^{1/n} \cdot (K)^B \quad (23)$$

where A and B are material constants equal to 1.0 and 0.9 respectively for ferrite-pearlite steels.

Although this approach was an improvement over previous methods, the predicted fatigue limits were not accurate in all cases and it could not deal adequately with major microstructural variations. For example, the approach was found to be inappropriate for ferrite-pearlite steels in which the grain size was markedly outside the original range.

Grozier and Bucher (159) produced a more meaningful correlation between composition, microstructure and fatigue limit in ferrite-pearlite steels. They used multiple regression analysis techniques to produce the following equation:-

$$\begin{aligned} \text{Fatigue limit} = & 163 + 99.2 (\% \text{ Si}) + 58 (\% \text{ Mn}) + 0.82 (\% \text{ P}) \\ & + 0.46 (d_a^{-1/2}) + 5.5(Y) \quad \text{N/mm}^2 \quad (24) \end{aligned}$$

where Y is a precipitation strengthening parameter due to vanadium or niobium carbide.

It can be seen that the Hall/Petch grain size relationship was again found to be satisfactory in accounting for microstructural size effects. This supports similar conclusions obtained for  $\alpha$ -brass and mild steel (70,160,161). The solid solution hardening effect due to silicon and manganese was shown by Grozier and Bucher, to influence the fatigue limit. This has also been verified by the work of Nishioka and Nishikawa (161).

### 3. PROJECT DETAILS

#### 3.1. Project Plan

The previous sections have outlined the recent developments in fatigue life prediction using the local stress-strain approach. In addition, some of the important micromechanisms associated with fatigue in iron based materials and the previous work relating metallurgical variables to properties have been discussed. The current research programme considers each of these subjects for a range of C/Si/Mn steels which contain ferrite-pearlite microstructures. The study is aimed at designers and metallurgists seeking improved methods of assessing the potential service performance of components and materials. The work can be conveniently divided into the following areas:-

- (i) An evaluation of the fatigue parameters of a range of C/Si/Mn steels.
- (ii) An assessment of the relationships between fatigue parameters and more conventional mechanical properties
- (iii) A quantitative evaluation of the relationships between metallurgical variables and fatigue related mechanical properties
- (iv) A study of the micromechanisms associated with the formation of fatigue cracks in ferrite-pearlite steels.
- (v) A study of the fatigue behaviour of C/Si/Mn steels subjected to variable amplitude loads.

#### 3.2. Project Design

In terms of experimental design, these topics could be studied by adopting the "classical approach" in which one factor is varied in turn while all other factors are held constant. The main problem with this method is that interaction effects between factors cannot be studied. A better approach is to carry out a full factorial experiment in which each factor

is fixed at a certain number of predetermined levels. This method is capable of coping with interaction effects but has the disadvantage of producing a large number of test conditions when multi-factor experiments are being studied.

A more practical approach is to use a fractional factorial design of experiment. With this technique both the main and second order effects can be obtained from a relatively small number of test conditions. For example, referring to fig.10 (obtained from ref.162), in an experiment for which there are seven factors at three different levels, the full factorial experiment would consist of 2187 test conditions. However the main and second order effects can be obtained from as little as 100 experiments, therefore a 1/9th fraction of the full factorial (243 conditions) is an adequate sample.

The design of the fractional factorial experiment is such that many of the highest order interactions are eliminated and those remaining are grouped with effects which are likely to be significant. In this way the main and second order effects are concentrated in the fractionalised experiment.

For some of the studies in this work, eight C/Si/Mn steels were used which were selected by adopting a fourth fraction, two level factorial design. However, for the quantitative assessment of relationships, more extensive data was required and therefore a third fraction, three level experiment was created which utilised five independent variables. The details of the individual experiments are discussed more fully in the appropriate sections.

It is important with this type of experimental design that the significance level of an effect can be obtained so that insignificant factors can be eliminated in the final analysis. One method of achieving this aim is to adopt an analysis of variants technique. At British Rail, a computer programme (ANOVA) is available for this purpose. The aim of the programme is to establish whether a change in the level of a particular factor has a significant effect on a potential dependent variable. The effect of a factor is taken as the variation in the response of the variable (measured at different levels) whereas the significance of the effect is assessed by comparing this variation with experimental scatter. The variances (or "mean squares") equivalent to the source of the variation are output and standard methods are then employed to determine the significance of the effect. When all the significant effects have been established, the regression coefficients associated with each one, are combined to construct a complete multiple regression equation.

### 3.3. Experimental Procedure

#### 3.3.1. Materials

The compositions of the steels used in the project were selected on the basis of the two fractional factorial experimental designs. It was established that the compositions required for the two level experiments could be taken from those produced for the three level experiment. In total twenty seven different compositions were necessary. All the steels were produced at the Corporate Laboratories of British Steel Corporation, Sheffield, using a vacuum melting process to minimise the non-metallic inclusion level. They were received as 1/2" diameter rods, approximately 6 ft long, in the as-rolled condition. The chemical analysis obtained on the steels is shown in table (1).

Prior to heat treatment and machining of test specimens, each rod was inspected microscopically for internal cleanliness and visually inspected for surface defects. Any defective parts were removed and discarded.

### 3.3.2. Heat Treatment

The steels were heat treated in order to produce a wide range of ferrite-pearlite microstructures in accordance with the design of the experiments. Preliminary experiments showed that the required microstructures could best be achieved by varying both the austenitising temperature and the isothermal transformation temperature. Austenitisation was carried out in a conventional resistance furnace purged with Argon gas, in which the temperature was controlled by feedback from a thermocouple placed just above the specimen blanks. The isothermal heat treatments were carried out in a lead bath.

### 3.3.3. Quantitative Microscopy

The microstructural characteristics of the steels were evaluated using several different techniques. The volume fraction of the ferrite or pearlite phase was obtained using a Quantimet 720 instrument. To obtain the greatest accuracy, the phase having the smallest volume (ferrite or pearlite) was selected for detection on this device. Ferrite grain size and the thickness of ferrite grain boundaries were measured by a mean linear intercept method using a lineal analyser attached to a Vickers photoplan bench microscope. The interlamellar spacing in the pearlite phase was obtained using the technique first proposed by Pellisier et al (142) and later developed by Birkbeck and Wells (163). This parameter together with the "free" ferrite size parameters was used to compute the "mean ferrite path" from the following equation:-

$$\bar{\lambda}_a = f_a \cdot d_a + 0.87 \cdot f_p \cdot S^0 \quad (25)$$

where  $\bar{\lambda}_a$  = mean ferrite path  
 $d_a$  = ferrite grain or grain boundary size  
 $S^\circ$  = interlamellar spacing  
 $f_a$  and  $f_p$  = fraction of ferrite and pearlite respectively.

The coefficient 0.87 was the assumed value for the ferrite fraction of the pearlite phase.

The non-metallic inclusion content in each steel was also assessed using the Quantimet 720.

#### 3.3.4. Fatigue Testing Procedure

Constant amplitude, strain controlled fatigue tests were carried out in an "M.T.S." servo-hydraulic testing machine. A sinusoidal waveform was used at frequencies ranging from 0.1 to 30 Hz. Prior to testing, each specimen (machined to the dimensions shown in fig.11) was polished to produce longitudinal markings on the gauge length, thereby reducing any stress concentrating effects resulting from the turning operation. All specimens were given a stress relieving treatment of 1 hour at 650°C in a vacuum furnace.

During the tests the load was measured by a load cell in series with the specimen and the strain by an extensometer attached to the specimen gauge length, fig.12. A high speed strip chart recorder was used throughout the tests to monitor these two parameters. In addition, an X-Y plotter was occasionally used to obtain a record of the stress-strain hysteresis loops.

#### 3.3.5. Monotonic Test Procedure

Monotonic tests were carried out under strain control conditions in the same servohydraulic machine as that used for the fatigue tests. A long arm extensometer was used, fig.13, from which engineering strains of 0.60 would be measured without having to reset the extensometer. This

level of strain was more than adequate for the materials tested in this work.

The loads and strains were monitored during the tests by the devices described for the fatigue tests i.e. an X-Y plotter and high speed strip chart recorder. From the outputs, the following properties were measured and calculated:-

1. Yield stress ( $\sigma_y$ ). This parameter was taken as the lower yield point in steels that exhibited a yield drop or the point at which the curve deviated from linearity in those steels without a yield drop.
2. Ultimate tensile strength ( $\sigma_u$ )
3. True fracture stress ( $\sigma_f$ )
4. True fracture strain ( $\epsilon_f$ )
5. Strain hardening exponents ( $n_x$ )
6. Strain hardening coefficient (Kx)

With reference to fig.14, these parameters were calculated using the following equations:-

a) Stress Parameters

$$\text{True stress } (\sigma_a) = \text{LOAD(P)}/\text{AREA(A)} \quad (26)$$

$$\text{Up to necking, } \sigma_a = S(1 + e) \quad (27)$$

$$\text{where } S = P/A_0$$

$$\text{and } e = L/L_0$$

$$\text{Uncorrected fracture stress } (\sigma_{f1}) = Pf/Af \quad (28)$$

To correct the axial fracture stress for necking the Yamashita method was adopted, (164). This method was formulated following extensive studies of the strain distribution which occurred in the necked portion of tensile specimens produced from three different types of material

(13% Cr steel, mild steel and copper). He established a correction factor that was independent of material composition, (within his range) based on an experimentally produced relationship between the true strain after the onset of necking. This relationship, which assumes isotropic behaviour in the material, is shown plotted in fig.15. Note that  $f_b$  equals the cross section area at maximum tensile load  $\left[ \frac{P}{S(1+e)} \right]$ .

b) Strain Parameters

$$\text{True fracture strain } \epsilon_f = \log_e A_0/A_f = \log_e (100/100-R.A) \quad (29)$$

$$\text{True strain } \epsilon_t = \log L/L_0 \quad (30)$$

$$\text{Up to necking, } \epsilon_t = \log (1+e) \quad (31)$$

$$\text{Plastic strain } \epsilon_p = \epsilon_t - \sigma_a/E \quad (32)$$

c) Work Hardening Parameters

To obtain n and K the Ramberg Osgood (16) relationship was used:-

$$\sigma_a = K(\epsilon_p)^n \quad (33)$$

Using this equation a best fit straight line is obtained in which the corrected fracture stress and the fracture strain are utilised in addition to the values of  $\sigma_a$  and  $\epsilon_p$  up to necking.

3.3.6. Production of Cyclic Stress-Strain Curves

It has been shown that cyclic  $\sigma - \epsilon$  properties are normally produced from either incremental step tests or multiple specimen tests.

i) Incremental Step Test (I.S. Test)

The I.S. test is one method of obtaining the cyclic stress-strain relationship in materials. The main advantage of using this technique is that a cyclic stress-strain curve can be accurately produced from testing one specimen. The clip on extensometer used for this test was the same as that used in the fatigue tests. In this test a specimen is subjected to a series of increasing and then decreasing strain amplitudes

forming a 30 cycle block in which only the lowest strain range is completely elastic. The maximum strain amplitude in the tests on the steels used in this study was .015, and several such blocks were required to cause fracture of a specimen. After a few blocks most materials tend to stabilise and once this stability is reached the locus of the stress-strain hysteresis loop tips describes the cyclic stress-strain curve for that material. Fig.5 illustrates the main features of the test.

In this work the strain hardening parameters from a cyclic stress-strain curve ( $n'$  and  $K'$ ) were originally obtained by manual graphical methods. This was found to be both time consuming and prone to "operator error" and therefore a computer programme was developed to produce values of the parameters more efficiently (165).

The programme is in two parts. In part 1 the output of the force cell and the strain measuring clip gauge are read simultaneously. The strain record is scanned for a local maximum and this value and the greatest stress to date are stored. The next minimum strain is then found and it and the minimum stress after the last maximum are also stored. From these the strain range and the associated stress range are calculated and the two values are punched out on paper tape. The next maximum strain and stress are then found and the ranges from the last minima to these maxima are punched out. Part 2 of the program runs off-line using this paper tape input. Initial tests showed that although  $n'$  was the same for the ascending and descending halves of the block,  $K'$  differed for the two. It was therefore necessary to consider these two halves of the block separately. In this work, all calculations have been done with the descending halves of blocks only.

One block of the incremental step test gives 58 ranges of stress and strain. 60 pairs of stress and strain range values are read and the

strain range values checked to ensure that they contain all of the descending values of one block (this is not always the case because they can contain parts of the descending halves of neighbouring blocks). If this condition is not satisfied additional pairs of values are read until it is.

The values of strain range which are read in are alternately ranges about zero mean and ranges about a non zero mean. The ranges about a non zero mean are discarded. The two greatest remaining ranges are also discarded since they are midway in characteristics between the ascending and the descending halves of the block. The ranges which remain are converted from integer values to stress and strain and the plastic strain is calculated from  $\epsilon_p = \epsilon_t - \sigma_a/E$ .

The final stage in choosing which values are valid is to reject those where the strain is so small that the error in  $\epsilon_p$  would be unacceptable.

For the remaining values of stress and plastic strain, a best fit straight line for  $\log \sigma_a = \log K' + n' \log \epsilon_p$  is calculated assuming equal weighting for all the points and equal % error in both stress and strain. This gives a first estimate for  $K'$  and  $n'$ . Points which lie outside of  $\pm 1\frac{1}{2}$  standard error in stress from this line are discarded and the best fit straight line recalculated.

Output on teletype may be extensive giving values for all the data assessed or it may print out just the vital information, e.g., block no.,  $K'$  and  $n'$ . The flow chart of the programme is shown in fig.16.

An additional parameter obtained from the I.S. test was the cyclic yield stress ( $\sigma_y'$ ). In this work  $\sigma_y'$  is defined as the point in the cyclic stress-strain relationship where the curve deviates from the linear elastic relationship. The parameter was obtained by manual graphical methods.

## 4. FATIGUE, MECHANICAL PROPERTY AND MATERIAL RELATIONSHIPS

### 4.1. Introduction

In this section, the first three objectives outlined in the project plan are studied in turn, ie,

- (i) To obtain the fatigue parameters for a range of C/Si/Mn steels.
- (ii) To compare these fatigue parameters with other mechanical properties
- (iii) To quantify the relationships between mechanical properties and material variables.

### 4.2. Constant Amplitude Fatigue Data

#### 4.2.1. Experimental Design

As stated in section 3, it was decided to adopt a two level partial factorial experimental design for this part of the work. The independent variables were considered to be carbon, silicon, manganese, austenitising temperature and isothermal transformation temperature; the latter two being required to produce a wide range of microstructures in the steels. Table (2) outlines the levels of the variables and the design selected.

#### 4.2.2. Materials

The partial factorial experiment required eight steels of different compositions which included steels with two levels of each of the elemental variables carbon, silicon and manganese. The chemical analysis of the steels used is shown in table (3) . The heat treatments given to the steels produced a range of microstructures, which are shown in figs.17 to 24 and for which the quantitative metallographic results shown in table (4), were obtained.

### 4.2.3. Results

#### 4.2.3.1. Results of Fatigue Tests

A series of constant amplitude strain controlled fatigue tests was carried out on each steel in order to produce basic fatigue-life data. The results of these tests are shown in table (5) . It should be noted that the elastic strain ( $\epsilon_e$ ) was calculated ( $\sigma/\epsilon$ ) whereas the plastic strain ( $\epsilon_p$ ) was the measured hysteresis loop width along the zero stress line. All the values quoted are for the stabilised material condition, which was found to exist in each steel after only a few cycles.

The best method of presenting the results graphically is shown in figs.25 to 32. Plots of total strain, plastic strain and elastic strain (stress) against life are all incorporated on the same graph. Fatigue life in each case is represented by the number of reversals to failure; the latter being defined in this work as the complete separation of the test specimen into two pieces.

It can be observed in these figures that the total strain - life relationship is represented by a smooth curve which tends to the horizontal in the long life regime. This end of the curve i.e. near the fatigue limit, was difficult to define accurately due to the very long testing times required. In the present study a "RUN OUT" was normally taken as  $3 \times 10^7$  cycles, which at the cycling rate adopted was equivalent to about two weeks testing time. Therefore, a limited number of "RUN OUTS" could be tolerated for each material and in fact only one was usually permitted.

The plastic strain and elastic strain - life relationships shown were produced manually. The lines obtained confirms that both the Coffin/Manson and Basquin empirical relationships are obeyed in C/Si/Mn steels. It was therefore possible to compute the four fatigue parameters from the test

data, table (6), and also to compare the results with both composition and microstructural variables.

#### 4.2.3.2. Composition - Fatigue Property Relationships

It is now an accepted fact that the initiation and development of fatigue cracks in metals is a result of cyclic plastic deformation. The effects of compositional variables on this process therefore, will be influenced by how an alloying element affects the generation and mobility of dislocations. In ferrite - pearlite steels the characteristics of plasticity in the soft phase (ferrite) is of prime concern in this respect.

The three alloying variables used in this work are carbon, silicon and manganese. Carbon forms with iron the stable carbide,  $Fe_3C$  and through microstructural changes, will affect the mobility of the ferrite based glide dislocations. Silicon however, forms a solid solution with iron which reduces the mobility of dislocations in the ferrite phase. Manganese, on the other hand affects both the microstructure and properties of the ferrite. It has the effect of reducing the transformation temperature of a steel which results in a reduced ferrite grain size and an increase in both content and fineness of the pearlite phase. In addition it also forms a solid solution with ferrite and hence affects the properties of this phase.

The combined effects of these elements on the fatigue parameters of a steel, has not been assessed previously. In this work the four fatigue parameters were each initially evaluated in terms of the three compositional variables, figs.33-36. In these figures the individual lines represent the effect of the compositional variable on the ordinate and the four lines per graph refer to various fixed levels of the non-varying elements.

(i) Fatigue Ductility Coefficient ( $\epsilon_f'$ )

Fig.33 summarises the effect of changes in composition on this parameter. Carbon has the largest effect; increases causing a marked reduction in the fatigue ductility coefficient. Increasing silicon and manganese levels also cause the parameter to be reduced, but to a much smaller degree.

These results were expected on the basis that all alloying elements will tend to reduce the ductility of pure iron. Carbon, represented by cementite, is known to reduce the monotonic fracture strain; a property thought to be equivalent to  $\epsilon_f'$ .

(ii) Fatigue Strength Coefficient ( $\sigma_f'$ )

A graph of composition against fatigue strength coefficient is shown in fig.34. Increases in carbon and manganese both increase the value of this parameter whereas the picture with silicon is more complex. The two lines showing a decrease in  $\sigma_f'$  with increasing silicon content, represent low manganese steels. This is an unexpected interaction which is difficult to explain metallurgically as both elements are solid solution strengtheners and therefore should increase  $\sigma_f'$ . This latter point is borne out when the high manganese steels are considered because in this case increasing silicon produces an increase in the fatigue strength coefficient.

(iii) Fatigue Ductility Exponent (c)

Composition interaction effects also occur with this parameter, as can be seen in fig.35. Increasing carbon significantly reduces (makes less negative) its value, whereas silicon and manganese effects are dependent on the level of carbon in the steel. For example, increases in silicon content produce an opposite effect on "c" when comparing low and high carbon steels. With the former,

"c" becomes more negative, whilst with the latter it becomes slightly more positive. The only effect of manganese is to cause a slight reduction in the exponent in low carbon steels.

(iv) Fatigue Strength Exponent (b)

Increases in carbon and silicon produce the opposite effect on this parameter, fig.36; higher carbon levels give higher values of "b" (more negative), whereas silicon additions cause the fatigue strength exponent to become less negative. However, the effect of manganese is influenced by the silicon content in the steel, as can be seen in the diagram. With low silicon steels manganese additions cause the Basquin slope to become flatter (more +ve), which is similar to the silicon effect. However, for high silicon steels, the very flat slope inherent in these steels, become less flat at the higher manganese levels.

(v) Fatigue Limit

The measured fatigue limits for the eight steels (listed in table (7), and shown in fig.37) indicate that this parameter is increased when the level of all three individual elements is raised. This result was anticipated as carbon, silicon and manganese additions all increase a material's strength; the property that influences the fatigue limit.

#### 4.2.3.3. Microstructure - Fatigue Property Relationships

In ferrite-pearlite steels certain microstructural features have been shown to influence monotonic properties. The ferrite grain size has been established as having a dominant influence on the strength properties of low carbon steels (147,148), whereas in fully pearlitic steels the interlamellar spacing is important (157). In mixed ferrite-pearlite structures, some workers (143,144) have shown that properties can be related to the "mean ferrite path". Finally the volume fraction of

ferrite or pearlite has been used by many workers to relate structure to properties in this type of steel.

The microstructure of the current steels is dominated by carbon content. The eight steels can be separated into two basic types, fully pearlitic high carbon steels, and low carbon steels containing appreciable free ferrite content. The structure - fatigue property comparisons therefore, are similar to the carbon content - property results, i.e. the fatigue strength coefficient is increased, the fatigue ductility coefficient is decreased, the fatigue strength exponent becomes more positive and the fatigue ductility exponent becomes less positive as the pearlite content is increased (or ferrite content decreased). The other major microstructural variables, ferrite grain size and mean ferrite path can be substituted for ferrite content in the above comments.

#### 4.2.4. Discussion

The comparison between composition, microstructure and the two fatigue coefficients ( $\sigma_f'$  and  $\epsilon_f'$ ) were in some cases unexpected. However, it is difficult to envisage that these parameters are characteristic material properties because of the way they are produced (long range extrapolation from the test data to the ordinate on a fatigue curve is required). The assumption is made therefore that the associated exponents are constant over the entire strain range from zero to the fracture strain. This may be a reasonable assumption to make for some materials but is unlikely to have general applicability. Some of the effects encountered in the current work could be due to this assumption being invalid for the high silicon steels under test. Work reported in later sections was used to study this phenomenon in more detail.

The results obtained for the two exponents can best be understood by considering their dependence on the cyclic strain hardening exponent,  $n'$ . Morrow (22) combined the Ramberg-Osgood relationship between stress and

plastic strain with the Coffin/Manson and Basquin fatigue life relationships to establish the correlation between  $n'$ , "c" and "b".

He showed that:-

$$n' = b/c \quad (34)$$

In order to establish a relationship between the individual fatigue life slope and  $n'$ , he adopted an energy approach. He assumed that the plastic strain energy per cycle ( $\Delta W$ ) was the area of a stable hysteresis loop and could be calculated as follows:-

$$\Delta W = 2\sigma_a \Delta \epsilon_p \left( \frac{1-n'}{1+n'} \right) \quad (35)$$

substituting for  $\Delta \epsilon_p$  by using the Ramberg-Osgood equation for the cyclic stress-strain curve, he produced the following relationship:-

$$\Delta W \propto \left( \frac{\sigma_a}{\sigma_{f'}} \right)^{\frac{1+n'}{n'}} \quad (36)$$

He then assumed that the total energy to fracture is equal to  $\Delta W \cdot N_f$  and established an empirical relationship between this combined parameter and stress amplitude as follows:-

$$\sigma_a \propto (\Delta W N_f)^{-1/4} \quad (37)$$

Using this relationship the fatigue life was solved in terms of the cyclic stress-strain properties:-

$$2N_f = \left( \frac{\Delta \epsilon_p}{2\epsilon_{f'}} \right)^{-(1+5n')} = \left( \frac{\sigma_a}{\sigma_{f'}} \right)^{-(1+5n')/n'} \quad (38)$$

Therefore:-

$$c = \frac{-1}{1+5n'} \quad \text{and} \quad b = \frac{-n'}{1+5n'} \quad (39)$$

In the current work the value of  $n'$  was initially obtained from the stabilised values of  $\sigma_a$  and  $\epsilon_p$  in each of the fatigue tests, ie, multiple specimen tests. The calculated results for the eight steels are shown in table (8). In quantitative terms, it can be seen that the high carbon steels have high  $n'$  values, the high silicon steels

possess low values for  $n'$  and the high manganese steels have average values. Therefore, it follows that high carbon steels should have a low Coffin/Manson exponent (less -ve) and a high Basquin exponent (more -ve) whereas high silicon steels should be the reverse. This hypothesis can generally be supported with the present results. Manganese, which has a very small effect on  $n'$ , also has a small effect on the Coffin/Manson and Basquin exponents.

### 4.3. Fatigue Parameter - Mechanical Property Relationships

#### 4.3.1. Experimental Design

The fatigue parameters obtained in the previous section for eight C/Si/Mn steels are also utilised in this section. For comparison, monotonic and cyclic data are used which were obtained from simple tension and I.S. tests on the same eight steels. The details of these tests have been given in previous sections.

#### 4.3.2. Results and Discussion

##### 4.3.2.1. Monotonic Test Results

###### (i) Reproducibility Assessment

At the outset of the testing programme it was decided to check the reproducibility of the testing technique. This was achieved by carrying out a series of identical tests on two steels from the main programme. The results of this assessment are summarised in table (9), where it can be seen that only a low level of dispersion in the test results was obtained. This was considered satisfactory and the main test programme was therefore carried out with the knowledge that little experimental "error" should accrue.

###### (ii) Results from Main Test Programme

The common properties from the tensile tests are shown in table (10). The strain hardening parameter quoted was obtained from the central

portion of the plots relating log plastic strain and log stress. It was found that this relationship was not linear for any of the steels over the complete plastic strain range and in fact could best be described as a combination of three straight lines. Fig.38 is a typical example. The work hardening rate of the second stage (denoted by the suffix II) was considered the most satisfactory in practical terms. In general the test results obtained (except those for  $n_{II}$ ), showed that the eight steels had widely varying mechanical properties. The effect of composition and microstructure on these properties will be discussed later.

#### 4.3.2.2. Cyclic Test Results

##### (i) Reproducibility Checks

Before the main test programme commenced, it was also decided to check the reproducibility of the I.S. test technique. Two of the steels were subjected to repeat tests and the results of this exercise are shown in table (11). It can again be seen that excellent reproducibility was obtained.

##### (ii) Cyclic Stress-Strain Data

From the I.S. tests and the fatigue tests (multiple specimen tests) reported in the previous section, a linear relationship between the logarithm of plastic strain and applied stress was obtained for each steel. Therefore an expression of the type proposed by Ramberg-Osgood can be used to describe this relationship. The results from both tests are shown in table (12).

The values of the work hardening parameters ( $n'$  and  $K'$ ) obtained by the two methods were similar with the results from the multiple specimen tests being slightly lower. However, the differences found were not considered to be significant.

The results quoted in table (12) also indicate the effects of compositional variations. In qualitative terms an increase in carbon content caused all the cyclic parameters to increase, whereas increasing the silicon and manganese levels only produced an increase in the strength parameters ( $K'$  and  $\sigma_y'$ ). Silicon had a dramatic effect on the cyclic strain hardening exponent  $n'$  with higher levels producing low values.

#### 4.3.2.3. Fatigue - Mechanical Property Relationships

##### (i) Relationship Between $\sigma_f$ and $\sigma_f'$

Several workers have suggested that the fatigue strength coefficient is related to the monotonic fracture stress. The basis of this proposition is that the intercept on the ordinate of a stress-life plot (ie, one reversal) is equivalent to a monotonic test. Many empirical equations have been reported in the literature which support this hypothesis (22,166,167,168), and multiplication factors of between 0.92 and 1.15 have been proposed for making  $\sigma_f$  equal to  $\sigma_f'$ . The closeness of these factors both to themselves and to unity indicate that the proposal is reasonable for many materials.

The comparison of  $\sigma_f$  and  $\sigma_f'$  obtained in the current work is shown in table (14) and graphically illustrated in fig.40. It can be seen that the  $\sigma_f$  values are higher than the corresponding  $\sigma_f'$  values for the high silicon steels whereas they are lower in the low silicon steels. The slope of the two lines in the figure are very similar but not equal to unity; the perfect correlation situation. This indicates that another variable must also be affecting the correlation. It can be seen from table (14) that this variable is the carbon content; in the high carbon steels,  $\sigma_f$  is usually greater than  $\sigma_f'$ .

A consideration of the way in which these two parameters are obtained suggests that they can only be equal if the Basquin exponent is a constant at all stress levels. However, the constancy of "b" cannot be established at high stress levels due to testing difficulties, ie, specimen buckling. Indirect methods of assessment therefore have to be utilised. It has already been shown that "b" is related to the cyclic strain hardening exponent,  $n'$  (22). Therefore, if  $n'$  varies with stress or strain amplitude, then "b" will vary and hence the intercept on the stress-reversals plot ordinate will also change.

It has also been shown in this work that the monotonic strain hardening rate is not a constant for ferrite-pearlite steels. In fact the graphs obtained for log stress and log plastic strain are best represented by three separate relationships. Similarly, some recent work published by Clayton (169) indicates that  $n'$  also varies at strain levels above 0.015 (the usual maximum of I.S. test). A cyclic stress-strain relationship of this type will therefore result in a complex correlation between stress amplitude and reversals to failure. A diagrammatic illustration of the relationship envisaged is shown in fig.39. In this case the monotonic fracture stress is equivalent to  $\sigma_f'$ . However, this parameter could be higher or lower than the conventionally computed  $\sigma_f'$ , being dependent on the complete cyclic strain hardening characteristics of the material.

The fact that increasing carbon and silicon have the opposite effect on both the  $\sigma_f/\sigma_f'$  correlation and on  $n'$  strongly suggests that this hypothesis is valid. In terms of the accuracy in predicting fatigue life curves, substituting  $\sigma_f'$  by  $\sigma_f$  will have only a minor effect for most of the steels in this study. A material dependency has been found in some steels and therefore, the correlation between the two parameters must be known before the substitution is used.

(ii) Relationships Between  $\epsilon_f$  and  $\epsilon_f'$

It has also been proposed that the monotonic true fracture strain is equal to the fatigue ductility coefficient, using the same arguments previously discussed for the strength parameters. To assess this hypothesis a plot of  $\epsilon_f$  against  $\epsilon_f'$ , has been constructed for the eight steels tested in this section, fig.41. It can be seen that a reasonable correlation exists between the two parameters; the monotonic true fracture strain has a slight tendency to over-estimate the fatigue ductility coefficient for high silicon steels but is equivalent for the low silicon steels. The slight inaccuracy in the high silicon steels may again be due to a non-linearity in the plastic strain-life relationship, (Coffin/Manson), caused by variations in  $n'$  at very high strain levels.

(iii) The Relationship Between b, c and  $n'$

The derivation of the Morrow equations relating these three parameters has been outlined in the previous section. It should be noted however, that the relationship between stress amplitude and total plastic strain energy to fracture is material dependent. Morrow found the slope of this line was approximately equal to  $-\frac{1}{4}$ , for SAE 4340 steel but values ranging from  $-\frac{1}{3}$  to  $-\frac{1}{8}$  have been quoted by some workers (23,170) for other materials and therefore the relationships between b,  $n'$  and c will vary.

The results of the current work are shown in tables (15) and (16). In table (15), the results of a linear regression analysis between the stress amplitude and the total plastic strain energy to fracture is shown. It can be seen that the slopes for most of the steels are in the range -0.30 to -0.39. Only the low carbon, high silicon steels have values below that found by Morrow for SAE4340 steel (22). The

average slope for the eight steels is  $-0.30$  and this can be used to obtain the following relationships for the steels studied in this work:-

$$c = \frac{-1}{1 + 4.3 n'} \qquad b = \frac{-n'}{1 + 4.3 n'}$$

Comparisons of the measured and calculated values of the two fatigue exponents, using both the Morrow equations and those derived in the current work are shown in table (16). Both equations can be seen to give reasonably accurate predictions with the empirical equation applicable to the present work being slightly better than the Morrow predictions. The largest errors, found in the low carbon high silicon steels, are due to the use of a single factor to represent all the materials.

(iv) Relationship Between the Cyclic Yield Stress and Fatigue Limit

Several investigators have suggested that the cyclic yield stress ( $\sigma_y'$ ) is equivalent to the fatigue limit of a material (22,32). The major argument supporting this proposal is that fatigue cannot occur without cyclic plasticity and the cyclic yield stress represents this limit. Values of  $\sigma_y'$  which were obtained from the X-Y plots from the I.S. tests are shown in table (12) and a plot of the two parameters has been drawn, fig.42. It can be seen that the fatigue limit is consistently slightly higher than the cyclic yield stress. This observation has been made by other workers (32,171). Mason, for example has shown that a transition zone exists between the elastic and plastic strain portion of a stress-strain curve that contains both anelastic and plastic strain components (172). The anelastic strains are a form of energy conversion associated with cyclic atomic diffusion and internal friction. Feltner and Morrow (32) have proposed that these anelastic strains are non-damaging in a fatigue sense and therefore the fatigue limit must be greater than the cyclic yield stress. The current work supports this view.

#### 4.4. Fatigue Parameter - Material Relationships

##### 4.4.1. Experimental Design

It has been shown previously that the fatigue behaviour of ferrite-pearlite steels can be described by the Coffin/Manson and Basquin laws. The four fatigue parameters derived from these relationships, are all that is required to define a materials fatigue characteristics. Additionally, it has been shown that properties obtained from either the monotonic test or the I.S. test are equivalent or similar to these fatigue parameters. Because the properties from these two tests are relatively easy to obtain, it was decided to base the work in this section on obtaining relationships between them and the metallurgical variables. A project was initiated in which five independent variables (carbon, silicon, manganese, austenitising temperature and isothermal transformation temperature) were each fixed at three, equally separated levels, table (17). A  $\frac{1}{3}$ rd fraction factorial experiment was created which required 81 monotonic and incremental step tests to be carried out. The details of the 81 conditions associated with these tests are shown in table (18). To meet the requirements of the design, 27 different material compositions were necessary. These compositions have previously been shown in table (1).

##### 4.4.2. Results

Monotonic and I.S. tests were carried out on all 27 steels in each of the three heat treated conditions. The testing techniques adopted and the method of data analysis for each test, have been described previously. Following the tests, a representative test specimen for each "experimental condition" was sectioned and prepared for microscopical examination. Quantitative metallography was then carried out on these specimens.

The results of the quantitative microscopy and the mechanical tests are combined in table (19). It can be seen from the results that a wide range of microstructures were produced in the steels, (ferrite content varied from zero to about 65%). These results can best be understood by considering the relationships between the independent variables and microstructure in more detail.

#### 4.4.2.1. Microstructural Considerations

The effect of increasing the carbon content of a steel is well known, i.e., the carbide and hence pearlite content is increased. As the volume fraction of pearlite increases, the microscopic size parameter associated with the "free" ferrite ( $d_{\alpha}$  in this work) decreases.

Additions of manganese cause the volume fraction of pearlite to increase due to its effect on the eutectoid composition; it reduces the level of carbon required to produce a fully pearlitic structure. In addition, the time required to complete the pearlite reaction increases with increasing manganese content, and therefore the interlamellar spacing also increases (173). The remaining elemental variable, silicon, produces a solid solution with ferrite and therefore the microstructure is unaffected.

Increasing the austenitising temperature has the initial effect of increasing the prior austenite grain size which in turn increases both the ferrite grain size and the interlamellar spacing. Cahn and Hagel (174) have shown that this is due to an increase in transformation time as the prior austenite grain size is increased and the growth rate is decreased, according to the equation:-

$$T = 0.5d_{\gamma}/G \quad (40)$$

where  $T$  = time to complete transformation  
 $d_\gamma$  = prior austenite grain size  
 $G$  = Growth rate of transformed product

The equation assumes that the rate of nucleation of the transformed product is not significant in the overall reaction time. Experimental results have validated this assumption by showing that transformation at the grain boundaries (the nucleation sites) occurs within the first few percent of the overall transformation time.

Raising the level of the other heat treatment variable (isothermal transformation temperature), increases the volume fraction of proeutectoid ferrite for a given carbon content and also increases the transformation time. This latter effect produces an increase in the ferrite grain size and the interlamellar spacing of the pearlite.

By adopting the shorthand method used by Feltner and Beardmore (175), the net effects of all the variables can be summarised as follows:-

$C \uparrow$  ,  $f_a \downarrow$  ,  $f_p \uparrow$  ,  $d_a \downarrow$  ,  $S^0 \leftrightarrow$  ,  $\bar{\lambda} \downarrow$

$Mn \uparrow$  ,  $f_a \downarrow$  ,  $f_p \uparrow$  ,  $d_a \leftrightarrow$  ,  $S^0 \uparrow$  ,  $\bar{\lambda} \downarrow$

$Si \uparrow$  , no microstructural change

$\gamma_{temp} \uparrow$  ,  $f_a \leftrightarrow$  ,  $f_p \leftrightarrow$  ,  $d_a \uparrow$  ,  $S^0 \uparrow$  ,  $\bar{\lambda} \uparrow$

I.T.T.  $\uparrow$  ,  $f_a \uparrow$  ,  $f_p \downarrow$  ,  $d_a \uparrow$  ,  $S^0 \uparrow$  ,  $\bar{\lambda} \uparrow$

In general, the anticipated microstructural characteristics of each steel, based on the above discussion, were borne out by the quantitative microscopy results shown in table (19). The anomolous results are probably due to either inaccuracies in the isothermal transformation heat treatments or microsegregation effects.

#### 4.4.2.2. Metallurgical Variables - Mechanical Property Relationships

In order to develop these relationships, the computer based "analysis of variants" programme, which has been described previously, was used. The relationships between metallurgical variables and fatigue related parameters were of major concern, but in addition some of the more common mechanical properties were evaluated. The programme used in the current work considered each composition factor in its linear form and also as the squared function. The significance of second order interactions (for example; C.Si, C.Si<sup>2</sup> or C.Si<sup>2</sup>) was also assessed.

##### i) Composition and Heat Treatment Effects

The results of this analysis indicated that the linear function of the composition variables had the greatest significance. Figs.43-45 are typical graphical examples that support this assessment because reasonable linear relationships exist between the elements and the mechanical properties. The computed regression equations obtained for the important mechanical properties are shown below:-

$$\begin{aligned}\sigma_y \text{ (N/mm}^2\text{)} &= 70 + 327(\%C) + 85(\%Si) + 83(\%Mn) && \left[ 82.7\% \right] \\ \sigma_{y'} \text{ (N/mm}^2\text{)} &= 104 + 53.5(\%C) + 61.4(\%Si) + 33.5(\%Mn) && \left[ 69.0\% \right] \\ \sigma_u \text{ (N/mm}^2\text{)} &= 241 + 621 (\%C) + 115(\%Si) + 75 (\%Mn) && \left[ 91.0\% \right] \\ \sigma_f \text{ (N/mm}^2\text{)} &= 542 + 557 (\%C) + 149(\%Si) + 132 (\%Mn) && \left[ 78.3\% \right] \\ \\ \epsilon_f &= 1.22 - 1.01(\%C) && \left[ 76.4\% \right] \\ \\ n' &= 0.148 + 0.148(\%C) - 0.035(\%Si) && \left[ 88.3\% \right]\end{aligned}$$

The figure in square brackets at the end of each equation is the degree of variation in the data that is explained by the equation. Fig.46 gives an indication of the equation accuracy. Actual and predicted values of the cyclic yield stress, for which the prediction equation represented only 69% of the variability in the data is shown. Although considerable scatter is present in this plot a definite relationship is

apparent. In metallurgical terms this level of scatter is common (153-157).

It can be seen from the equations that all the strength parameters are increased by additions of carbon, silicon and manganese. However, the heat treatment variables were not found to be significant. This latter result is probably due to the few unexpected microstructures that were produced.

(ii) Microstructural Effects

The carbon content in these steels is related to the dispersion hardening caused by cementite particles. This effect can be assessed quantitatively if a microstructural parameter which reflects the interbarrier spacing (important in dispersion strengthening) is substituted for the carbon content.

In order to produce structure-property relationships applicable to all the steels studied, a single microstructural parameter was required. Because deformation in mixed ferrite-pearlite structures is largely confined to the ferrite phase, the mean ferrite path was considered the most appropriate parameter to use. This was calculated by substituting several measurements obtained from the microstructure of the steels, into equation (25), ie,

$$\bar{\lambda}_a = f_a \cdot d_a + 0.87 f_p S^\circ$$

The computed values of this parameter were then transformed into the two following forms in the regression analysis:-

- |      |                          |                              |
|------|--------------------------|------------------------------|
| (i)  | $\log \bar{\lambda}_a$   | .... Gensamer and co-workers |
| (ii) | $\bar{\lambda}_a^{-1/2}$ | .... Hall/Petch              |

The following equations were obtained from this analysis:-

$$\begin{aligned}
 \sigma_y \text{ (N/mm}^2\text{)} &= 256 - 93.2(\log \bar{\lambda}_a) + 81.2(\%Si) + 55(\%Mn) && [72.6\%] \\
 \sigma_y \text{ (N/mm}^2\text{)} &= 151 + 88.2(\bar{\lambda}_a^{-1/2}) + 83.4(\%Si) + 52(\%Mn) && [75.0\%] \\
 \\
 \sigma_{y'} \text{ (N/mm}^2\text{)} &= 135 - 14.2(\log \bar{\lambda}_a) + 61 (\%Si) + 29(\%Mn) && [68.0\%] \\
 \sigma_{y'} \text{ (N/mm}^2\text{)} &= 117 + 15.2(\bar{\lambda}_a^{-1/2}) + 61 (\%Si) + 28(\%Mn) && [68.0\%] \\
 \\
 \sigma_u \text{ (N/mm}^2\text{)} &= 595 - 179 (\log \bar{\lambda}_a) + 112(\%Si) + 61(\%Mn) && [77.0\%] \\
 \sigma_u \text{ (N/mm}^2\text{)} &= 394 + 168 (\bar{\lambda}_a^{-1/2}) + 114(\%Si) + 60(\%Mn) && [76.0\%] \\
 \\
 \sigma_f \text{ (N/mm}^2\text{)} &= 862 - 184 (\log \bar{\lambda}_a) + 143(\%Si) + 76(\%Mn) && [78.0\%] \\
 \sigma_f \text{ (N/mm}^2\text{)} &= 662 + 167 (\bar{\lambda}_a^{-1/2}) + 147(\%Si) + 72(\%Mn) && [78.0\%] \\
 \\
 \epsilon_f &= 0.65 + 0.23 (\log \bar{\lambda}_a) && [57.0\%] \\
 \epsilon_f &= 0.91 - 0.22 (\bar{\lambda}_a^{-1/2}) && [61.0\%] \\
 \\
 n' &= 0.232 - 0.042(\log \bar{\lambda}_a) - 0.37(\%Si) - 0.017(\%Mn) && [78.0\%] \\
 n' &= 0.185 + 0.040(\bar{\lambda}_a^{-1/2}) - 0.036(\%Si) - 0.019(\%Mn) && [80.0\%]
 \end{aligned}$$

It can be seen in these results that the coefficients associated with the two forms of the mean ferrite path are very similar. This was not surprising because the two transformations considered reduce the overall range of  $\bar{\lambda}_a$  values by about the same amount. Therefore the slopes of correlations with mechanical properties are similar. However, because the individual values are transformed by different amounts, the equation constant (intercept) will vary for each case.

The similarity in the overall range of the transformed  $\bar{\lambda}_a$  values, also means that the variability in the correlations will be similar. This can be seen from the result for each equation shown in square brackets. Therefore, the postulations of Gensamer and Hall/Petch are in essence very similar, although in metallurgical terms the latter is more satisfactory.

#### 4.4.3. Discussion

The results presented in this section show how composition and microstructure relate to some important mechanical properties. There are different aspects to what is meant by this latter term. In this work the strength and ductility of a material subjected to cyclic loads are of prime interest. However, through the correlations between cyclic and monotonic fracture strength and ductility, the monotonic fracture properties are also considered important.

##### a) Monotonic Properties

Strength properties can be subdivided into two types; those related to flow and those to fracture. Both are functions of numerous variables in addition to composition and microstructure (strain, strain rate and temperature, for example). In the current work these latter variables were held constant so that the effects of metallurgical variables could be assessed.

In steels, the resistance to initial flow is complicated by the presence of interstitial elements (C and N), which are associated with a high monotonic yield stress (upper yield point) and a sudden reduction in stress immediately yield has occurred. Cottrell's theory (176), postulates that dislocations are "locked" by the interstitial atoms that segregate to positions around dislocations made favourable by the lattice distortion. The upper yield point reflects the shear stress required to tear a dislocation away from its "atmosphere". On reaching this stress level numerous dislocations are released into the slip planes which allows deformation to occur momentarily at a very low stress. In ferrite-pearlite steels the dislocations pile-up at microstructural barriers producing microscopic back stresses on the glide planes. A higher stress is then required to produce further deformation. This point, which is equivalent to the lower yield stress, is obviously

influenced by the ability of dislocations to move through the ferrite. This in turn will be dependent on the solute atoms in the ferrite phase and on the interbarrier spacing which is influenced by the ferrite grain size and the separation of cementite particles.

The equation for the monotonic lower yield stress ( $\sigma_y$ ) shows that dispersion hardening has the biggest effect on this property. Carbon content and mean ferrite path, which combines the ferrite content and grain size with the cementite content and interparticle spacing, reflect this effect. However, the solid solution strengthening effects due to silicon and manganese are also significant.

Further increases in load result in permanent plastic deformation. In steels, the early stages of plasticity is also unusual in that it often occurs in strain bursts with little associated increase in macroscopic stress, (Lüders extension). The mechanism responsible for this behaviour is related to a local increase in stress at the tip of an array of piled-up dislocations. This stress concentration, combined with the applied stress in an adjacent grain, unlock the dislocations in that grain. Repetitions of this behaviour lead to the propagation of a Lüders band through the specimen. Several bands or strain bursts usually occur before a macroscopic increase in stress is observed.

This latter point is characterised by homogeneous deformation throughout the specimen.

The low strain, work hardening rate ( $n_1$  in table (13)) is very low in each steel studied. This result probably indicates that initial plasticity occurred by a Lüders band mechanism. This feature is also illustrated by the flat stress-strain curves shown in figs.47-54. It is also evident that increasing the silicon content of the steel results in a lower work hardening rate in this region. In fact, in some of the high silicon steels virtually no work hardening occurs in the early stages of plasticity.

The effect of alloying elements on the low strain, monotonic work hardening characteristics of iron based materials has not been systematically studied. Therefore in order to comment on this behaviour, the current work is considered in association with indirect observations found in the literature. In this region of the true stress-true strain curve, the work hardening characteristics of a material are dependent on two main factors:-

(i) The degree to which dislocations interact with each other or with microstructural barriers, and

(ii) The degree and ease of dispersion or propagation of deformation throughout the material.

The rate of work hardening will be high if dislocation interaction is extensive but will be low in polycrystalline materials that exhibit homogenous deformation. This is because each new part of the material that becomes active will initially have a low work hardening rate due to the low initial dislocation density in undeformed material.

Ferrite, having a high stacking fault energy, cross-slips readily on many planes (110), (112) and (113) and deformation is characterised by wavy slip markings in the most favourably oriented surface grains. Specimen extension in this stage is by a Lüders band mechanism. When carbon is alloyed with iron to produce pearlite, the work hardening rate in the early stages do not alter very much (compare  $n_T$  values for low and high carbon steels in table (13)). However, the extent of the Lüders extension is reduced (compare figs.49 and 50 with figs.53 and 54 respectively). This indicates that homogeneous deformation is reached more quickly in pearlite than in ferrite. This is a result of two effects:-

(i) The ferrite content in a pearlitic steel, in which virtually all the strain occurs, is lower than in a ferritic steel.

(ii) The cementite particles act as a source for dislocation generation. Burns and Pickering (177) have observed that many dislocations are generated from ferrite-cementite interfaces during the monotonic deformation of pearlite.

Additions of silicon to iron reduces the stacking fault energy, restricting slip to the (110) planes. Cross-slip becomes difficult at high silicon concentrations and deformation is characterised by planar slip markings at the surface of the metal. McEvily and Johnston have reported that in iron-silicon irons this type of slip leads to a greater dispersion of deformation throughout the specimen (68). Feltner and Beardmore (175) have gone further in stating that "in general the weight of evidence indicates that in single phase materials, alloying with substitutional atoms to achieve a more planar slip character will produce a more homogeneous slip distribution". Therefore, the observed decrease in  $n_I$  as the concentration of silicon in ferrite is increased, can be explained by the greater distribution of deformation in this material compared with pure ferrite.

The effect of manganese additions in steels is to raise the volume fraction of pearlite and to produce a solid solution with the ferrite component of the microstructure. From the previous discussion, it can be deduced that these material variations will have only a small effect on the low strain work hardening characteristics of the metal.

The other strength properties quoted in this work,  $\sigma_U$  and  $\sigma_f$ , are also dependent on the work hardening characteristics of the steels. In these cases, the work hardening rate at higher strains ( $n_{II}$  and  $n_{III}$ ) are relevant. The results of table (13) indicate that  $n_{II}$  values are considerably higher than the corresponding  $n_I$  values. The major reason for this effect can be deduced by comparing the regression equations for  $\sigma_y$  and  $\sigma_U$ . It can be seen that the regression coefficient for

carbon related parameters in the case of  $\sigma_U$ , are approximately twice those for  $\sigma_Y$ . This indicates that the dispersion of cementite in ferrite has a dominant effect on  $n_{II}$ . This is probably due to the restricted dislocation mobility caused by the proximity of cementite lamellae. Burns and Pickering's observations are again pertinent to this behaviour.

The high strain work hardening rate,  $n_{III}$ , tends to be lower than  $n_{II}$ . In the regression equations this change is reflected in a lower coefficient for carbon (and related parameters) in the expressions for  $\sigma_f$  compared with  $\sigma_u$ . Again the  $\sigma_f$  coefficients for silicon and manganese are similar to those obtained for  $\sigma_U$ . This indicates that a dispersed second phase has the greatest effect on dislocation mobility even at very high strains.

#### b) Cyclic Properties

An interesting feature of the results is the much reduced effect of the second phase particles when the yield stress is obtained under cyclic loading ( $\sigma_y'$ ). The equations quantify the descriptive hypothesis given in the literature review, ie, plastic deformation under cyclic loading is aided by,

- i) back stresses caused by dislocation pile-ups at second phase particles, and
- ii) a relatively low dislocation density which is maintained during cycling by annihilation of the oppositely signed screw dislocations that are produced from a sessile source.

However, the solid solution hardening effect is still apparent under cyclic loading; the coefficients for silicon are virtually unchanged. With manganese the coefficients for cyclic properties are down but it should be noted that manganese additionally influences the volume fraction of the cementite particles.

The series of regression equations also include those for the cyclic strain hardening exponent,  $n'$ . The results are quantitative representations of the observations made in the first part of the section, ie, increasing carbon content causes  $n'$  to increase whereas additions of silicon have the opposite effect. This behaviour is probably associated with a material's capacity for reversible slip which in turn is influenced by the inherent flexibility of dislocation movement. In high stacking fault energy materials (unalloyed ferrite for example) a high flexibility in dislocation mobility, allied with the complex dislocation pattern produced during cycling, results in a low level of dislocation reversibility when the loading direction is changed. When cementite particles are present in unalloyed ferrite the dislocation structures produced are even more complex and the degree of dislocation reversibility will be reduced. This results in a higher  $n'$  value. However, when silicon is present in ferrite the movement of dislocations is changed considerably. Slip is confined to the (110) planes and planar slip results. This type of deformation behaviour leads to more homogeneous slip and also to a higher potential for dislocation reversibility. In cyclic tests this is characterised by homogeneous, low notch-peak surface deformation and a low cyclic strain hardening exponent.

Additions of manganese increase the volume fraction of cementite in addition to entering into solid solution in ferrite. In terms of the cyclic strain hardening exponent, these two characteristics will tend to cancel each other out and therefore variations in manganese do not affect the value of  $n'$ .

### c) Ductility Parameters

Finally, the ductility parameter considered to be important in this work,  $\epsilon_f$ , was found to be affected significantly by the cementite content and spacing only. This result is related to the localised nature of deformation that occurs in materials containing hard particles in a soft matrix. If microscopic strain gradients are large, as can be expected in ferrite containing cementite particles, then deformation will be concentrated in the softer phase. In order to maintain continuity in the material, many dislocations are necessary at the particle/matrix interface. (This has been predicted by Ashby (85).and also observed by Burns and Pickering (177)). Therefore, such interfaces are vulnerable to debonding, and hence materials containing hard particles in a soft matrix will have a lower fracture ductility than the matrix material. For a given overall strain in a specimen, the degree of deformation in the soft matrix will increase as the volume fraction of the second phase increases. Therefore, the fracture ductility will be reduced correspondingly.

Elements in solid solution in the ferrite will play little or no part in the debonding - fracture mechanism. It can be anticipated therefore that such elements will not affect the monotonic fracture ductility.

### d) Prediction of Fatigue Curves

The regression equations produced in this section have also been used to predict fatigue or equivalent fatigue parameters, table (20). The two suffixes associated with the parameters (pc and pm) in this table, indicate the predicted values using (a) the equation containing just the elemental variables (pc) and (b) those calculated from the equation containing the microstructural parameter (pm). One method of assessing these predictions is to compare constructed fatigue life curves

with actual fatigue test data. Fig.55 shows this comparison for casts 40 and 74 on a strain-life basis whereas fig.56 shows the same comparison in terms of stress-life. For the predicted curves, the fatigue limits were evaluated using calculated values of the cyclic yield stress,  $\sigma_y'$ , and then adding  $20 \text{ N/mm}^2$  in accordance with the discrepancy previously established (see fig.42).

The results for the strain-life curve were fairly typical in that an excellent correlation was found between the actual and predicted values. However, the inferior results shown in fig.56 indicates the strong influence of the intercept  $\sigma_f'$  on the predicted stress-life curve. It is clear from the results that the regression equations do not accurately predict the values of  $\sigma_f'$ . This problem is not due to the poor regression equation but the uncertain correlation between the monotonic fracture stress and the fatigue strength coefficient. This point has been discussed in a previous section.

## 5. CHARACTERISTICS OF FATIGUE DAMAGE AND FRACTURE IN C/Si/Mn STEELS

### 5.1. Introduction

The aim of the work in this section was to produce qualitative information on the nature of crack initiation and propagation in ferrite-pearlite steels. It should be noted that this was not a major objective of the project and therefore an extensive, systematic approach was not adopted. In essence, the fracture faces of some of the longer life specimens from each material were examined in a scanning electron microscope (SEM). The characteristic features of both stage I and stage II crack growth were studied. In addition, surface fatigue damage was observed on specimens from other tests in which the cycling was occasionally interrupted to allow the specimen to be examined. For this work the gauge length of the specimens was electropolished prior to testing, using the following solution at a temperature of 20° C :-

Glacial acetic acid	133 ml
Chromium trioxide	25 ml
Water	7 ml

Electropolishing was carried out for 30 minutes using a bath voltage of 20.5 volts.

In order to assess the notch-peak topography developed on the electropolished surfaces, a taper-section technique was occasionally employed which gave a 5:1 magnification in a perpendicular direction to the surface.

### 5.2. Surface Damage and Microcracks

The initial fatigue damage was observed after only a small fraction of the specimen life in all the materials examined. Fine surface markings developed quickly in some areas and then the affected areas grew in size and number as the test proceeded. In the steels containing a high ferrite content, the surface damage was initially confined to the

ferrite grains. Fig.57 shows the familiar surface slip bands that developed; in this case from cast 40 which has more than 60% of ferrite in the microstructure. The height of the peaks was relatively small (typically 2  $\mu\text{m}$ ) and microcracks were often associated with the slip bands. These can be clearly seen in fig.57b. A further characteristic of these high ferrite steels, including those with 2% silicon, was that the slip markings had a wavy appearance.

The initial fatigue damage in the lamellar pearlite structures occurred preferentially in those colonies in which the cementite plates were oriented at approximately  $45^\circ$  to the applied stress axis. As the tests progressed the surface area showing damage increased markedly.

The observations of surface damage made on the high ferrite steels were similar to those reported by other workers (66,67,113). Surface damage develops locally in shallow slip bands and microcracks often form in one favourably oriented grain before any appreciable damage is created in adjacent grains. Evidence of extrusion formation was not found in the steels examined and therefore it is possible that the microcracks developed by a slip band mechanism similar to that proposed by Neumann (114). In addition the observation of wavy slip characteristics in the high silicon steels supports the work of Boettner and McEvily (67) and indicates that a silicon content in excess of 2% is required in order to completely restrict slip to the (110) planes. However, because increasing silicon clearly had a marked effect on the fatigue properties of the steels studied, some constraint on the available slip systems must have occurred. This apparent anomaly is probably due to the limited and qualitative assessment of slip marking "waviness" made in the work.

The surface deformation characteristics found in the pearlitic steels were similar to previous observations made by Taylor (84) and by the

author (178). Decohesion of the favourably oriented ferrite-cementite interfaces initially occurs, due probably to dislocation generation from these interfaces. The pertinent observations of Burns and Pickering (177) and the theory of Ashby (85) have already been discussed in this respect.

### 5.3. Stage I Fracture Characteristics

The actual initiation point of a fatigue crack is usually very difficult to find when examining fracture faces. However, this feature, together with the stage I cracks was observed in several high ferrite containing steels. The best example found is that shown in figs.58 and 59. The specimen, from cast 07, had two initiation points as can be seen in fig.58a, which were characterised by a number of similar features:-

1. The surface of the cracks was very smooth compared to the stage II cracks.
2. The stage I cracks formed at an angle of between  $30^{\circ}$  and  $60^{\circ}$  to the direction of the applied load. This was assessed by tilting the specimen in the S.E.M. and noting the angle between the specimen surface and the stage I crack.
3. Non-metallic inclusions were associated with the stage I cracks.  
(These are indicated by the small arrows in figs.58b and 59b).

Similar characteristics were usually observed on other specimens which contained a clearly delineated stage I crack. However, in the fully pearlitic steels, the initiation point was less clear and no definite stage I cracks were observed.

The results for the steels containing appreciable ferrite content clearly show the influence of non-metallic inclusions in generating the major microcracks from which the stage II cracks ultimately developed. This is despite the fact that these steels were vacuum melted and

contained a very low density of small inclusions. The inclusions associated with the stage I cracks for example, were only 10 to 15  $\mu\text{m}$  long, and about 5  $\mu\text{m}$  in diameter.

The observations made by Lankford (94) which were discussed previously, are obviously pertinent to this finding, ie, debonding of inclusions was probably responsible for the formation of the stage I cracks in the ferritic steels. The angle of the cracks was associated with the maximum shear stress and the crystallography of the grains in the critical location, whereas their smooth surface can be attributed to the initially slow crack growth through the material in this region.

Specimens from the pearlitic steels did not contain stage I cracks and evidence on which to postulate a crack initiation mechanism was not obtained from these studies. However, the previously reported observations made on the specimen surface, indicate that debonding of the ferrite/cementite interface is probably the dominant factor. It is suggested that the closeness of the carbide lamellae prevents the formation of an observable stage I crack.

#### 5.4. Stage II Fracture Characteristics

The general appearance of the stage II fractures at low magnifications was very similar for all the steels tested. Typical photographs, shown in figs.60 and 61, are for the high ferrite steel (cast 34) and the fully pearlitic steel (cast 36) respectively. The main feature of the fractures was the multitude of steps, which could often be classified as one or other of two major types:-

- a) Major irregular shaped steps that lie in planes almost parallel to the direction of crack growth (bottom to top in the photographs shown). Examples of this feature, which can be classified as "brittle striations" are marked by "A" in figs.60 and 61.

- b) Numerous irregular shaped steps, located between the brittle striations, which were often oriented at approximately  $45^{\circ}$  to the direction of crack growth.

Viewing the fractures at higher magnifications revealed only one major difference between the steel types. The steels containing appreciable ferrite had very fine striations in some of the ferritic areas. An example is shown in fig.62 which is from cast 07. In the lower left hand quarter of this photograph the markings produced by the crack penetrating a circular shaped pearlite colony can be seen. Adjacent to this colony is a ferritic region which contains fine striations. It should be noted that even in steels containing more than 60% ferrite, the striations were always difficult to observe in the S.E.M., and considerably less than 60% of the fracture surface contained the markings.

In the fully pearlitic steels and in the pearlite colonies of the ferritic steels, no fatigue striations were observed over the entire fracture surface. Fig.63 is a good example of the fracture characteristics in pearlite; in this case from steel 74 tested at a strain amplitude of 0.003 ( $N_f \approx 10^5$ ). The different orientations of the cementite lamellae can be seen to have had a marked effect on the surface topography. On the right hand side of the photograph the cementite plates are almost in the same plane as the growing crack, whereas in many regions on the left hand side, the plates are perpendicular to the crack. Also visible in this photograph are several secondary cracks which appear to have developed at growth faults in the pearlite colonies. A better example of secondary cracking, in this case along the ferrite-cementite interfaces, is shown in fig.64a and b. This form of crack was a very common feature on all the fractures examined at relatively long crack lengths. A better way to assess the influence of cementite lamellae on the fracture surface topography, was

to view the fractures after etching in 2% Nital. Figs.65 and 66 are examples of this technique. It can be seen that the orientation of the cementite plates in each colony has caused the crack to propagate in a different direction.

From the observations made, a mechanism of fatigue crack growth in ferrite-pearlite steels can be postulated:-

Cementite lamellae have a strong influence on the fracture characteristics even in steels containing large volume fractions of ferrite. The numerous secondary steps at approximately  $45^{\circ}$  to the growth direction are "macroscopic" indications of their effect. It is probable that debonding of the favourably oriented ferrite/ cementite interfaces occurs as the crack front approaches a pearlite colony. A "bridge" containing undamaged material can remain between adjacent pearlite colonies that have incurred fatigue damage (debonding). These bridges eventually fracture to produce the brittle striations running parallel with the crack front. Fig.67 is a diagrammatic representation of this hypothesis. It is suggested therefore that a mechanism similar to that proposed by Forsyth and Ryder (134) applies to pearlitic steels. They envisaged small cleavage cracks developing ahead of the crack front which was followed by the necking down and fracture of the ligament of material separating the two, as the local stress increased.

The limited number of "classical" striations in the high ferrite steels, also suggests that cracking of the pearlite regions may have a strong influence on the crack growth mechanism in these materials. It is proposed that debonding ahead of the crack tip is again favoured in the pearlite colonies. Crack penetration through the ferrite grains can be both rapid and extensive being affected by the relative position of adjacent pearlite colonies. Thus, not all ferrite grains exhibit surface markings.

## 6. FATIGUE RESISTANCE OF C/Si/Mn STEELS IN VARIABLE LOAD ENVIRONMENTS

### 6.1. Introduction

An important feature of the development of fatigue resistant components is the ability to predict their life and hence anticipate potential problems. This requirement necessitates the understanding of material behaviour when subjected to variable amplitude loads, as most service loading conditions are of this type. In the literature review, the important information required for an accurate prediction of fatigue life was outlined. In recent years this information has been gathered together and computer based fatigue life prediction programmes which incorporate these features, have been produced.

The Society of Automotive Engineers has organised an extensive programme of work aimed at evaluating the accuracy of some of these programmes, and in general many of the results obtained were encouraging (ref.179 contains several papers on the subject). The aim of the work reported in this section is to use some of the data and variable amplitude load signals incorporated in the SAE work in order to assess the characteristics of a prediction programme (180,181) and also to consider the influence of metallurgical parameters in variable load environments.

### 6.2. The SAE Test Programme

The test programme designed by SAE included three different types of service strain-time histories selected from over thirty such records submitted by committee members. The three histories can be briefly described as follows:-

#### (i) Suspension history

This history was obtained from a vehicle-suspension component which was driven over an accelerated durability course. The signal consisted of random inputs from the road surface superimposed on less frequent inputs from the vehicle manoeuvres. In general a compressive mean load was present in the majority of the cycles.

(ii) Bracket history

This history was produced from a load carrying bracket attached to the side of a road vehicle. Most cycles had a zero mean load.

(iii) Transmission history

This history was characterised by a changing mean load. It was obtained from the transmission torque measured on a tractor engaged in front-end loader work.

The three histories were considered to be typical for the ground vehicle industry and sufficiently different to be useful in this exercise of checking the accuracy of fatigue life prediction programmes. A sample of each loading history is shown in fig.68.

An extensive test programme was carried out by several of the participating American laboratories. The main features were as follows:-

- (a) Variable amplitude fatigue tests on centre notch specimens of the type shown in fig.69, using the selected random histories as input to the test specimens. The test series utilised two materials (MAN-TEN and RQC-100) and crack initiation life, crack propagation life and life to failure were monitored.
- (b) Constant amplitude fatigue tests on the same specimen type and in the same materials.
- (c) Monotonic and cyclic tests on the two materials to obtain the basic mechanical property data required in many of the prediction programmes.

During the last few years many workers have used this data to assess their own fatigue life prediction techniques. In the current study the prediction programme outlined in (180) and (181) is first assessed using the SAE data and subsequently, the response of C/Si/Mn steels to variable load histories is evaluated.

### 6.3. The Life Prediction Programme

#### 6.3.1. Description

A random history (usually strain or load-time) is processed by the programme on a reversal by reversal basis. Initially, the nominal signal is subjected to a cycle counting routine (Rainflow) which reduces the measured history into a series of cycles and half cycles consistent with material behaviour. Also incorporated in the rainflow algorithm is a "material memory" feature. The output from the rainflow routine is next converted to the local condition by taking account of the geometric concentrating effects in the component being studied. This is achieved using Neubers rule (8). In order to achieve this objective the cyclic stress-strain relationship of the component material is used and it is assumed that the material obeys Masing's hypothesis (21).

For each reversal or cycle, the parameter ( $\sigma_{\max} \epsilon_f$ ) (40) is next calculated in the following way:-

- (i) For each stress range identified by cycle counting, the  $\Delta\sigma \Delta\epsilon_f$  product is calculated from,

$$\Delta\sigma \Delta\epsilon_f = K_f^2 \Delta S^2 / E \quad (41)$$

- (ii) For the calculated  $\Delta\sigma \Delta\epsilon_f$  value, the unique values of  $\sigma_a$  and  $\epsilon_f$  are obtained from a pre-calculated table of results produced using the cyclic stress-strain curve and Masing's description of the hysteresis loop shape.
- (iii)  $\sigma_{\max}$  is then calculated by reference to the previous relevant turning point followed by the  $\sigma_{\max} \epsilon_f$  parameter.

Finally, the fatigue damage ( $1/N_f$ ) resulting from each reversal or cycle is assessed and accumulated. To obtain the fatigue curve for this assessment the four fatigue parameters ( $\sigma_f'$ ,  $\epsilon_f'$ , c and b) are fed into the computer and the following equation is used:-

$$(\sigma_{\max} \epsilon_f E)^{1/2} = \left[ (\sigma_f')^2 (2N_f)^{2b} + E \sigma_f' \epsilon_f' (2N_f)^{b+c} \right]^{1/2} \quad (42)$$

Miners rule is adopted in order to define failure of the component, i.e. failure is assumed when the accumulated damage value reaches unity.

### 6.3.2. Evaluation of the Programme

The basic material properties for Man-Ten and RQC-100 steel are shown in table (21). For the SAE exercise, Man-Ten was used in the as-rolled condition and had a pearlitic microstructure whereas RQC-100 had been quenched and tempered to produce a bainitic structure. The results of the life predictions and a comparison with the test data is shown in tables (22) and (23). Figure 70 is a typical graphical representation of some of the data, in this case for Man-Ten steel subjected to the suspension history. For this material the life predictions fell between the initiation line and the total failure line. This is exactly the desired result as the programme intends to predict the life to develop a short crack and hence includes initiation life and part of the crack growth life.

The predictions for the RQC-100 steel however, were generally below the lower bound crack initiation line for all the histories. There was therefore a consistency in the "error". Due to the complex nature of the prediction programme, it is difficult to assess the source of this error. The possibilities are the failure of Neubers rule, Miners rule or the material model created for this material.

Although fine tuning of the programme is obviously still required, the fact that consistent results are obtained indicates that it can be used for material comparison purposes, providing that the major characteristics of each material ("Masing" and material memory behaviour) are similar.

### 6.3.3. Evaluation of the Masing Hypothesis for C/Si/Mn Steels

In order to evaluate the accuracy of the Masing hypothesis for predicting hysteresis loop shapes in C/Si/Mn steels the X-Y outputs obtained during the I.S. tests were utilised. For each of the steels studied, the 5th, 10th and 15th loops ( $\epsilon_a$  of 0.005, 0.010 and 0.015 respectively) were replotted with a common zero and for comparison the Masing modified cyclic stress-strain curve was incorporated into the plot. All the steels revealed similar characteristics; as the strain range increased the curve was raised vertically on the plot. A typical example is shown in fig.71, which represent the results for cast 40.

Morrow first noticed this effect in OFHC Copper (22) and he attributed it to a variation in the cyclic strain hardening exponent ( $n'$ ) as the loop size was increased. Jhansale, however (19), considered that the work hardening parameters were constant and in fact it was the hysteresis loop yield stress that varied when the strain range was increased. He proposed a new parameter (Yield range increment) which is influenced by strain range and which must be used in the Ramberg-Osgood expression in order to improve the relationship between plastic strain and stress amplitude. For example,

$$\epsilon_p = \left( \frac{\sigma_a - \delta\sigma_y'}{K'} \right)^{1/n'} \quad (43)$$

where  $\delta\sigma_y' =$  Yield range increment.

These two theories were evaluated in the current work by using the data from cast 40. First, the work hardening parameters were calculated assuming a constant value for the hysteresis loop yield stress (Morrow). The results obtained for the three loops of varying strain range from the I.S. tests supported Morrow's observations that as strain range is increased both  $n'$  and  $K'$  are decreased, table (24). Secondly, Jhansale's proposal for a varying hysteresis loop yield stress was

adopted, and a relationship between this parameter and strain range was produced, fig.72. Incorporating this data with the co-ordinates of the hysteresis loop data from the same three I.S. test loops as before, the work hardening parameters were calculated. In this case both  $n'$  and  $K'$  were found to be constant. The results from the two exercises can be compared in table (24).

From metallurgical considerations, the theory of Jhansale is more acceptable. The hysteresis loop yield stress can be regarded as a measure of the resistance of a material to the onset of macroscopic plastic deformation at the beginning of each strain reversal. It will almost certainly be strain history dependent therefore, because it will be affected by the number of free dislocations on the glide planes. An increasing number of dislocations will be trapped as the applied strain is increased due to the type of dislocation structures produced; the range of structures will vary from small isolated clusters at low strains, to the complete cellular networks typical of very high strains. Thus, there will be a greater resistance to macroscopic dislocation movement with this latter type of structure, and hence the hysteresis loop yield stress will be higher.

Variations in hysteresis loop yield stress for C/Si/Mn steels were found to be approximately  $100 \text{ N/mm}^2$ , for a strain range of up to 0.03 (see fig.73). If ignored, a serious error may result in the predicted fatigue lives. The effect is complex as it is material and sequence dependent, and therefore the final outcome is difficult to estimate. In essence the fatigue damage parameter will often be incorrectly computed as the signal is processed. It can be too high (more damaging) or too low (less damaging), compared to the true value, depending on the signal characteristics. Because of the uncertainty involved it is recommended that future life prediction programmes should account for this effect.

The additional information required is simply the relationship between hysteresis loop yield stress (or yield range increment) and applied strain range.

Following the assessment of the life prediction programme several conclusions have emerged:-

- (i) The programme can produce accurate predictions for some materials and strain histories. The results for Man-Ten steel are particularly good.
- (ii) Prediction errors can result which are material dependent.
- (iii) C/Si/Mn steels all exhibit non-Masing behaviour but the variation in hysteresis loop yield stress with applied strain range is similar. Therefore, the programme can be used in a material comparison exercise, even though the actual predictions may be slightly inaccurate.

#### 6.4. A Comparison of C/Si/Mn Steels Subjected to Variable Load Histories

##### 6.4.1. Procedure

The comparison was achieved by obtaining a life prediction for each steel when subjected to various levels of the SAE histories. The relevant mechanical properties were fed into the computer on request together with the load history. The life prediction for each set condition was then printed out within a few seconds. Fig.74 represents the input and output of the programme for just one of the case studies.

The first list of questions in this figure is for creating the material model and for modification of the basic load history. The mechanical properties of interest ( $E$ ,  $K'$  and  $n'$ ), are used to "construct" a cyclic stress-strain curve from the following relationship:-

$$\epsilon_f = \sigma_a/E + \left( \frac{\sigma_a}{K'} \right)^{1/n'} \quad (44)$$

The computed curve is then separated into a variable number of short straight lines for subsequent analysis to find the strain corresponding to the next stress-range in the signal. In the example shown, 200 model elements were selected to represent the curve.

The SAE histories used in this work were produced as nominal load histories. However, the life prediction programme operates on stress and therefore conversion was required. This was achieved by using a calibration factor based on an elastic analysis of the notched specimen used in the SAE programme produced by Landgraf et al (179). They showed that the nominal stress at the notch root (S) was related to the applied load (P) by:-

$$S \text{ (N/mm}^2\text{)} = 11.25.P \text{ (kN)} \quad (45)$$

Thus, to calculate the calibration factor for producing the maximum absolute stress corresponding to the maximum load, this equation was used. For example, a common test load was 71.2 kN, which converts to a stress of 800 N/mm<sup>2</sup>. Now, the maximum load in each variable amplitude signal had been normalised to a value of 999, therefore the calibration factor for each applied input history is 800 divided by 999 which is 0.7995.

The next question to answer is associated with the use of Neubers rule for converting nominal to local stress. The stress concentration factor for the notched specimen under consideration has been assessed by several workers and the mean value was found to be 3.0. This value was therefore used in the current work. The second list of questions, fig.74b is to establish the fatigue-life curve for subsequent estimation of damage from every cycle and reversal. The four fatigue parameters and the fatigue limit are substituted into the equation representing the fatigue-life curve for this purpose.

The third series of questions is required for identifying the history to be used in the analysis (SAESRE in example is the suspension history). These histories are all stored in digital form on five megabyte hard discs.

#### 6.4.2. Life Prediction Results

Life predictions were made using each of the three service histories at four different maximum stress levels (800, 450, 230 and 125 N/mm<sup>2</sup>). Each steel was considered therefore, for a total of twelve "history/stress level" conditions. The predicted lives, which were produced as blocks of the signal, are illustrated graphically in figs.75-77 and from these results several interesting features were noted:-

- (i) The difference between steels increases as the magnitude of the signal stress is reduced, ie, in the high cycle region.
- (ii) High strength steels generally have a better fatigue resistance.
- (iii) Some cross-overs occur in the curves (particularly with the high silicon steels) indicating that material superiority can be stress dependent.
- (iv) The anticipated signal dependency of the predicted life was observed. When the life in blocks was converted to cycles, the suspension history was found to be much less damaging than either the bracket or transmission histories which tended to be similar. This is probably a reflection of the generally compressive mean stress in the suspension signal.

The effect of metallurgical variables on variable amplitude fatigue life can also be assessed quantitatively from this data. Table (25) shows the predicted lives in cycles ( $N_p$ ) for variations in composition, stress level and signal. A multiple regression analysis was carried out on this data to establish the influence of the elements carbon, silicon and manganese on fatigue life and the following results were obtained:-

(i) For suspension history

(a) Maximum absolute stress =  $800 \text{ N/mm}^2$

$$\text{Log life (Nf.10}^3) = 1.37 + 0.791 (\% \text{ C}) + 0.171 (\% \text{ Mn})$$

(b) Maximum absolute stress =  $450 \text{ N/mm}^2$

$$\text{Log life (Nf.10}^3) = 2.11 + 1.17 (\% \text{ C}) + 0.297 (\% \text{ Mn}) + 0.121 (\% \text{ Si})$$

(c) Maximum absolute stress =  $230 \text{ N/mm}^2$

$$\text{Log life (Nf.10}^3) = 3.07 + 1.50 (\% \text{ C}) + 0.717 (\% \text{ Mn}) + 0.614 (\% \text{ Si})$$

(ii) For Bracket history

(a) Maximum absolute stress =  $800 \text{ N/mm}^2$

$$\text{Log life (Nf.10}^3) = 0.516 + 0.561 (\% \text{ C}) + 0.118 (\% \text{ Mn}) - 0.053 (\% \text{ Si})$$

(b) Maximum absolute stress =  $450 \text{ N/mm}^2$

$$\text{Log life (Nf.10}^3) = 1.17 + 0.87 (\% \text{ C}) + 0.242 (\% \text{ Mn}) + 0.077 (\% \text{ Si})$$

(c) Maximum absolute stress =  $230 \text{ N/mm}^2$

$$\text{Log life (Nf.10}^3) = 2.14 + 1.11 (\% \text{ C}) + 0.557 (\% \text{ Mn}) + 0.467 (\% \text{ Si})$$

(iii) For Transmission history

(a) Maximum absolute stress =  $800 \text{ N/mm}^2$

$$\text{Log life (Nf.10}^3) = 0.852 + 0.382 (\% \text{ C}) + 0.112 (\% \text{ Mn}) - 0.049 (\% \text{ Si})$$

(b) Maximum absolute stress =  $450 \text{ N/mm}^2$

$$\text{Log life (Nf.10}^3) = 1.53 + 0.64 (\% \text{ C}) + 0.216 (\% \text{ Mn}) + 0.043 (\% \text{ Si})$$

(c) Maximum absolute stress =  $230 \text{ N/mm}^2$

$$\text{Log life (Nf.10}^3) = 2.52 + 0.722 (\% \text{ C}) + 0.458 (\% \text{ Mn}) + 0.371 (\% \text{ Si})$$

In all cases the equations represent at least 96% of the observed variation.

#### 6.4.3. Discussion

The equations indicate that the magnitude of the "alloy effect" is dependent on the maximum absolute stress level in the signal and on some other signal characteristic. This point is illustrated graphically in

fig.78, which is a plot of the regression coefficients associated with each of the elements, and the maximum stress in the signal. It can be seen that iron containing carbon and/or manganese has better fatigue properties than pure iron for all the stress conditions considered. However, the degree of improvement increases as the stress level in the signal is reduced. With carbon this effect is almost linear whereas with manganese much greater benefit is obtained if the maximum stress in the signal is below  $450 \text{ N/mm}^2$ .

Silicon additions to iron do not necessarily produce an improvement in the fatigue properties. In fact, if the service stresses are high, the fatigue behaviour of an iron/silicon alloy may be slightly inferior to that of pure iron. However, when the service stresses are low (below  $400 \text{ N/mm}^2$ ) increasing the level of silicon will result in a substantial benefit.

It is also apparent from fig.78, that alloying effects are influenced by the type of signal; the benefits always being greater with the suspension history followed next by the signal from the bracket. The main differences between these signals are mean stress and loading sequence. For example, the suspension history has very different mean stress characteristics compared to the other two and therefore the longer predicted lives (in cycles) with this history indicates the important role played by this parameter. In fact, the differences in life between the suspension history and the other two is greater than the differences found between the others. Thus, it can be concluded that mean stress effects are greater than loading sequence effects; the major difference between the bracket and transmission histories.

The apparent relationship between the "alloying effect" and signal characteristics is only a reflection of the type of fatigue life curve

used in the prediction programme. This can best be understood by considering compositional variations in relation to this curve, ie, the  $\sigma_{\max} \cdot \epsilon_f$  - life curve. From the equation that describes the curve (No.42), it can be seen that the two intercepts are  $\sigma_f' \cdot \epsilon_f'$  and  $(\sigma_f')^2$ , whereas the corresponding slopes are  $(b + c)$  and  $2b$  respectively. By adopting the shorthand system used previously, an assessment of the effect of compositional changes on this curve can be quickly achieved:-

(i) Effect of increasing carbon

$$C \uparrow, \sigma_f' \uparrow, \epsilon_f' \downarrow, \sigma_f' \epsilon_f' \leftrightarrow, (\sigma_f')^2 \uparrow, n' \uparrow, c \text{ less } \text{-ve}, b \text{ more } \text{-ve}, b+c \text{ less } \text{-ve}, 2b \text{ more } \text{-ve}$$

In the low cycle region, the intercept is unaltered in higher carbon steels but the slope of the line is less negative and thus a benefit in life accrues. In the high cycle region, the increase in the intercept value resulting from increases in carbon content, are offset to some extent by the change in the slope. The net effect however, is still beneficial.

(ii) Effect of increasing manganese

$$Mn \uparrow, \sigma_f' \uparrow, \epsilon_f' \leftrightarrow, \sigma_f' \epsilon_f' \uparrow, (\sigma_f')^2 \uparrow, n' \leftrightarrow, c \leftrightarrow, b \leftrightarrow, b+c \leftrightarrow, 2b \leftrightarrow$$

Additions of manganese only affects the two intercepts which in both cases attain higher values. Hence, increasing the weight percentage of this element is generally beneficial to fatigue life.

(iii) Effect of increasing silicon

$$Si, \sigma_f' \uparrow, \epsilon_f' \downarrow, \sigma_f' \epsilon_f' \downarrow, (\sigma_f')^2 \uparrow, n' \uparrow, c \text{ more } \text{-ve}, b \text{ less } \text{-ve}, b+c \text{ more } \text{-ve}, 2b \text{ less } \text{-ve}$$

In the low cycle region, the higher level of the intercept is devalued by the detrimental change to the slope; little overall effect results. However, in the high cycle region the variation in intercept and slope are both beneficial and therefore the degree of improvement brought about by this element increases rapidly as the stress level in the signal is reduced.

The metallurgical aspects associated with this fatigue behaviour have been discussed in a previous section. The reasons for the increases in the "strength" parameters and the changes in work hardening characteristics of the steels have been outlined.

## 7. CONCLUDING REMARKS

The main interest in fatigue from an engineering viewpoint, lies in the successful prediction of component life under different service conditions. The potential use of fatigue analysis in design has received increased attention in the last few years. At British Railways, as in several other major organisations, a serious attempt is currently being made to improve the efficiency of material usage whilst at the same time maintaining a high level of component safety. The local stress-strain approach to life prediction, which considers the material response to cyclic, variable amplitude loading, forms the basis of this attempt.

The progress towards computer aided design which includes a fatigue analysis is inevitably slow. However, at the present time the analytical life prediction procedure previously discussed is being assessed by British Rail. This is in a number of service failure investigations. For example, when studying certain problem components, a model of the service failure is initially set up in the computer. This includes a sample of the actual service strain history and the relevant properties of the material. An assessment of changes to the model variables (service environment or material properties) can then be made in the computer. Thus, the optimum solution to the problem can be quickly established.

Modelling of service failures in this way is obviously very useful. The most effective and efficient method of improvement can be selected with confidence. In addition it also allows a very realistic assessment of the value of material changes. There is no doubt that some problems cannot be solved by using a different material. Whilst metallurgically this is not a very satisfactory finding, it does prevent the wasteful attempts at material solutions based on the non-realistic fatigue assessments used previously.

In the current work some of the major characteristics of the life prediction programme that are associated with material behaviour, have been assessed. A range of C/Si/Mn steels, which encompass many railway products, has been used for this purpose. Conversely, the fatigue life prediction procedure has been used to evaluate the significance of material variables in variable amplitude fatigue situations, ie, composition and microstructure.

The life prediction programme used, requires an accurate knowledge of a material's response to constant amplitude cyclic loads. The major inputs are the relationships between stress and strain under cyclic loading and between the number of load reversals and life. The former is required for creating the model of material response to cyclic loads, whereas the latter forms the basis of the fatigue damage summation routine.

The relationship between stress and strain that is used in the programme is obtained after cyclic stabilisation of the material. It has been shown in this work that the cyclic stress-strain properties of C/Si/Mn steels are very different to those produced by monotonically loading virgin material. The major differences are in the yield stress and the work hardening characteristics at low strains (up to 0.015). For example, the monotonic yield stress was found to be always higher than the cyclic yield stress. The major reason for this observation is associated with the cementite phase in the microstructure. Under monotonic loading cementite particles act as barriers to dislocation motion. They therefore cause dislocation pile-ups which in turn produce long range back stresses on the glide planes. These reduce the ability of a dislocation source to generate new dislocations. Hence the stress to produce monotonic yielding is increased as the cementite volume fraction is increased or the interparticle spacing decreased. However,

when a material undergoes a load reversal, the mobility of dislocations is increased due to the supplementary back stresses on the glide planes and to a reduction in the dislocation density caused by annihilation of screw dislocations. Thus, the cyclic yield stress is lower than the monotonic yield stress.

The substitutional elements silicon and to some extent manganese, do not appear to influence this mechanism. The regression coefficients associated with the yield stress parameters  $\sigma_y$  and  $\sigma_y'$  show silicon to have the same effect on each whereas under cyclic loading the effect of manganese is only slightly reduced. This latter observation can be attributed to the increased volume fraction of pearlite that results from an increase in manganese content, ie, the strength contribution of manganese is only partially due to solid solution strengthening.

After yielding, the material behaviour under cyclic loading is also initially different to that observed in monotonic tests. In the latter case this region is characterised by a very flat curve representing a low work hardening rate (Lüders extension), whereas in the former a smoother, steeper curve is observed. Hence it appears that low strain cyclic deformation in ferrite-pearlite steels is more uniform than the irregular and intermittent deformation which characterises monotonic loading.

The effect of composition and microstructural variables on the cyclic strain hardening behaviour of ferrite-pearlite steels is substantial. The major effects can again be attributed to the different mechanisms produced by a dispersed phase and by substitutional elements. Dislocation interactions in ferrite are increased as the cementite volume fraction is increased and hence the strain hardening rate is also increased.

Conversely, as the level of a substitutional element is raised the ability

of dislocations to cross-slip is reduced (lower stacking fault energy) which results in greater reversibility of dislocation movement on the glide planes, ie, planar slip is more reversible than wavy slip. It is proposed that this effect leads to a lower strain hardening rate in planar slip materials. Thus, in the steels used in this investigation increasing carbon content produces an increase in  $n'$ , increasing silicon reduces  $n'$  and increasing manganese has little effect because it contributes to both mechanisms.

Another feature of the material model used in the life prediction programme is the assumed shape of the hysteresis loops. This is required for calculating the stress produced by each strain reversal in a variable amplitude strain history. A common assumption that is used is that the hysteresis loop shape is simply the cyclic stress-strain curve multiplied by the factor two (Masing hypothesis). However, this assumption has been shown to be invalid for C/Si/Mn steels because the hysteresis loop yield stress is dependent on prior history. It is recommended therefore that future life prediction programmes should take these observations into account.

The calculation of fatigue damage that accrues from each strain reversal in a variable amplitude signal, requires a fatigue-life curve. The one used in this work employs a combined stress-strain parameter which is able to cope with mean stress variations. This type of curve can be constructed accurately using four parameters which have recently been termed fatigue properties. They are the intercept and slope of the two straight lines which are obtained from plotting log plastic strain against log cycles (Coffin/Manson) and log stress against log cycles (Basquin). This situation has been simplified still further by the relationships proposed by Morrow between the slopes of these lines and the cyclic strain hardening exponent, and because the two intercepts are equivalent in many materials

to the monotonic fracture stress and strain. It is possible therefore to construct a fatigue curve from the results of just two tests; a monotonic test and an incremental step test.

In this work all of these concepts have been evaluated for C/Si/Mn steels. It has been found that the Coffin/Manson and Basquin relationships are obeyed. The Morrow relationships between the cyclic strain hardening exponent and the Coffin/Manson and Basquin exponents have been found to be quite good, ie, the equations that fit the current data best are very similar to Morrow's equations. The equivalence of the fatigue strength and ductility coefficients and the monotonic fracture stress and strain has also been assessed. In general, the results showed comparability. A discrepancy was found in the high silicon steels which is probably due to variability in the cyclic strain hardening exponent at high strains. Construction of fatigue curves using the four fatigue parameters has been carried out. The predictions used regression equations which related the equivalent fatigue parameters and metallurgical variables. In general adequate predictions were obtained.

All the fatigue data generated during the study indicated that additions of carbon, silicon and manganese had a beneficial effect on fatigue life in the high cycle region. However, this is much reduced in the low cycle region and it is probable that at very high strains, pure iron can resist cyclic deformation for longer than any of the alloys considered. In order to appreciate the effect of the individual elements in fatigue, the mechanisms occurring over the entire life range must be considered. In the tests carried out in this work, failure was taken as complete separation of the specimen. Therefore, the life parameter used contained a component of crack initiation and crack propagation. Over the complete life range the importance of initiation and propagation, and material strength and ductility will vary. It is now well established that in the

low cycle region of a fatigue curve, ductility and crack propagation are dominant, whereas in the high cycle region, strength and crack initiation are more important.

Additions of carbon to iron produce a dispersion of hard cementite particles in a soft ferrite matrix (pearlite). This has a marked effect on the movement of dislocations and hence on the fatigue behaviour of the steel. Cementite in ferrite reduces the fatigue ductility coefficient and also the steepness of the Coffin/Manson slope ( $c$  becomes less -ve). A schematic representation of the effect is shown in fig.79. Therefore, at ultra high strains ferrite is superior to pearlite but at strain levels of about  $\pm 2\%$  (still very much in the low cycle region) a cross-over occurs and pearlite is slightly more fatigue resistant than ferrite. At these testable strain levels pearlite has a superior resistance to crack initiation than ferrite which is probably due to two effects associated with the second phase particles.

(i) The cyclic yield stress increases with carbon content and therefore for a given strain range the level of plasticity in pearlite will be less than in ferrite.

(ii) The dispersion of second phase particles results in more homogeneous deformation.

The significance of these effects on crack initiation resistance increases in magnitude as the strain level of the test is reduced and hence they are also responsible for the superiority of pearlite over ferrite in the high cycle region of a fatigue curve.

When silicon is alloyed with iron it forms a solid solution. This reduces the mobility of dislocations due to the higher friction on the glide planes and also restricts deformation to the (110) planes reducing the ability of dislocations to cross-slip. Silicon has little effect on the

fatigue ductility coefficient but it produces a steeper Coffin/Manson slope (more -ve). Iron-silicon alloys are therefore inferior to pure iron in the low cycle fatigue region. It has been shown by several workers that the action of restricting cross-slip leads to more homogeneous deformation throughout the metal and to a greater reversibility of dislocation movement. This results in a lower cyclic strain hardening rate which has been clearly validated in this work. It will also result in a larger plastic zone size at a growing crack tip which will cause a crack to propagate at a faster rate. It is probable therefore that the inferiority of Fe-Si alloys in the low cycle region is due to a faster fatigue crack propagation rate in these materials.

In the high cycle region, strength and crack initiation resistance are important. Silicon irons have a higher cyclic yield stress compared to pure iron which is caused by a solid solution strengthening mechanism (precise details unknown). Therefore silicon irons have a better resistance to crack initiation in this region.

Manganese additions to iron (with carbon) induces two microstructural strengthening effects; dispersion and solid solution strengthening. Its effect on fatigue life therefore falls between that produced by carbon and silicon.

The fatigue life prediction programme was used to assess the influence of metallurgical parameters on variable amplitude fatigue life. In this context, quantitative data has been produced that shows the benefits to be gained from alloying. However, in a more general way the results produced have greater significance to future material development research programmes. It is clear that the performance of a material is strongly influenced by the variable load environment. Therefore, the use of empirical relationships in material selection procedures that do not consider this environment is inadequate. The often used ratio of

fatigue limit and ultimate tensile strength falls into this category.

In addition, material development programmes aimed at producing fatigue resistant materials, must also be related to realistic, dynamic loading histories.

Different material strengthening mechanisms have been assessed in this work and therefore the results can be used in the more general context of material design for fatigue resistance. In this respect, the fatigue parameter concept can again be adopted. It has been shown by many workers that the fatigue resistance of stabilising materials is dependent on several fatigue parameters, ie, the intercepts and slopes of the plastic strain and stress-life lines and the fatigue limit. In general terms, if high plastic strain resistance is required a material should have a high fatigue ductility coefficient and a fatigue ductility exponent as close as possible to zero. Similarly, for the maximum resistance to low plastic strains a high value of the fatigue strength coefficient is required in combination with a zero fatigue strength exponent (when the fatigue limit is equal to the fatigue strength coefficient). All of these parameters are influenced by the cyclic strain hardening exponent of the material,

$$\sigma_f' = K'(\epsilon_f')^{n'} \quad n' = b/c$$

Thus it can be seen that the cyclic strain hardening exponent ( $n'$ ) is the best guide to a materials fatigue resistance.

Using the now familiar shorthand method:-

For good resistance to low plastic strains

$$n' \downarrow, \sigma_f' \uparrow, b \text{ less -ve}$$

For good resistance to high plastic strains,

$$n' \uparrow, \epsilon_f' \uparrow, c \text{ less -ve}$$

Unfortunately these desirable combinations of individual properties are not often attainable. For example, if alloying is used to produce a low  $n'$  value, it will also cause a reduction of  $\sigma_f$  (unless the yield stress is increased accordingly). Similarly, modifications in microstructure that bring about an increase in  $n'$  will usually cause the fracture ductility to decrease. This is because the reduced level of dislocation reversibility, which is required to increase  $n'$ , will inevitably favour the crack formation mechanism in the material and hence reduce fracture ductility.

For the range of materials studied in this work, the solid solution effects due to silicon come closest to the ideals discussed. In the long life fatigue régime increasing silicon is beneficial because  $n'$  is reduced and  $\sigma_f'$  is increased. However, the resistance to high plastic strains is reduced due to the low  $n'$  value. Therefore, employing a steel with a high silicon content will only be useful if the service strains are known to be about the fatigue limit of the unalloyed material.

Increases in carbon is also beneficial in the long life regime due to its effect on  $\sigma_f'$ . However, the improvement is not as high as could be expected from its effect on monotonic properties due to a high  $n'$  and a large Bauschinger effect.

A different way to study fatigue resistance is to consider stress-strain hysteresis (energy approach). The fracture of a metal specimen caused by repetitive reversals of load, requires a conversion of energy. Several workers have adopted this theme in an attempt to quantify the fatigue process in terms of energy absorption. The assumption has usually been made that a constant amount of energy is required to fracture a specimen. The area of a stress-strain hysteresis loop can be taken as a measure of the energy converted in each cycle of a fatigue test. The best attempts

to quantify fatigue using this approach, have been those which relate the accumulated energy associated with plasticity in a fatigue test, and the area under a true stress - true strain monotonic curve (22,31).

An index of fatigue resistance can be obtained by considering hysteresis loop shape in combination with the mechanisms of fatigue damage. In fig.80, two fatigue resistant loop "shapes" are highlighted. Fig.80a represents a typical hysteresis loop shape that may be obtained from a commercial steel subjected to a strain range of  $\epsilon_f$ . Improved fatigue resistance can be produced by:-

(i) using a material with zero plasticity for the same strain range, fig.80b,

or (ii) using a material for which plastic deformation is not fatigue damaging. The literature review and the current work indicates that materials that do not cyclically work harden should possess these properties. Fig.80c is a diagrammatic representation of this behaviour.

The loops shown in fig.80b can be achieved in two ways. Either increase the cyclic yield stress in a material by improving the dislocation locking mechanism or develop a non stabilising material that has a very high cyclic strain hardening exponent. The dislocation locking by solute atoms and by dispersed particles was found to be similar in the ferrite-pearlite steels studied, (see the regression equation for  $\sigma_y'$  given previously). Other alloy systems however, may show that one strengthening mechanism is significantly superior to the other. It is suggested therefore that the individual effects of the strengthening procedures should be assessed in order to optimise material selection in terms of fatigue.

It is now well established that ferrite-pearlite steels cyclically stabilise very quickly. Thus, the material improvement mechanism that

relies on non-stability cannot be utilised in this range of steels. There are indications in the literature however, that face centred cubic materials are more amenable to this type of development (53,182). Certainly annealed austenitic steels and some of the aluminium alloys exhibit rapid cyclic hardening that extends right up to specimen fracture. The reason for this behaviour is related to either the ability of these materials to disperse or propagate deformation or to cyclic induced transformations. Thus, the ratio of plastic to elastic deformation decreases continuously during a test towards zero. In this case, the energy criterion for failure, ie, a critical plastic strain energy, may never be reached. Thus it can be seen that certain materials can withstand considerable plastic deformation either without forming fatigue cracks or by developing conditions that lead to non-propagating cracks.

Finally, the non-damaging plasticity case (fig.80c) is an ideal situation represented by elastic-perfectly plastic materials. In reality no such material exists but the principle of reducing the cyclic strain hardening exponent to improve fatigue resistance is valid. In this work for example, the additions of silicon to iron have been shown to improve fatigue resistance in the long life regime. In metallurgical terms this trend can be brought about by using alloying additions that restrict a material's ability to cross-slip. It is clear that planar slip is more reversible than wavy slip, which results in two fatigue related phenomena,

- (i) a shallow notch-peak topography is produced at the specimen surface,
- and (ii) the cyclic strain hardening exponent is reduced.

The ability to restrict dislocation movement to individual slip planes can only be brought about by solid solution elements. Precipitates of

hard particles in a soft matrix will not alter dislocation mobility in this respect. In fact, as shown in this work, a dispersion of cementite in ferrite will cause the cyclic strain hardening exponent to increase.

The hypotheses quoted above are both important in terms of designing fatigue resistant steels. In the past, the philosophy of alloy strengthening in steels has been based on improving the monotonic yield or ultimate tensile strength. Dispersion or precipitation hardening is particularly good for achieving these aims (see the regression equation for these two parameters). It is now suggested however, that a better parameter on which to base alloy development is the cyclic strain hardening exponent  $n'$ . This should be low in ferrite based stabilising steels, but should be as high as possible in non stabilising austenitic steels. Therefore, for maximum fatigue resistance (long life regime) the former type of steel should be strengthened by solid solution elements whereas the latter will probably be better if a precipitate is present in the matrix.

It is interesting to note that the major strengthening mechanisms employed in commercial ferritic and austenitic steels are often of the opposite type to the ones suggested in this discussion. Ferritic steels are inevitably strengthened by carbides of various type and morphology whereas many austenitic steels are preferred as single phase alloys. Future metallurgical research will hopefully reverse this trend and produce commercial materials with superior fatigue resistance than those available today.

## 8. CONCLUSIONS

1. The observations of Basquin that a linear relationship exists between log stress and log cycles to failure applies to C/Si/Mn steels.
2. The observations of Coffin and Manson that a linear relationship exists between log plastic strain and log cycles to failure applies to C/Si/Mn steels.
3. The four fatigue parameters (an expression coined by Morrow) adequately describe the constant amplitude fatigue characteristics of C/Si/Mn steels.
4. Increasing carbon content produces an increase in the fatigue strength coefficient, reduces the fatigue ductility coefficient and increases the cyclic strain hardening exponent. The latter effect causes the fatigue ductility exponent to become less negative and the fatigue strength exponent to become more negative.
5. Increasing silicon content produces an increase in the fatigue strength coefficient, has little effect on the fatigue ductility coefficient and reduces the cyclic strain hardening exponent. This leads to the fatigue ductility exponent becoming more negative and the fatigue strength exponent becoming less negative.
6. Increasing manganese content produces an increase in the fatigue strength coefficient, but has little effect on the fatigue ductility coefficient, cyclic strain hardening exponent, fatigue strength exponent or fatigue ductility exponent.
7. Ferrite volume fraction and grain size strongly influence the fatigue parameters in low carbon steels whereas interlamellar spacing is important in high carbon steels.

8. Dispersions of cementite in ferrite have a much greater effect on monotonic strength properties than on cyclic properties.
9. The increase in strength produced by the substitutional atoms of silicon and manganese in ferrite, is independent of loading type (monotonic and cyclic).
10. The relationship between the fatigue strength exponent, fatigue ductility exponent and cyclic strain hardening exponent for C/Si/Mn steels, closely agrees with Morrow's predictions.
11. C/Si/Mn steels cyclically soften at low strains but harden at high strains.
12. The fatigue ductility and strength coefficients are not necessarily equivalent to the monotonic fracture strain and stress respectively, for C/Si/Mn steels.
13. Accurate predictions of fatigue curves can be obtained by considering either compositional variables either alone or in combination with a general microstructural variable ( $\bar{\lambda}_d$ ).
14. The cyclic yield stress ( $\sigma_y'$ ) is not equivalent to the fatigue limit, being always of a lower value.
15. C/Si/Mn steels exhibit non-Masing behaviour, ie, hysteresis loop shapes are not an exact reflection of the cyclic stress-strain curve multiplied by a factor 2.
16. The hysteresis loop yield stress is a variable which is dependent on the previous strain history. The degree of variability is similar in the C/Si/Mn steels studied in this work.
17. The life prediction programme used in this work is capable of producing comparable results when applied to materials possessing similar cyclic behaviour.

18. Iron containing carbon and/or manganese has better fatigue properties than pure iron for the majority of stress conditions. The degree of improvement increases markedly as the stress level in the signal is reduced.
19. Silicon additions to iron do not necessarily produce an improvement in fatigue life. In the low cycle fatigue regime there is usually a disbenefit but in the high cycle regime a significant improvement can be expected for all service environments.
20. The magnitude of the alloying effects in terms of fatigue resistance is dependent on the strain history.
21. Mean stress effects influence variable amplitude fatigue life more than loading sequence.

## 9. RECOMMENDATIONS FOR FUTURE WORK

The future demands a closer and better relationship between the material's scientist and the engineer. Therefore metallurgical research must be strongly linked to engineering practice. In this context the following recommendations can be made:-

1. Metallurgical studies of fatigue mechanisms must be related to fatigue parameters.
2. Metallurgists must study cyclic material deformation behaviour under variable amplitude loading. This information is needed for the better modelling of materials in the computer.
3. Metallurgists should consider the energy approach to fatigue as it provides a more fundamental account of the processes involved which may lead to the elimination of the many empirical relationships currently used.
4. Material development programmes should be based on the established fatigue parameters, particularly the cyclic strain hardening exponent  $n'$ . A detailed evaluation of individual strengthening mechanisms in both body centred cubic and face centred cubic materials may lead to a new range of fatigue resistant materials.

## 10. REFERENCES

1. ROWE, G.H.  
"Models of the fatigue process".  
"Fatigue - An Interdisciplinary Approach". - Syracuse University  
Press, 1964.
2. WOHLER, A.  
"Bericht über die versuche, welche auf der Königl. Niederschlesisch -  
Markischen Eisenbahn mit apparaten zum messen der biegung und  
verdrehung von Eisenbahnwagen achsen während der fahrt,  
angestellt wurden".  
Zeitschrift für Bauwesen, Vol. 8, 1858, pp 641-652.
3. WOHLER, A.  
"Versuche zur ermittlung der auf die eisenbahnwagen - achsen  
einwirkenden kräfte und der widerstands fähigkeit der wagen - achsen".  
Zeitschrift für Bauwesen, Vol. 10, 1860, pp 583-616.
4. WOHLER, A.  
"Resultate der in der Central-Werstatt der Niederschlesisch -  
Markischen eisenbahn zu Frankfurt a.d.o. angestellten versuche  
über die relative festigkeit von eisen, stahl and Kupfer".  
Zeitschrift für Bauwesen, Vol. 16, 1866, pp 67-84.
5. WOHLER, A.  
"Ueber die festigkeits - versuche mit eisen und stahl".  
Zeitschrift für Bauwesen, Vol. 20, 1870, pp 73-106.

6. ENDO, T. and MORROW, J.  
"Cyclic stress-strain and fatigue behaviour of representative aircraft metals".  
J. Mat, J.M.L.S.A., Vol. 4, No. 1, March 1969, pp 159-175.
7. TOPPER, T.H. and BYRE GOWDA, C.V.  
"Local stress-strain approach to fatigue analysis and design".  
A.S.M.E. Conference, May 1970, "Design Engineering".
8. NEUBER, H.  
"Theory of stress concentration for shear strained prismatical bodies with arbitrary non-linear stress-strain law".  
J. Appl. Mech, Dec. 1961, pp 544-550.
9. BYRE GOWDA, C.V. and TOPPER, T.H.  
"On the relation between stress and strain concentration factors in notched members in plane stress."  
J. Appl. Mech, Trans A.S.M.E., Vol. 37, No. 1, 1970.
10. BYRE GOWDA, C.V.  
"Fatigue behaviour of notched mild steel plates in plane stress".  
PhD. Thesis, University of Waterloo, Waterloo, Ontario, Canada,  
March 1969.
11. TOPPER, T.H., WETZEL, R.M. and MORROW, J.  
"Neubers rule applied to fatigue of notched specimens".  
J. Mat, J.M.L.S.A., Vol. 14, No. 1, March 1969, pp 200-209.
12. PETERSON, R.E.  
"Stress Concentration Design Factors".  
John Wiley & Sons publication, 1953.

13. WATSON, P., and DABELL, B.J.  
"Cycle counting fatigue damage".  
S.E.E. Conference "Statistical Aspects of Fatigue Testing".  
Warwick University, Feb., 1975.
14. MATSUIISHI, M., and ENDO, T.  
"Fatigue of metals subjected to various stress".  
Paper presented to Japan Society of Mechanical Engineers,  
Fukuoka, Japan, March 1968.
15. LUDWIG, P.  
"Elemente der technologischen Mechanik".  
Springer-Verlag OHG, Berlin, 1909.
16. RAMBERG, W., and OSGOOD, W.R.  
"Description of stress-strain curves by three parameters".  
Technical Note 902, N.A.C.A., July 1943.
17. LANDGRAF, R.W., MORROW, J., and ENDO, T.  
"Determination of the cyclic stress-strain curve".  
J. Mat., Vol. 4, No. 1, 1969, p 176.
18. JHANSALE, H.R.  
"Inelastic deformation and fatigue response of spectrum loaded  
strain controlled axial and flexural members".  
Ph.D. Thesis, University of Waterloo, Waterloo, Ontario, Canada,  
March 1971.
19. JHANSALE, H.R.  
"A new parameter for the hysteretic stress-strain behaviour of  
metals".  
J. Engineering Materials and Technology, Jan. 1975, pp 33-38.

20. BAUSCHINGER, J.  
Mitt, Mech. Tech. Lab., 25, Technischen Hochschule, Munich, 1897.
21. MASING, G.  
"Eigen spannungen und Verfestigung beim messing".  
Proc. 2nd International Congress of App. Mech., Zurich, 1926,  
pp 332-335.
22. MORROW, J.  
"Cyclic plastic strain energy and fatigue of metals".  
Symposium on "Internal Friction, Damping and Cyclic Plasticity",  
A.S.T.M. S.T.P. 378, 1965, pp 45-87.
23. HALFORD, G.R., and MORROW, J.  
"Low cycle fatigue in torsion".  
Proc. A.S.T.M., Vol. 62, 1962, pp 697-707.
24. BAIRSTOW, L.  
"The elastic limits of iron and steel under cyclical variations of  
stress".  
Phil. Transactions (A), Vol. 210, 1909-1910, pp 35-55.
25. SMITH, J.H. and WEDGWOOD, G.A.  
"Stress-strain loops for steel in the cyclic state".  
J.I.S.I., Vol. XCI, No. 1, 1915, pp 365-397.
26. BASQUIN, O.H.  
"The exponential law of endurance tests".  
Proc. A.S.T.M., Vol. 10, 1910, pp 625-630.
27. HANSTOCK, R.F.  
"Damping capacity, strain hardening and fatigue".  
Proc. Phys. Soc., Vol. 59, 1947, pp 275-287.

28. MANSON, S.S.  
"Behaviour of materials under conditions of thermal stress".  
NACA report No. 1170, 1953.
29. SACHS, G., GEORGE, H., BROWN, W.F.J.  
"A survey of embrittlement and notch sensitivity of heat resisting steels".  
A.S.T.M. Spec. Tech. pub., No. 128, 1952.
30. COFFIN, L.F.  
"A study of the effects of cyclic thermal stresses on a ductile metal".  
Trans. A.S.M.E., Vol. 76, 1954, pp 931-950.
31. MARTIN, D.E.  
"An energy criterion for low cycle fatigue".  
Jnl. of Basic Engineering, Dec. 1961, p 565.
32. FELTNER, C.E., and MORROW, J.  
"Microplastic strain hysteresis energy as a criterion for fatigue fracture".  
Jnl. of Basic Engineering, Dec. 1961, pp 15-21.
33. GATTS, R.R.  
"Application of a cumulative damage concept to fatigue".  
Jnl. of Basic Engineering, Dec. 1961, pp 529-534.
34. HALFORD, G.R.  
"The energy required for fatigue".  
Jnl. of Mat., Vol. 1, part 1, March 1966, pp 3-18.

35. ESIN, A.  
"The microplastic strain energy criterion applied to fatigue".  
Trans. A.S.M.E., March 1968, pp 28-36.
36. MORROW, J.  
"Cyclic plastic strain energy and fatigue of metals".  
A.S.T.M. S.T.P. 378, 1965, pp 45-87.
37. MORROW, J.  
"Fatigue Design Handbook".  
S.A.E., New York, 1968, chapter 3.2.
38. GERBER, W.  
"Bestimmung der Zulossigene Spannugen in Eisen Constructionen".  
Z. Bay. Arch. Ing. Ver., Vol. 6, 1874, p 101.
39. GOODMAN, J.  
"Mechanics Applied to Engineering".  
Longmans, Green and Co., London, 1899.
40. SMITH, K.N., WATSON, P., and TOPPER, T.H.  
"A stress-strain function for the fatigue of metals".  
Jnl. of Mat., Vol. 5, No. 4, Dec 1970.
41. MOWBRAY, C.F., and McCONNALEE, J.E.  
"Applications of finite element stress analysis and stress-strain  
properties in determining notch fatigue specimen deformation and  
life".  
A.S.T.M., S.T.P. 519, Dec 1971, p 151.
42. MUSIOL, C., and MORTON, K.  
"Analytical approach to fatigue in disc-braked railway wheels".  
S.E.E. Conference, City University, 1977.

43. THOMPSON, N., and WADSWORTH, N.J.  
"Metal Fatigue".  
Advances in Physics, Vol. 7, 1958, pp 72-166.
44. FROST, N.E.  
"The effect of cold work on the fatigue properties of two steels".  
Metallurgia, Vol. 62, 1960, pp 85-90.
45. MOORE, H.F., and KOMMERS, J.B.  
"An investigation of the fatigue of metals".  
Engineering Experimental Station Bulletin 124, University of  
Illinois, 1921.
46. TOPPER, T.H., and SANDOR, B.I.  
"Effects of mean stress and prestrain on fatigue damage summation".  
A.S.T.M. S.T.P. 462, 1970, pp 93-104.
47. WATSON, P., and TOPPER, T.H.  
"The effect of overstrains on the fatigue behaviour of five steels".  
Presented at 1970 Fall Meeting, The Metallurgical Society of AIME,  
Cleveland, Ohio.
48. OWENS, J.P., WATSON, P., and PLUMTREE, A.  
"The effect of prestrain on the cyclic behaviour of  $\alpha$ -titanium".  
Presented at International Conference on Mechanical Behaviour of  
Materials, Kyoto, Japan, Aug. 1971.
49. WATSON, P., HODDINOTT, D.S., and NORMAN, J.P.  
"Periodic overloads and random fatigue behaviour".  
A.S.T.M. S.T.P. 519, 1973, pp 271-284.

50. PALMGREN, A.  
"Die Lebensdauer von Kugellagern".  
A.V.D.L., Vol. 68, 1924, p 339.
51. MINER, M.A.  
"Cumulative damage in fatigue".  
J. Appl. Mech., Vol. 12, 1945, p A-159.
52. BAUSCHINGER, J.  
"On the change of the elastic limit and strength of Iron and steel,  
by drawing out, by heating and cooling, and by repetition of loading".  
Minutes Proc. Inst. Civil Engineers, Vol. 87, London, 1886-87, p 463.
53. LANDGRAF, R.W.  
"The resistance of metals to cyclic deformation".  
A.S.T.M. S.T.P. 467, 1970, pp 3-36
54. JHANSALE, H.R., and TOPPER, T.H.  
"Engineering analysis of the inelastic stress response of a  
structural metal under variable cyclic strains".  
A.S.T.M. S.T.P. 519, 1973, pp 246-270.
55. WATSON, P., and TOPPER, T.H.  
"An evaluation of the fatigue performance of automotive steels".  
S.A.E. Mid-Year meeting, Montreal, June 1971.
56. ABDEL-RAOUF and PLUMTREE, A.  
"On the steady state deformation of Iron".  
Met. Trans., Vol. 2, No. 4, April 1971, p 1251.
57. JAMES, H.R., and SLEESWYK, A.W.  
"Influence of intrinsic stacking fault energy on cyclic hardening".  
Acta. Met. Vol. 26, No. 11, Nov. 1978, pp 1721-1726.

58. PLUMBRIDGE, W.J., and RYDER, D.A.  
"The metallography of fatigue".  
Metals and Materials, Vol. 3, No. 8, Aug 1969.
59. GROSSKREUTZ, J.C.  
"The mechanisms of metal fatigue".  
Phys. stat. sol. (b), Vol. 47, No. 11, 1971, pp 11-31.
60. LAIRD, C.  
"Fatigue Resistance".  
"Alloy and Microstructural Design", Edited by Tien and Ansell,  
Chapter VI, 1976.
61. FELTNER, C.E., and LAIRD, C.  
"Cyclic stress-strain response of F.C.C. metals and alloys,  
Parts I and II".  
Acta Met, Vol. 15, 1967, pp 1621 and 1633.
62. KUHLMANN - WILSDORF, D., and LAIRD, C.  
"Dislocation behaviour in fatigue".  
Material Science and Engineering, Vol. 27, 1977, pp 137-156.
63. FINNEY, J.M.  
Ph.D. Thesis, University of Pennsylvania, Philadelphia, Pa., 1974.
64. PRATT, J.E.  
"Dislocation substructure in strain cycled copper as influenced  
by temperature".  
Acta. Met, Vol. 15, 1967, p 319.
65. KREJCI, J., and LUCAS, P.  
"Dislocation substructure in fatigued - Iron single crystals".  
Phys. Stat, Sol. (a), Vol. 5, 1971, p 315.

66. FOX, P.  
"Fatigue crack initiation and propagation in plain carbon-manganese steels".  
M. Phil. Thesis, Sheffield City Polytechnic, 1969.
67. BOETTNER, R.C., and McEVILY, A.J.  
"Fatigue slip band formation in silicon-iron".  
Acta. Met, Vol. 13, No. 9, Sept 1965, pp 937-946.
68. McEVILY, A.J., and JOHNSTON, T.L.  
"The role of cross-slip in brittle fracture and fatigue".  
Proc. International Conference on Fracture, Sendai, Japan, Sept 1965.
69. MILLER, G.A.  
Ph.D. Thesis, M.I.T. 1965.
70. KLESNIL, M., HOLZANN, M., LUCAS, P., and RYS, P.  
"Some aspects of the fatigue process in low carbon steels".  
J.I.S.I., Jan. 1965, pp 47-53.
71. SUZUKI, H., and BARRETT, C.S.  
"Deformation twinning in Silver-Gold alloys".  
Acta. Met, Vol 6, 1958, p 156.
72. COTTRELL, A.H.  
"Interaction of Dislocations and Solute Atoms".  
A.S.M. publication "Relations of properties to microstructure", 1954.
73. COTTRELL, A.H., HUNTER, C.S., and NABARRO, F.R.N.  
"Electrical interaction of a Dislocation and a Solute Atom".  
Phil. Mag, 44, 1953, p 1064.

74. FRIEDEL, J.  
"Les Dislocations".  
Published by Gauthier-Villars, Paris, 1956.
75. MOTT, N.F., and NABARRO, F.R.N.  
"Dislocation theory and transient creep".  
Bristol Conference "Strength of Solids", Phys. Soc. (London),  
1948, p 1.
76. FLEISCHER, R.L.  
"Solution hardening".  
Acta. Met, Vol. 9, 1961, p 996.
77. FLEISCHER, R.L.  
"Substitutional solution hardening".  
Acta. Met, Vol. 11, 1963, p 203.
78. FISHER, J.C.  
"On the strength of solid solution alloys".  
Acta. Met, Vol 12, 1954, p 9.
79. FLINN, P.A.  
"Solute hardening of close packed solid solutions".  
Acta. Met, Vol 6, 1958, p 631.
80. BARRETT, C.S., ANSEL, G., and MEHL, R.F.  
"Slip, twinning and cleavage in iron and silicon ferrite".  
Trans. ASM., Vol. 25, 1937, pp 702-736.
81. GOLLAND, D.I., and JAMES, P.L.  
"Fatigue crack initiation and propagation in iron and iron-  
silicon alloys".  
Metal Science Journal, Vol. 4, 1970, pp 113-118.

82. JENKINS, C.H.M., and MELLOR, G.A.  
"Investigation of the behaviour of metals under deformation at high temperatures".  
J.I.S.I., Vol. 37, 1942, p 86.
83. McGRATH, J.T., and BRATINA, W.J.  
"Dislocation structures in fatigued iron-carbon alloys".  
Phil. Mag, Vol. 12, No. 120, Dec. 1965, pp 1293-1305.
84. TAYLOR, J.G.  
"Fatigue in pearlite structures".  
Ph.D. Thesis, Sheffield City Polytechnic, Oct. 1976.
85. ASHBY, M.F.  
"The deformation of plastically non-homogeneous materials".  
Phil. Mag, Vol. 21, No. 170, Feb. 1970.
86. CALABRESE, C., and LAIRD, C.  
"Cyclic stress-strain response of two phase alloys".  
Materials Science and Engineering, Vol. 13, 1974, p 141.
87. RANSOM, J.T., and MEHL, R.F.  
"The statistical nature of the fatigue properties of SAE 4340 steel forgings".  
A.S.T.M. S.T.P. 137, 1953, p 3.
88. EPREMIAN, E., and MEHL, R.F.  
"The statistical behaviour of fatigue properties and the influence of metallurgical factors".  
A.S.T.M. S.T.P. 137, 1953, p 25.

89. RANSOM, J.R.  
"The effect of inclusions on the fatigue strength of SAE 4340 steel".  
Trans. A.S.M., Vol. 46, 1954, p 1254.
90. CUMMINGS, H.N., STULEN, R., and SCHULTE, W.  
"Tentative fatigue strength reduction factors for silicate-type inclusions in high strength steels".  
Proc. A.S.T.M., Vol. 58, 1958, p 505.
91. DUCKWORTH, W.E.  
"The achievement of high fatigue strength in steels".  
Metallurgia, Vol. 69, 1964, p 53.
92. HAUSER, J.J., and WELLS, M.G.H.  
"Inclusions in high strength and bearing steels".  
"Air Force Mat. Lab. Tech. Rep. No. AFML-TR-69-339, Feb. 1970.
93. LANKFORD, J.  
"Effect of oxide inclusions on fatigue failure".  
International Metals Reviews, Sept. 1977, pp 221-228.
94. LANKFORD, J.  
"Initiation and early growth of fatigue cracks in high strength steel".  
Engineering Fracture Mechanics, Vol. 9, 1977, pp 617-624.
95. BROOKSBANK, D., and ANDREWS, K.W.  
"Stress associated with duplex oxide-sulphide inclusions in steel".  
J.I.S.I., Vol. 208, 1970, p 582.

96. BROOKSBANK, D., and ANDREWS, K.W.  
"Stress fields around inclusions and their relation to mechanical properties".  
J.I.S.I., Vol. 210, 1972, p 246.
97. THORNTON, P.A.  
"The influence of non-metallic inclusions on the mechanical properties of steel - a review".  
J. Mater. Sci., Vol. 6, 1971, pp 347.
98. KIESSLING, R.  
"Non-metallic inclusions in steel". Part III.  
The Iron and Steel Institute publication, London, 1968.
99. KIESSLING, R.  
"The influence of non-metallic inclusions on the properties of steel".  
J. Met., Vol. 21, 1969, p 48
100. KIESSLING, R., and NORDBERG, H.  
"Production and application of clean steels".  
The Iron and Steel Institute publication, London, 1972, p 179.
101. THOMPSON, N., and WADSWORTH, N.J.  
"Metal Fatigue".  
Advances in Physics, Vol. 7, 1958, p 72.
102. GROSSKREUTZ, J.C.  
"Fatigue mechanisms in the sub-creep range".  
A.S.T.M. S.T.P. 495, pp 5-60, 1971.

103. ALDEN, T.H., and BACKOFEN, W.A.  
"The formation of fatigue cracks in aluminium single crystals".  
Acta. Met, Vol. 9, 1961, p 352.
104. AVERY, D.H., and BACKOFEN, W.A.  
"Nucleation and growth of fatigue cracks".  
Proc. International conference on fracture of solids, New York, 1963.
105. GROSSKREUTZ, J.C., and BENSON, D.K.  
"The effects of the surface on the mechanical properties of  
metals".  
"Surfaces and Interfaces", Syracuse University Press, New York,  
1968, p 61.
106. HOLDEN, J.  
"Observations of cyclic structure at large ranges of plastic  
strain".  
International Conference on mechanisms in fatigue, Acta. Met,  
Vol. 11, 1963, p 639.
107. MAY, A.N.  
"A model of metal fatigue".  
Nature, Vol. 185, 1960, p 303, and Vol. 188, 1963, p 573.
108. COTTRELL, A.H., and HULL, D.  
"Extrusion and intrusion by cyclic slip in copper".  
Royal Society Discussions, Proc. Roy. Soc. A242, 1957, p 145.
109. MOTT, N.F.  
"A theory of the origin of fatigue cracks".  
Acta. Met, Vol. 6, 1958, p 195.

110. THOMPSON, N.  
"Some observations on the early stages of fatigue fracture".  
International Conference in fracture, Averbach, New York, 1959.
111. KENNEDY, A.J.  
"Possible dislocation gating mechanisms for fatigue extrusion".  
Phil. Mag., Vol. 6, No. 49, 1961.
112. WATT, D.F.  
"A mechanism for the production of intrusions and extrusions during fatigue".  
Phil. Mag., Vol. 14, No. 127, July 1966, p 87.
113. KOCANDA, A.  
"On some fatigue phenomena in steel with very low carbon content".  
Supplement to WAT Bulletin, No. 9/10, 1962.
114. NEUMANN, P.  
"Bildung und Ausbreitung von Rissen bei der Wechselverformung".  
Zeitschrift F. Metallkunde H.11, pp 780-789, 1967.
115. BROEK, D.  
"The effect of intermetallic particles on fatigue crack propagation in aluminium alloys".  
Int. Conf. on Fracture, paper 66, Brighton, 1969.
116. KERSHAW, J., and LIU, H.W.  
"Electron Fractography and fatigue crack propagation in 7075-T6 aluminium sheet".  
Syracuse University Research ITR, Aug. 1968.

117. KOCANDA, S., and KOZUBOWSKI, J.  
"On some details of the microstructure of fatigue fractures  
of PA6 aluminium alloy".  
WAT Bulletin, No. 11, pp 61-77, 1969.
118. KOCANDA, S., and KOZUBOWSKI, J.  
"Ermüdungsbrüche von Ausscheidungen in Aluminiumlegierungen".  
Zeitschrift f. Metallkunde, H.6, pp 453-456, 1974.
119. BROEK, D.  
"Some contributions of electron fractography to the theory  
of fracture".  
National Aeroplane Laboratory, NLR, Amsterdam, 1973.
120. GAUTHIER, P., DERABAUDY, H., and AUVINET, J.  
"Secondary cracking process during fatigue crack propagation".  
Engineering Fracture mechanics, Vol. 5, No. 4, pp 977-981, 1973.
121. McCLINTOCK, F.A., and PELLOUX, R.M.N.  
"Crack extension by alternating shear".  
Boeing Scientific Research Laboratories, D1-82-0708, 1968.
122. PELLOUX, R.M.N.  
"Mechanisms of formation of ductile striation".  
Trans. A.S.M., Vol. 62, 1969, pp 281-284.
123. KOCANDA, S.  
"Fatigue failure of metals".  
Published by Sijthoff and Noordhoff, 1978.
124. ZAPPFE, C.A., and WORDEN, C.  
"Fractographic registrations on fatigue".  
Trans. A.S.M., Vol. 43, 1951, pp 958-969.

125. TOKUDA, A.  
"Observations of the fatigue fracture surfaces of some carbon steels by electron microscopy".  
Trans. Journ. Japan of Metals, No. 24, 1960, pp 171-190.
126. KOCANDA, S., and KUR, J.  
"Studies of fatigue fractures with the aid of the electron microscope".  
WAT Bulletin, No. XLV, 1959, pp 63-66.
127. KOCANDA, S.  
"On microstructure of the machine elements of constructional carbon steel, fatigue resistance of materials and metal structural parts".  
Proc. Int. Conf., Warsaw 1960, Pergamon Press, Oxford/PWN, Warsaw, 1964, pp 101-111.
128. DELEIRIS, H., MENCARELLI, E., and LACQUET, P.  
"Techniques de derovillage des cassures des pieces en acier destinees a la microfractographic electronique".  
Memoirs Scient. Revue de Metallirgie, LXIII, No. 5, 1966, pp 463-472.
129. TAIRA, S., and TANAKA, K.  
"Fractography of low carbon steel in fatigue fracture".  
Journal of the Society of Materials Japan, No. 21, Feb. 1972, pp 97-103.
130. LAIRD, C., and SMITH, G.C.  
"Crack propagation in high stress fatigue".  
Phil. Mag, Vol. 7, No. 77, pp 847-857.

131. MATTING, A., and JACBY, G.  
"Die Zerrutung metallischer werkstoffe bei schwingbeanspruchung  
in der Fractographie".  
Aluminium, No. 5, 1962, pp 309-319.
132. PELLOUX, R.M.N.  
"Corrosion-fatigue crack propagation".  
Int. Conf. on Fracture, Brighton, 1969, Session V, Paper 64.
133. BOWLES, C.Q., and BROEK, D.  
"On the formation of fatigue striations".  
Int. Journ. of Fracture Mechanics, Vol. 8, No. 1, 1972, pp 75-85.
134. FORSYTH, P.J.E., and RYDER, D.A.  
"Some results of the examination of aluminium alloy specimens  
fracture surfaces".  
Metallurgia, Vol. 63, 1961, pp 117-127.
135. STYFFE, K.  
"Effect of increasing carbon on tensile properties".  
London, 1869.
136. POURCEL, A.  
"Relations of Manganese and Carbon in Iron and Steel".  
Trans. ASME, Vol. 11, 1882, p 187.
137. TURNER, T.  
"Influence of Silicon on Steels".  
Trans. Chemical Society, 1887, p 134.
138. HADFIELD, R.A.  
"On alloys of Iron and Silicon".  
J.I.S.I., 1889, pp 222-255.

139. ARNOLD, J.O.  
"Physical Influence of Elements on Iron".  
J.I.S.I., No. 1, 1894, p 107.
140. STEAD, J.E.  
"Influence of Some Elements on the Mechanical Properties of Steel".  
J.I.S.I., No. II, 1916, p 5.
141. McWILLIAM, A.  
"The Influence of Some Elements on the Tenacity of Basic Steels".  
J.I.S.I., No. II, 1918, p 43.
142. PELLISIER, G.E., HAWKES, M.F., JOHNSON, W.A., and MEHL, R.F.  
"The interlamellar spacing of pearlite".  
Trans. A.S.M. Vol. 30, 1942, pp 1049-1086.
143. GENSAMER, M., PEARSALL, E.B., PELLINI, W.S., and LOW, J.R.  
"The tensile properties of pearlite, bainite and spheroidite".  
Trans. A.S.M., Vol. 30, 1942, p 983.
144. LACY, C., and GENSAMER, M.  
"The tensile properties of alloyed ferrites".  
Trans. A.S.M. Vol. 32, 1944, p 88.
145. GENSAMER, M., PEARSALL, E.B., and SMITH, G.V.  
"The Mechanical Properties of the Isothermal Decomposition Products of Austenite".  
Trans. A.S.M. Vol. 28, 1940, p 380.
146. GENSAMER, M.  
"Strength and Ductility".  
Trans. A.S.M. Vol. 36, 1946. p 30.

147. HALL, E.O.  
"The deformation and ageing of mild steel".  
Proc. Phys. Soc., Vol. 648, 1951, p 747.
148. PETCH, N.J.  
"The cleavage strength of polycrystals".  
J.I.S.I., Vol. 174, No. II, 1953, pp 25-28.
149. ESHELBY, J.D., FRANK, F.G., and NABARRO, F.R.N.  
"The Equilibrium of Linear Arrays of Dislocations".  
Phil. Mag, Vol. 42, 1951, pp 351-364.
150. NABARRO, F.R.N., BASINSKI, Z.S., and HOLT, D.B.  
"Plasticity of Pure Single Crystals".  
Advances in Physics, Vol. 13, 1964, p 193.
151. EMBURY, J.D., and FISHER, R.M.  
"The Structure and Properties of Drawn Pearlite".  
Acta. Met, Vol. 14, 1966, p 147.
152. LANGFORD, G.  
"A Study of the Deformation of Patented Steel Wire".  
Met. Trans, Vol. 1, Feb. 1970, p 465.
153. IRVINE, K.J., and PICKERING, F.B.  
"Low Carbon Steels with Ferrite-Pearlite Structures".  
J.I.S.I., Nov. 1963, p 944
154. PICKERING, F.B., and GLADMAN, T.  
"An Investigation into Some Factors which Control the Strength  
of Carbon Steels".  
BISRA Conference on Carbon Steels, Harrogate.

155. IRVINE, K.J., PICKERING, F.B., and GLADMAN, T.  
"Grain Refined Carbon-Manganese Steels".  
J.I.S.I., Vol. 205, Feb. 1967, p 161.
156. GLADMAN, T., HOLMES, B., and PICKERING, F.B.  
"Work Hardening of Low Carbon Steels".  
J.I.S.I., Vol. 208, Feb. 1970, p 172.
157. GLADMAN, T., McIVOR, I.D., and PICKERING, F.B.  
"Some aspects of the structure-property relationships in  
high carbon ferrite-pearlite steels".  
J.I.S.I., Vol. 210, Dec. 1972, p 916.
158. ROWE, G.H.  
"Correlation of High-Cycle Fatigue Strength with True  
Stress-Strain behaviour".  
J of Materials, Vol. 1, No. 3, Sept. 1966, p 689.
159. GROZIER, J.D., and BUCHER, J.H.  
"Correlation of fatigue limit with microstructure and  
composition of ferrite-pearlite steels".  
Journal of Materials, Vol. 2, No. 2, June 1967, pp 393-407.
160. OKUBO, H., MURIKAMI, S., and HOSONO, K.  
"Microscopic Strain Distribution and Endurance Limit in Alpha-Brass".  
Journal Inst. of Metals, Vol. 91, 1962-63, pp 95-98.
161. NISHIOKA, K., and NISHIKAWA, T.  
"The Effect of Metallurgical Factors on Fatigue Strength".  
Bulletin of J.S.M.E., Vol. 16, No. 91, Jan. 1973, p 12.

162. DAVIES, O.L.  
"Statistical methods in research and production".  
Published by Oliver and Boyd, London, 1967.
163. BIRKBECK, G., and WELLS, T.C.  
"Pearlite Morphology in three low carbon steels".  
Trans. Met. Soc. AIME, Vol. 242, Oct. 1968, pp 2217-2220.
164. YAMASHITA, N.  
"The stress and strain distribution at the neck of a tensile specimen".  
Bulletin of JSME, Vol. 9, No. 36, Nov. 1966, p 637.
165. MORTON, K., REBBECK, R.G., DABELL, B.J., and WATSON, P.  
"Cyclic Material Properties and Resistance to Fatigue".  
British Rail R & DD Technical Note FM26, Feb. 1974.
166. MANSON, S.S.  
Machine Design, MADEA, June 1960, p 153.
167. MANSON, S.S., and HIRSCHBERG, M.H.  
"Fatigue an Interdisciplinary Approach".  
Syracuse University Press, 1964, p 133.
168. LANDGRAF, R.W.  
"The resistance of metals to cyclic deformation".  
A.S.T.M. S.T.P. 467, 1969, pp 3-36.
169. CLAYTON, P.  
"The wear behaviour of pearlite steels with particular reference to rails".  
PhD. Thesis, Brunel University, 1978.

170. BENHAM, P.P.  
"Torsional strain cyclic fatigue of copper at low endurance".  
Journal Inst. of Metals, Vol. 91, 1962-63, pp 404-417.
171. LAZAN, B.J.  
"Damping and resonance fatigue properties of materials  
considering elevated temperatures".  
Mechanical Behaviour of Materials at Elevated Temperature,  
McGraw-Hill, New York, 1961, pp 477-515.
172. MASON, W.P.  
"Internal friction, plastic strain and fatigue in metals and  
semi-conductors".  
A.S.T.M. S.T.P. 237, 1958, pp 36-50.
173. "Atlas of Isothermal Transformation and Cooling Transformation  
Diagrams".  
Published by the American Society for Metals, March 1977.
174. CAHN, J.W., and HAGEL, W.C.  
"Theory of the Pearlite Reaction".  
From "Decomposition of Austenite by Diffusional Processes" Edited  
by V.F. Zackay and H.I. Aaronson, New York (John Wiley and Sons),  
1962.
175. FELTNER, C.E., and BEARDMORE, P.  
"Strengthening mechanisms in fatigue".  
A.S.T.M. S.T.P. 467, 1969, pp 77-112.

176. COTTRELL, A.H.  
"Theory of dislocations".  
Progress in Metal Physics, Vol. 1 (London: Butterworths  
Scientific Publications), 1949, p 77.
177. BURNS, K.W., and PICKERING, F.B.  
"Deformation and fracture of ferrite-pearlite structures".  
J.I.S.I., Vol. 202, 1964, p 899.
178. MORTON, K.  
"Fatigue damage in pearlite".  
A.C.T. Research Report, Sheffield City Polytechnic, April 1968.
179. "Fatigue Under Complex Loading. Analyses and Experiments".  
S.A.E. Publication "Advances in Engineering", Vol. 6, 1977.
180. DABELL, B.J., and HILL, S.J.  
"The use of computers in fatigue design and development".  
Int. J. Fatigue, Jan. 1979, p 29.
181. WATSON, P., and DABELL, B.J.  
"A realistic computer-based fatigue comparison of spheroidal  
graphite cast iron and cast steel".  
Int. J. Fatigue, April 1979, p 69.
182. LANDGRAF, R.W.  
"Cyclic stress-strain response in Commercial Alloys".  
Proceedings of symposium "Work Hardening in Tension and Fatigue",  
Cincinnati, Nov. 1975, p 240.

## 11. STATEMENT OF POST GRADUATE STUDY

During the period in which the research work was carried out, a number of courses and conferences were attended. The following list outlines the main events which were related to the current work,

1. The presentation of a paper concerning the project approach at a research colloquium at Sheffield City Polytechnic.
2. The presentation of a paper entitled "Techniques for Predicting the Fatigue Performance of Materials" at SEECO 76, London.
3. The presentation of a paper entitled "The influence of Chemical Composition on the cyclic behaviour of ferrite-pearlite steels" ICF4, Waterloo University, Canada.
4. Attendance of a series of lectures at Sheffield City Polytechnic on "Quantitative Metallography".
5. Attendance of a series of lectures at Sheffield City Polytechnic on "High Strength Steels" by F.B. Pickering.

TABLE 1

CHEMICAL COMPOSITION OF EXPERIMENTAL STEELS

CAST NO.	C	Si	Mn	S	P	O <sub>2</sub>	N	Sn	Al
40	0.30	0.30	0.54	0.013	0.004	0.0005	0.001	0.005	0.005
31	0.32	0.28	1.01	0.012	0.006	0.0013	0.002	0.014	"
34	0.32	0.27	1.44	0.010	0.005	0.0011	0.001	0.005	"
28	0.30	1.20	0.54	0.011	0.003	0.0005	0.001	0.005	"
37	0.34	1.09	1.03	0.012	0.006	0.0018	0.002	0.010	"
43	0.32	1.10	1.60	0.013	0.006	0.0017	0.002	0.006	"
07	0.29	2.04	0.54	0.013	0.004	0.0010	0.001	0.005	"
48	0.32	1.83	1.02	0.011	0.003	0.0028	0.002	0.010	0.03
72	0.32	1.91	1.51	0.011	0.004	0.0010	0.002	"	"
41	0.50	0.33	0.56	0.012	0.004	0.0005	0.001	0.006	0.005
32	0.51	0.28	0.99	0.011	0.007	0.0009	0.001	0.010	"
35	0.52	0.29	1.50	0.011	0.006	0.005	0.002	0.006	"
42	0.51	1.11	0.57	0.012	0.004	0.0013	0.001	0.005	"
38	0.51	1.13	1.08	0.011	0.007	0.008	"	0.007	"
45	0.51	1.09	1.51	0.013	0.006	0.0011	"	0.007	"
70	0.50	1.84	0.52	0.013	0.003	0.0035	0.002	0.01	0.03
71	0.52	1.90	1.01	0.011	0.003	0.0018	"	"	0.02
73	0.49	1.80	1.46	0.011	0.004	0.005	"	"	"
26	0.78	0.30	0.58	0.011	0.003	0.0006	"	"	0.005
79	0.79	0.27	1.01	0.011	0.004	0.0007	"	"	0.03
36	0.71	0.29	1.51	0.013	0.007	0.0015	0.001	"	.006
44	0.74	1.07	0.59	0.012	0.004	0.0005	0.001	0.014	"
39	0.71	1.09	1.01	0.012	0.007	0.0015	0.002	0.009	"
47	0.69	1.08	1.50	0.011	0.003	0.0018	0.001	0.01	"
78	0.65	2.00	0.58	0.012	0.002	0.0007	0.002	"	0.02
75	0.68	1.83	1.03	0.012	0.003	0.002	0.01	"	0.01
74	0.70	1.86	1.49	0.013	0.006	0.0007	0.002	"	0.01

SAMPLE NUMBER	INDEPENDENT VARIABLES					
	CARBON	MANGANESE	SILICON	AUSTENITISING TEMPERATURE	ISOTHERMAL TRANSFORMATION TEMPERATURES	
1	L(0.3%)	L(0.5%)	L(0.3%)	L(850 °C)	L540 °C)	
2	L	H	L	H	H	
3	L	L	H	H	H	
4	L	H	H	L	L	
5	H	L	L	H	L	
6	H	H	L	L	H	
7	H	L	H	L	H	
8	H(0.7%)	H(1.5%)	H(2.0%)	H(1050 °C)	L(660 °C)	

L = LOW LEVEL

H = HIGH LEVEL

TABLE (2)

FACTORIAL DESIGN FOR BASIC FATIGUE PROPERTY STUDIES

CAST NO.	C	Si	Mn	S	P	Cu	O <sub>2</sub>	N	Sn	Al
40	0.30	0.30	0.54	0.013	0.004	0.04	0.0005	0.001	0.005	0.005
34	0.32	0.27	1.44	0.010	0.005	0.06	0.0011	0.001	0.005	0.005
07	0.29	2.04	0.54	0.013	0.004	0.05	0.0010	0.001	0.005	0.005
72	0.32	1.91	1.51	0.011	0.004	0.01	0.0010	0.002	0.010	0.03
26	0.78	0.30	0.58	0.011	0.003	0.01	0.0006	0.002	0.010	0.0005
36	0.71	0.29	1.51	0.013	0.007	0.06	0.0015	0.001	0.010	0.0005
78	0.65	2.00	0.58	0.012	0.002	0.01	0.0007	0.001	0.010	0.02
74	0.70	1.86	1.49	0.013	0.006	0.01	0.0007	0.002	0.010	0.01

All values are in wt %

TABLE (3)

CHEMICAL COMPOSITION OF EIGHT STEELS USED IN FATIGUE STUDIES

TABLE (4)QUANTITATIVE MICROSTRUCTURAL ANALYSIS

CAST NO.	$f_{\alpha}$	$f_p$	$d_{\alpha}$	$S^{\circ}$	$\bar{\lambda}_{\alpha}$
40	68.0	32.0	16.2	0.30	11.10
34	46.5	53.5	18.3	0.35	8.67
07	64.0	36.0	17.1	0.28	11.03
72	40.0	60.0	5.3	0.30	2.28
26	0.2	99.8	1.5	0.45	0.39
36	ZERO	100	ZERO	0.32	0.28
78	ZERO	100	ZERO	0.42	0.36
74	ZERO	100	ZERO	0.36	0.31

All length parameters are in  $\mu\text{m}$

Where:-

$f_{\alpha}$  = volume fraction of ferrite

$f_p$  = volume fraction of pearlite

$d_{\alpha}$  = ferrite grain size

$S^{\circ}$  = interlamellar spacing in pearlite

$\bar{\lambda}_{\alpha}$  = mean ferrite path in mixed structures

TABLE (5)

FATIGUE TEST RESULTS

TEST NO.	$\sigma_a$ N/mm <sup>2</sup>	$\epsilon_c$	$\epsilon_p$	$\epsilon_t$	$2N_f$
40/1	413	.00200	.01670	.0187	1084
40/2	382	.00186	.00780	.0966	3800
40/8	350	.00170	.0060	.0077	6212
40/3	314	.00153	.0034	.0049	16840
40/4	226	.00110	.0005	.0022	137600
40/5	198	.00096	.0003	.0019	245000
40/7	185	.00090	.00015	.0014	675600
40/6	171	.00083	.0001	.0009	$1 \times 10^7$
34/1	508	.00254	.0161	.0186	1060
34/2	423	.00211	.0069	.0090	4340
34/6	398	.00199	.0056	.0076	6956
34/7	370	.00185	.0035	.0053	13137
34/5	337	.00168	.0017	.0034	46920
34/4	270	.00135	.0004	.0017	632000
34/8	253	.00127	.0003	.0016	1184827
34/3	220	.00110	-	.0011	$3 \times 10^7$ R.O.
07/2	530	.00265	.0151	.0178	416
07/3	490	.00245	.0064	.0088	1780
07/6	475	.00238	.0045	.0068	3182
07/7	440	.00220	.0029	.0051	5456
07/4	420	.00210	.0018	.0039	15800
07/5	365	.00183	.0006	.0024	124700
07/8	315	.00158	-	.0016	$3 \times 10^7$ R.O.
07/1	290	.00145	-	.0014	$4.07 \times 10^7$

TABLE 2 (CONT'D)

TEST NO.	$\sigma_a$ N/mm <sup>2</sup>	$\epsilon_e$	$\epsilon_p$	$\epsilon_f$	$2N_f$
72/2	659	.00330	.0151	.0184	276
72/3	580	.00290	.0063	.0092	2592
72/9	540	.00270	.0039	.0066	7762
72/4	486	.00240	.0011	.0035	33980
72/5	410	.00205	.0005	.0027	94420
72/10	390	.00195	.0002	.0022	684351
72/6	350	.00175	-	.0017	$3.0 \times 10^7$ R.O.
72/8	330	.00165	.00005	.0016	$1.19 \times 10^7$
26/1	624	.00312	.0156	.0187	740
26/2	560	.00280	.0070	.0098	3540
26/8	495	.00248	.0048	.0073	6846
26/5	440	.00220	.0027	.0049	19200
26/3	375	.00188	.0013	.0032	64500
26/6	305	.00150	.0006	.0021	420000
26/7	262	.00131	.0003	.0017	926000
26/4	240	.00120	-	.0012	$3.0 \times 10^7$ R.O.
36/1	714	.00357	.0161	.0186	980
36/2	575	.00288	.0064	.0092	4950
36/10	535	.00268	.0043	.0070	10255
36/5	462	.00231	.0020	.0043	24700
36/4	410	.00205	.0012	.0032	93400
36/9	362	.00181	.0006	.0024	433000
36/8	353	.00177	.0005	.0023	702100
36/3	327	.00164	-	.0016	$3.0 \times 10^7$ R.O.

TABLE (5) (Cont'd)

TEST NO.	$\sigma_a$ N/mm <sup>2</sup>	$\epsilon_e$	$\epsilon_p$	$\epsilon_t$	$2N_f$
78/2	725	.00360	.0160	.0196	404
78/1	600	.00300	.0066	.0096	1980
78/6	550	.00275	.0045	.0072	4368
78/3	470	.00235	.0020	.0043	20360
78/4	412	.00206	.0010	.0031	86000
78/5	350	.00175	.0004	.0021	818000
78/7	330	.00165	-	.0017	9576300
74/1	818	.00410	.0132	.0173	428
74/2	683	.00340	.0050	.0084	2600
74/11	599	.00300	.0025	.0055	8173
74/3	536	.00270	.0010	.0037	25220
74/12	462	.00230	.0007	.0030	204675
74/5	405	.00200	.0003	.0023	320000
74/10	345	.00170	-	.0017	$3 \times 10^7$ R.O.

TABLE (6)

THE MEASURED FATIGUE PARAMETERS  
FOR EACH STEEL

CAST NO.	$\epsilon_f'$	c	$\sigma_f'$ (N/mm <sup>2</sup> )	b
40	0.95	-.58	876	-.112
34	0.83	-.57	946	-.096
07	0.75	-.63	714	-.053
72	0.53	-.59	968	-.068
26	0.51	-.53	1479	-.124
36	0.56	-.53	1436	-.107
78	0.35	-.52	1237	-.095
74	0.28	-.52	1550	-.101

TABLE (7)

THE MEASURED FATIGUE LIMIT  
OF EACH STEEL

CAST NO.	FATIGUE LIMIT	
	STRAIN	STRESS (N/mm <sup>2</sup> )
40	.00085	175
34	.0012	245
07	.0015	310
72	.0017	350
26	.0012	245
36	.0016	330
78	.0017	350
74	.00175	360

TABLE (8)

CYCLIC STRAIN HARDENING PARAMETERS  
OBTAINED FROM THE FATIGUE TESTS

CAST NO.	$n'$	$K' (N/mm^2)$
40	.160	806
34	.151	853
07	.096	785
72	.117	1088
26	.204	1638
36	.238	1915
78	.187	1467
74	.197	1834

TABLE (9)

RESULTS FROM REPRODUCIBILITY ASSESSMENT  
OF MONOTONIC TEST

Cast Number	$\sigma_y$ N/mm <sup>2</sup>	$\sigma_u$ N/mm <sup>2</sup>	$\sigma_f$ N/mm <sup>2</sup>	$\epsilon_f$	$n_{II}$	$K_{II}$
40/41	239	596	887	0.99	0.26	938
40/42	203	579	878	1.03	0.28	988
40/43	250	581	737	0.81	0.26	917
Mean	231	585	834	0.94	0.27	952
STD Deviation	24.6	9.3	84	0.11	0.014	50.2
26/21	288	849	1069	0.43	0.25	1625
26/22	212	860	1061	0.47	0.30	1721
26/23	281	833	1043	0.46	0.22	1414
26/24	223	873	1082	0.47	0.28	1680
Mean	239	854	1064	0.45	0.26	1610
STD Deviation	37.1	17.0	16.3	0.02	0.035	136

TABLE (10)

## MONOTONIC TEST RESULTS FOR EIGHT C/Si/Mn STEELS

CAST NO.	$\sigma_y$ (N/mm <sup>2</sup> )	0.2%P.S (N/mm <sup>2</sup> )	$\sigma_u$ (N/mm <sup>2</sup> )	$\sigma_f$ (N/mm <sup>2</sup> )	$\epsilon_f$	$n_{II}$	$K_{II}$ (N/mm <sup>2</sup> )
40	280	250	515	800	0.98	0.29	1130
34	410	325	580	954	0.95	0.30	1254
07	370	320	560	898	0.77	0.31	1205
72	565	485	742	1153	0.84	0.28	1551
26	460	420	741	1054	0.46	0.26	1532
36	520	500	776	1160	0.53	0.25	1579
78	450	500	937	1286	0.48	0.30	2132
74	470	505	949	1320	0.49	0.31	2254

\*  $n_{II}$  and  $K_{II}$  are strain hardening properties in stage II of  $\log \sigma_d - \log \epsilon_p$  curve.

TABLE (11)RESULTS FROM REPRODUCIBILITY ASSESSMENT  
OF INCREMENTAL STEP TEST

	$\sigma_{yc}$	$n'$	$K'$
34/30	357	0.179	1080
34/31	359	0.176	1055
34/32	356	0.175	1046
34/33	360	0.177	1067
34/34	346	0.178	1065
Mean	355	0.177	1063
STD Deviation	6.4	0.001	12.85
74/70	619	0.179	1707
74/71	627	0.180	1791
74/72	625	0.177	1704
Mean	626	0.178	1747
STD Deviation	1.41	0.002	61.5

\*  $\sigma_{yc}$  = monotonic yield stress in compression in  $N/mm^2$

TABLE (12)

CYCLIC STRESS-STRAIN DATA  
FOR THE EIGHT STEELS

CAST NO.	n' VALUES		K' VALUES		$\sigma_y'$
	I.S.T.	M.S.T.	I.S.T.	M.S.T.	I.S.T.
40	.179	.160	879	806	165
34	.165	.151	967	853	220
07	.118	.096	882	785	290
72	.134	.117	1110	1088	330
26	.232	.204	1713	1638	240
36	.202	.238	1618	1915	325
78	.197	.187	1616	1467	325
74	.198	.197	1963	1834	350

M.S.T. = Multiple Specimen Test

I.S.T. = Incremental Step Test

CAST NO.	MONOTONIC STRAIN HARDENING PROPERTIES						CYCLIC PROPERTIES	
	$n_I$	$K_I^2$ N/mm <sup>2</sup>	$n_{II}$	$K_{II}^2$ N/mm <sup>2</sup>	$n_{III}$	$K_{III}^2$ N/mm <sup>2</sup>	$n'$	$K'$ N/mm <sup>2</sup>
40	.131	542	.290	1130	.156	803	.179	879
34	.047	430	.300	1254	.197	964	.165	967
07	.012	345	.310	1205	.221	952	.118	882
72	.001	490	.282	1551	.181	1191	.134	1110
26	.088	709	.261	1532	.177	1211	.232	1713
36	.044	660	.253	1579	.175	1299	.202	1618
78	.028	604	.302	2132	.211	1532	.197	1616
74	.013	552	.313	2254	.188	1480	.198	1963

TABLE (13)

COMPARISON OF MONOTONIC AND CYCLIC STRAIN HARDENING PARAMETERS

CAST NO.	$\epsilon_f'$	c	$\sigma_f'$	b	$\sigma_f$	$\epsilon_f$	n'	K'	$\sigma_y$	$\sigma_y'/\sigma_u$
40	0.95	-.58	876	-.112	800	.98	.179	879	165	.32
34	0.83	-.57	946	-.096	954	.95	.165	967	220	.38
07	0.75	-.63	714	-.053	898	.77	.118	882	290	.52
72	0.53	-.59	968	-.068	1153	.84	.134	1110	330	.44
26	0.51	-.53	1479	-.124	1054	.46	.232	1713	240	.32
36	0.56	-.53	1436	-.107	1160	.53	.202	1618	325	.42
78	0.35	-.52	1237	-.095	1286	.48	.197	1616	325	.35
74	0.28	-.52	1550	-.101	1320	.49	.198	1963	350	.37

All stress parameters are in N/mm<sup>2</sup>

TABLE (14)

FATIGUE AND CYCLIC STRESS-STRAIN PARAMETERS

Table (15)

RESULTS OF LINEAR REGRESSION ANALYSIS OF  
STRESS AMPLITUDE AND TOTAL PLASTIC STRAIN  
ENERGY TO FAILURE

CAST NO.	SLOPE	INTERCEPT	CORRELATION COEFFICIENT
40	-0.32	7948	-.98
34	-0.36	15606	-.98
07	-0.19	2686	-.95
72	-0.14	2140	-.94
26	-0.35	15868	-.97
36	-0.39	31595	-.99
78	-0.30	10810	-.99
74	-0.36	20297	-.97

TABLE (16)

MEASURED AND CALCULATED VALUES OF THE  
FATIGUE EXPONENTS "b" AND "c"

CAST NO.	MEASURED		MORROW		CURRENT WORK	
	c	b	$c = \frac{-1}{1+5n'}$	$b = \frac{-n'}{1+5n'}$	$c = \frac{-1}{1+4.3n'}$	$b = \frac{-n'}{1+4.3n'}$
40	-.58	-.112	-.53	-.094	-.56	-.101
34	-.57	-.096	-.55	-.090	-.58	-.096
07	-.63	-.053	-.63	-.074	-.66	-.078
72	-.59	-.068	-.60	-.080	-.63	-.084
26	-.53	-.124	-.46	-.107	-.50	-.115
36	-.53	-.107	-.50	-.100	-.53	-.107
78	-.52	-.095	-.50	-.099	-.54	-.106
74	-.52	-.101	-.50	-.099	-.54	-.106

TABLE (17)

LIST OF INDEPENDENT VARIABLES AND THE THREE  
LEVELS SELECTED FOR EACH

C	Si	Mn	AUSTENITISING TEMPERATURE	ISOTHERMAL TRANSFORMATION TEMPERATURE
0.3%	0.3%	0.5%	850°C	540°C
0.5%	1.15%	1.0%	950°C	600°C
0.7%	2.00%	1.5%	1 050°C	660°C

Table (18)

FACTORIAL DESIGN FOR STRUCTURE - PROPERTY STUDIES

SAMPLE NUMBER	INDEPENDENT VARIABLES				
	CARBON	MANGANESE	SILICON	AUSTENITISING TEMPERATURE	ISOTHERMAL TRANSFORMATION TEMPERATURE
1	L	L	L	L	L
2	H	L	M	L	H
3	M	L	H	L	M
4	H	M	L	L	L
5	M	M	M	L	H
6	L	M	H	L	M
7	M	H	L	L	L
8	L	H	M	L	H
9	H	H	H	L	M
10	H	L	L	M	H
11	M	L	M	M	M
12	L	L	H	M	L
13	M	M	L	M	H
14	L	M	M	M	M
15	H	M	H	M	L
16	L	H	L	M	H
17	H	H	M	M	M
18	M	H	H	M	L
19	M	L	L	H	M
20	L	L	M	H	L
21	H	L	H	H	H
22	L	M	L	H	M
23	H	M	M	H	L
24	M	M	H	H	H
25	H	H	L	H	M
26	M	H	M	H	L
27	L	H	H	H	H

L = Lowest level

M = Medium level

H = Highest level

TABLE 18 (Cont'd)

SAMPLE NUMBER	INDEPENDENT VARIABLES				
	CARBON	MANGANESE	SILICON	AUSTENITISING TEMPERATURE	ISOTHERMAL TRANSFORMATION TEMPERATURE
28	M	L	L	L	H
29	H	L	L	L	M
30	L	L	M	L	M
31	M	L	M	L	L
32	L	L	H	L	H
33	H	L	H	L	L
34	L	M	L	L	H
35	M	M	L	L	M
36	L	M	M	L	L
37	H	M	M	L	M
38	M	M	H	L	L
39	H	M	H	L	H
40	L	H	L	L	M
41	H	H	L	L	H
42	M	H	M	L	M
43	H	H	M	L	L
44	L	H	H	L	L
45	M	H	H	L	H
46	L	L	L	M	M
47	M	L	L	M	L
48	L	L	M	M	H
49	H	L	M	M	L
50	M	L	H	M	H
51	H	L	H	M	M
52	L	M	L	M	L
53	H	M	L	M	M
54	M	M	M	M	L
55	H	M	M	M	H
56	L	M	H	M	H
57	M	M	H	M	M
58	M	H	L	M	M
59	H	H	L	M	L

TABLE 18 (Cont'd)

SAMPLE NUMBER	INDEPENDENT VARIABLES				
	CARBON	MANGANESE	SILICON	AUSTENITISING TEMPERATURE	ISOTHERMAL TRANSFORMATION TEMPERATURE
60	L	H	M	M	L
61	M	H	M	M	H
62	L	H	H	M	M
63	H	H	H	M	H
64	L	L	L	H	H
65	H	L	L	H	L
66	M	L	M	H	H
67	H	L	M	H	M
68	L	L	H	H	M
69	M	L	H	H	L
70	M	M	L	H	L
71	H	M	L	H	H
72	L	M	M	H	H
73	M	M	M	H	M
74	L	M	H	H	L
75	H	M	H	H	M
76	L	H	L	H	L
77	M	H	L	H	H
78	L	H	M	H	M
79	H	H	M	H	H
80	M	H	H	H	M
81	H	H	H	H	L

CAST NO.	COMPOSITION			HEAT TREATMENT		QUANTITATIVE MICROSCOPY				MONOTONIC PROPERTIES				CYCLIC PROPERTIES		
	%C	%Si	%Mn	$\gamma$ TEMP ( $^{\circ}$ C)	I.T. TEMP ( $^{\circ}$ C)	$f_{\alpha}$	$d_{\alpha}$	$S^{\circ}$	$\bar{\lambda}_{\alpha}$	$\sigma_y$	$\sigma_U$	$\sigma_f$	$\epsilon_f$	$n'$	$K'$	$\sigma'_y$
40A	0.30	0.30	0.54	850	540	64.12	14.85	0.30	9.62	238	492	771	0.94	.163	840	164
40B				950	600	5.75	8.42	0.55	0.94	248	515	812	1.11	.190	920	140
40C				1050	660	50.17	17.10	0.40	8.75	223	490	793	0.89	.174	850	138
31A	0.32	0.28	1.01	1050	540	4.30	7.04	0.42	0.65	316	575	850	1.10	.178	880	158
31B				850	600	29.10	12.06	0.38	3.74	297	524	959	1.08	.177	850	150
31C				950	660	36.66	16.03	0.40	6.10	282	514	788	0.90	.179	950	158
34A	0.32	0.27	1.44	950	540	1.00	6.12	0.20	0.23	341	603	978	1.05	.165	950	195
34B				850	660	41.96	21.24	0.28	9.05	328	580	928	0.86	.195	1020	139
34C				1050	600	0.95	8.65	0.50	0.51	317	598	954	0.93	.191	1080	176

Units of microstructure =  $\mu$ m, of stress = N/mm<sup>2</sup>

TABLE (19)

METALLURGICAL VARIABLES AND MECHANICAL PROPERTIES FOR SOME C/Si/Mn STEELS

CAST NO.	COMPOSITION			HEAT TREATMENT		QUANTITATIVE MICROSCOPY				MONOTONIC PROPERTIES			CYCLIC PROPERTIES			
	%C	%Si	%Mn	$\gamma$ TEMP ( $^{\circ}$ C)	I.T. TEMP ( $^{\circ}$ C)	$f_{\alpha}$	$d_{\alpha}$	$S^{\circ}$	$\bar{\lambda}_{\alpha}$	$\sigma_y$	$\sigma_u$	$\sigma_f$	$\epsilon_f$	$n'$	$K'$	$\sigma_y'$
28A	0.30	1.20	0.54	1050	600	12.53	10.06	0.45	1.60	290	621	960	0.74	.135	880	213
28B				850	660	63.72	12.08	0.25	7.78	285	610	900	0.75	.135	900	221
28C				950	540	54.10	17.00	0.40	9.36	313	600	980	0.90	.137	900	248
37A	0.34	1.09	1.03	950	600	8.07	9.00	0.44	1.08	339	622	1047	0.86	.150	1050	207
37B				850	540	30.12	10.69	0.36	3.44	351	636	1010	0.76	.145	1010	215
37C				1050	660	32.79	17.51	0.32	5.93	323	634	1043	0.77	.149	1080	242
43A	0.32	1.10	1.60	850	600	30.54	15.25	0.31	4.84	377	672	1120	1.02	.139	1000	275
43B				950	660	26.89	15.87	0.44	4.55	371	631	1014	0.86	.135	1000	270
43C				1050	540	15.00	3.50	0.33	0.77	387	723	1148	0.83	.135	1050	261

Units of microstructure =  $\mu$ m, of stress = N/mm<sup>2</sup>

TABLE (19)

METALLURGICAL VARIABLES AND MECHANICAL PROPERTIES FOR SOME C/Si/Mn STEELS

CAST NO.	COMPOSITION			HEAT TREATMENT		QUANTITATIVE MICROSCOPY				MONOTONIC PROPERTIES				CYCLIC PROPERTIES		
	%C	%Si	%Mn	$\gamma$ TEMP ( $^{\circ}$ C)	I.T. TEMP ( $^{\circ}$ C)	$f_{\alpha}$	$d_{\alpha}$	$S^{\circ}$	$\bar{\lambda}_{\alpha}$	$\sigma_y$	$\sigma_U$	$\sigma_f$	$\epsilon_f$	$n'$	$K'$	$\sigma'_y$
07A	0.29	2.04	0.54	950	660	63.72	18.92	0.30	12.15	348	640	923	0.80	.130	1010	300
07B				850	600	64.64	12.10	0.32	7.92	360	660	903	0.83	.115	890	218
07C				1050	540	28.17	10.56	0.50	3.29	375	673	868	0.67	.120	1020	255
48A	0.32	1.83	1.02	850	660	56.12	6.32	0.32	3.67	434	703	1208	0.96	.115	1000	305
48B				950	540	17.59	8.20	0.40	1.73	443	741	1229	1.01	.145	1110	260
48C				1050	600	1.01	2.94	0.50	0.46	393	763	1243	1.01	.125	1090	310
72A	0.32	1.91	1.51	1050	660	42.60	13.43	0.40	5.92	462	687	1081	0.73	.114	980	280
72B				850	540	0.05	-	0.45	0.39	486	742	1232	0.94	.134	1020	361
72C				950	600	4.96	1.69	0.38	0.40	466	766	1146	0.85	.130	1110	271

Units of microstructure =  $\mu\text{m}$ , of stress =  $\text{N}/\text{mm}^2$

TABLE (19)

METALLURGICAL VARIABLES AND MECHANICAL PROPERTIES FOR SOME C/Si/Mn STEELS

CAST NO.	COMPOSITION			HEAT TREATMENT		QUANTITATIVE MICROSCOPY				MONOTONIC PROPERTIES			CYCLIC PROPERTIES			
	%C	%Si	%Mn	$\gamma$ TEMP (°C)	I.T. TEMP (°C)	$f_{\alpha}$	$d_{\alpha}$	$S^{\circ}$	$\bar{\lambda}_{\alpha}$	$\sigma_y$	$\sigma_u$	$\sigma_f$	$\epsilon_f$	$n'$	$K'$	$\sigma_y'$
41A	0.50	0.33	0.56	1050	600	0.10	4.50	0.50	0.43	339	647	1079	0.83	.208	1250	196
41B				850	660	6.29	11.71	0.40	1.06	278	615	985	0.67	.177	1300	181
41C				950	540	0.50	3.95	0.46	0.42	300	642	990	0.66	.225	1320	153
32A	0.51	0.28	0.99	950	600	0.45	4.33	0.35	0.32	328	696	997	0.52	.215	1320	183
32B				850	540	0.51	6.19	0.28	0.27	366	669	1022	0.70	.230	1380	171
32C				1050	660	0.85	6.50	0.35	0.36	338	670	989	0.54	.231	1450	144
35A	0.52	0.29	1.50	850	600	0	0	0.41	0.36	429	785	1107	0.67	.202	1420	178
35B				950	660	2.16	8.16	0.36	0.48	341	678	994	0.53	.227	1330	205
35C				1050	540	0.05	1.00	0.45	0.39	429	670	1032	0.77	.208	1380	197

Units of microstructure =  $\mu\text{m}$ , of stress =  $\text{N}/\text{mm}^2$

TABLE (19)

METALLURGICAL VARIABLES AND MECHANICAL PROPERTIES FOR SOME C/Si/Mn STEELS

CAST NO.	COMPOSITION			HEAT TREATMENT		QUANTITATIVE MICROSCOPY				MONOTONIC PROPERTIES				CYCLIC PROPERTIES		
	%C	%Si	%Mn	$\gamma$ TEMP (°C)	I.T. TEMP (°C)	$f_{\alpha}$	$d_{\alpha}$	$S^{\circ}$	$\bar{\lambda}_{\alpha}$	$\sigma_{\gamma}$	$\sigma_{U}$	$\sigma_f$	$\epsilon_f$	$h'$	$K'$	$\sigma'_y$
42A	0.51	1.11	0.57	950	650	10.00	9.85	0.44	1.33	318	723	1071	0.59	.170	1200	207
42B				850	600	3.94	6.19	0.35	0.54	347	722	1157	0.80	.189	1290	227
42C				1050	540	0.65	3.27	0.32	0.30	456	799	1120	0.70	.185	1390	233
38A	0.51	1.13	1.08	850	660	5.55	8.62	0.40	0.81	401	769	1203	0.66	.180	1300	182
38B				950	540	1.20	4.74	0.30	0.31	440	801	1317	0.79	.197	1470	304
38C				1050	600	0.30	1.00	0.30	0.26	435	826	1230	0.62	.182	1370	230
45A	0.51	1.09	1.51	1050	660	2.56	5.12	0.32	0.40	395	751	1142	0.65	.176	1470	241
45B				850	540	2.82	3.26	0.35	0.39	455	822	1244	0.78	.213	1620	213
45C				950	600	0.20	3.00	0.30	0.27	397	824	1230	0.70	.192	1520	259

Units of microstructure =  $\mu\text{m}$ , of stress =  $\text{N}/\text{mm}^2$

TABLE (19)

METALLURGICAL VARIABLES AND MECHANICAL PROPERTIES FOR SOME C/Si/Mn STEELS

CAST NO.	COMPOSITION			HEAT TREATMENT	QUANTITATIVE MICROSCOPY				MONOTONIC PROPERTIES			CYCLIC PROPERTIES				
	%C	%Si	%Mn		$\gamma$ TEMP (°C)	I.T. TEMP (°C)	$f_{\alpha}$	$d_{\alpha}$	$S^{\circ}$	$\bar{\lambda}_{\alpha}$	$\sigma_y$	$\sigma_U$	$\sigma_f$	$\epsilon_f$	$n'$	$K'$
70A	0.50	1.84	0.52	850	540	16.02	5.89	0.34	1.19	518	833	1222	0.56	.148	1280	323
70B				950	600	6.81	8.69	0.35	0.86	455	818	1230	0.59	.158	1320	219
70C				1050	660	6.47	8.17	0.50	0.94	481	888	1173	0.47	.155	1320	259
71A	0.52	1.90	1.01	1050	540	2.00	4.13	0.32	0.36	530	916	1282	0.55	.165	1370	269
71B				850	600	1.25	6.32	0.40	0.42	496	838	1268	0.56	.165	1450	242
71C				950	660	3.00	6.05	0.32	0.45	510	859	1158	0.47	.166	1480	260
73A	0.49	1.80	1.46	950	540	0.20	2.60	0.34	0.30	570	903	1360	0.76	.143	1320	289
73B				850	660	1.12	6.05	0.45	0.45	458	862	1385	0.63	.148	1280	317
73C				1050	600	0.10	1.00	0.30	0.26	573	932	1454	0.68	.162	1500	283

Units of microstructure =  $\mu\text{m}$ , of stress =  $\text{N}/\text{mm}^2$

TABLE (19)

METALLURGICAL VARIABLES AND MECHANICAL PROPERTIES FOR SOME C/Si/Mn STEELS

CAST NO.	COMPOSITION			HEAT TREATMENT	QUANTITATIVE MICROSCOPY					MONOTONIC PROPERTIES			CYCLIC PROPERTIES			
	%C	%Si	%Mn		$\gamma$ TEMP ( $^{\circ}$ C)	I.T. TEMP ( $^{\circ}$ C)	$f_{\alpha}$	$d_{\alpha}$	$S^{\circ}$	$\bar{\lambda}_{\alpha}$	$\sigma_y$	$\sigma_u$	$\sigma_f$	$\epsilon_f$	$n'$	$K'$
26A	0.78	0.30	0.58	950	660	0.50	6.24	0.35	0.33	373	785	1032	0.40	.260	1750	177
26B				850	600	0.50	3.00	0.32	0.29	407	741	1112	0.57	.255	2000	182
26C				1050	540	0.10	2.00	0.45	0.39	383	759	1019	0.42	.245	1680	152
79A	0.79	0.27	1.01	850	660	0	0	0.25	0.22	382	789	1037	0.44	.244	1900	241
79B				950	540	0	0	0.25	0.22	416	797	1140	0.45	.270	2100	231
79C				1050	600	0.05	1.00	0.33	0.29	400	819	1148	0.40	.250	2020	220
36A	0.71	0.29	1.51	1050	660	0.10	1.50	0.35	0.31	442	793	1135	0.49	.220	1680	212
36B				850	540	0.05	1.00	0.30	0.26	499	776	1168	0.51	.240	1850	230
36C				950	600	0	0	0.28	0.24	452	811	1181	0.58	.220	1850	231

Units of microstructure =  $\mu$ m , of stress = N/mm<sup>2</sup>

TABLE (19)

METALLURGICAL VARIABLES AND MECHANICAL PROPERTIES FOR SOME C/Si/Mn STEELS

CAST NO.	COMPOSITION		HEAT TREATMENT	QUANTITATIVE MICROSCOPY				MONOTONIC PROPERTIES			CYCLIC PROPERTIES					
	%C	%Si		%Mn	$\gamma$ TEMP ( $^{\circ}$ C)	I.T. TEMP ( $^{\circ}$ C)	$f_{\alpha}$	$d_{\alpha}$	$S^{\circ}$	$\bar{\lambda}_{\alpha}$	$\sigma_y$	$\sigma_u$	$\sigma_f$	$\epsilon_f$	$n'$	$K'$
44A	0.74	1.07	0.59	850	540	0.20	2.00	0.37	0.32	484	906	1268	0.53	.210	1780	296
44B				950	600	0.20	1.00	0.35	0.30	422	859	1244	0.51	.240	1800	214
44C				1050	660	0.05	1.00	0.32	0.28	530	889	1192	0.47	.214	1790	251
39A	0.71	1.09	1.01	1050	540	0.01	0	0.44	0.38	544	888	1185	0.49	.195	1600	278
39B				850	600	0.10	1.00	0.35	0.31	475	877	1262	0.61	.214	1700	211
39C				950	660	0.05	1.00	0.36	0.31	474	925	1247	0.53	.210	1710	217
47A	0.69	1.08	1.50	950	540	0.01	0	0.30	0.26	616	917	1305	0.62	.180	1580	303
47B				850	660	0.05	1.00	0.38	0.33	519	843	1227	0.45	.206	1520	218
47C				1050	600	0.05	1.00	0.40	0.35	530	882	1254	0.50	.197	1750	270

Units of microstructure =  $\mu$ m, of stress = N/mm<sup>2</sup>

TABLE (19)

METALLURGICAL VARIABLES AND MECHANICAL PROPERTIES FOR SOME C/Si/Mn STEELS

CAST NO.	COMPOSITION			HEAT TREATMENT		QUANTITATIVE MICROSCOPY				MONOTONIC PROPERTIES			CYCLIC PROPERTIES			
	%C	%Si	%Mn	$\gamma$ TEMP ( $^{\circ}$ C)	I.T. TEMP ( $^{\circ}$ C)	$f_{\alpha}$	$d_{\alpha}$	$S^{\circ}$	$\bar{\lambda}_{\alpha}$	$\sigma_y$	$\sigma_u$	$\sigma_f$	$\epsilon_f$	$n'$	$K'$	$\sigma'_y$
78A	0.65	2.00	0.58	1050	600	1.20	5.00	0.30	0.32	530	910	1300	0.41	.165	1620	281
78B				850	660	1.06	3.95	0.32	0.32	464	937	1291	0.47	.177	1500	259
78C				950	540	0	0	0.40	0.35	461	970	1274	0.57	.170	1550	284
75A	0.68	1.83	1.03	950	600	0.20	2.00	0.31	0.27	518	963	1275	0.39	.163	1540	286
75B				850	540	0.05	1.00	0.30	0.26	541	969	1354	0.51	.186	1740	245
75C				1050	660	0.10	1.00	0.35	0.31	455	988	1303	0.40	.165	1630	288
74A	0.70	1.86	1.49	850	600	0	0	0.32	0.28	536	1064	1360	0.48	.173	1720	280
74B				950	660	0	0	0.40	0.35	539	949	1284	0.42	.180	1610	317
74C				1050	540	0.05	1.00	0.45	0.39	552	978	1325	0.56	.170	1640	255

Units of microstructure =  $\mu\text{m}$ , of stress =  $\text{N/mm}^2$

TABLE (19)

METALLURGICAL VARIABLES AND MECHANICAL PROPERTIES FOR SOME C/Si/Mn STEELS

CAST NO.	$\sigma_{fpc}$	$\sigma_{fpm}$	$\sigma'_f$	$\epsilon_{fpc}$	$\epsilon_{fpm}$	$\epsilon'_f$	$C_{pc}$	$C_{pm}$	C	$b_{pc}$	$b_{pm}$	b
40	845	860	876	.88	1.06	.95	-.56	-.57	-.58	-.103	-.101	-.112
34	934	923	946	.86	1.06	.83	-.55	-.55	-.57	-.104	-.102	-.096
07	1047	1106	714	.89	1.08	.75	-.66	-.68	-.63	-.078	-.074	-.053
72	1132	1331	968	.86	.53	.53	-.64	-.59	-.59	-.083	-.094	-.068
26	1081	1032	1479	.39	.53	.51	-.47	-.51	-.53	-.122	-.113	-.124
36	1129	1124	1436	.46	.45	.56	-.48	-.50	-.53	-.119	-.115	-.107
78	1218	1299	1237	.52	.46	.35	-.57	-.59	-.52	-.099	-.095	-.095
74	1334	1323	1550	.49	.53	.28	-.58	-.59	-.52	-.095	-.095	-.101

\* Suffix pc = predictions using chemical composition only

Suffix pm = predictions using chemical composition and microstructure

Units of stress parameters =  $N/mm^2$

TABLE (20)

COMPARISON OF CALCULATED AND ACTUAL MECHANICAL PROPERTIES

TABLE (21)

COMPOSITION AND MECHANICAL PROPERTIES  
FOR MAN-TEN AND RQC-100 STEELS

CHEMICAL COMPOSITION	MAN-TEN	RQC-100
Carbon	0.23	0.19
Silicon	0.01	0.24
Manganese	1.57	0.79
Sulphur	0.022	0.021
Phosphorus	0.016	0.005
Copper	0.22	-
Boron	-	0.0028
MECHANICAL PROPERTIES		
Youngs Modulus (N/mm <sup>2</sup> )	203 000	203 000
n'	0.193	0.100
K' (N/mm <sup>2</sup> )	1 190	1 150
$\sigma_f'$ (N/mm <sup>2</sup> )	930	1 165
b	-0.095	-0.075
$\epsilon_f'$	0.26	1.06
c	-0.47	-0.75

TABLE (22)

PREDICTIONS FOR SAE HISTORIES - MAN-TEN STEEL

Test I.D. No.	Max/Min Load (kN)	Max Load Range (kN)	Actual Life to Initiation (Blocks)	Actual Life to Failure (Blocks)	Predicted Life (Blocks)
SM 1	- 71.2	95.7	7.7 - 28	10.5 - 48	20.28
SM 2	- 40.0	53.8	162 - 430	767 - 2 200	313.5
SM 3	- 26.7	35.9	1 410 - 2 240	31 884	3 000
SM 4	- 20.0	26.9	4 700	24 666	20 460
SM 5	- 13.3	17.9	-	85 370	82 000
BM 1	- 71.2	123.6	1.5 - 2.6	2.2 - 3.0	1
BM 2	- 35.6	61.8	11.5 - 23	19.5 - 44	15.23
BM 3	- 15.6	27.0	270 - 1 588	1 054 - 4 944	2 319
BM 4	- 13.3	23.20	2 666	4 076 - 9 910	8 436
BM 5	- 11.1	19.3	-	20 630	55 400
TM 1	+ 71.2	106.3	8.4 - 12.8	8.9 - 16	4
TM 2	+ 35.6	53.2	74 - 420	86 - 537	77.2
TM 3	+ 15.6	23.2	3 755 - 5 800	5 780 - 6 957	6 946

\* SM = Suspension History

BM = Bracket History

TM = Transmission History

TABLE (23)

PREDICTIONS FOR SAE HISTORIES - RQC-100 STEEL

Test I.D. No.	Max/Min Load (kN)	Max Load Range (kN)	Actual Life to Initiation (Blocks)	Actual Life to Failure (Blocks)	Predicted Life (Blocks)
SR 1	- 71.2	95.7	20 - 64	27.5 - 218	24
SR 2	- 40.0	53.8	1 710	5 535	463
SR 3	- 31.1	41.8	11 200	51 124	3 317
SR 4	- 26.7	35.9	48 000	106 732	16 820
BR 1	- 71.2	123.6	3.3 - 5.1	5.3 - 7.4	1
BR 2	- 35.6	61.8	47 - 113	108 - 212	27.6
BR 3	- 15.6	27.0	2 773 - 5 020	7 673 - 12 519	19 000
TR 1	+ 71.2	106.3	22.2 - 29.9	24 - 35.6	5.8
TR 2	+ 35.6	53.2	269 - 460	297 - 520	126.3
TR 3	+ 15.6	23.2	-	88 020	25 200

\* SR = Suspension History

BR = Bracket History

TR = Transmission History

TABLE (24)

DIFFERENT ASSESSMENTS OF NON-MASING MATERIAL BEHAVIOUR

		n'	K'	Correlation Coefficient
(1) <u>Morrow</u> $\epsilon_p = \left(\frac{\sigma_a}{K'}\right)^{1/n'}$	Loop 5	.162	1384	.999
	Loop 10	.153	1372	.995
	Loop 15	.140	1351	.994
(2) <u>Jhansale</u> $\epsilon_p = \left(\frac{\sigma_a - \delta\sigma_{y'}}{K'}\right)^{1/n'}$	Loop 5	.164	1386	.995
	Loop 10	.164	1381	.995
	Loop 15	.163	1376	.993

$\delta\sigma_{y'}$  = Yield range increment

TABLE (25)

## COMPOSITION AND LIFE PREDICTION RESULTS

Cast No.	C (wt %)	Si (wt %)	Mn (wt %)	Np 800 (reversals)	Np 450 (reversals)	Np 230 (reversals)
40 S	0.30	0.30	0.54	$4.75 \times 10^4$	$4.40 \times 10^5$	$1.07 \times 10^7$
34 S	0.32	0.27	1.44	$8.09 \times 10^4$	$9.62 \times 10^5$	$4.36 \times 10^7$
07 S	0.29	2.04	0.54	$4.72 \times 10^4$	$6.62 \times 10^5$	$1.66 \times 10^8$
72 S	0.32	1.91	1.51	$7.75 \times 10^4$	$1.44 \times 10^5$	$8.74 \times 10^8$
26 S	0.78	0.30	0.58	$1.23 \times 10^5$	$1.66 \times 10^6$	$8.80 \times 10^7$
36 S	0.71	0.29	1.51	$1.45 \times 10^5$	$2.38 \times 10^6$	$2.94 \times 10^8$
78 S	0.65	2.00	0.58	$1.07 \times 10^5$	$2.06 \times 10^6$	$3.84 \times 10^8$
74 S	0.70	1.86	1.49	$1.48 \times 10^5$	$3.82 \times 10^6$	$1.67 \times 10^9$
40 B	0.30	0.30	0.54	$5.46 \times 10^3$	$3.88 \times 10^4$	$6.64 \times 10^5$
34 B	0.32	0.27	1.44	$7.72 \times 10^3$	$7.03 \times 10^4$	$2.26 \times 10^6$
07 B	0.29	2.04	0.54	$3.92 \times 10^3$	$4.69 \times 10^4$	$6.28 \times 10^6$
72 B	0.32	1.91	1.51	$5.88 \times 10^3$	$9.35 \times 10^4$	$2.05 \times 10^7$
26 B	0.78	0.30	0.58	$1.00 \times 10^4$	$1.04 \times 10^5$	$3.49 \times 10^6$
36 B	0.71	0.29	1.51	$1.10 \times 10^4$	$1.39 \times 10^5$	$9.46 \times 10^6$
78 B	0.65	2.00	0.58	$7.72 \times 10^3$	$1.16 \times 10^5$	$1.09 \times 10^7$
74 B	0.70	1.86	1.49	$9.80 \times 10^3$	$1.92 \times 10^5$	$3.15 \times 10^7$
40 T	0.30	0.30	0.54	$9.87 \times 10^3$	$6.84 \times 10^4$	$9.84 \times 10^5$
34 T	0.32	0.27	1.44	$1.43 \times 10^4$	$1.21 \times 10^5$	$2.84 \times 10^6$
07 T	0.29	2.04	0.54	$8.07 \times 10^3$	$8.00 \times 10^4$	$6.53 \times 10^6$
72 T	0.32	1.91	1.51	$1.13 \times 10^4$	$1.40 \times 10^5$	$1.82 \times 10^7$
26 T	0.78	0.30	0.58	$1.60 \times 10^4$	$1.46 \times 10^5$	$3.59 \times 10^6$
36 T	0.71	0.29	1.51	$1.83 \times 10^4$	$2.08 \times 10^5$	$8.00 \times 10^6$
78 T	0.65	2.00	0.58	$1.26 \times 10^4$	$1.56 \times 10^5$	$8.55 \times 10^6$
74 T	0.70	1.86	1.49	$1.51 \times 10^4$	$2.26 \times 10^5$	$1.85 \times 10^7$

Np = Life Predictions : suffix refers to max stress level.

Fig.1 (a)

Example of a star-crack failure  
at a rail end.

Fig.1 (b)

Fracture face of a star-crack  
rail failure showing the  
initiating fatigue crack.

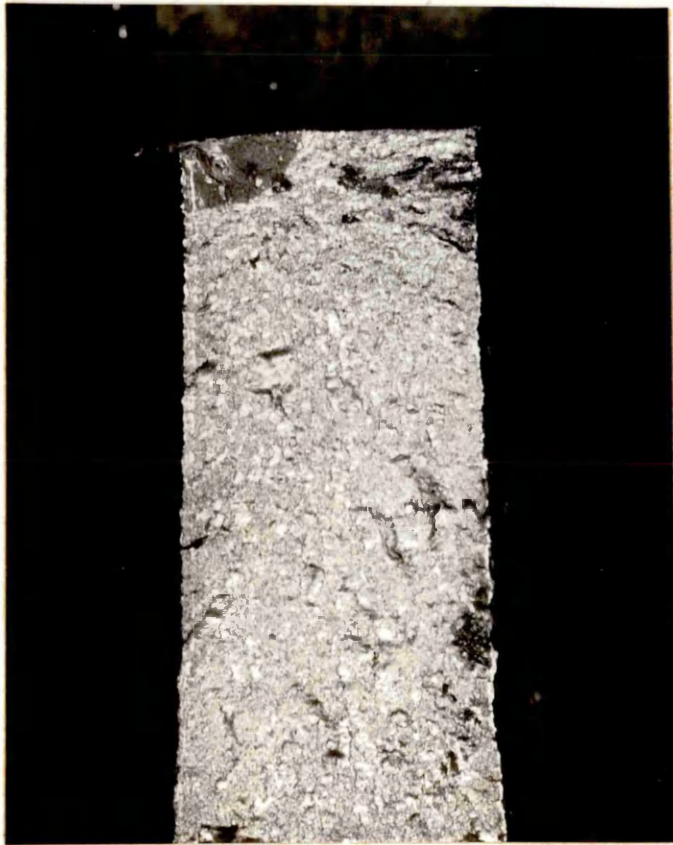
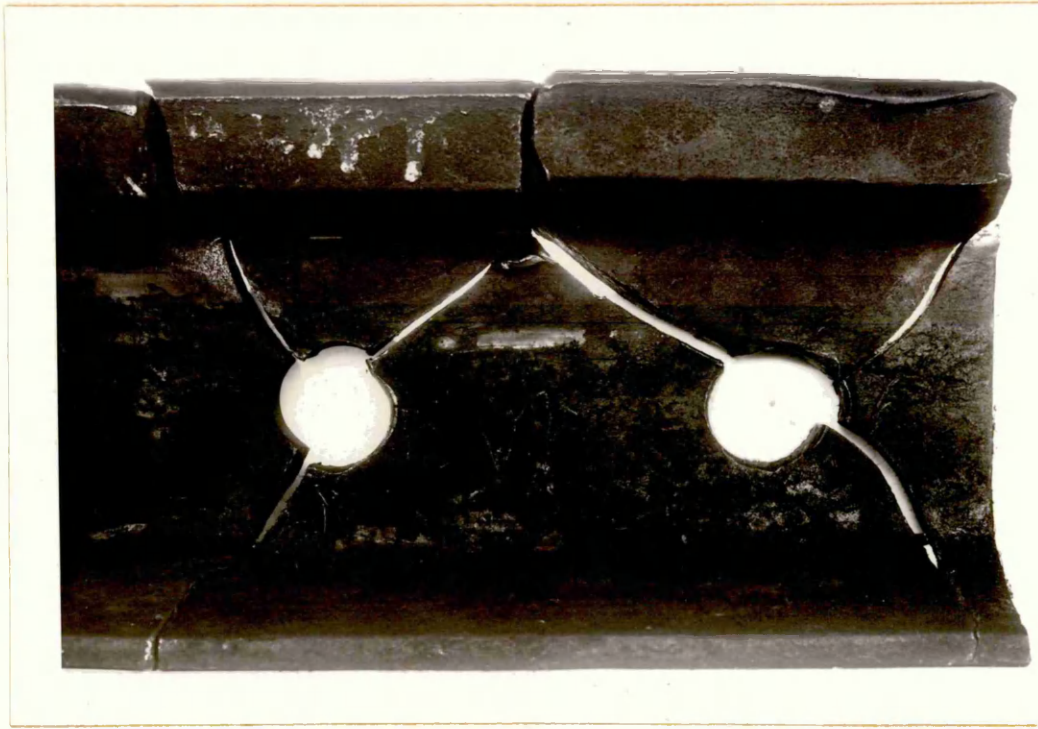


Fig.2

Example of a fractured wheel.  
The initial fatigue crack developed  
from the small, threaded bolt hole  
marked "A".



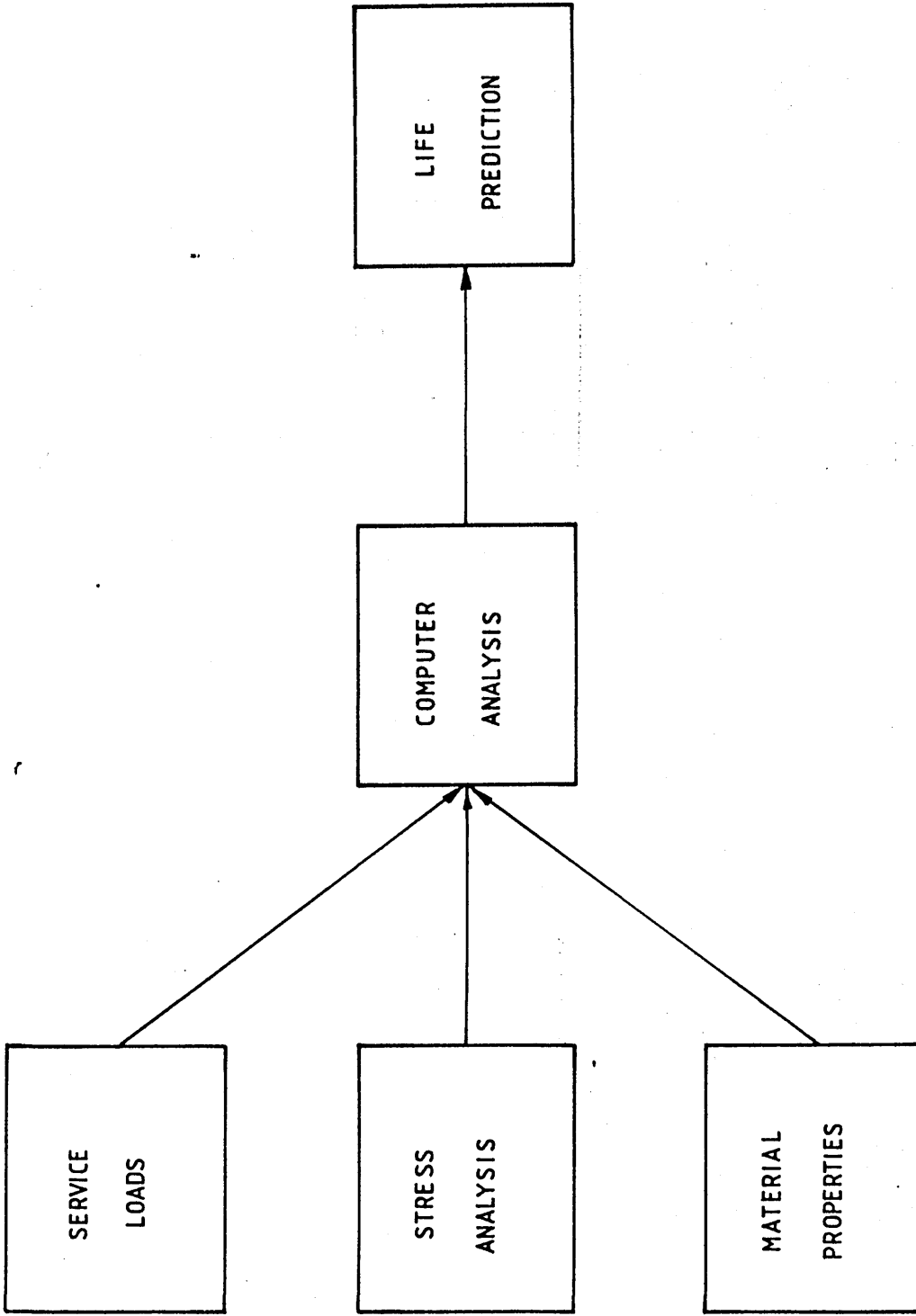


FIG. 3. BASIC ELEMENTS FOR FATIGUE LIFE PREDICTION.

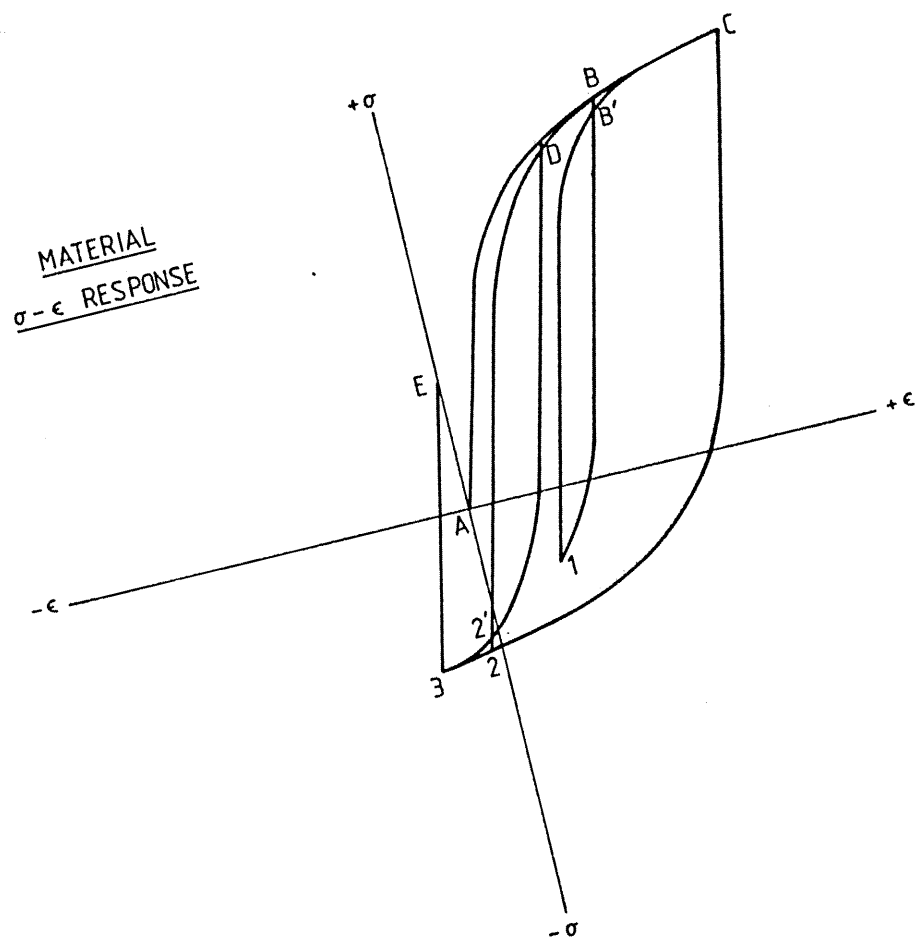
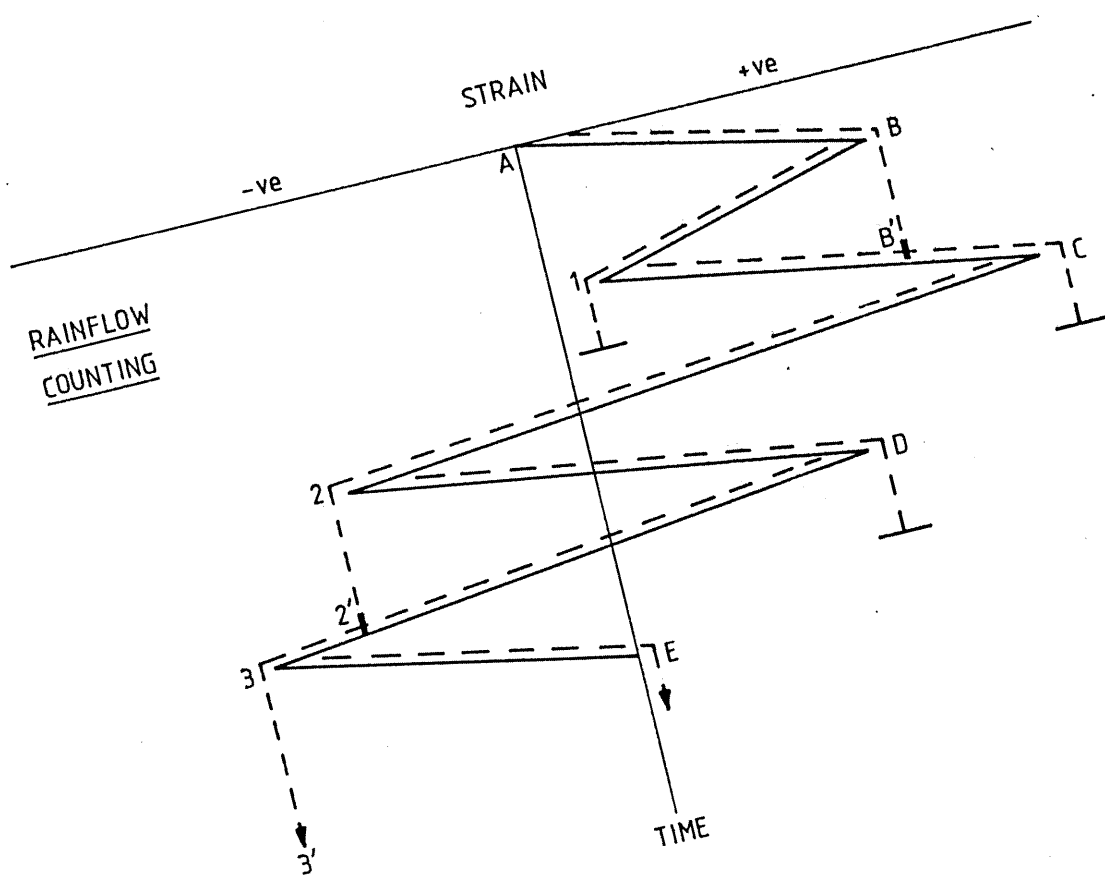
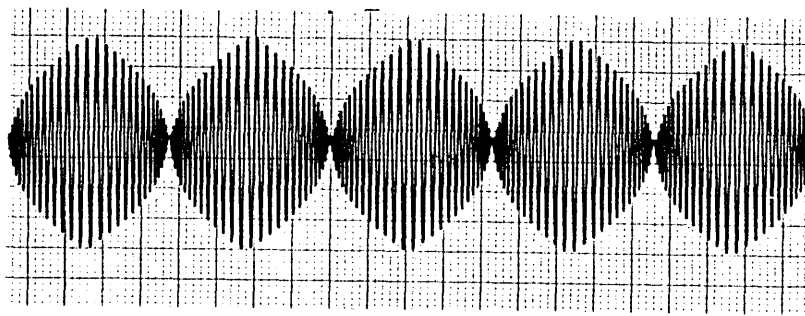
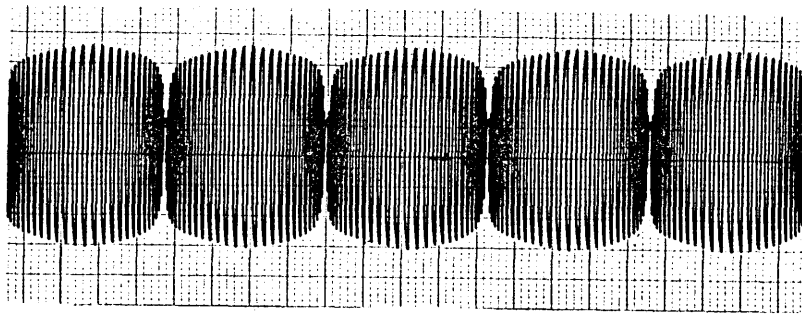


FIG. 4. RAINFLOW COUNTING OF VARIABLE AMPLITUDE SIGNALS

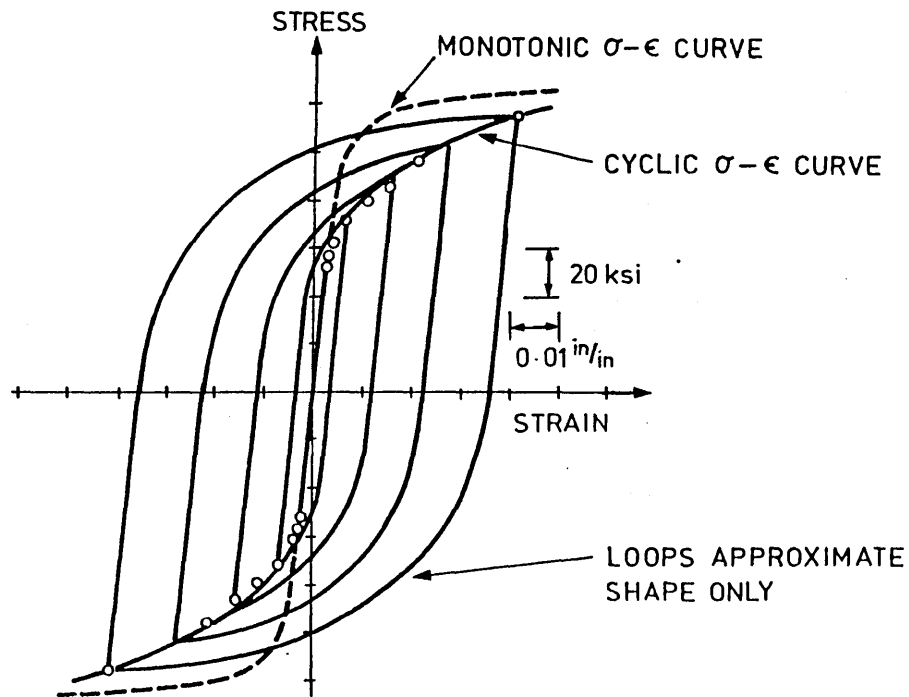
FIG. 5.



(i) STRAIN INPUT



(ii) STRESS RESPONSE



(iii)  $\sigma$ - $\epsilon$  HYSTERESIS LOOPS (REF. 17)

FIG. 5. PRODUCTION OF CYCLIC  $\sigma$ - $\epsilon$  CURVE FROM INCREMENTAL STEP TEST.

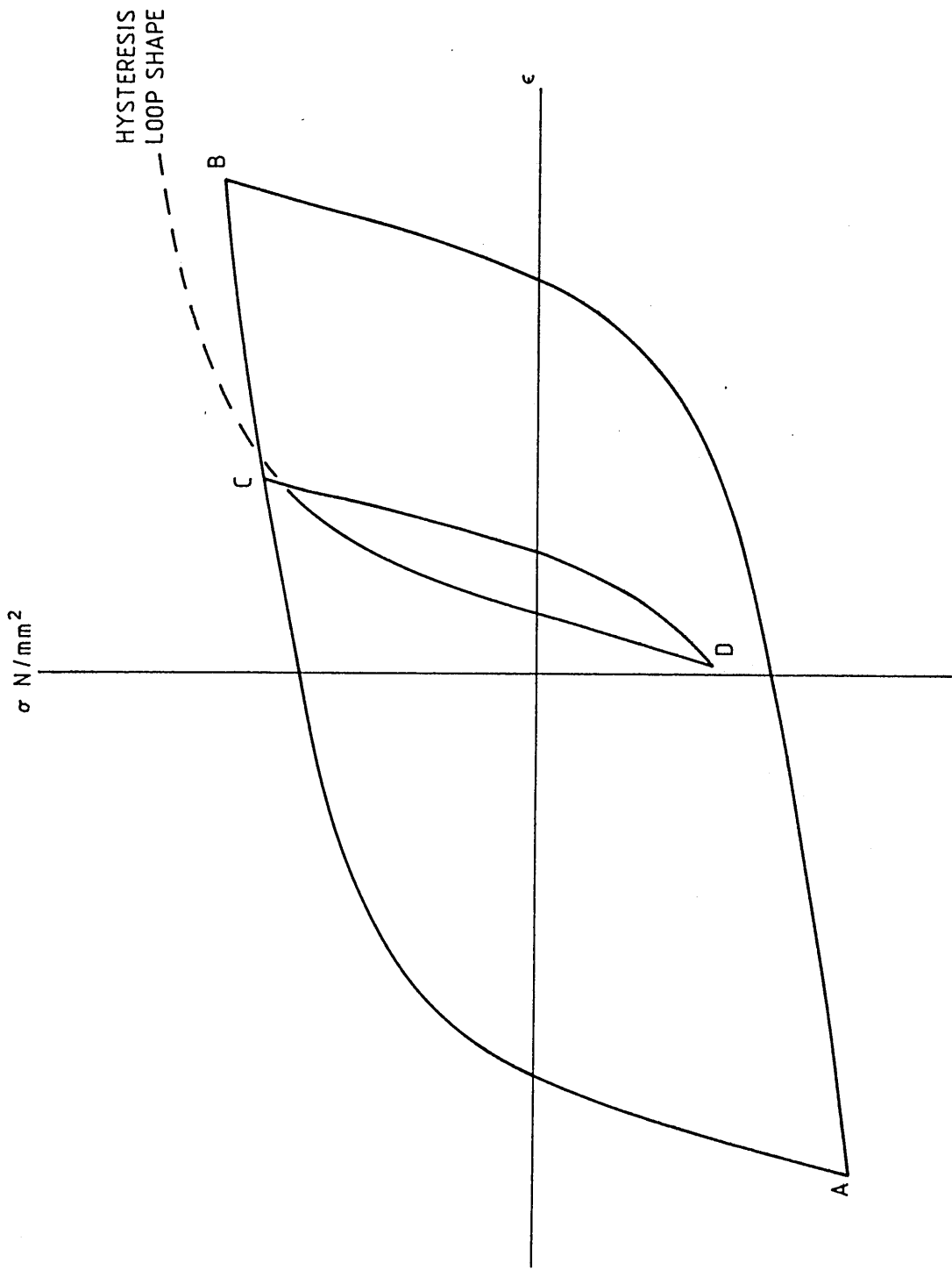


FIG. 6. DEMONSTRATION OF 'MATERIAL MEMORY' EFFECT

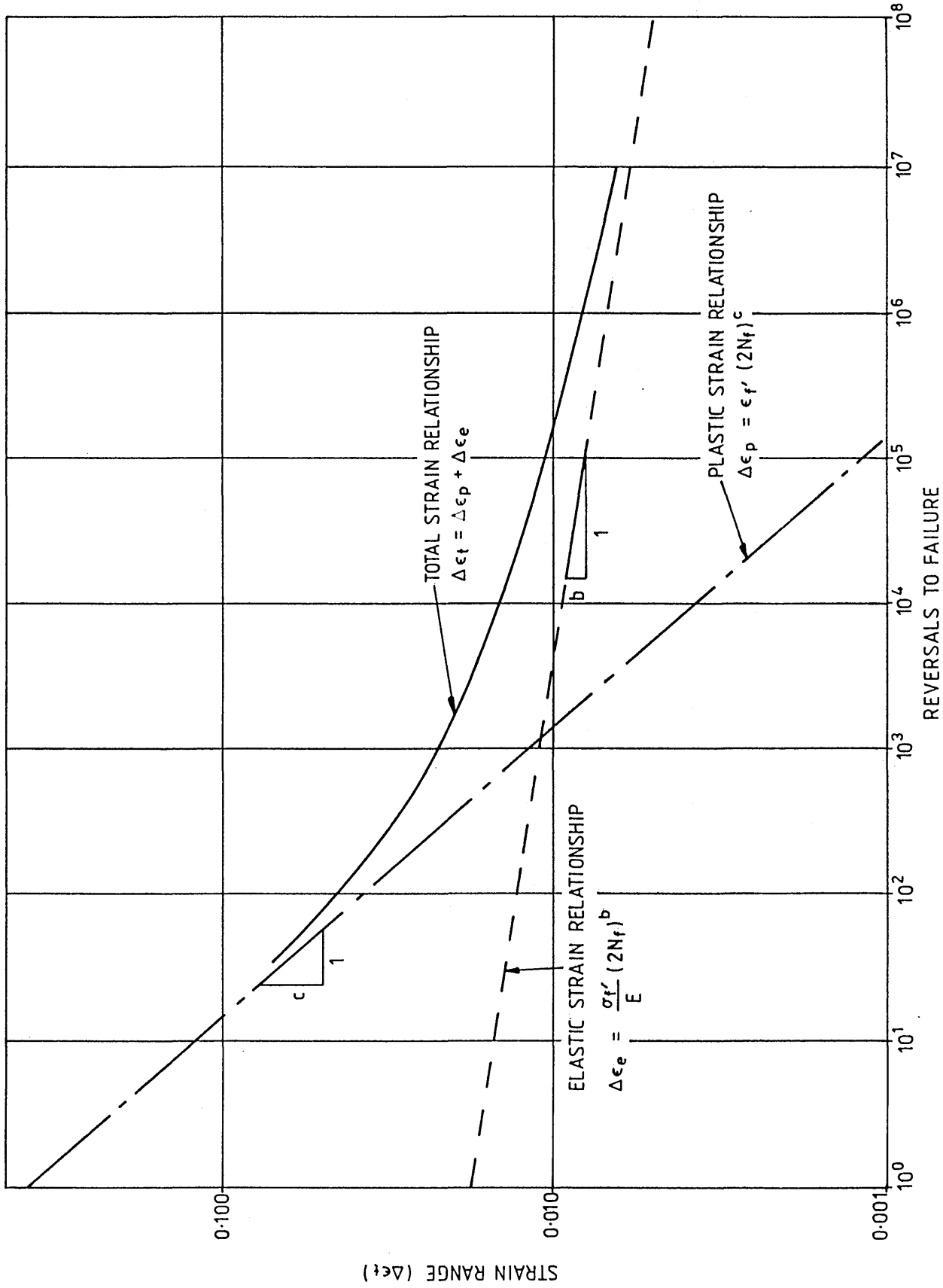


FIG. 7. DIAGRAMMATIC REPRESENTATION OF TOTAL, ELASTIC AND PLASTIC STRAIN - LIFE CURVES

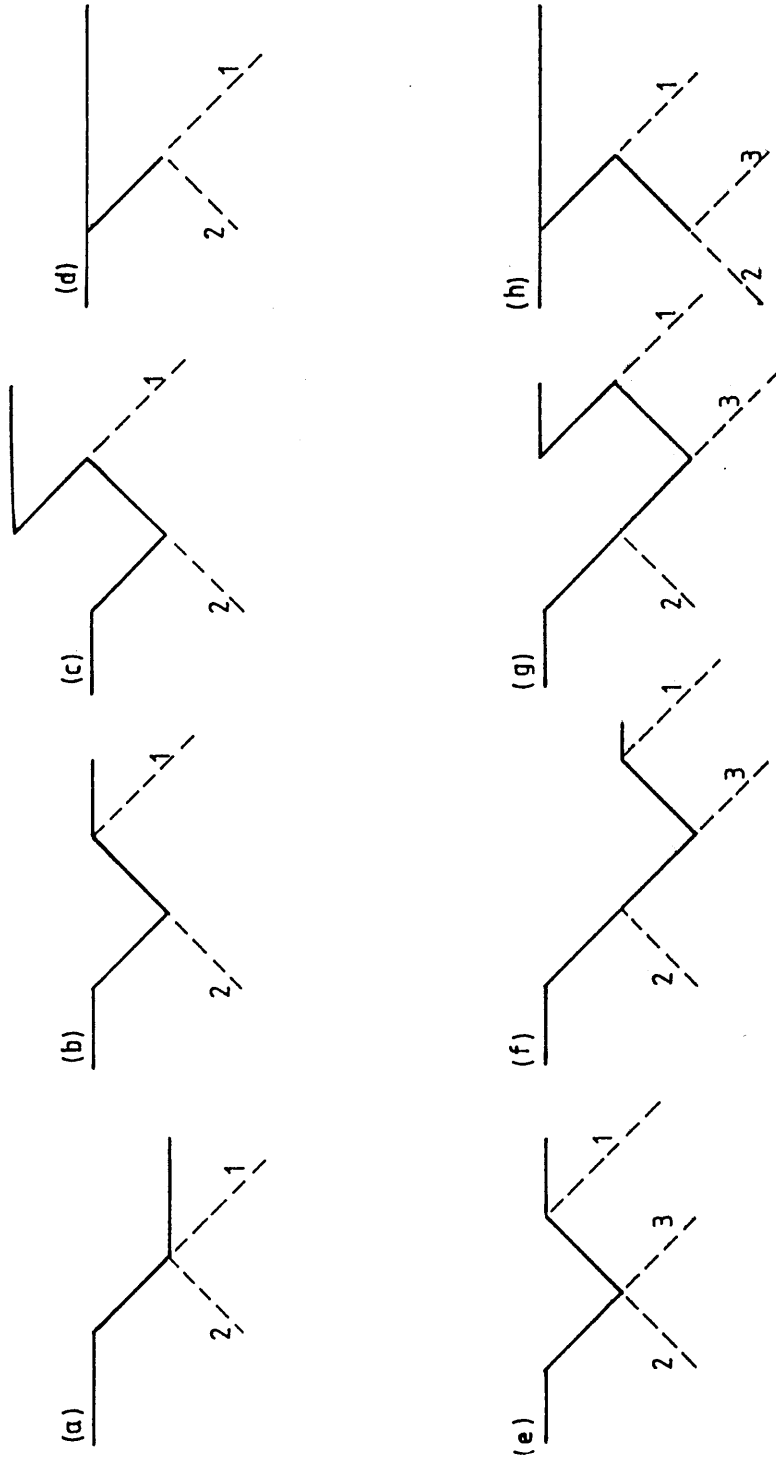


FIG. 8. THE FATIGUE CRACK INITIATION AND GROWTH MODEL OF P. NEUMANN. (114)

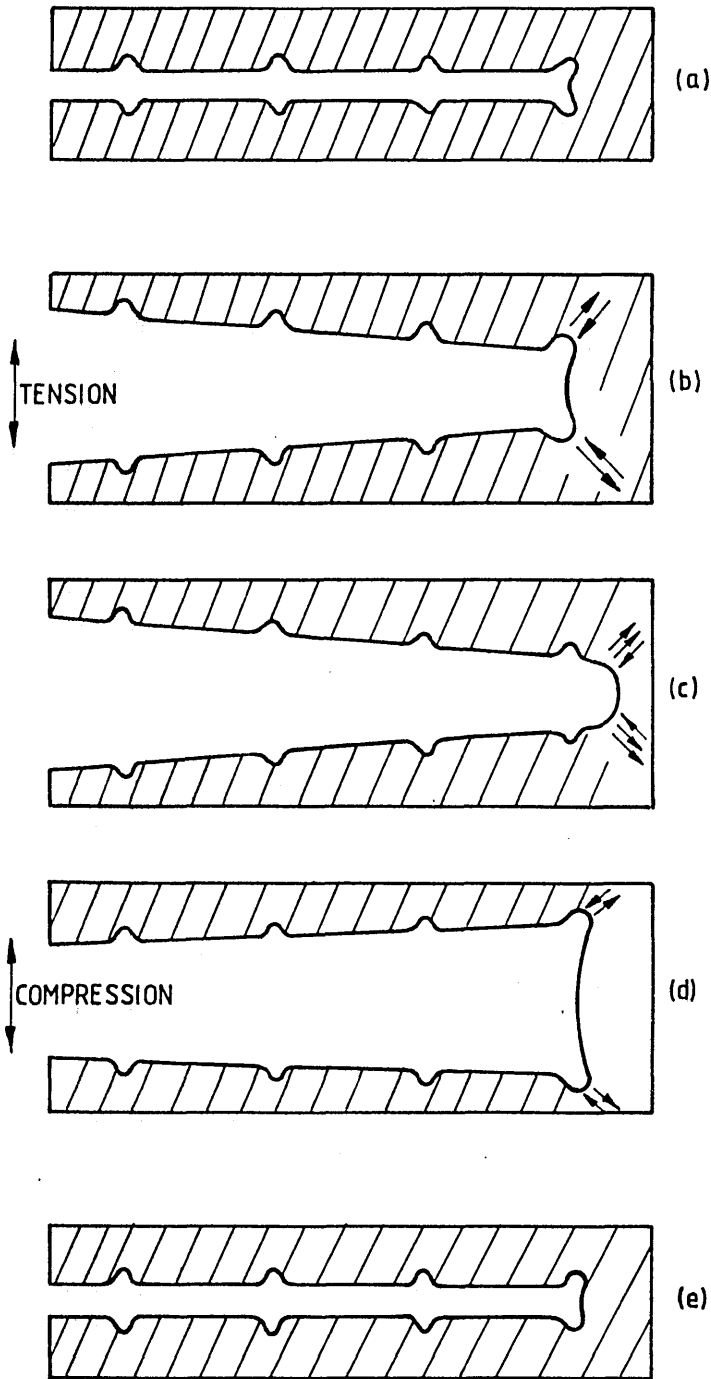
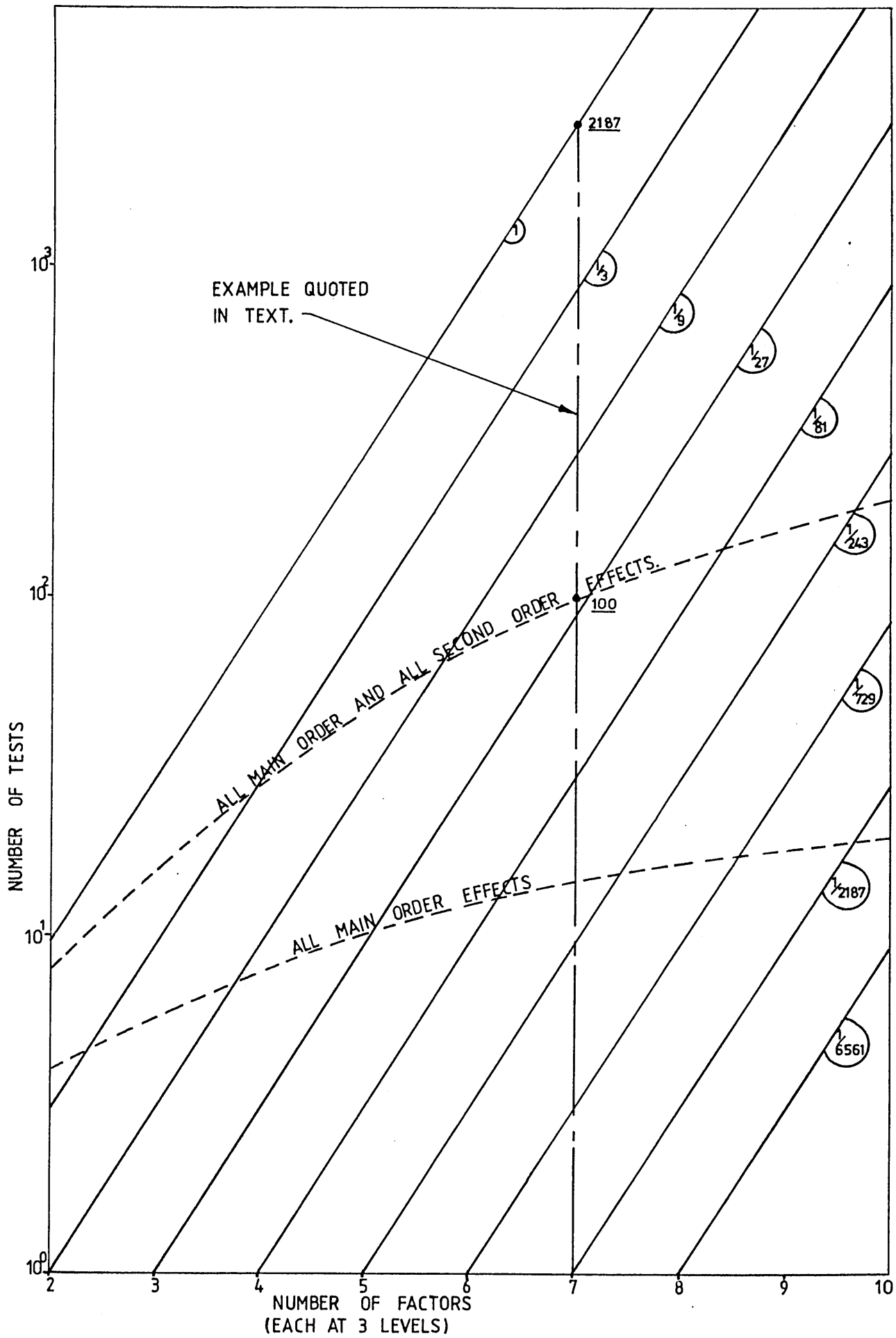
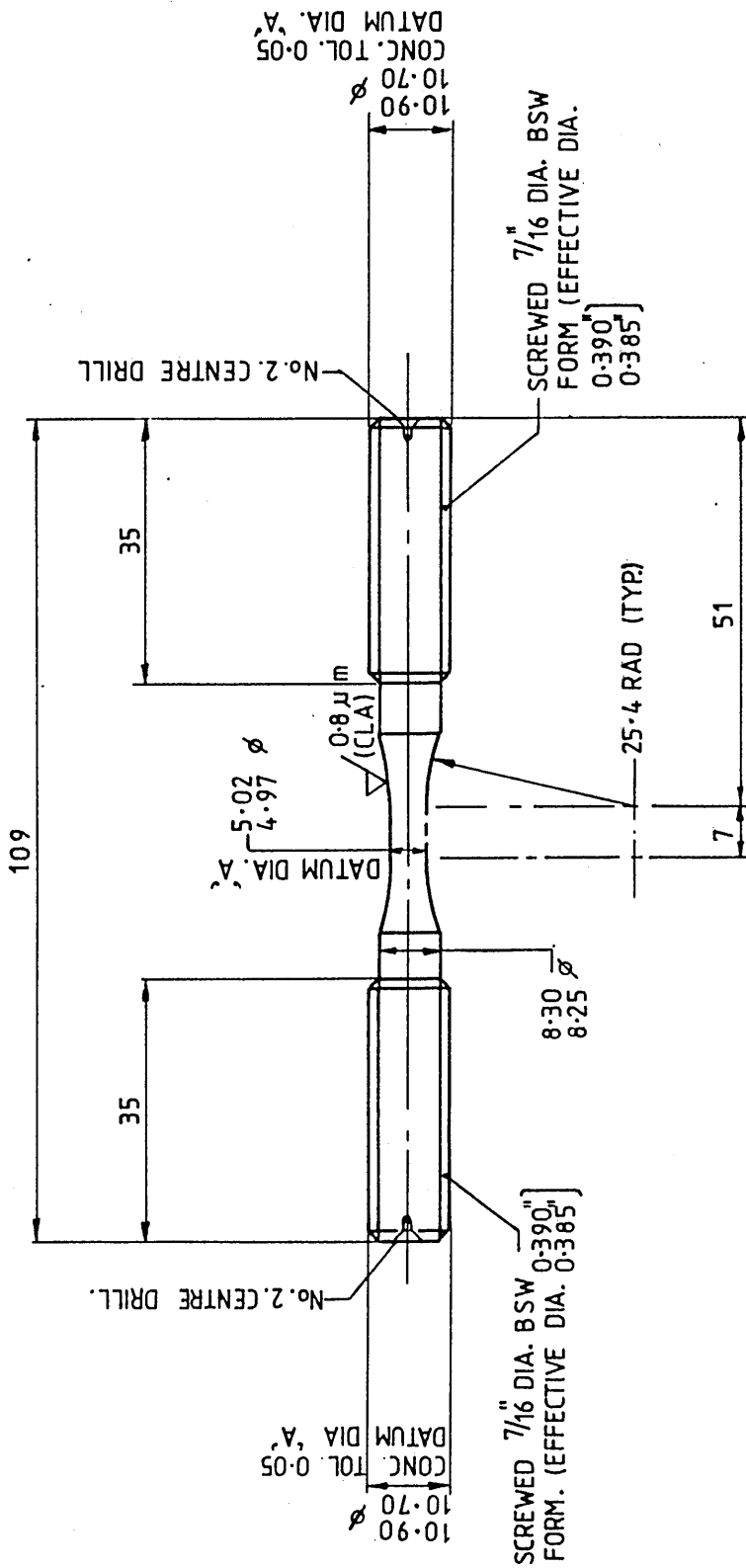


FIG 9. THE FATIGUE CRACK PROPAGATION MODEL OF LAIRD AND SMITH (130).



**FIG. 10. BASIS OF FRACTIONAL FACTORIAL DESIGNED EXPERIMENTS.**



ALL DIMENSIONS ARE IN mm.

FIG.11. SPECIMEN DESIGN.

Fig. 12

The photograph shows the small, clip-on extensometer used in the fatigue tests and the incremental step tests.

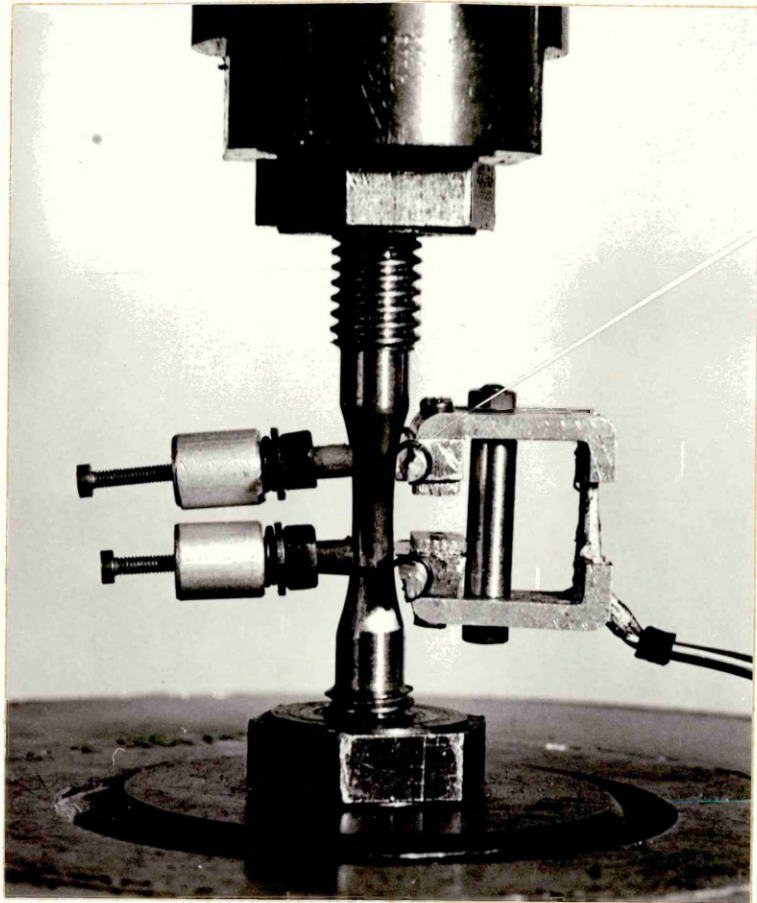
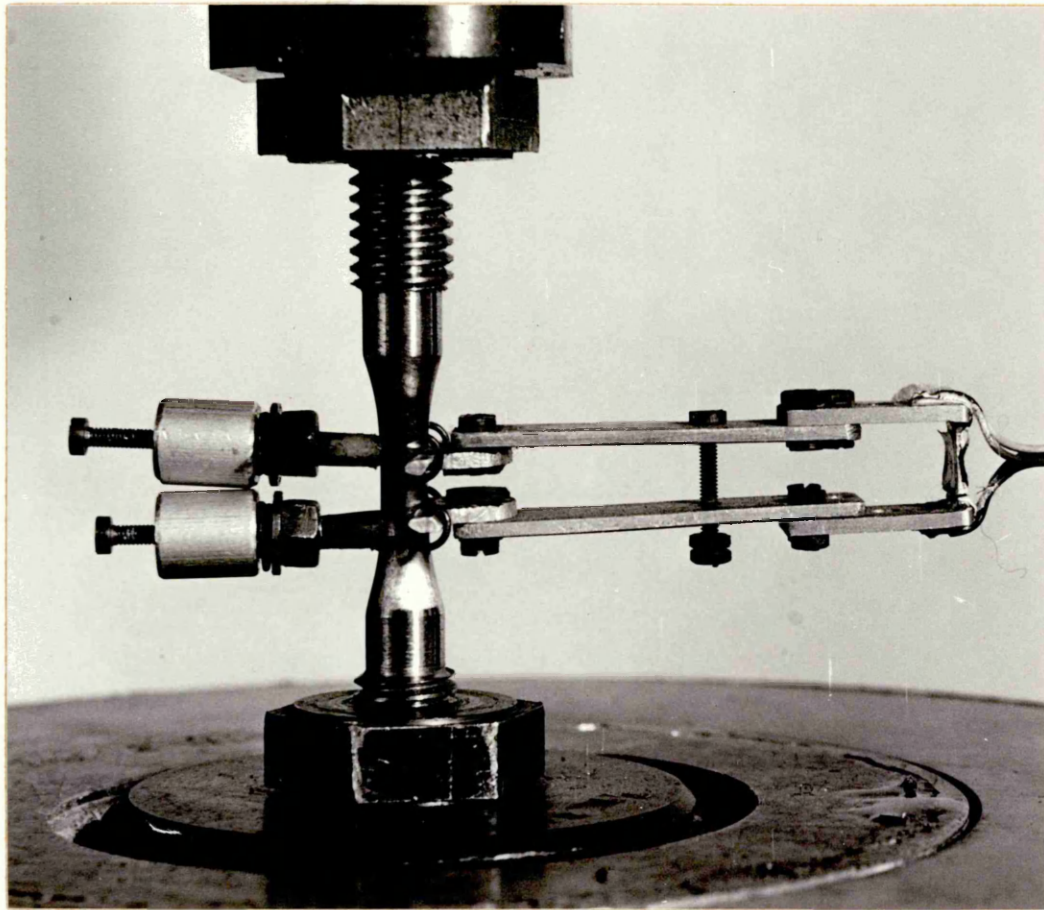
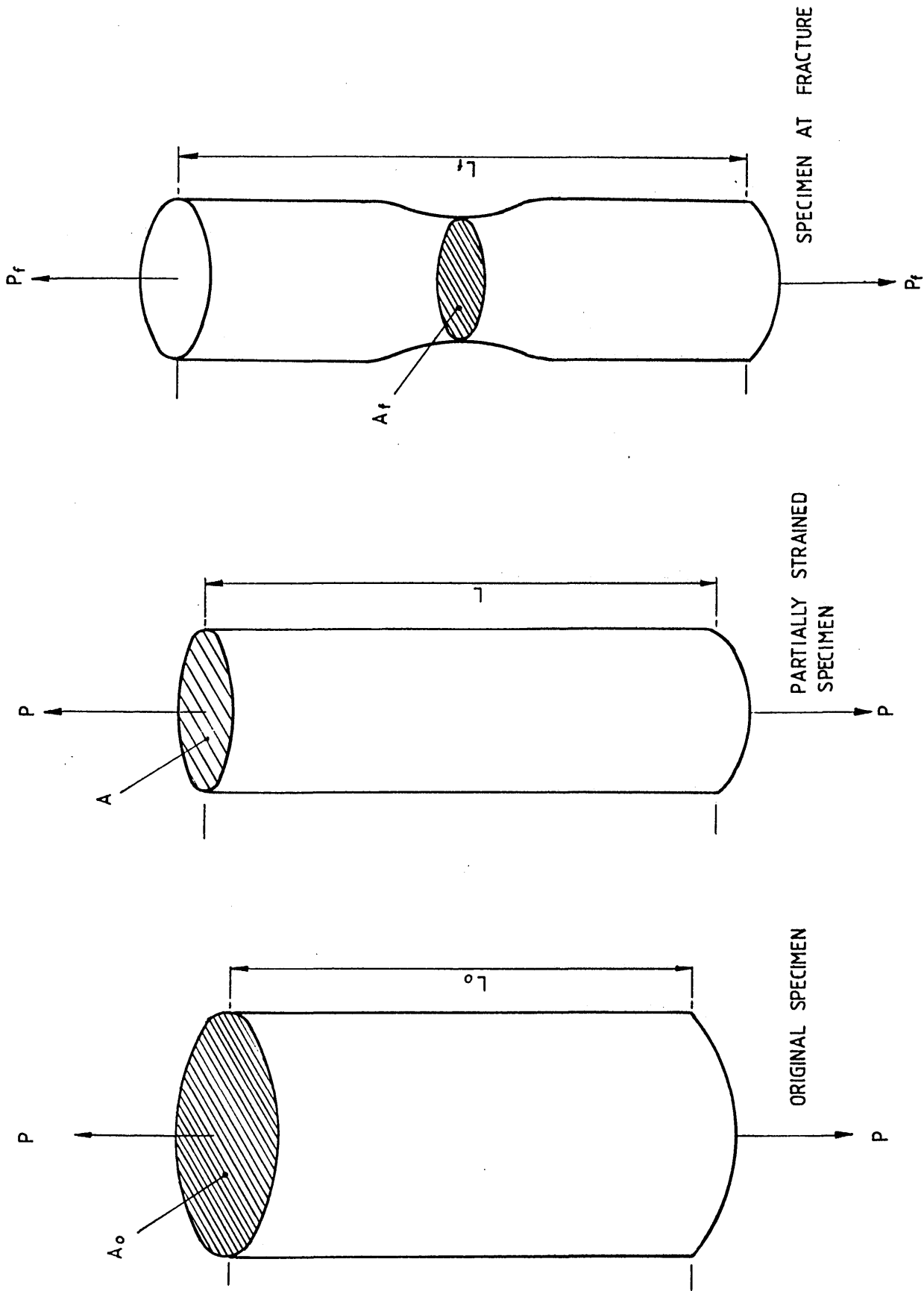


Fig.13

The photograph shows the long arm extensometer used in the monotonic tests.





**FIG. 14. GAUGE SECTION FROM A LONGITUDINAL TENSILE SPECIMEN**

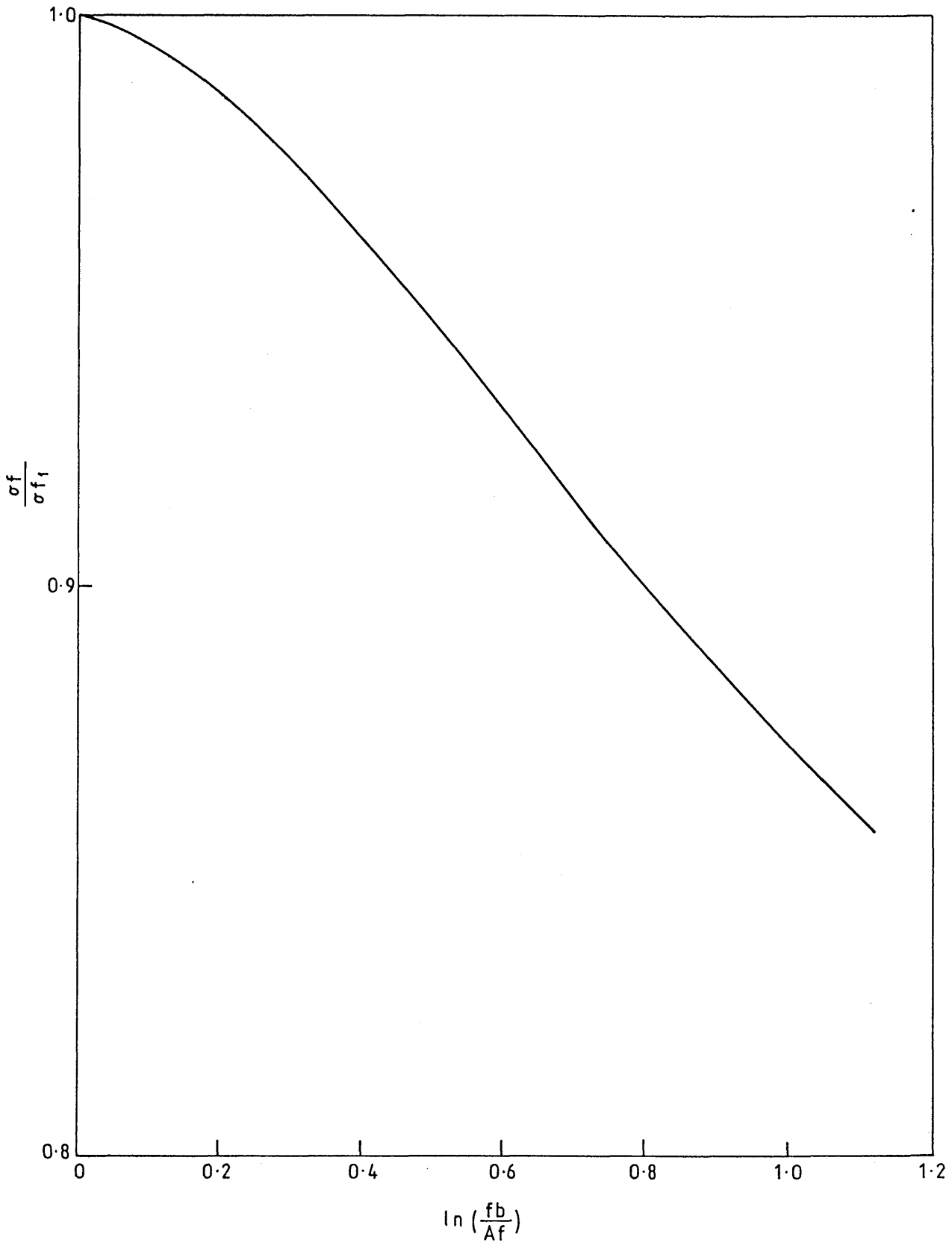


FIG. 15. YAMASHITA'S CORRECTION FOR NECKING

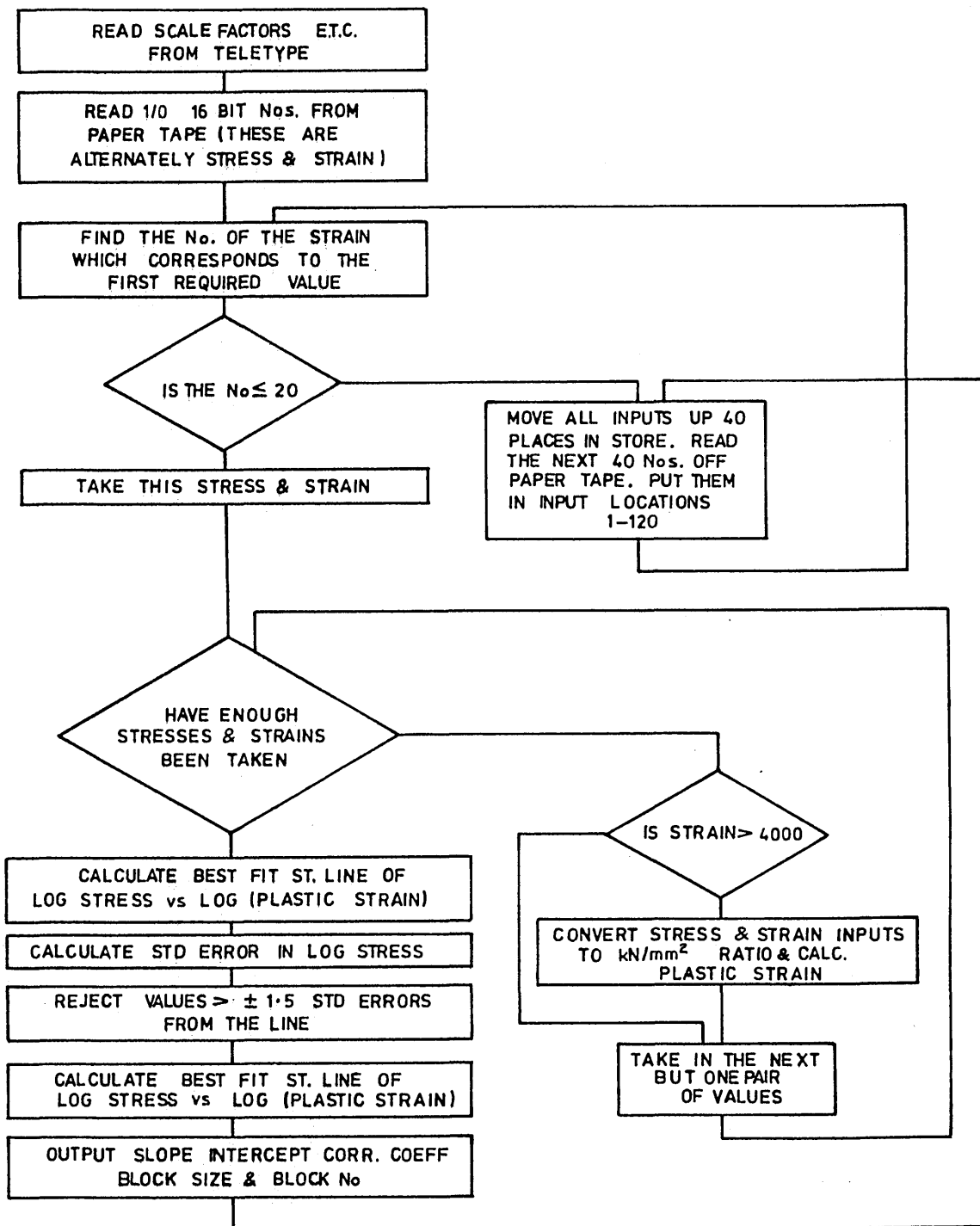


FIG.16. THE FLOW CHART FOR THE COMPUTER PROGRAMME USED TO OBTAIN VALUES OF 'n'

Fig.17

Microstructure of cast 40  
x 250

Fig.18

Microstructure of cast 34  
x 250

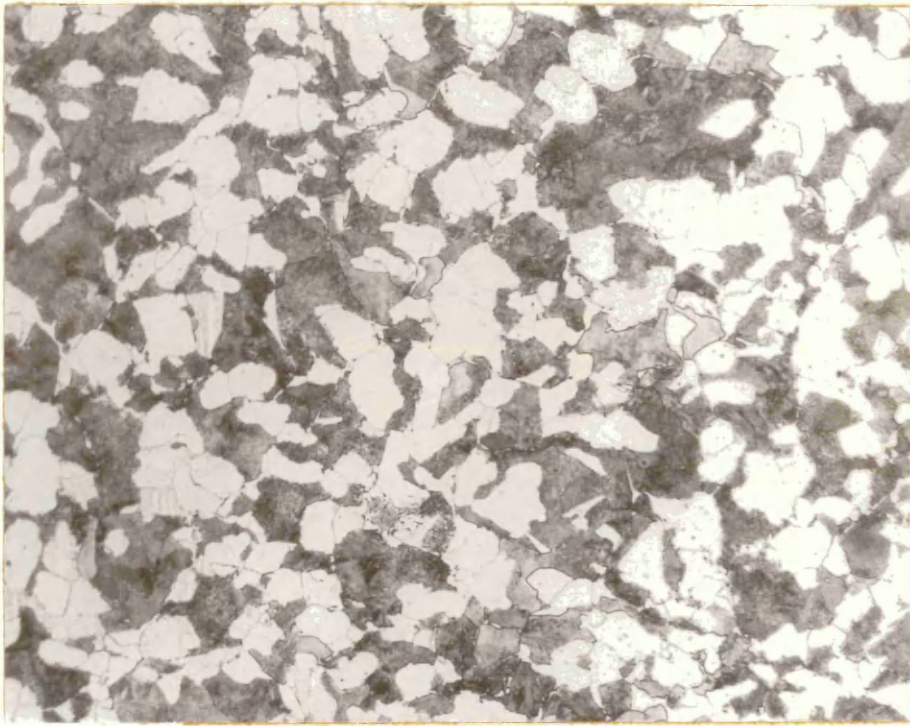


Fig.19

Microstructure of cast 07  
x 250

Fig.20

Microstructure of cast 72  
x 250

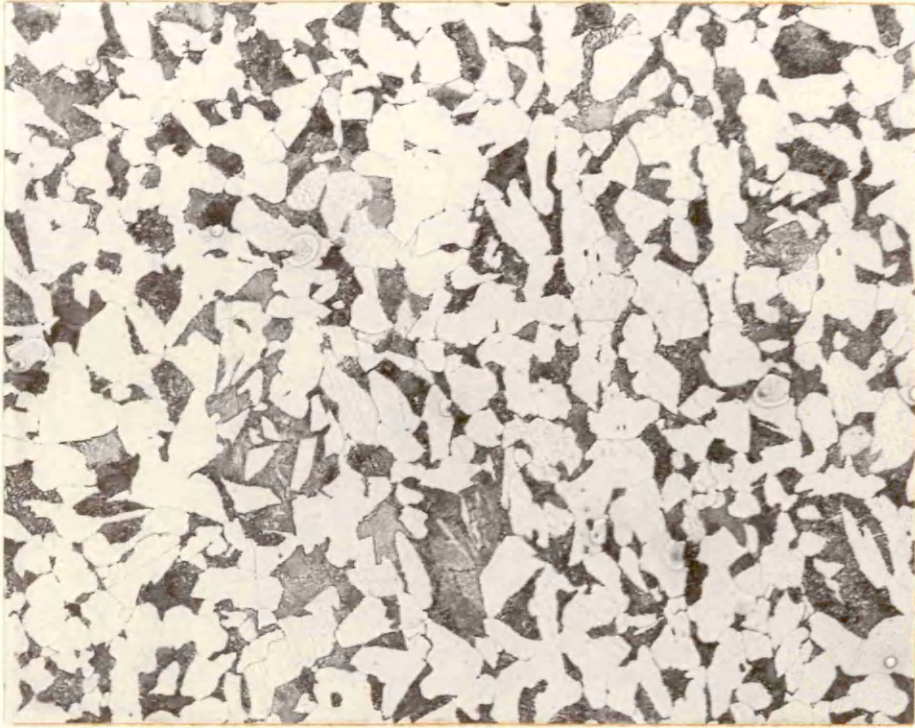


Fig.21

Microstructure of cast 26  
x 250

Fig.22

Microstructure of cast 36  
x 250





Fig.23

Microstructure of cast 78

x 250

Fig.24

Microstructure of cast 74 .

x 250



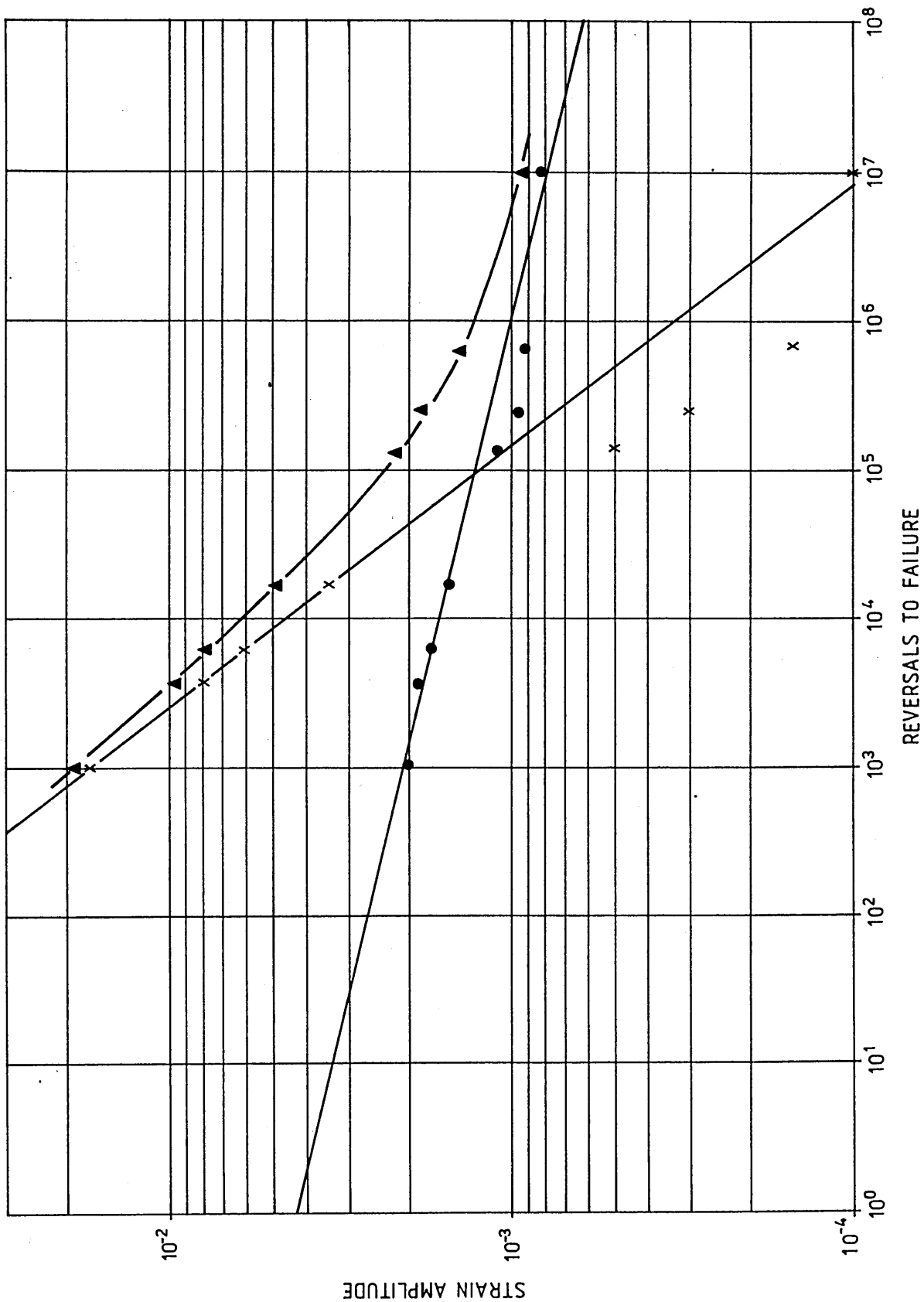


FIG. 25. FATIGUE CURVES FOR CAST 40

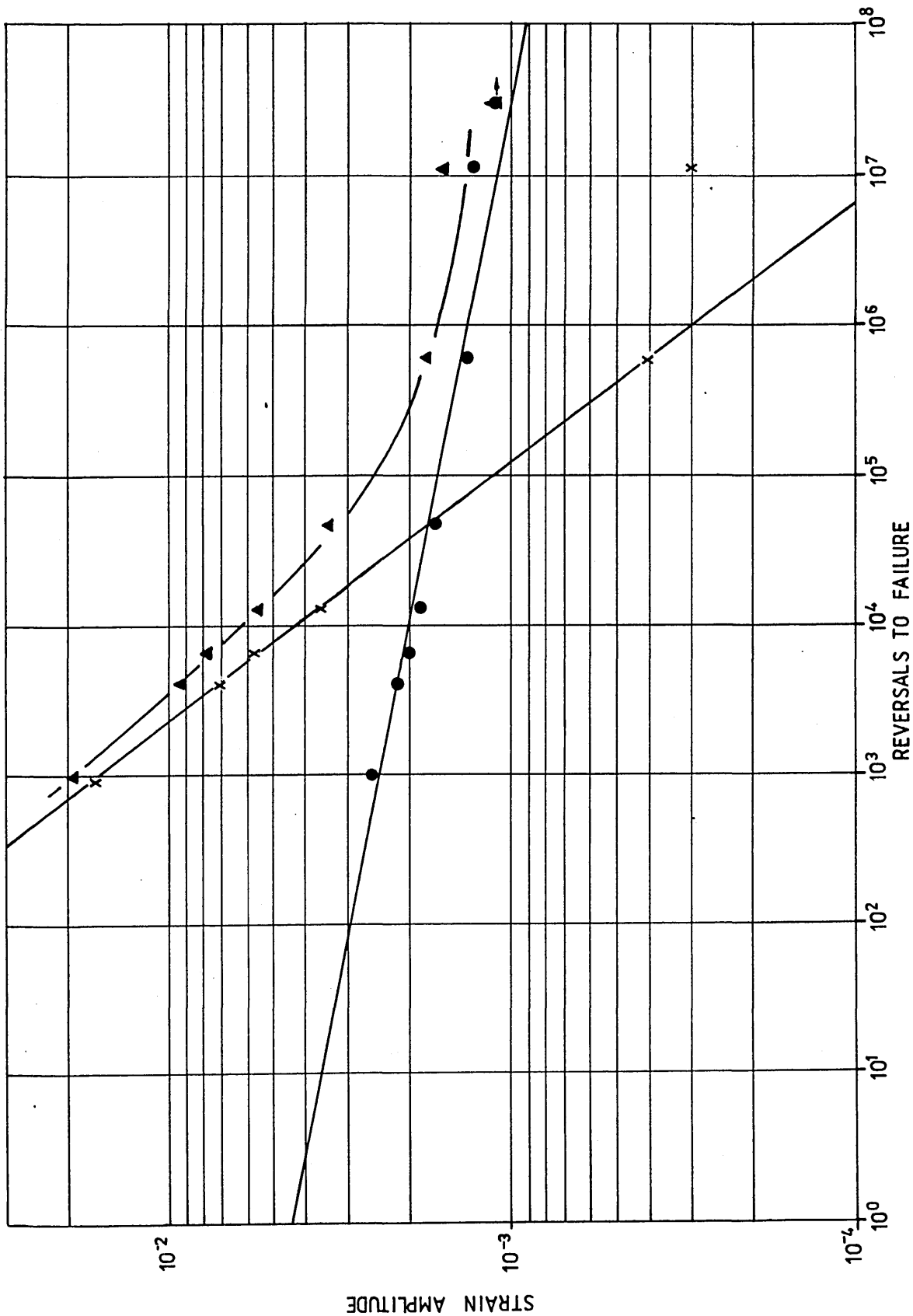


FIG. 26. FATIGUE CURVES FOR CAST 34.

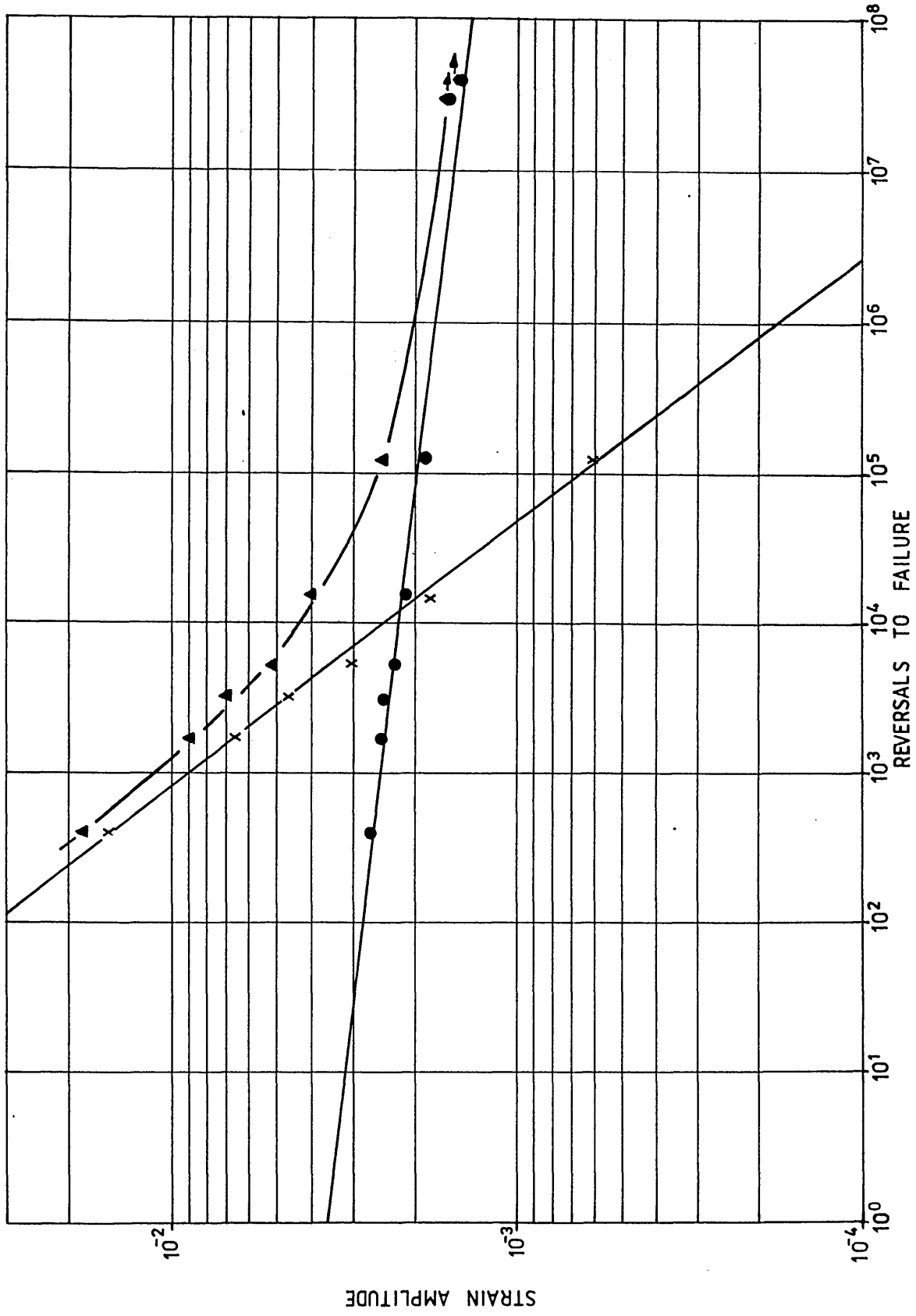


FIG. 27. FATIGUE CURVES FOR CAST 07.

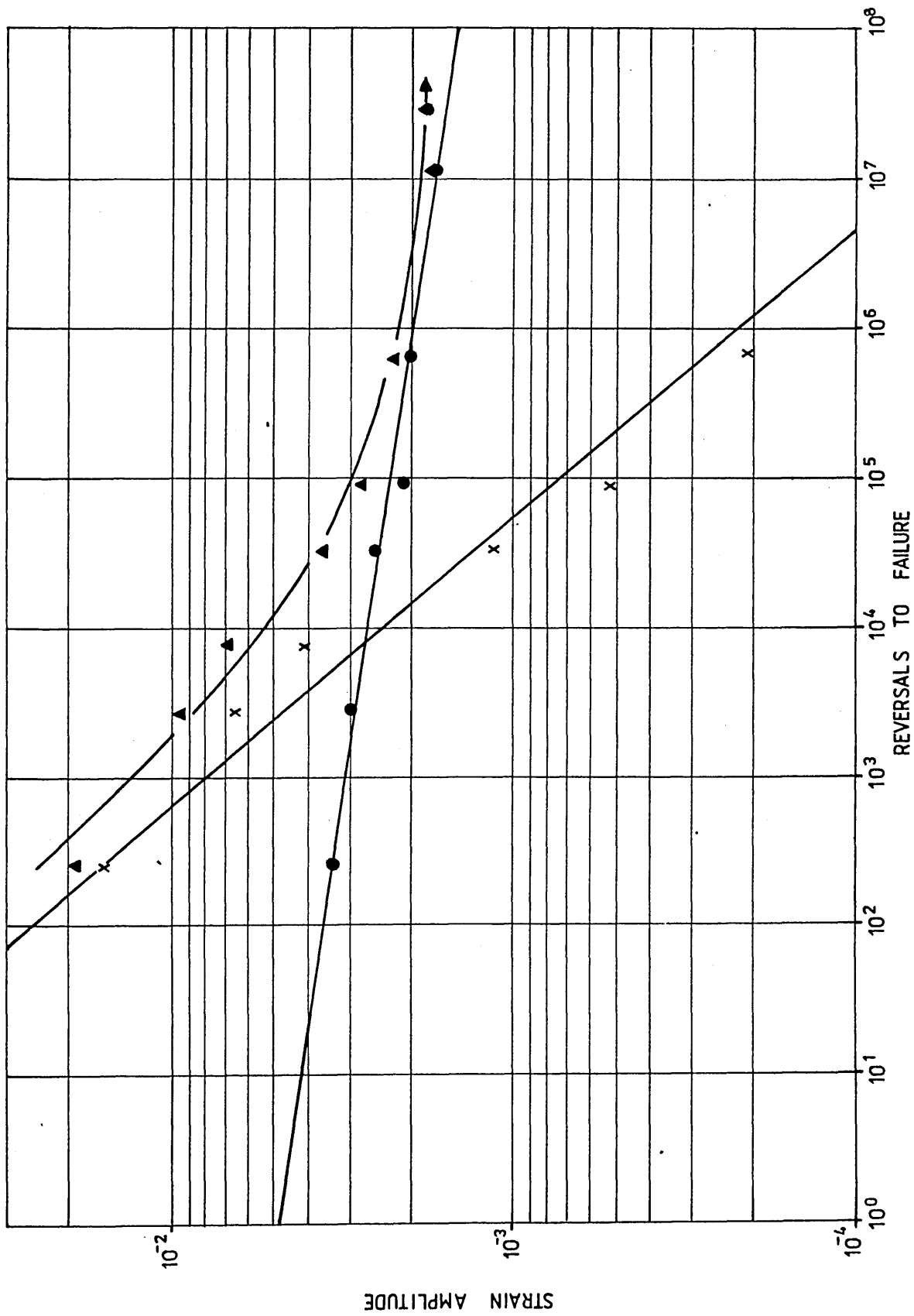


FIG. 28. FATIGUE CURVES FOR CAST 72.

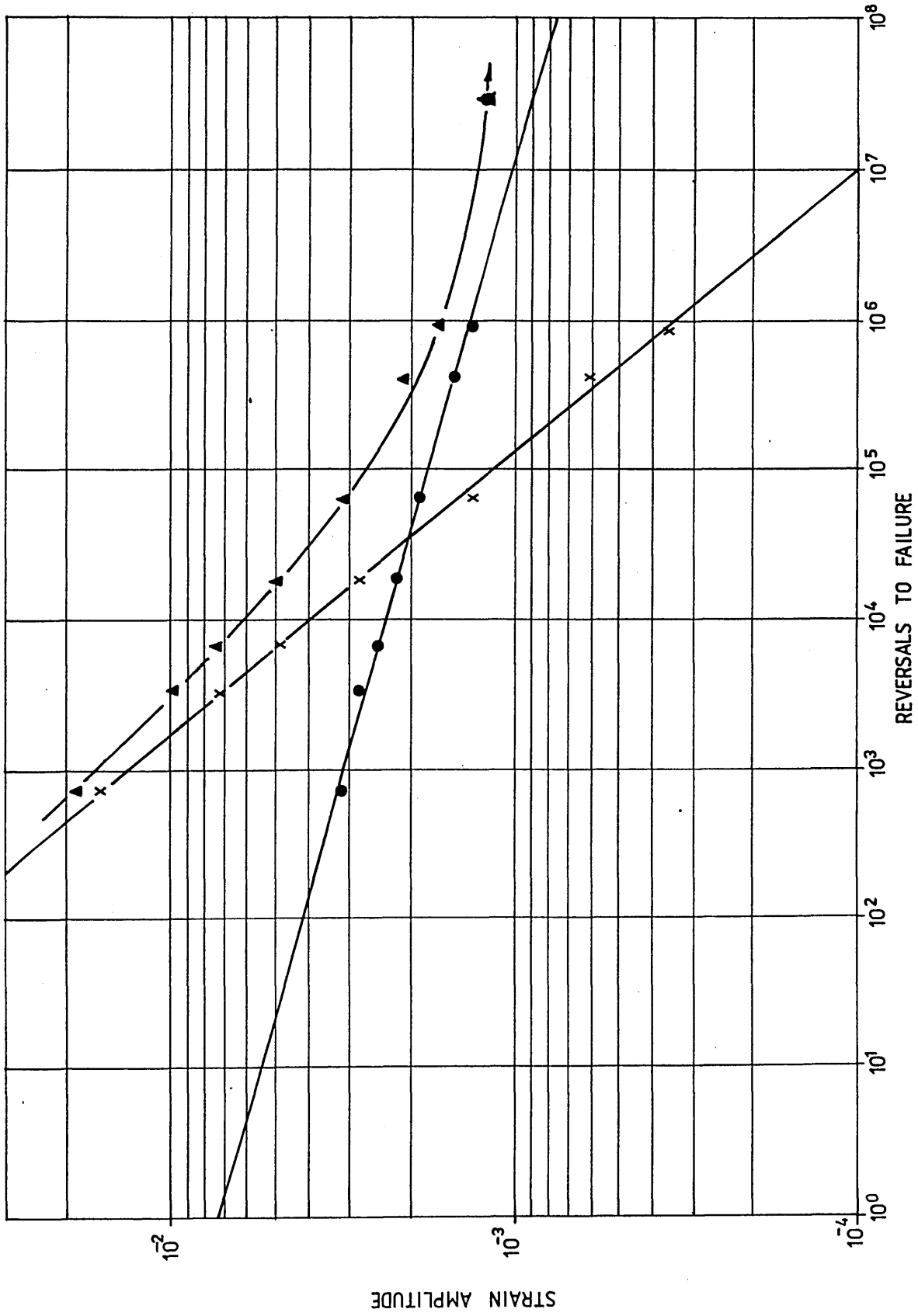
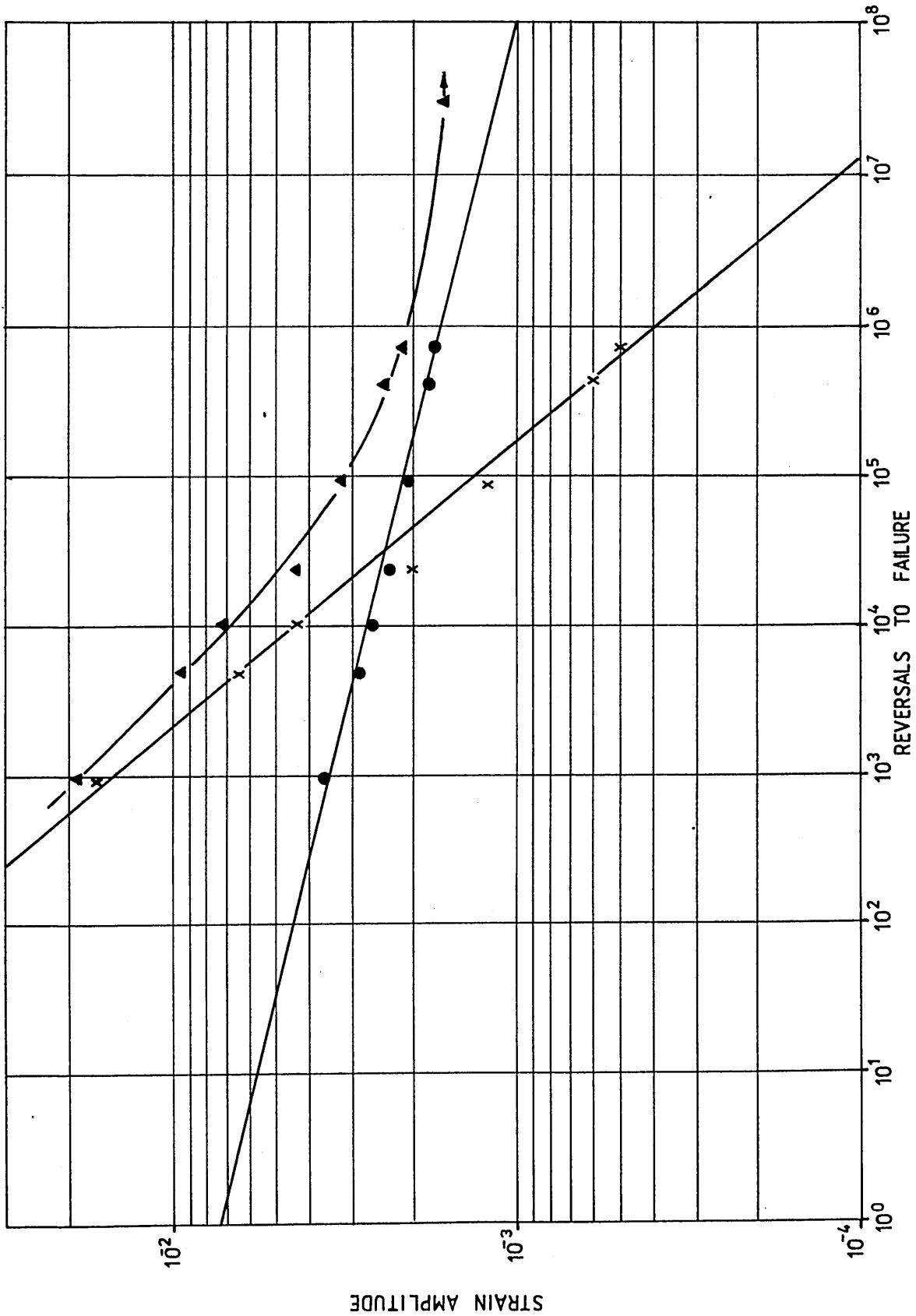


FIG. 29. FATIGUE CURVES FOR CAST 26



**FIG. 30. FATIGUE CURVES FOR CAST 36.**

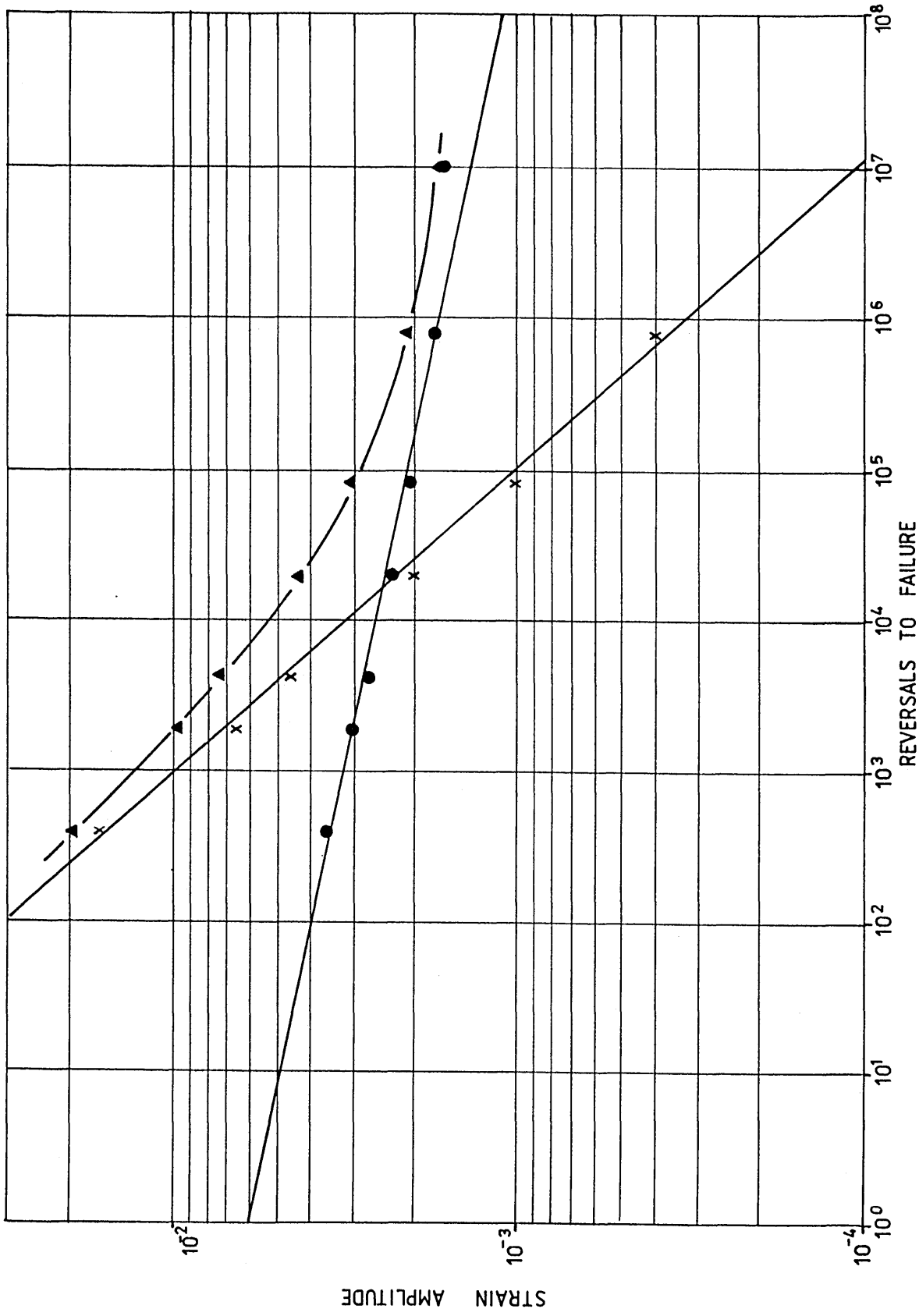


FIG. 31. FATIGUE CURVES FOR CAST 78.

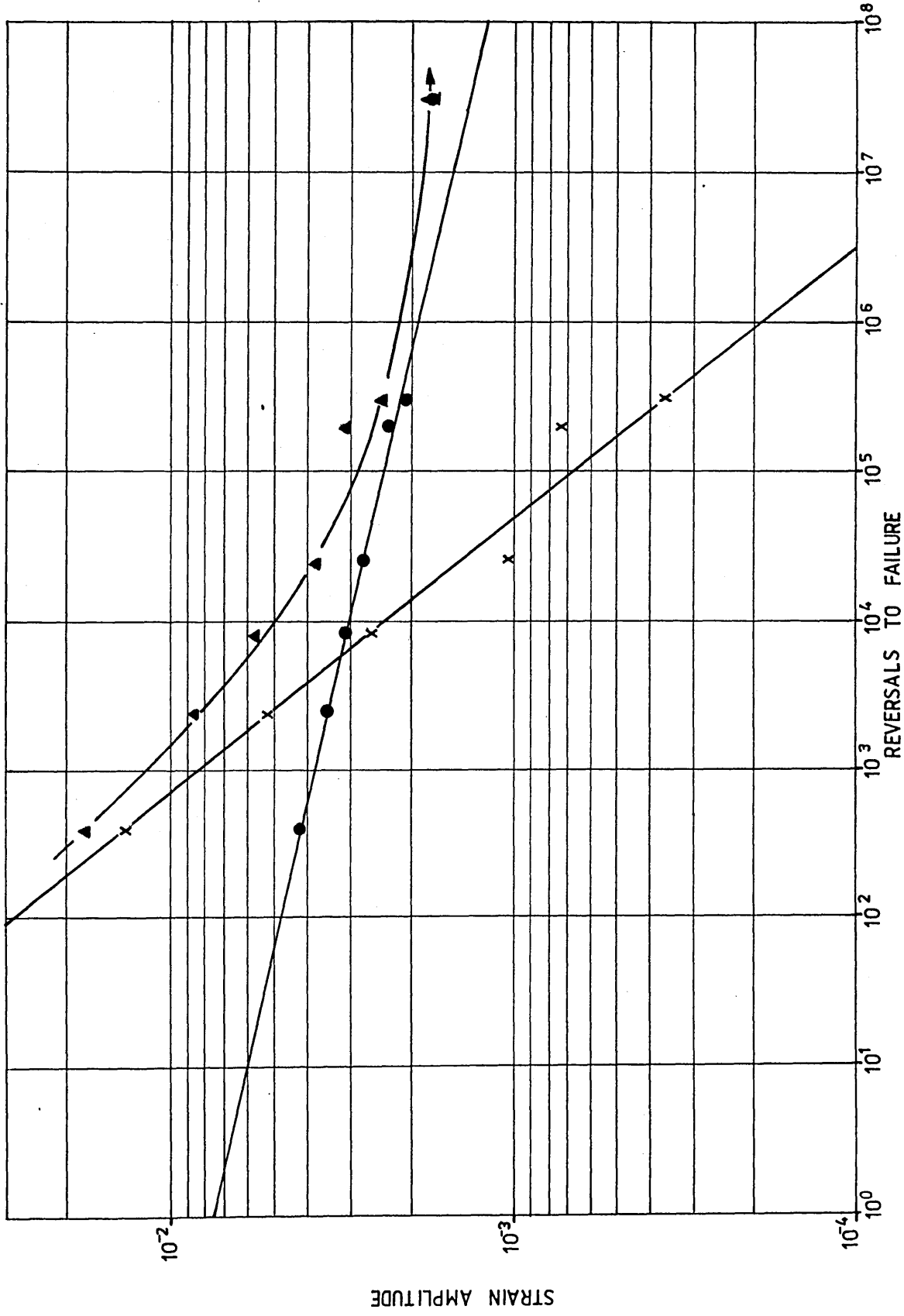


FIG. 32. FATIGUE CURVES FOR CAST 74

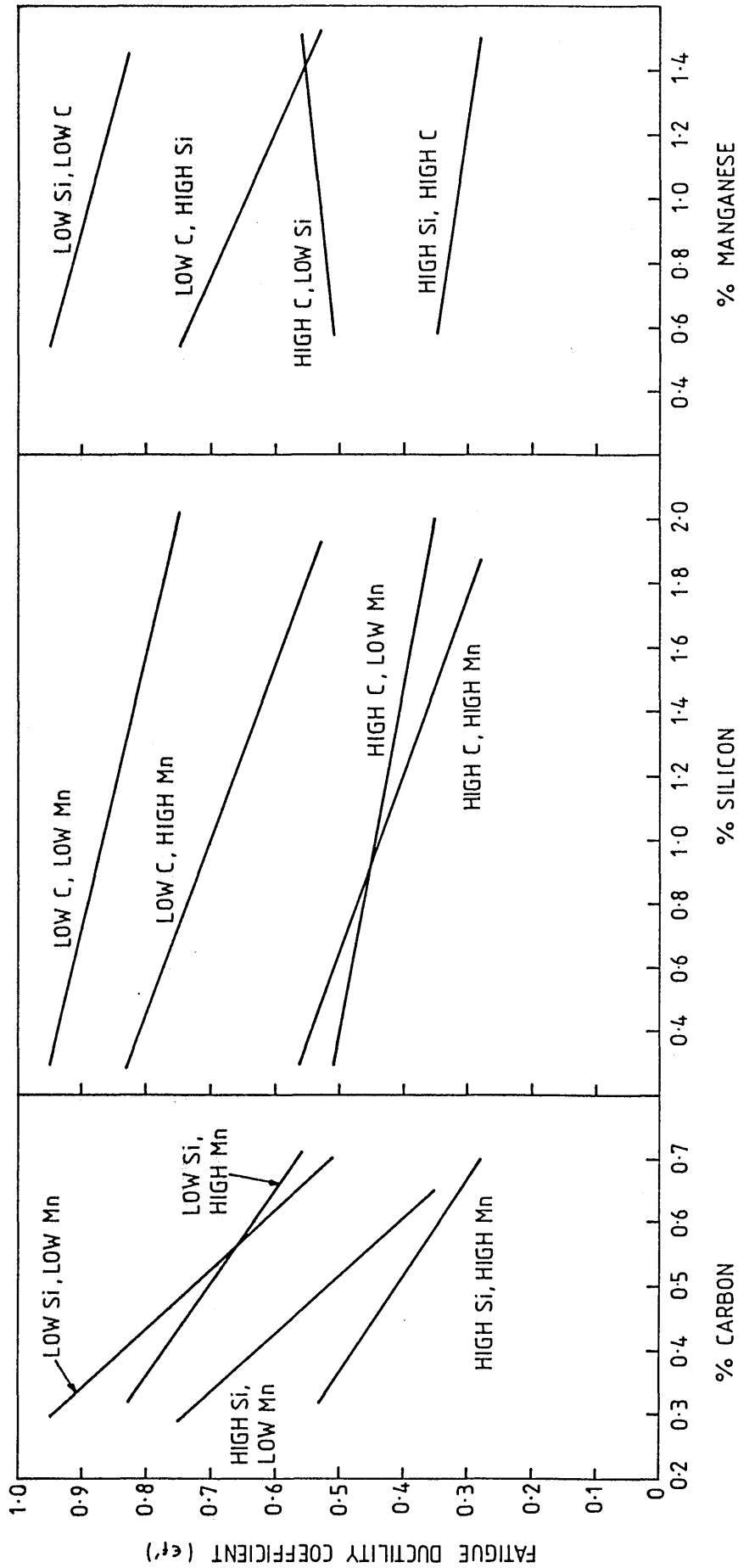


FIG. 33. EFFECT OF CARBON, SILICON AND MANGANESE ON FATIGUE DUCTILITY COEFFICIENT

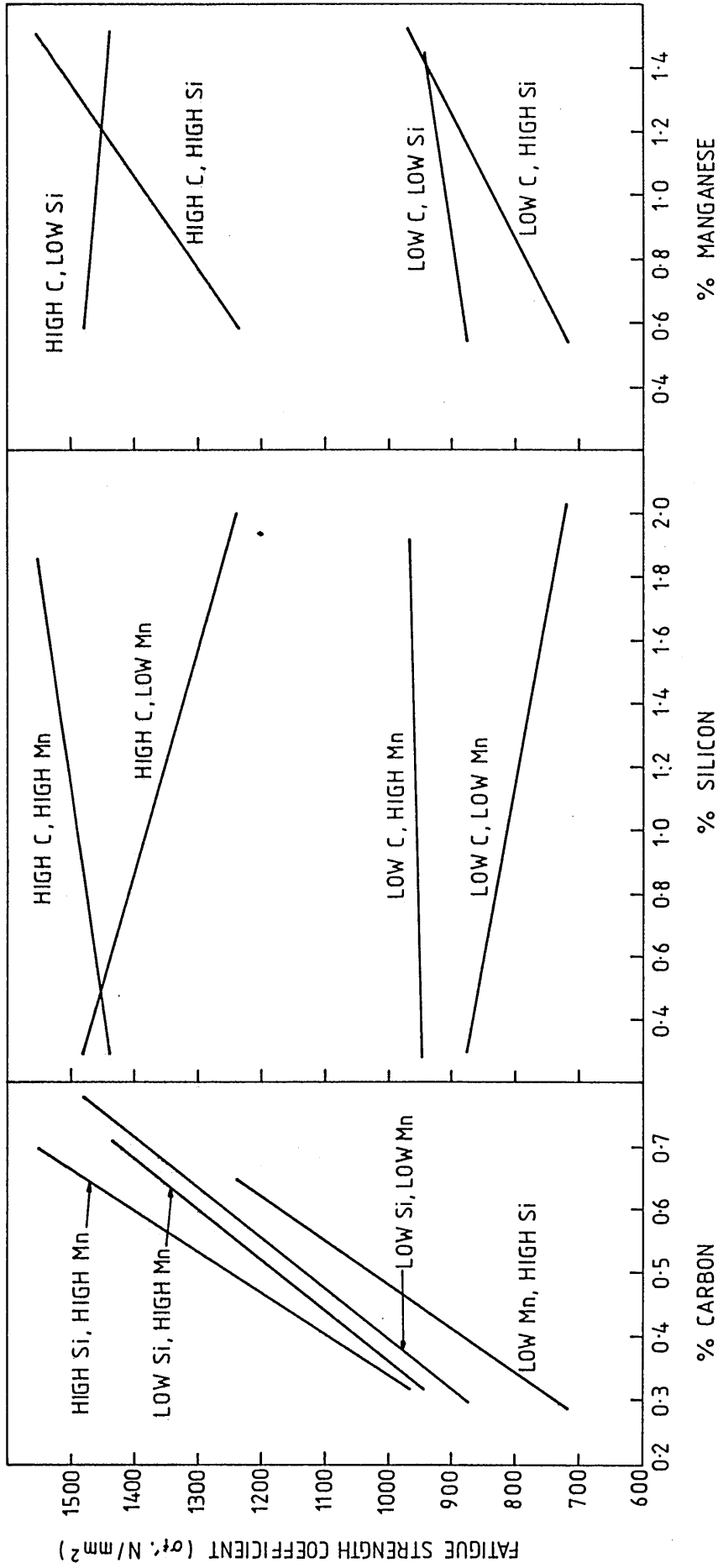
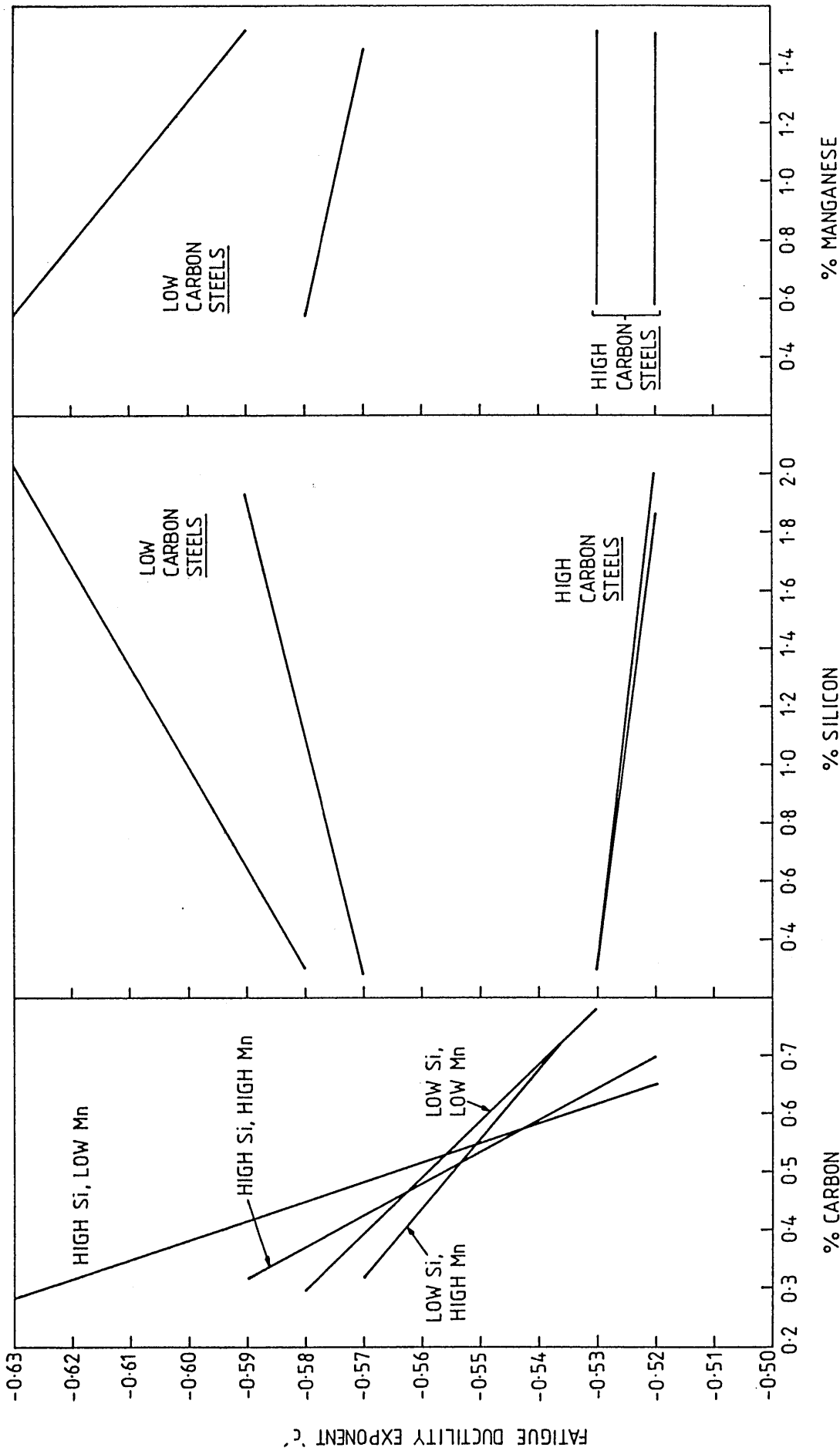


FIG. 34. EFFECT OF CARBON, SILICON AND MANGANESE ON FATIGUE STRENGTH COEFFICIENT



**FIG. 35. EFFECT OF CARBON, SILICON AND MANGANESE ON FATIGUE DUCTILITY EXPONENT**

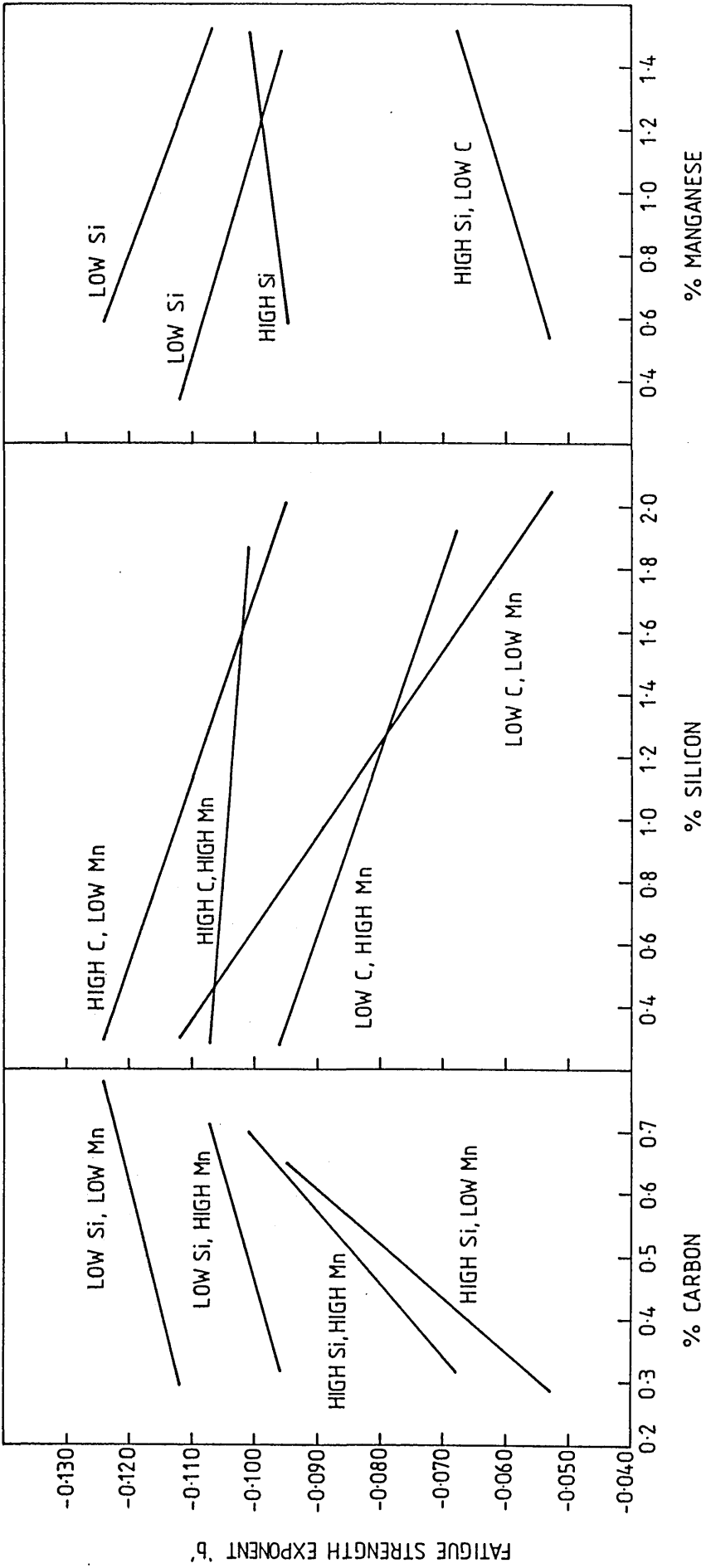


FIG. 36. EFFECT OF CARBON, SILICON AND MANGANESE ON FATIGUE STRENGTH EXPONENT

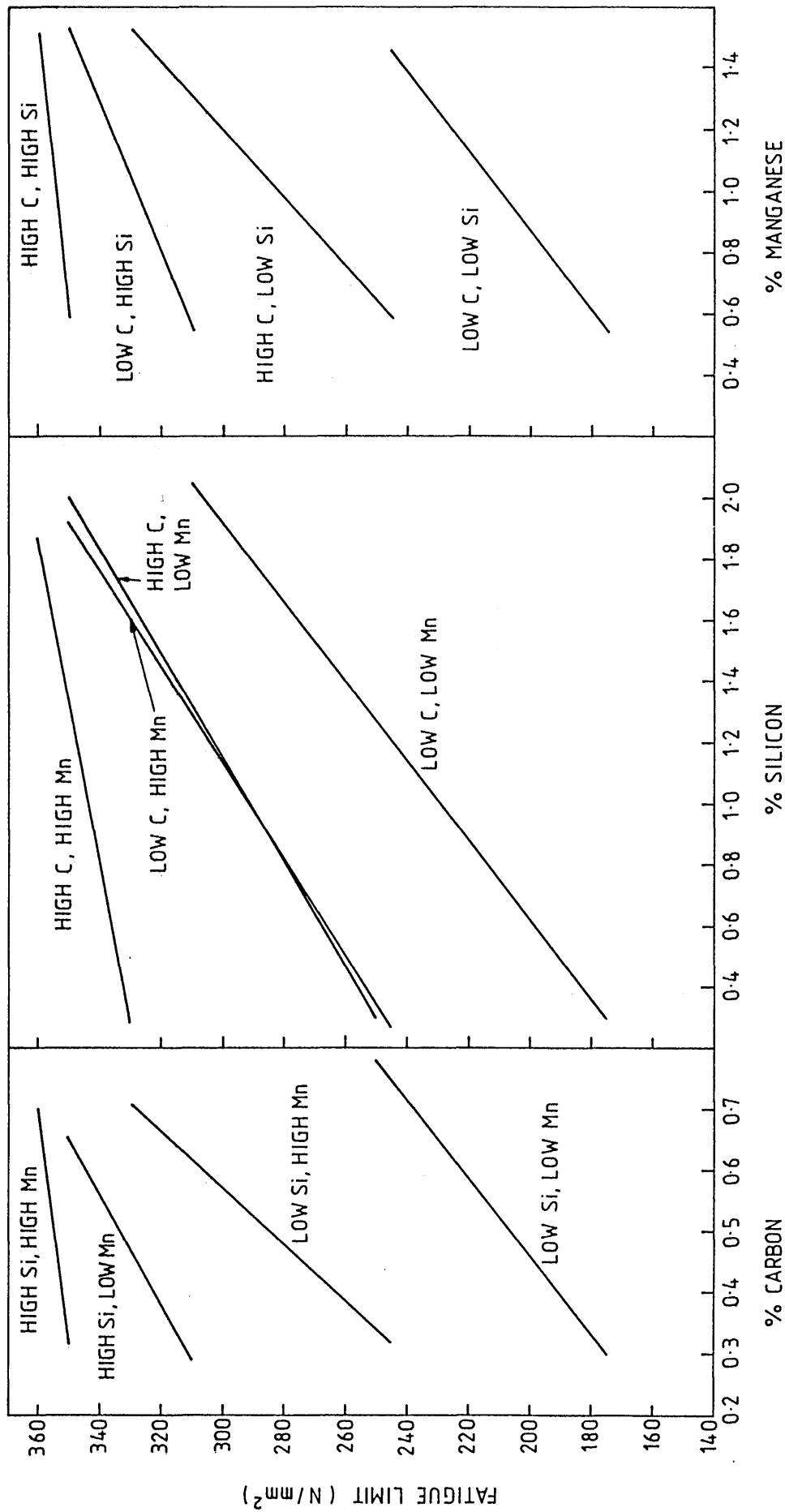


FIG. 37. EFFECT OF CARBON, SILICON AND MANGANESE ON FATIGUE LIMIT

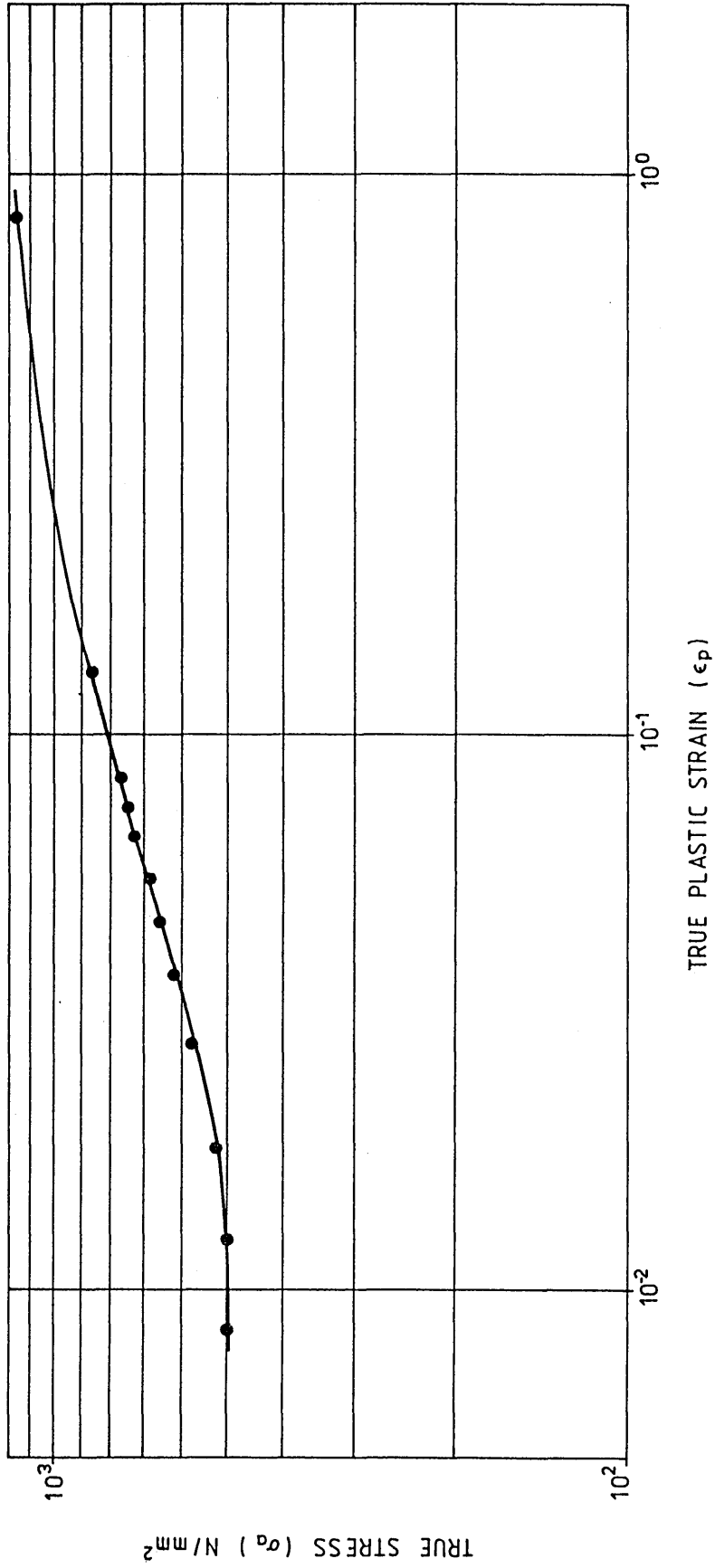


FIG. 38. MONOTONIC TRUE STRESS - TRUE PLASTIC STRAIN PLOT FOR CAST 72

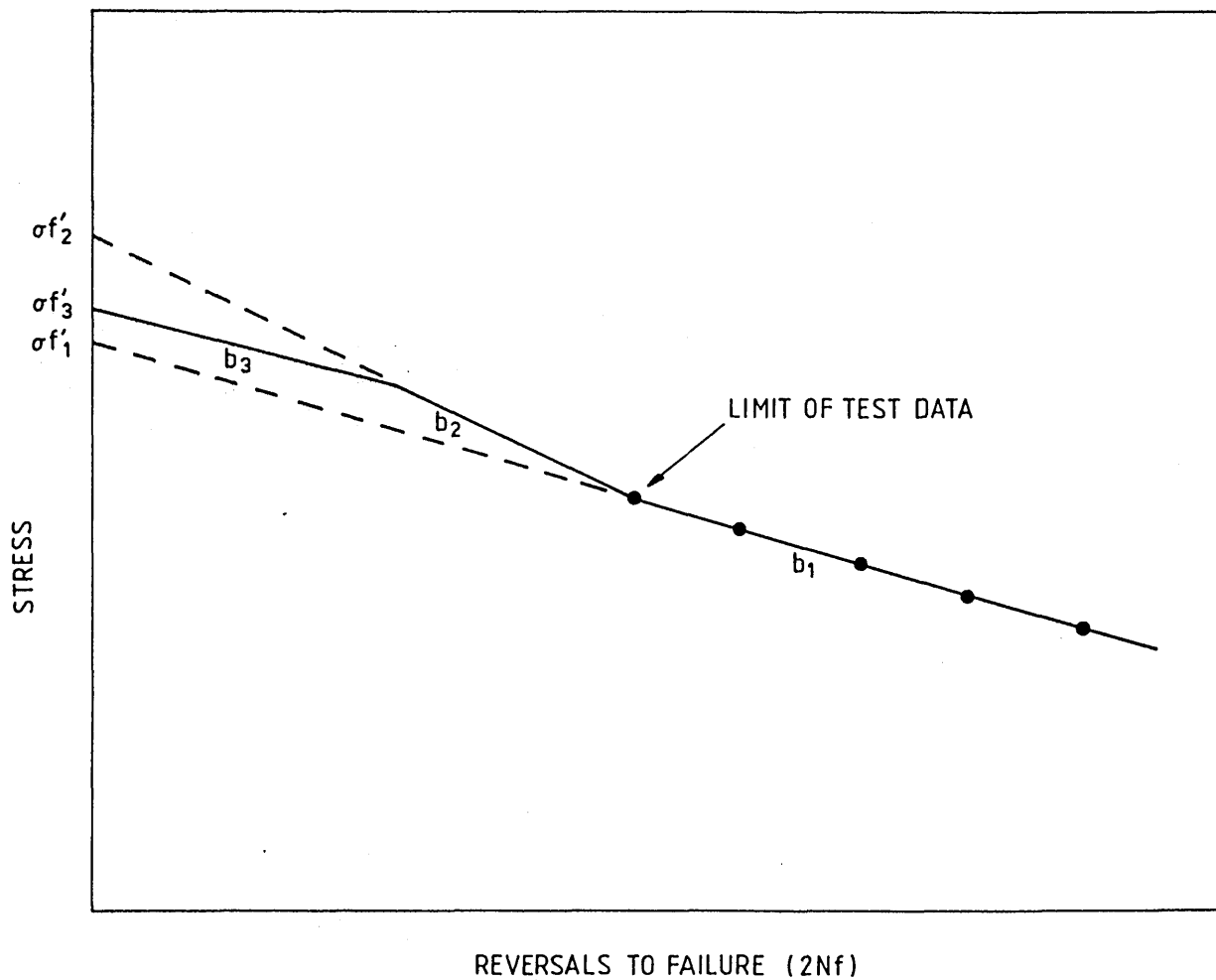


FIG. 39. DIAGRAMMATIC REPRESENTATION OF PROPOSED STRESS-LIFE RELATIONSHIP

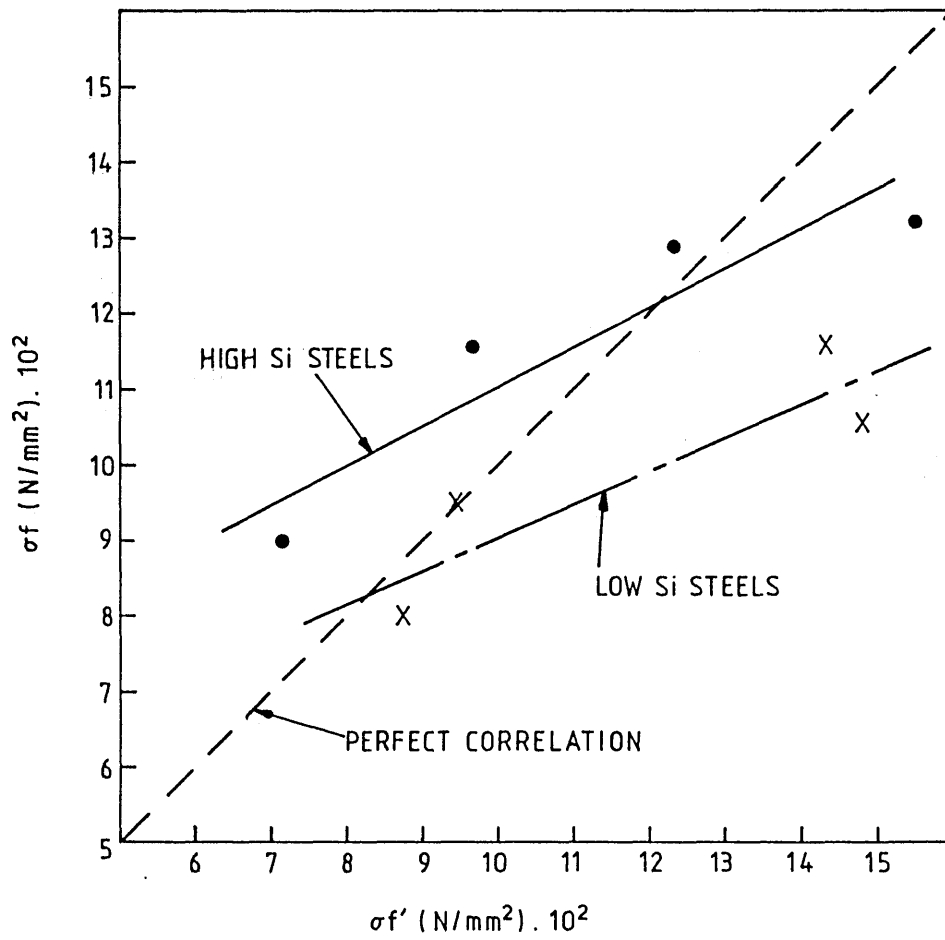


FIG. 40. CORRELATION BETWEEN FATIGUE STRENGTH COEFFICIENT AND MONOTONIC FRACTURE STRESS

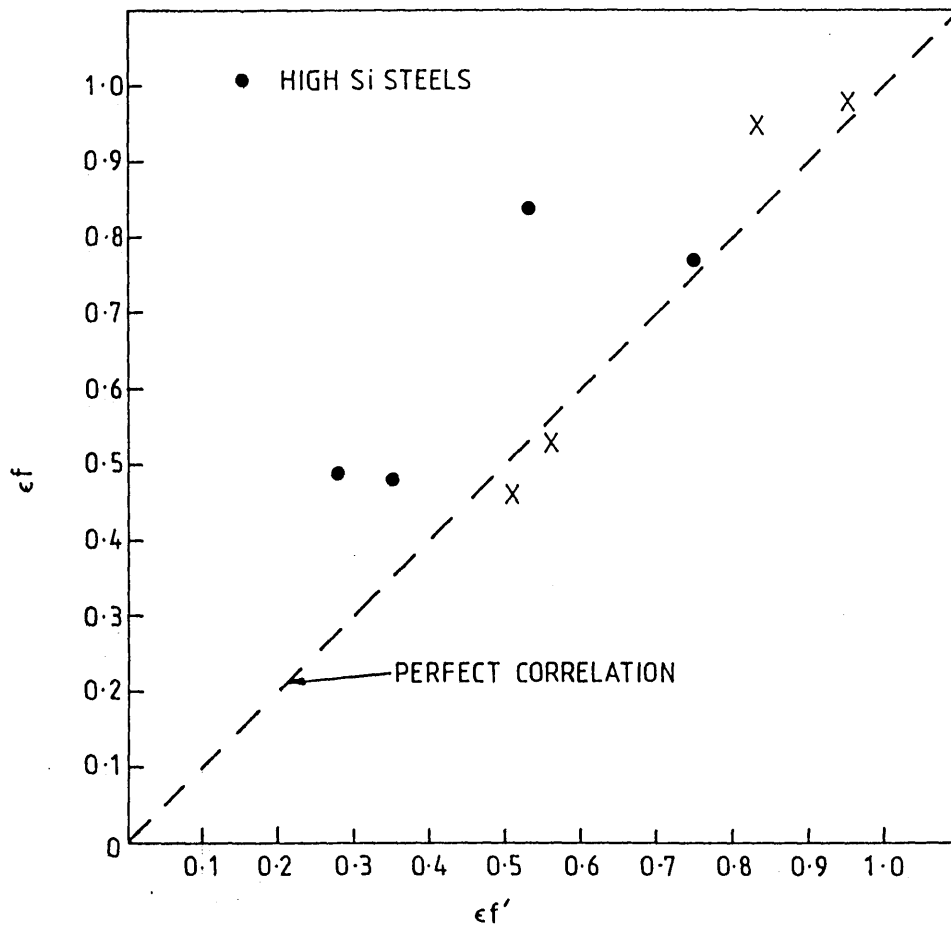


FIG. 41. COMPARISON BETWEEN FATIGUE DUCTILITY COEFFICIENT AND MONOTONIC FRACTURE STRAIN

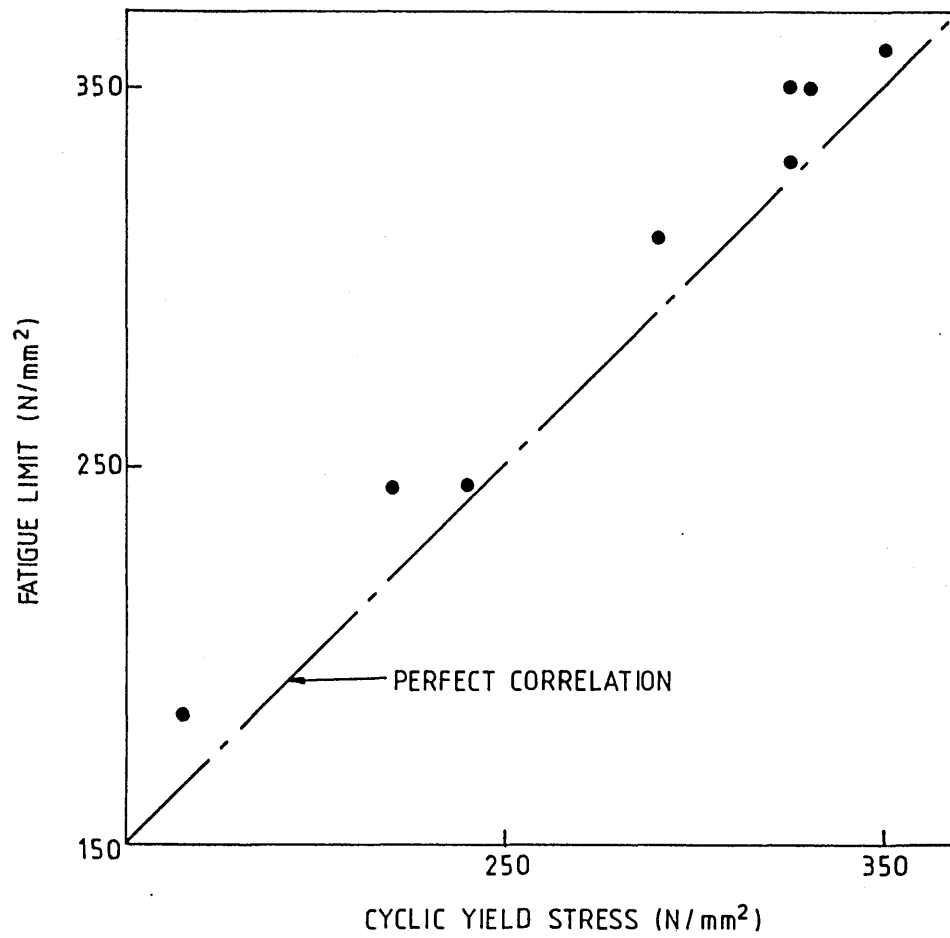


FIG. 42. COMPARISON BETWEEN CYCLIC YIELD STRESS AND MEASURED FATIGUE LIMIT

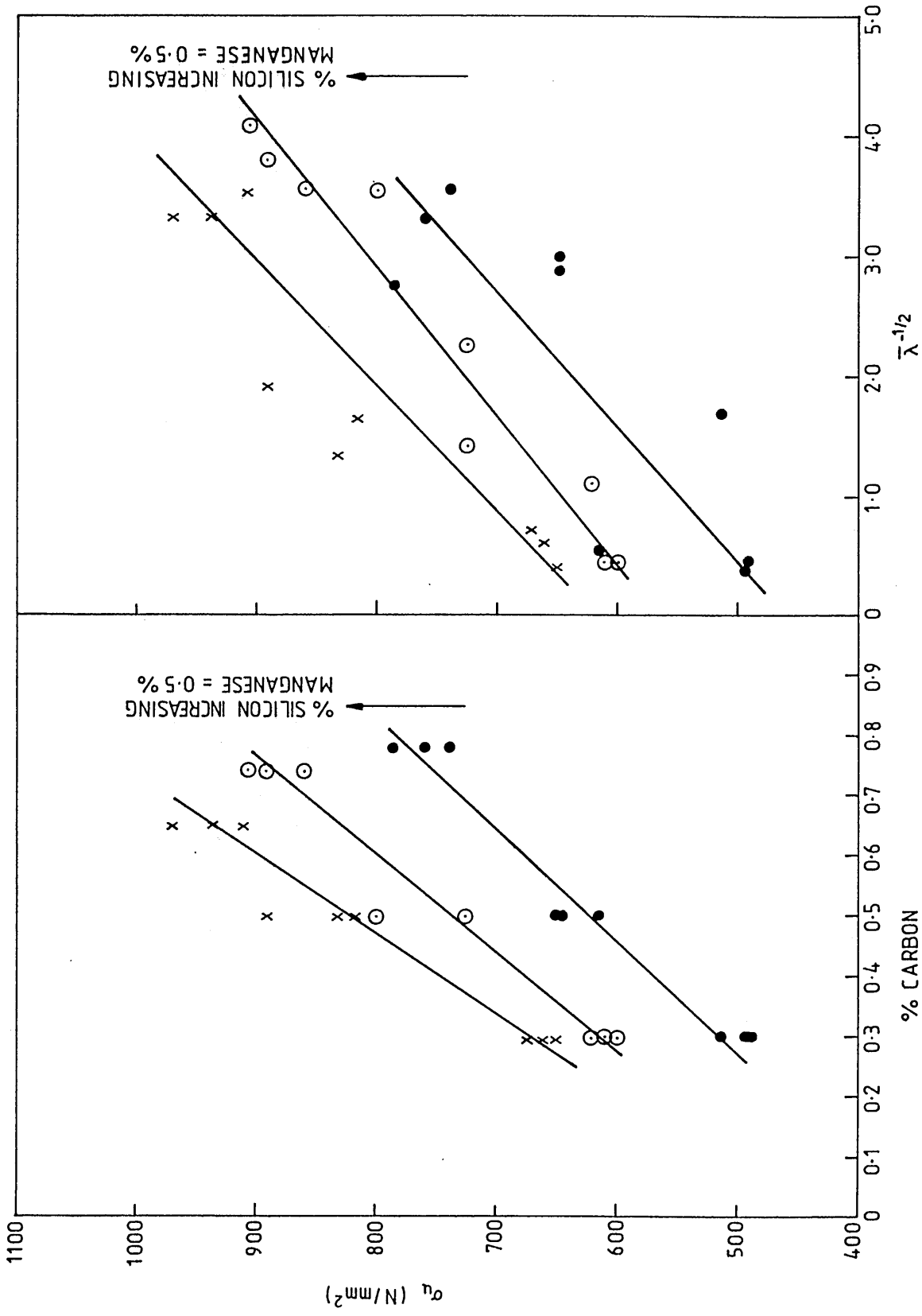


FIG. 4.3. STRUCTURE, COMPOSITION - PROPERTY CURVES

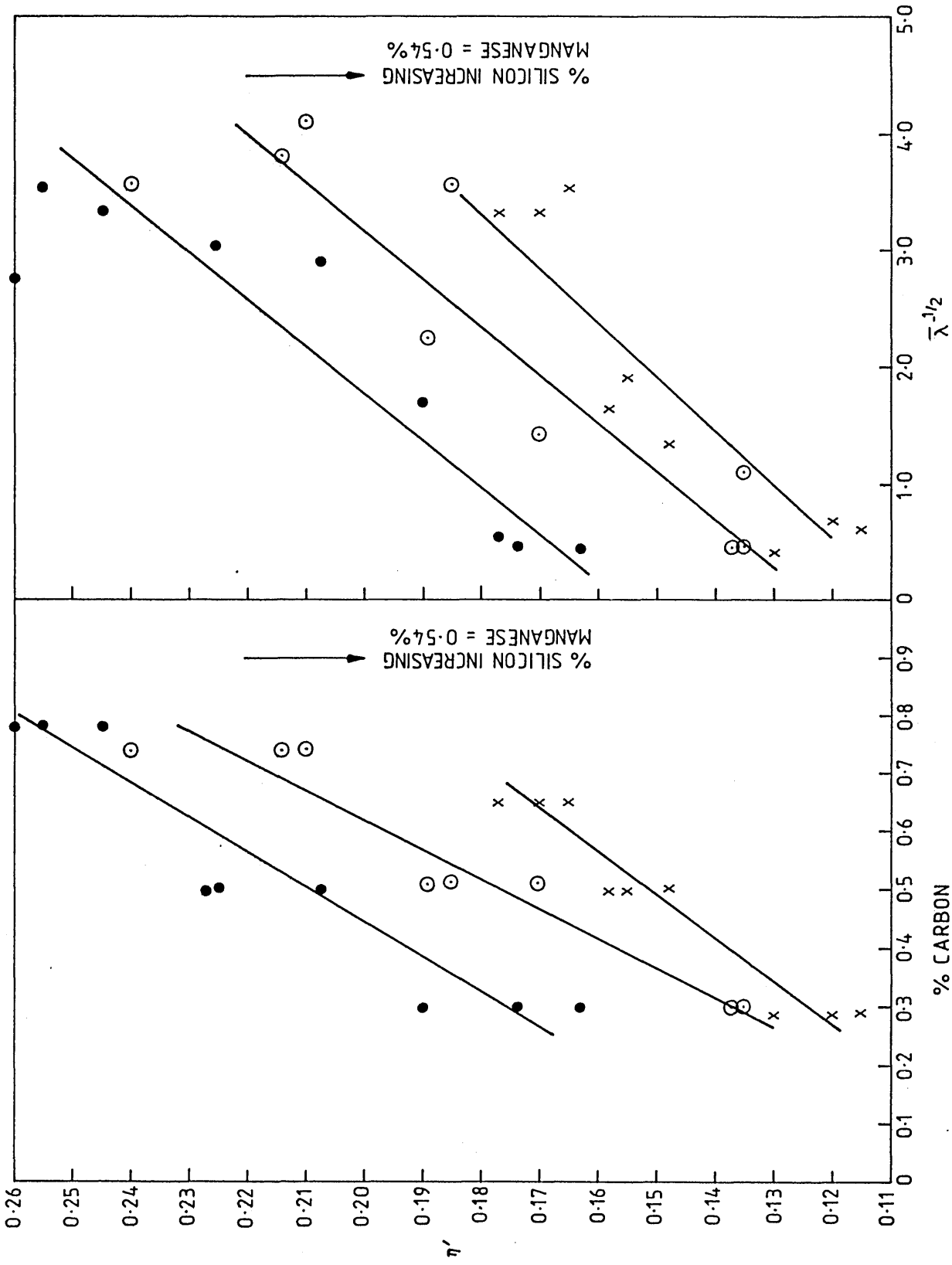


FIG. 4.4. STRUCTURE, COMPOSITION - PROPERTY CURVES

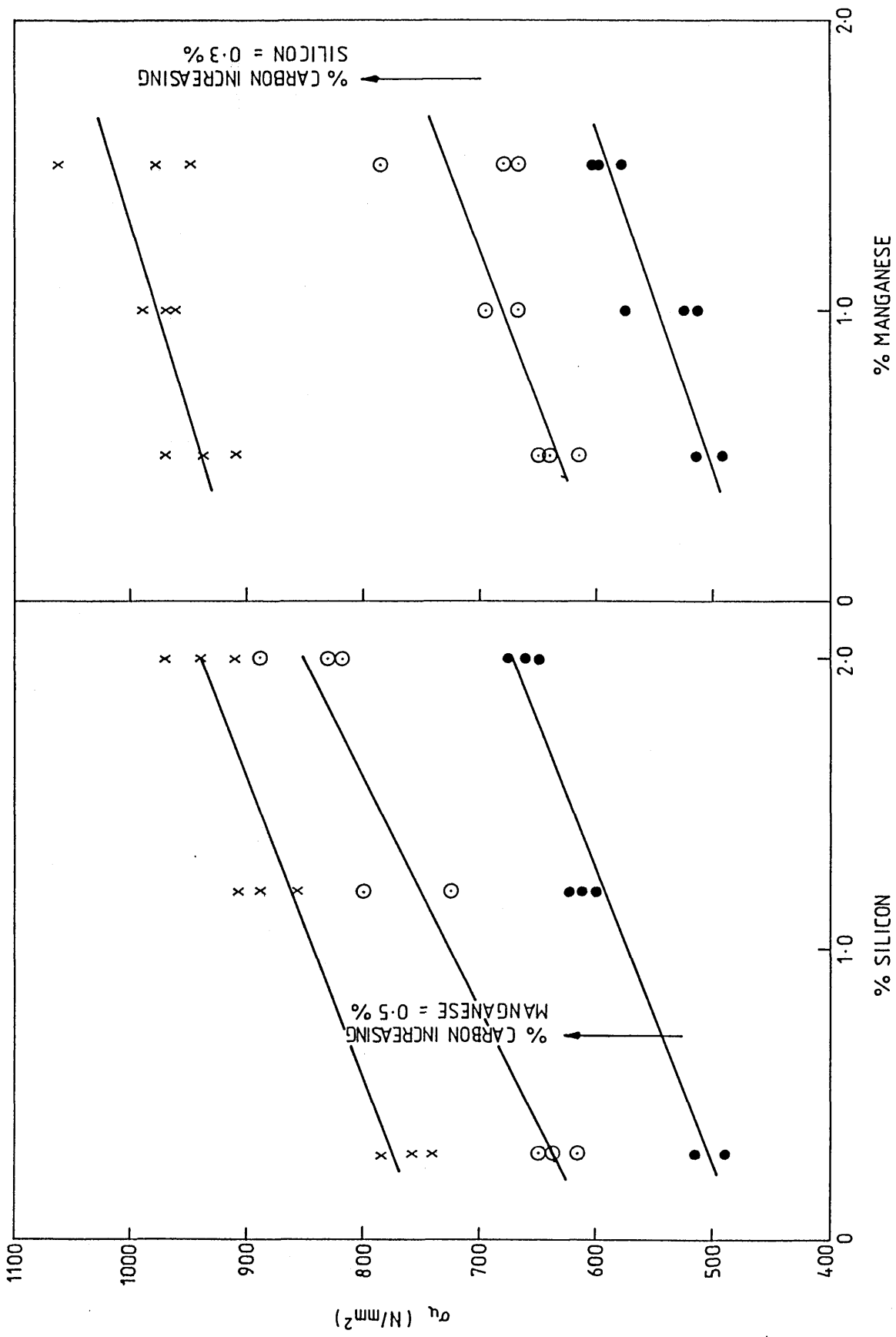


FIG. 45. COMPOSITION - PROPERTY CURVES

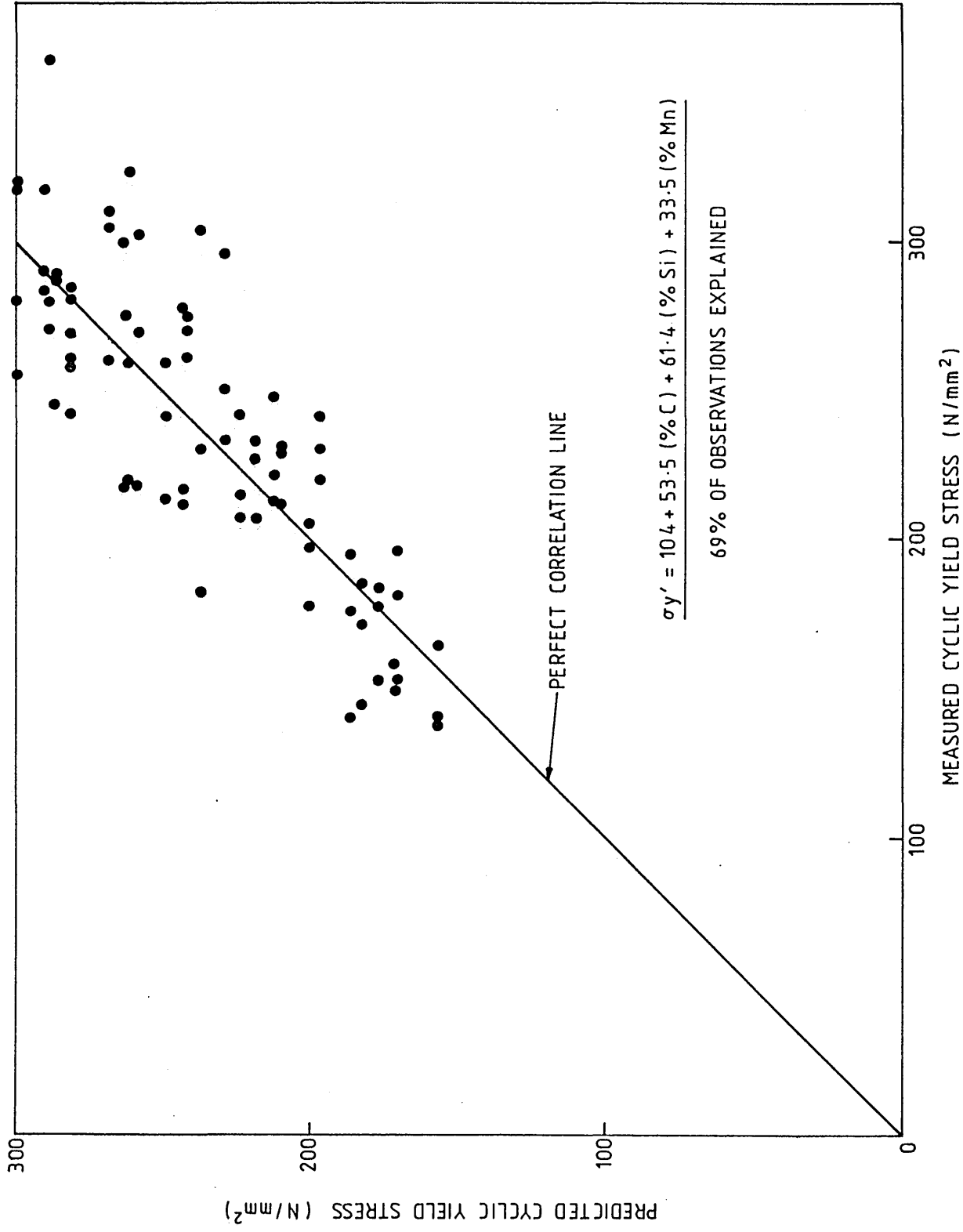


FIG. 46. PREDICTED AND MEASURED CYCLIC YIELD STRESS VALUES

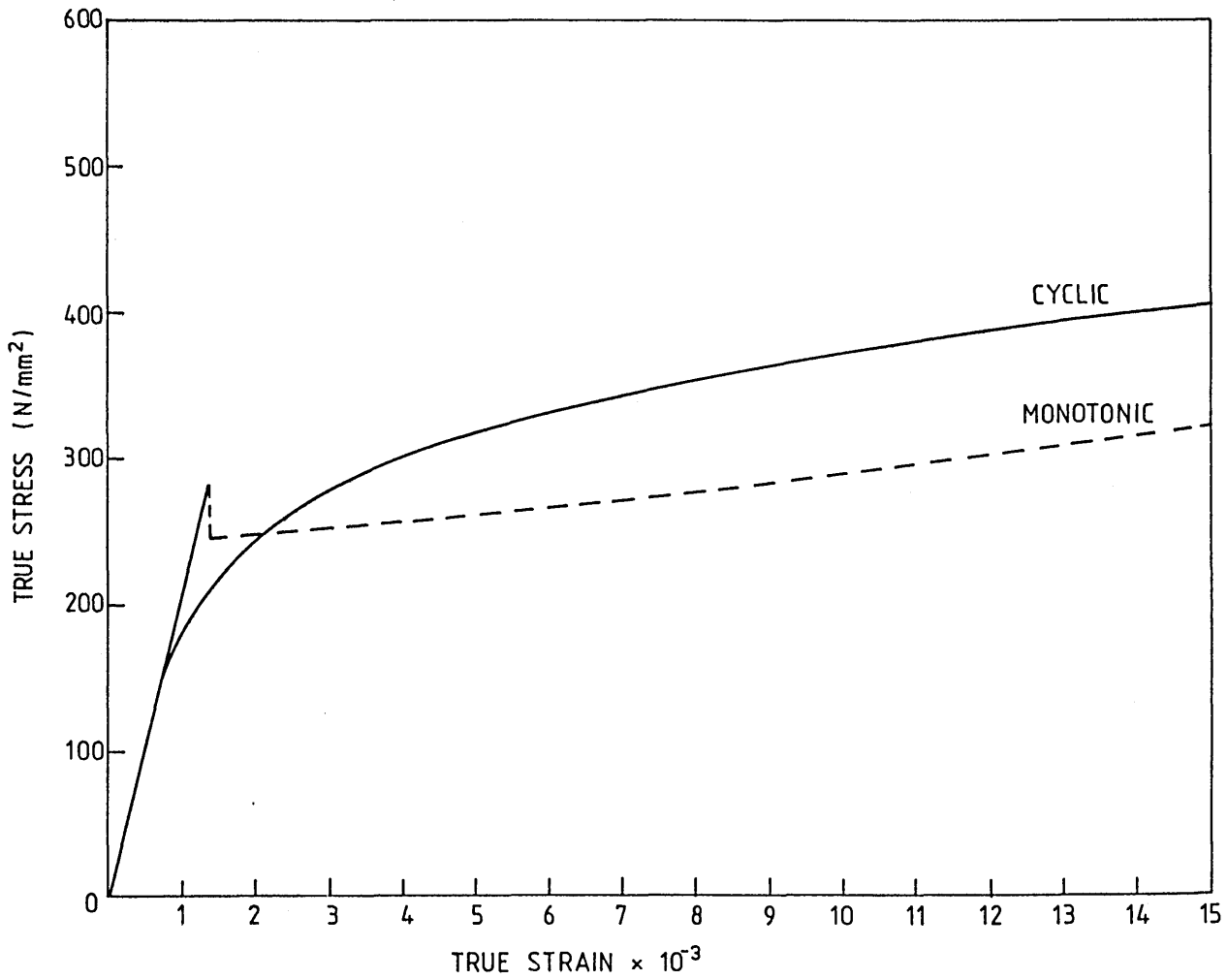


FIG. 47. CYCLIC AND MONOTONIC  $\sigma_a - \epsilon_t$  CURVES FOR CAST 40

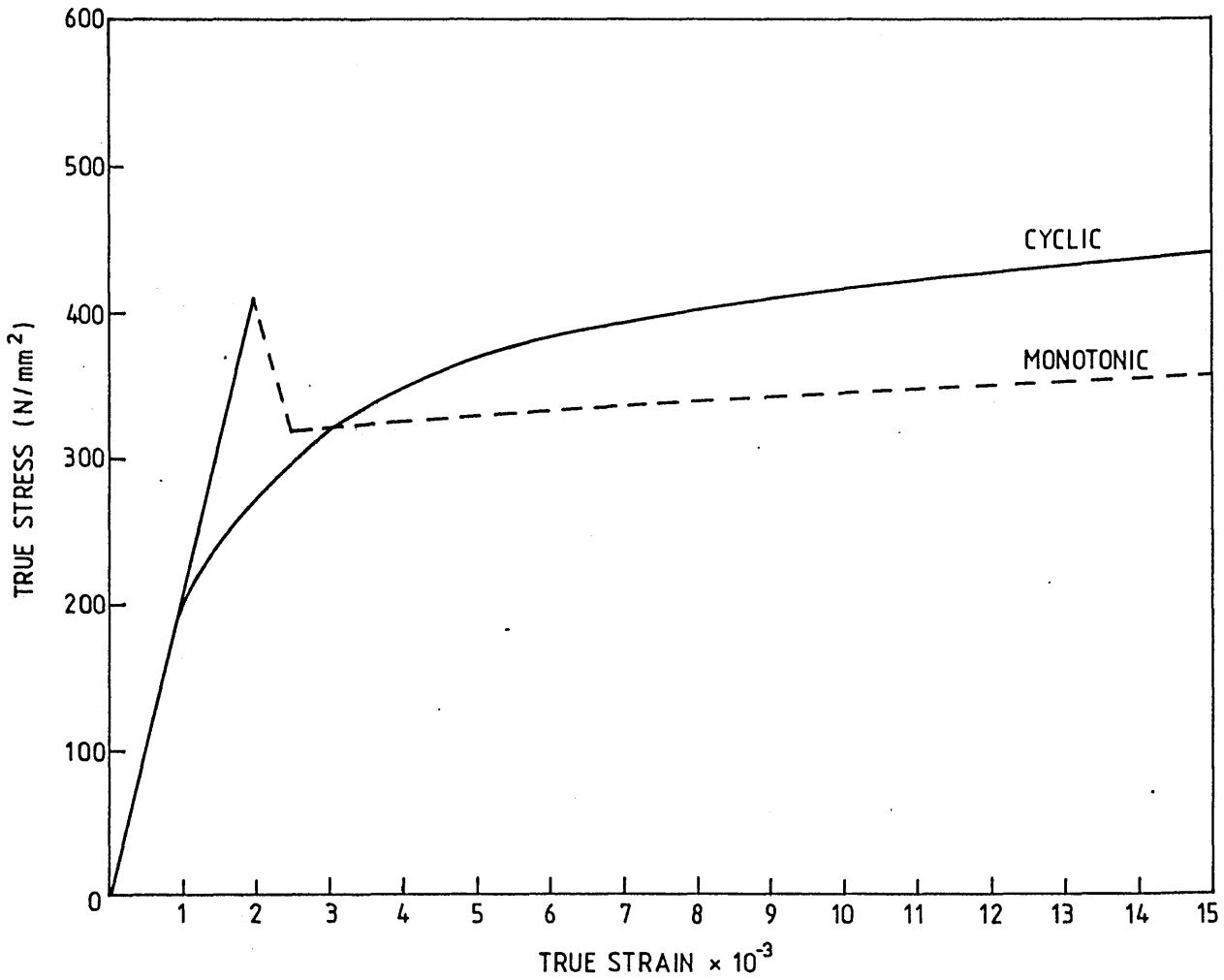


FIG. 48. CYCLIC AND MONOTONIC  $\sigma_a - \epsilon_t$  CURVES FOR CAST 34

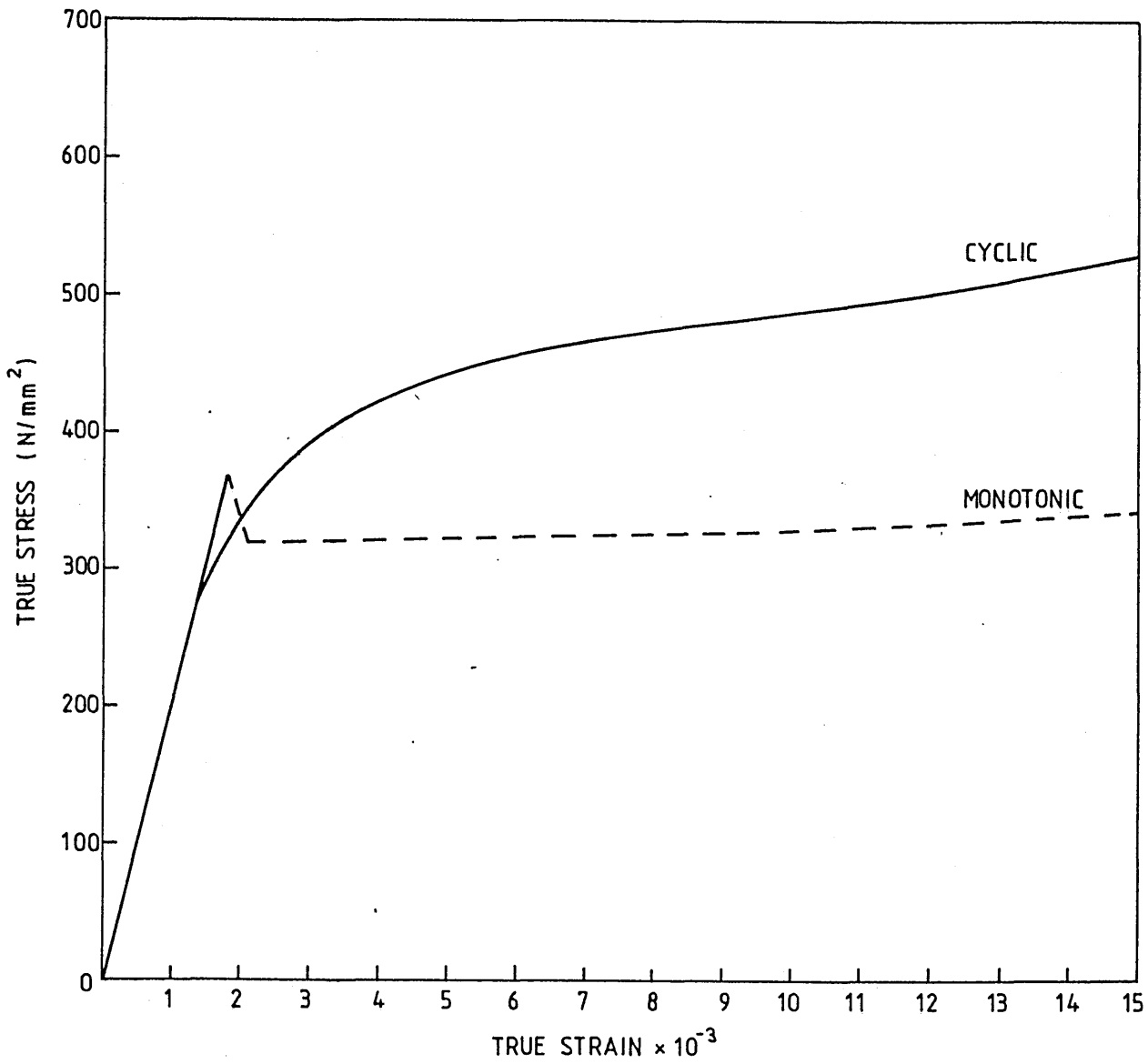


FIG. 49. CYCLIC AND MONOTONIC  $\sigma_a - \epsilon_t$  CURVES FOR CAST 07

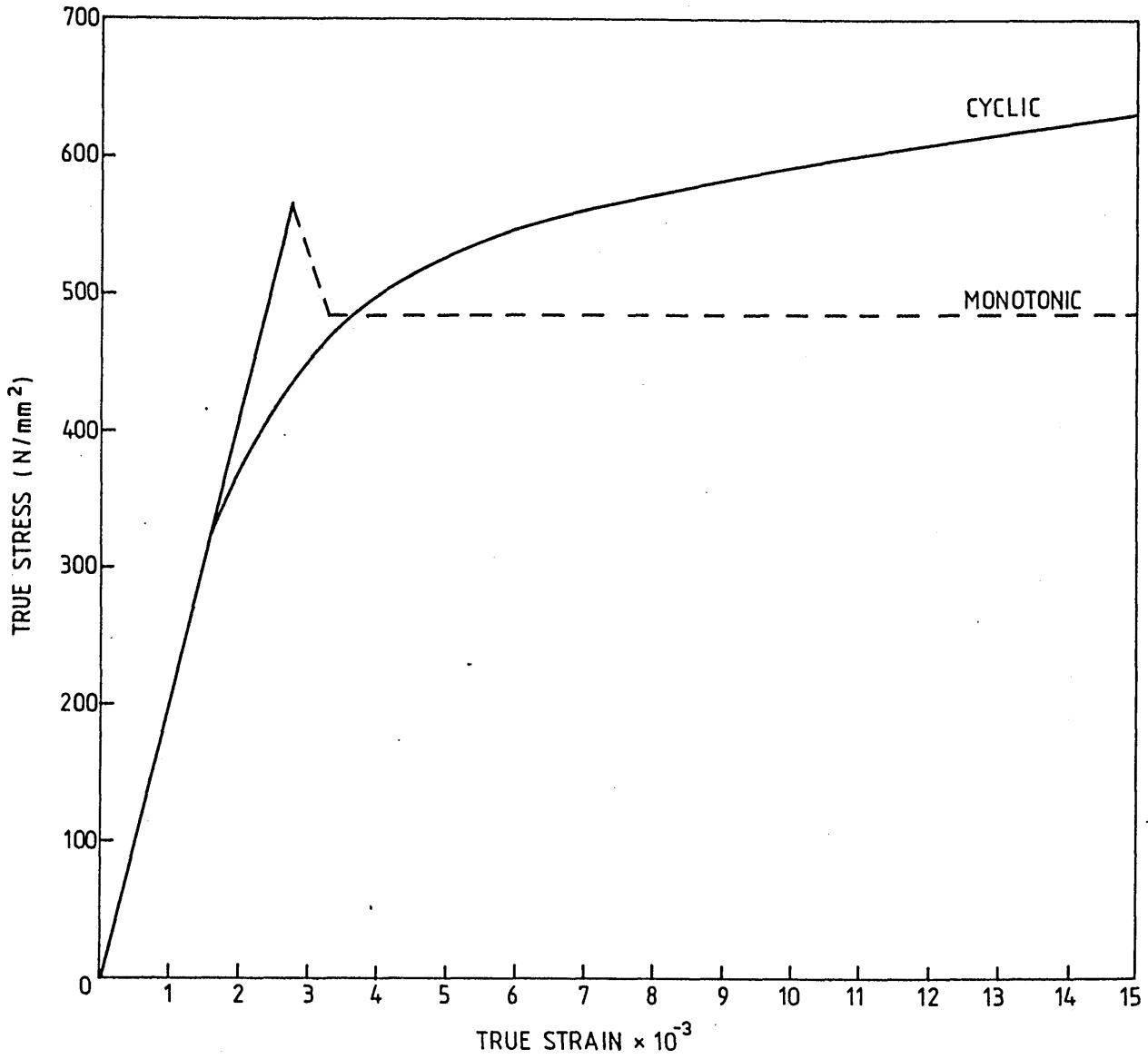


FIG. 50. CYCLIC AND MONOTONIC  $\sigma_a - \epsilon_t$  CURVES FOR CAST 72

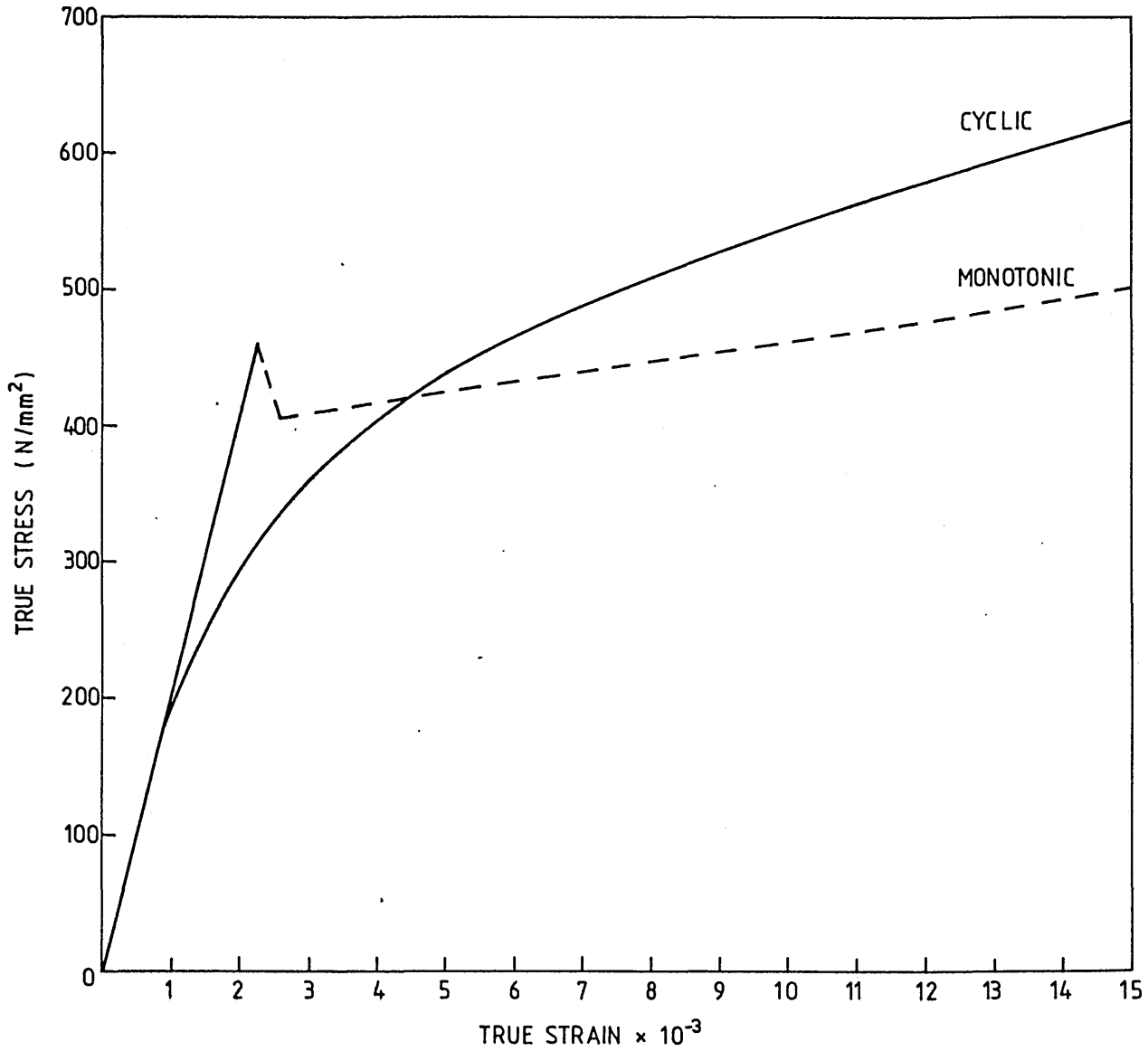


FIG. 51. CYCLIC AND MONOTONIC  $\sigma_a - \epsilon_t$  CURVES FOR CAST 26

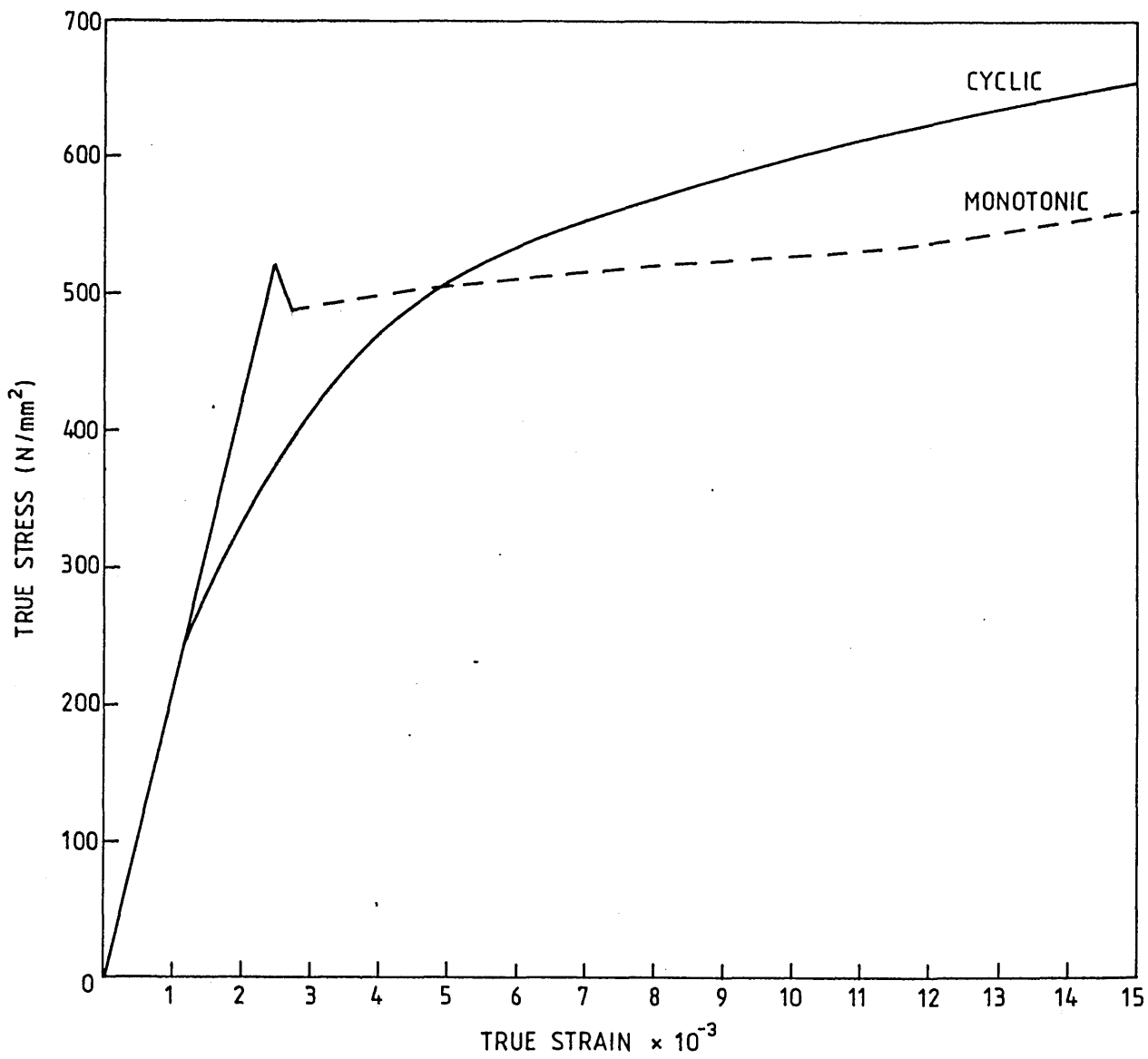


FIG. 52. CYCLIC AND MONOTONIC  $\sigma_a - \epsilon_t$  CURVES FOR CAST 36

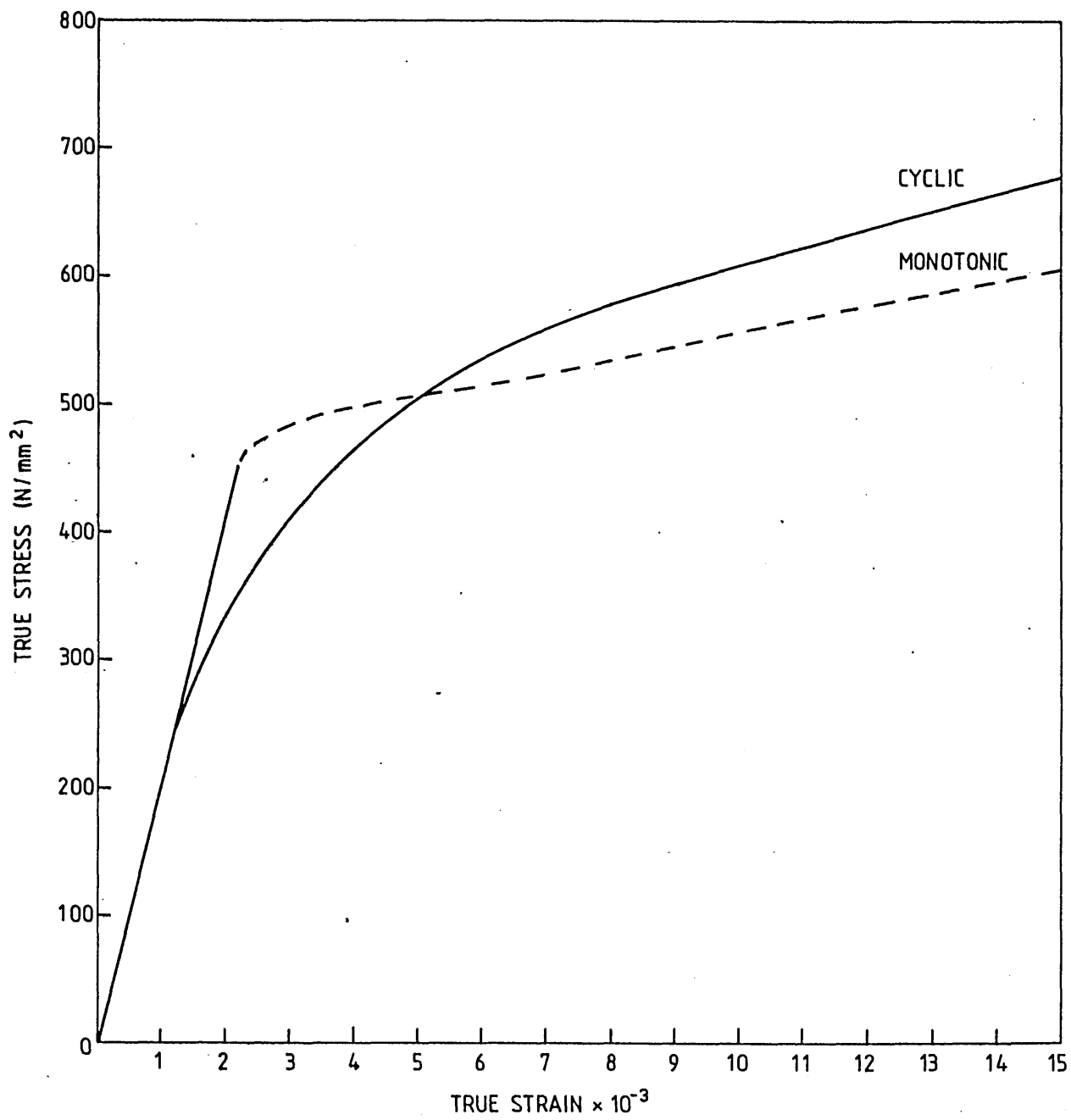


FIG. 53. CYCLIC AND MONOTONIC  $\sigma_a - \epsilon_t$  CURVES FOR CAST 78

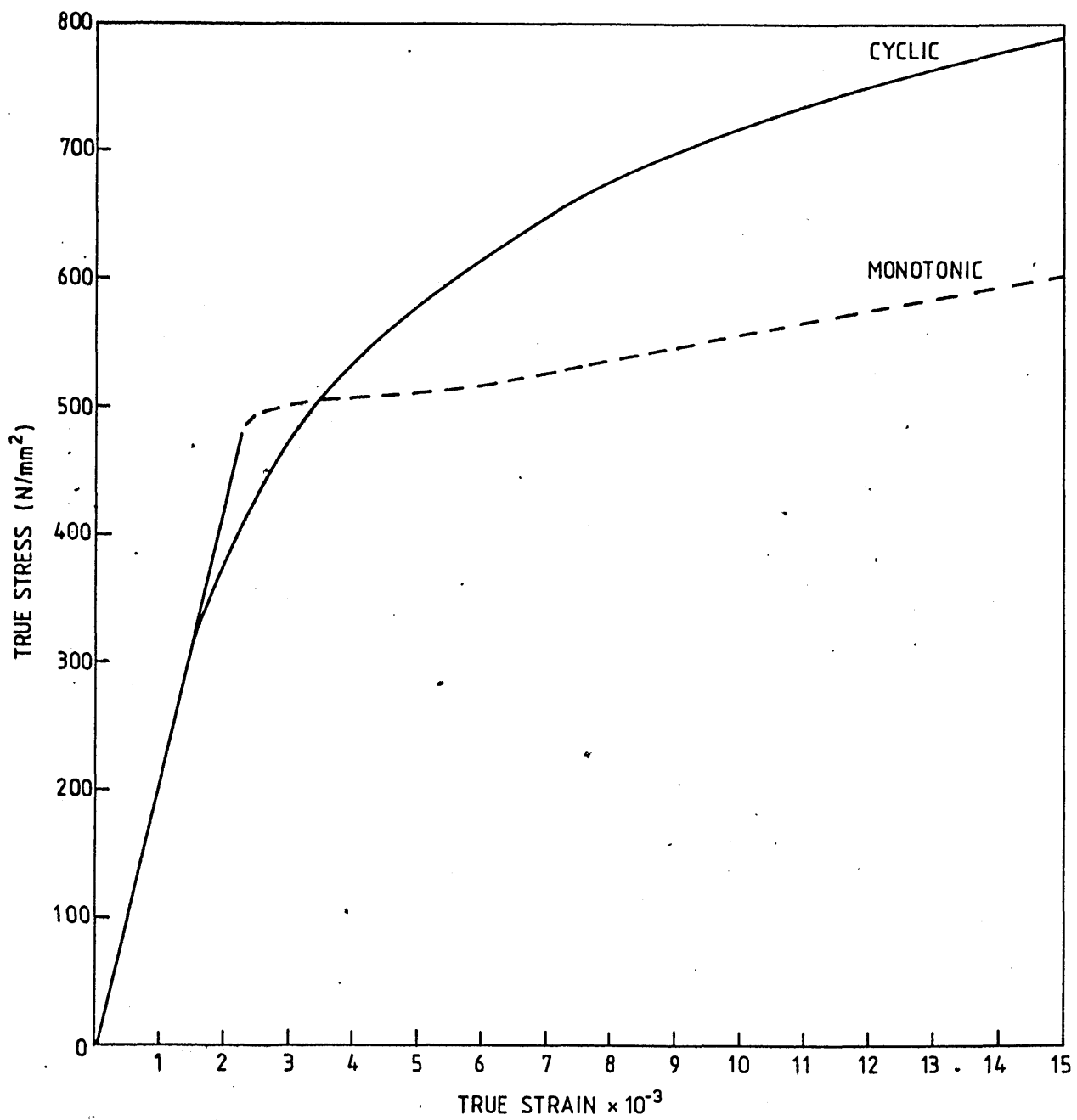


FIG. 54. CYCLIC AND MONOTONIC  $\sigma_a - \epsilon_t$  CURVES FOR CAST 74

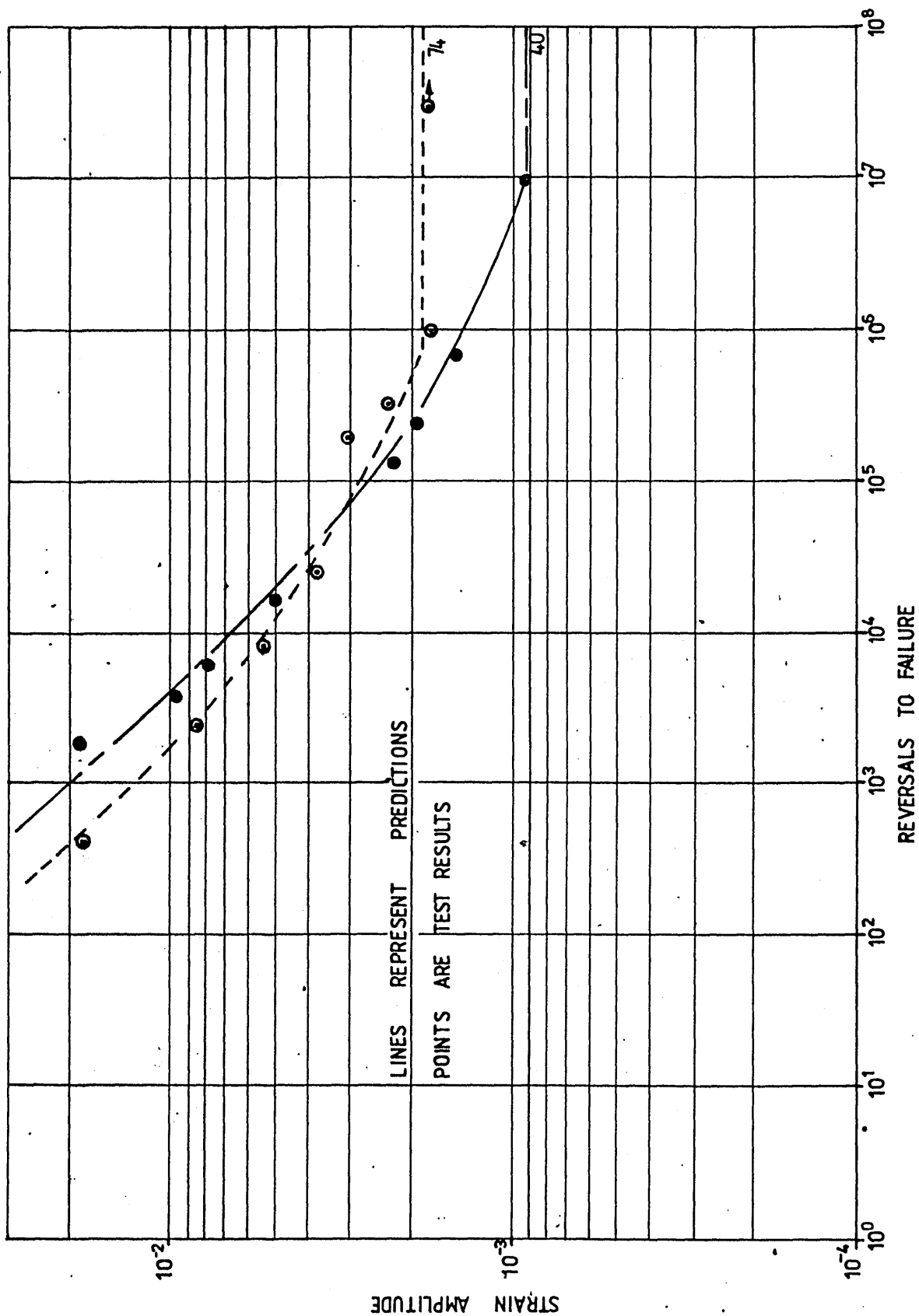


FIG. 55. PREDICTED CURVE AND ACTUAL TEST DATA.

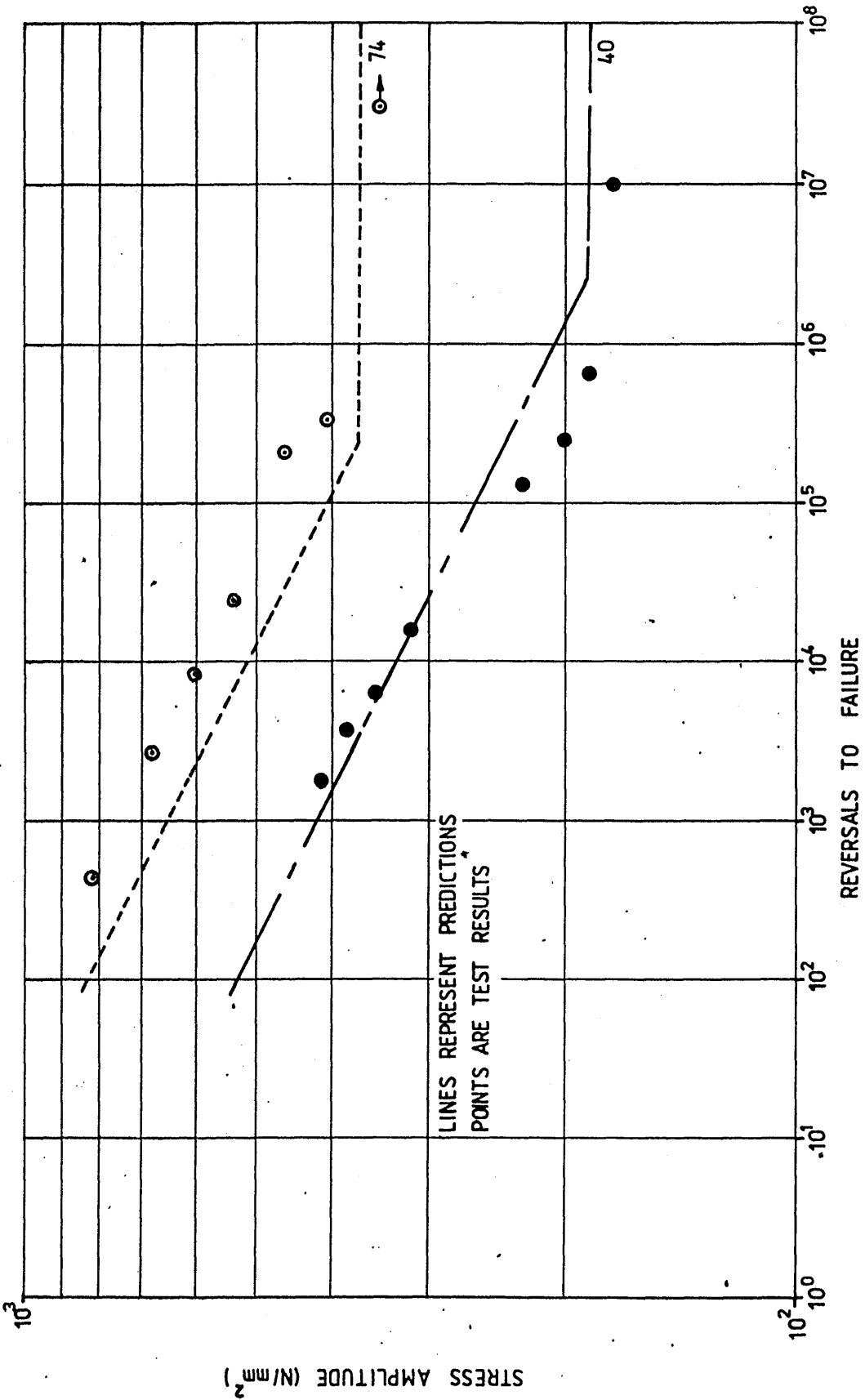


FIG. 56. PREDICTED LINES AND ACTUAL TEST DATA.

Fig.57(a)

Example of surface damage in  
ferrite (cast 40).

x 2.1K

Fig.57(b)

View of same area as above at a  
higher magnification

x 5.3K

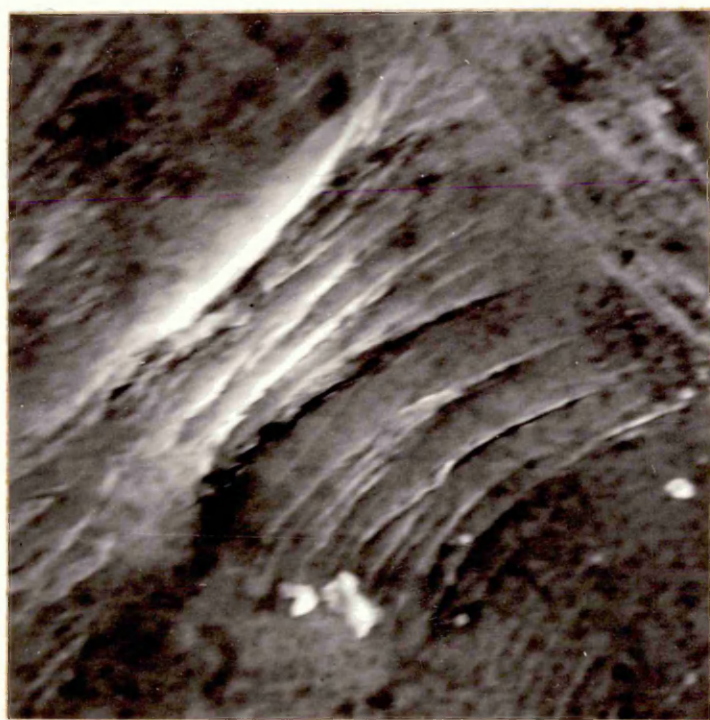


Fig. 58(a)

Example of stage I cracks in  
cast 07.

x 240

Fig. 58(b)

Stage I crack with an associated  
non-metallic inclusion.

x 1.2K

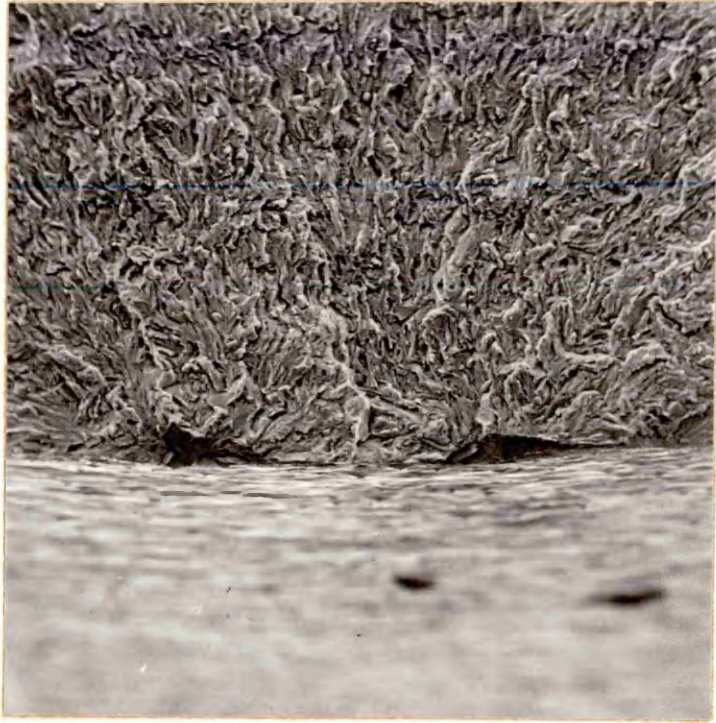


Fig.59(a)

One of the stage I cracks from  
cast 07 shown at a higher  
magnification.

x 600

Fig.59(b)

The other stage I crack from  
cast 07. In this case two non-  
metallic inclusions are associated  
with the crack.

x 1.3K.

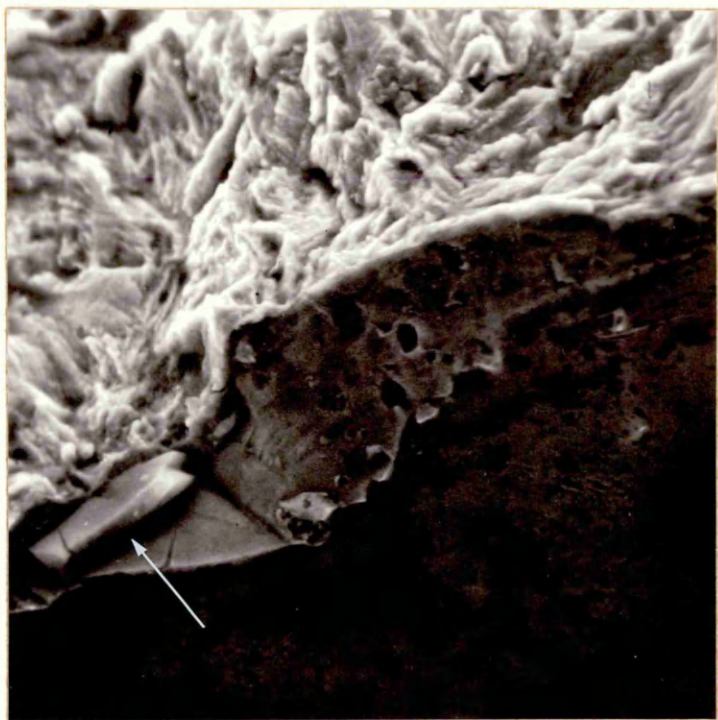
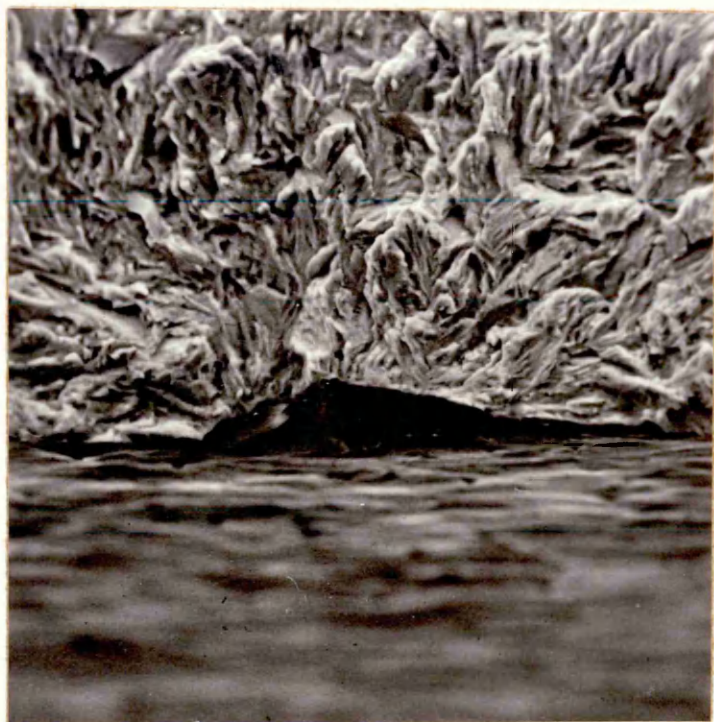


Fig.60

Stage II crack in ferritic steel  
(cast 34). An example of a brittle  
striation is marked "A".

x 275

Fig.61

Stage II crack in pearlitic steel  
(cast 36). An example of a brittle  
striation is marked "A".

x 275

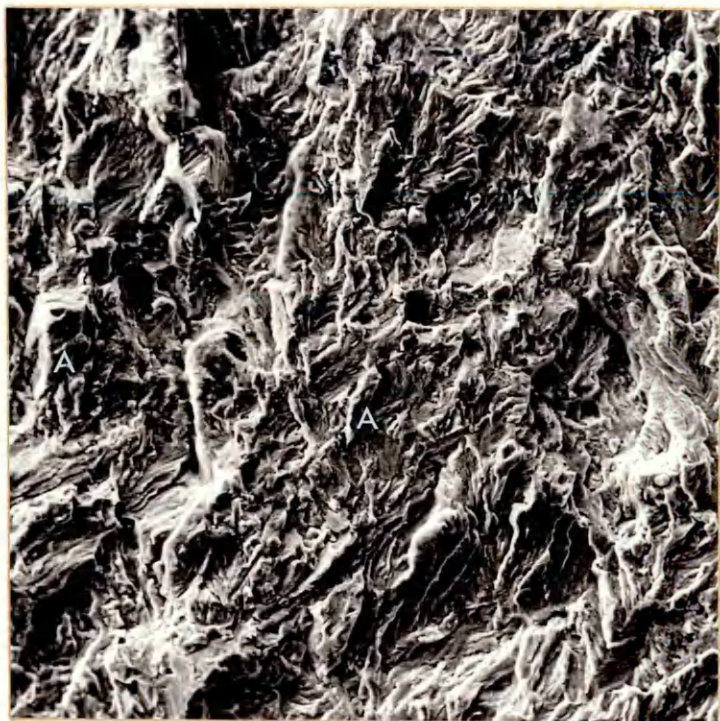


Fig.62

Example of fatigue striations in a steel containing appreciable ferrite in the microstructure.

x 2.75K

Fig.63

High magnification photograph showing the characteristics of stage II cracks in pearlite, (cast 74).

x 2.4K

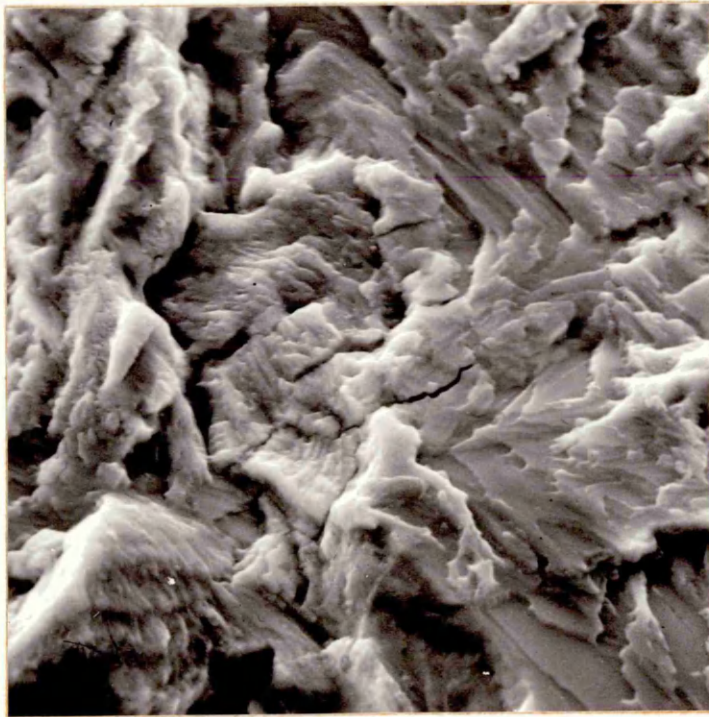


Fig.64(a)

Example of secondary cracks which developed in the later stages of the tests.

x 2.0K

Fig.64(b)

View of same area as shown above but at a higher magnification.

x 6.2K

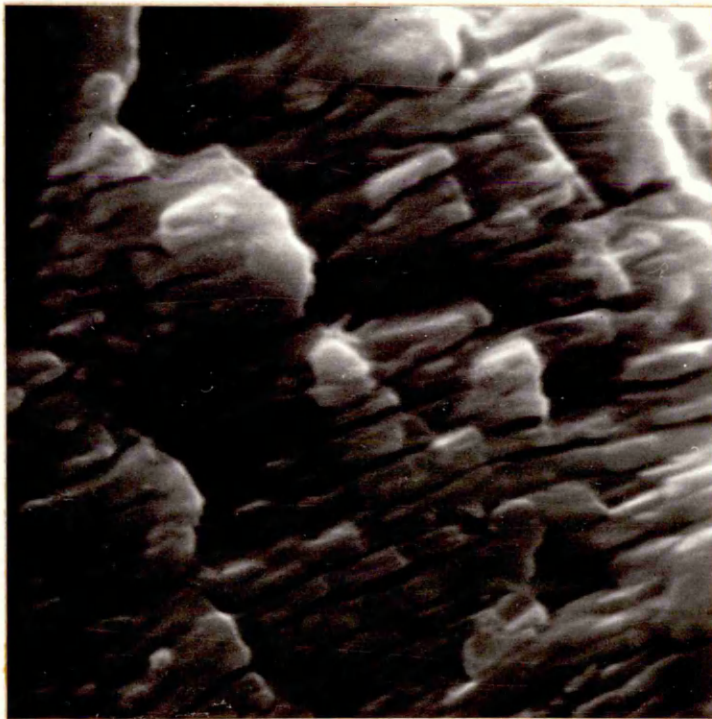
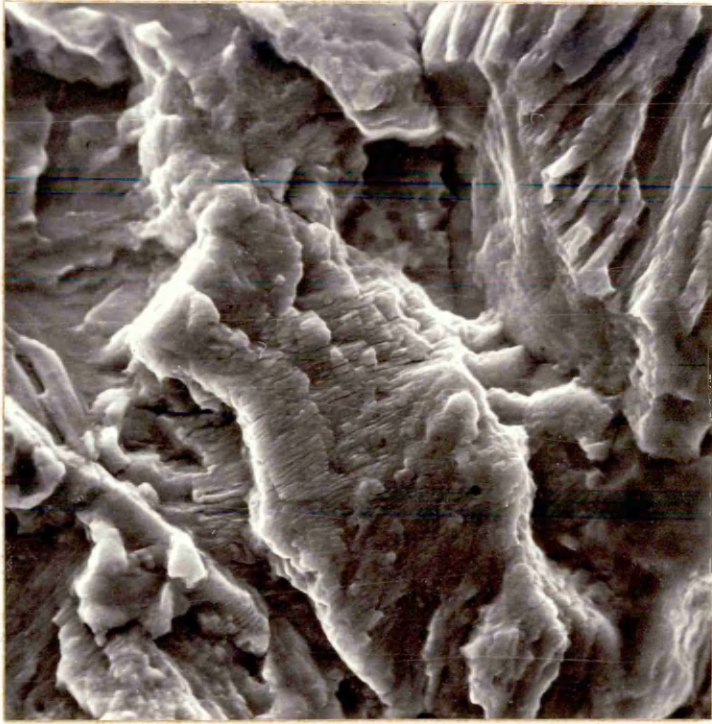


Fig.65(a)

An example of a stage II crack  
in pearlite.

x 2.1K

Fig.65(b)

View of same area as above, after  
etching in 2% nital.

x 2.1K

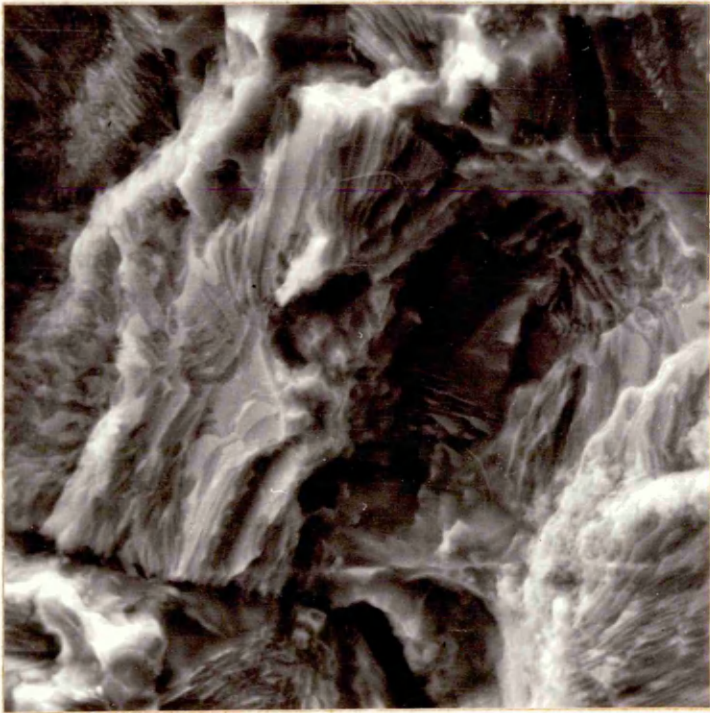


Fig.66(a)

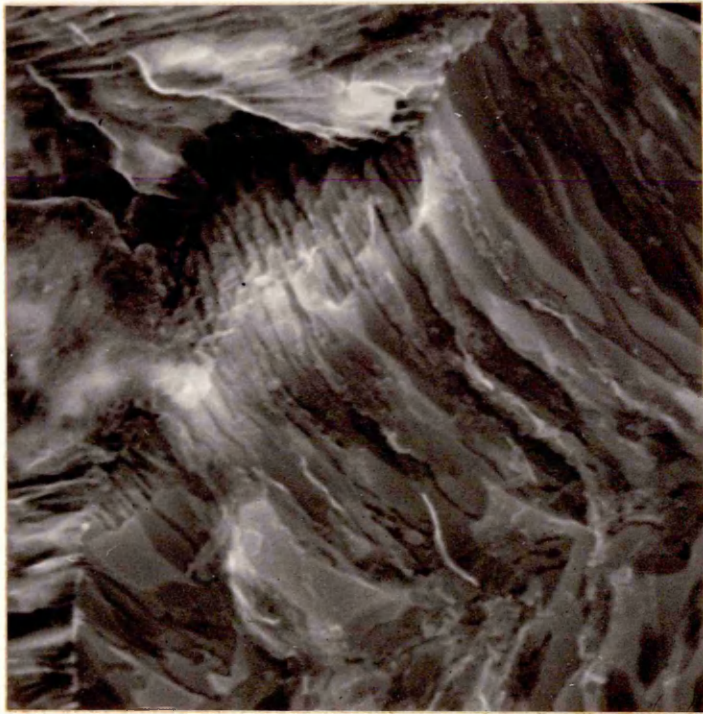
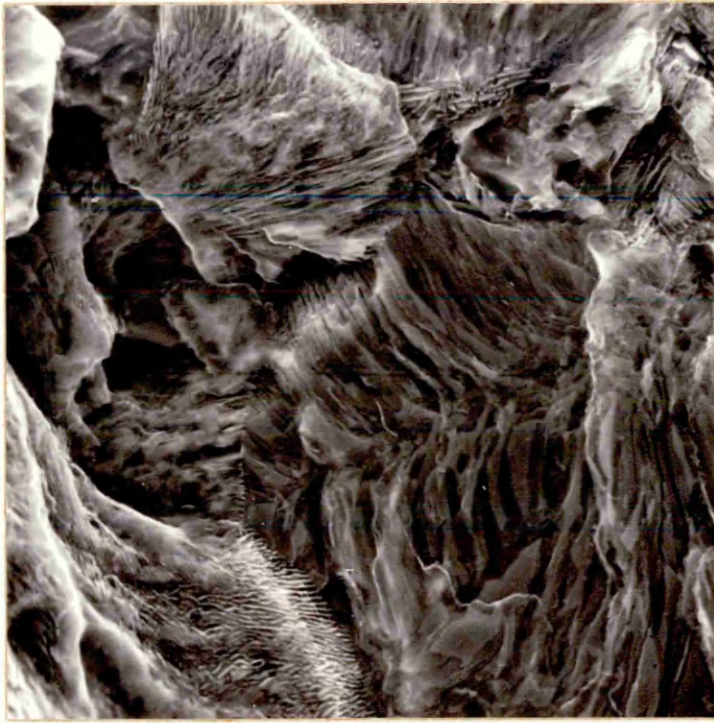
An example of a stage II crack in  
pearlite after etching in 2% nital.

x 2.4K

Fig.66(b)

View of same area as above but at  
higher magnification.

x 6.0K



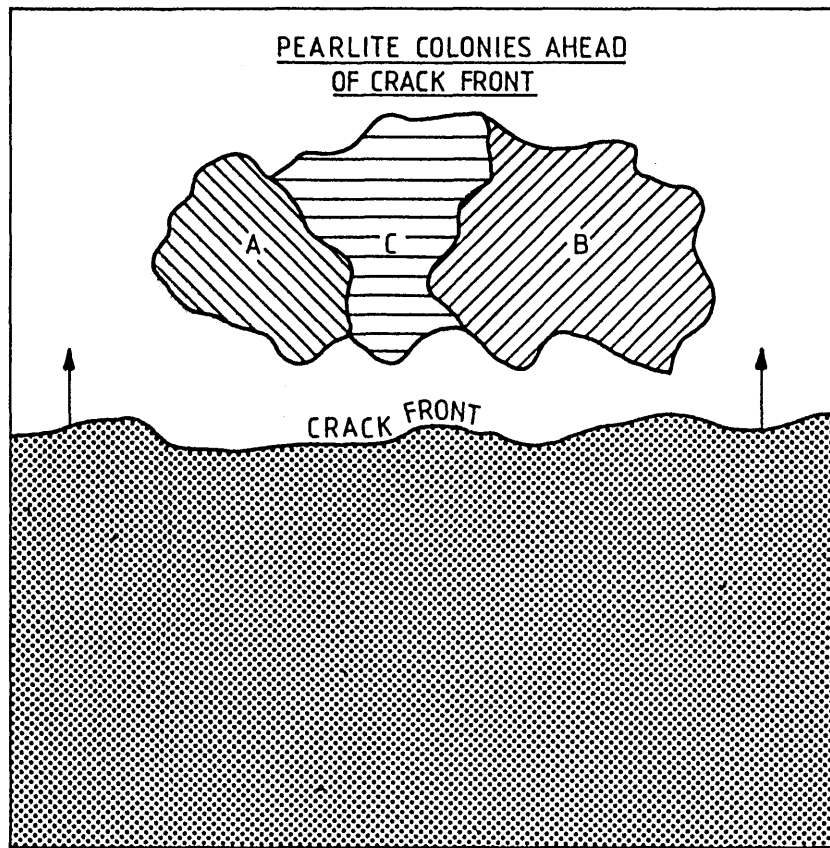


FIG. 67. DIAGRAMMATIC REPRESENTATION OF CRACK GROWTH MECHANISM IN PEARLITE. DEBONDING INITIALLY OCCURS AT THE FERRITE / CEMENTITE INTERFACES IN THE FAVOURABLY ORIENTED COLONIES 'A' AND 'B'. STRESS THEN BUILDS UP IN THE UNFAVOURABLY ORIENTED COLONY 'C' LEADING TO THE FORMATION OF A BRITTLE STRIATION WHEN FRACTURE OF THIS LIGAMENT OCCURS

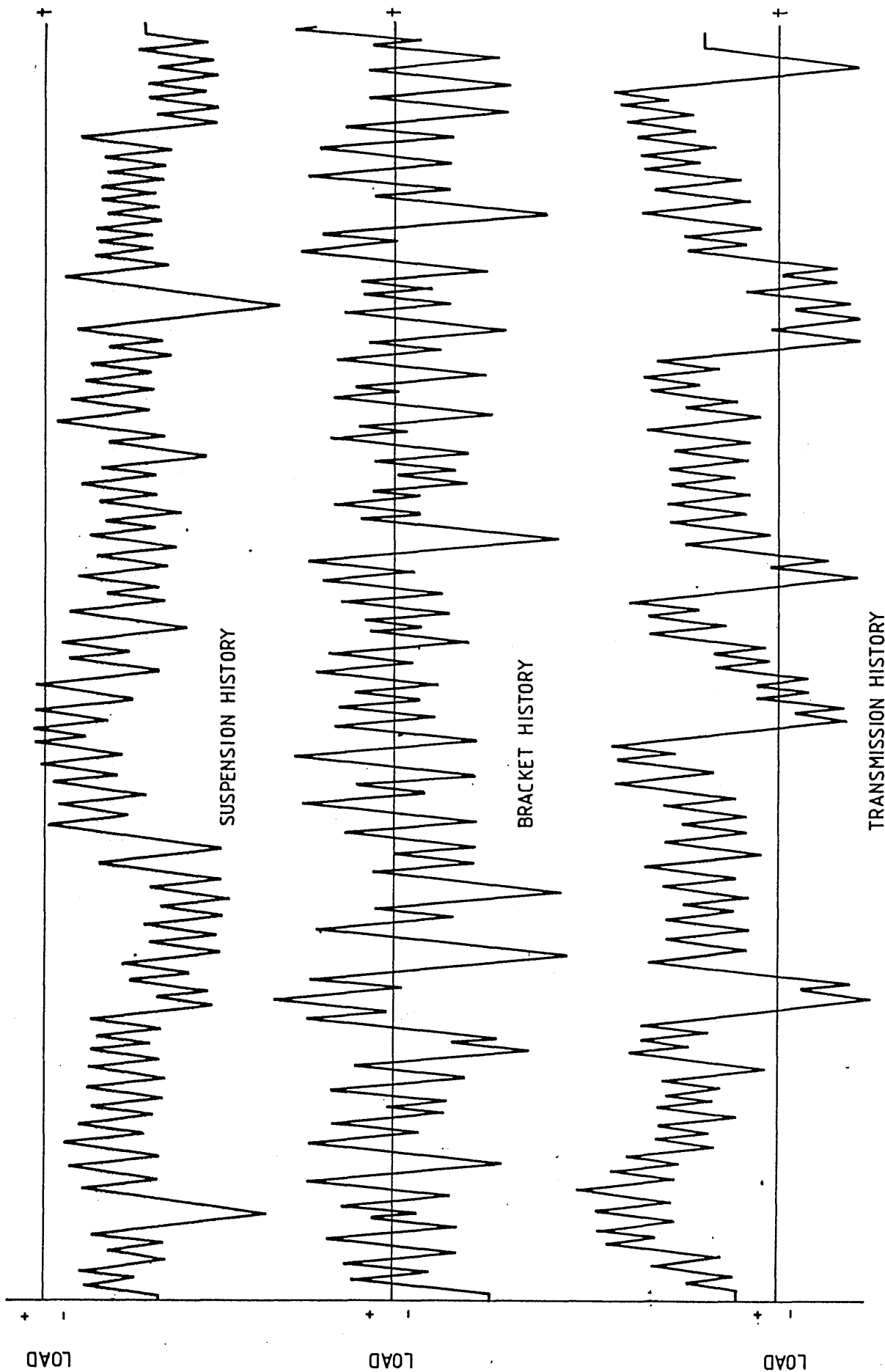


FIG. 68. EXTRACTS FROM THE THREE S.A.E. HISTORIES



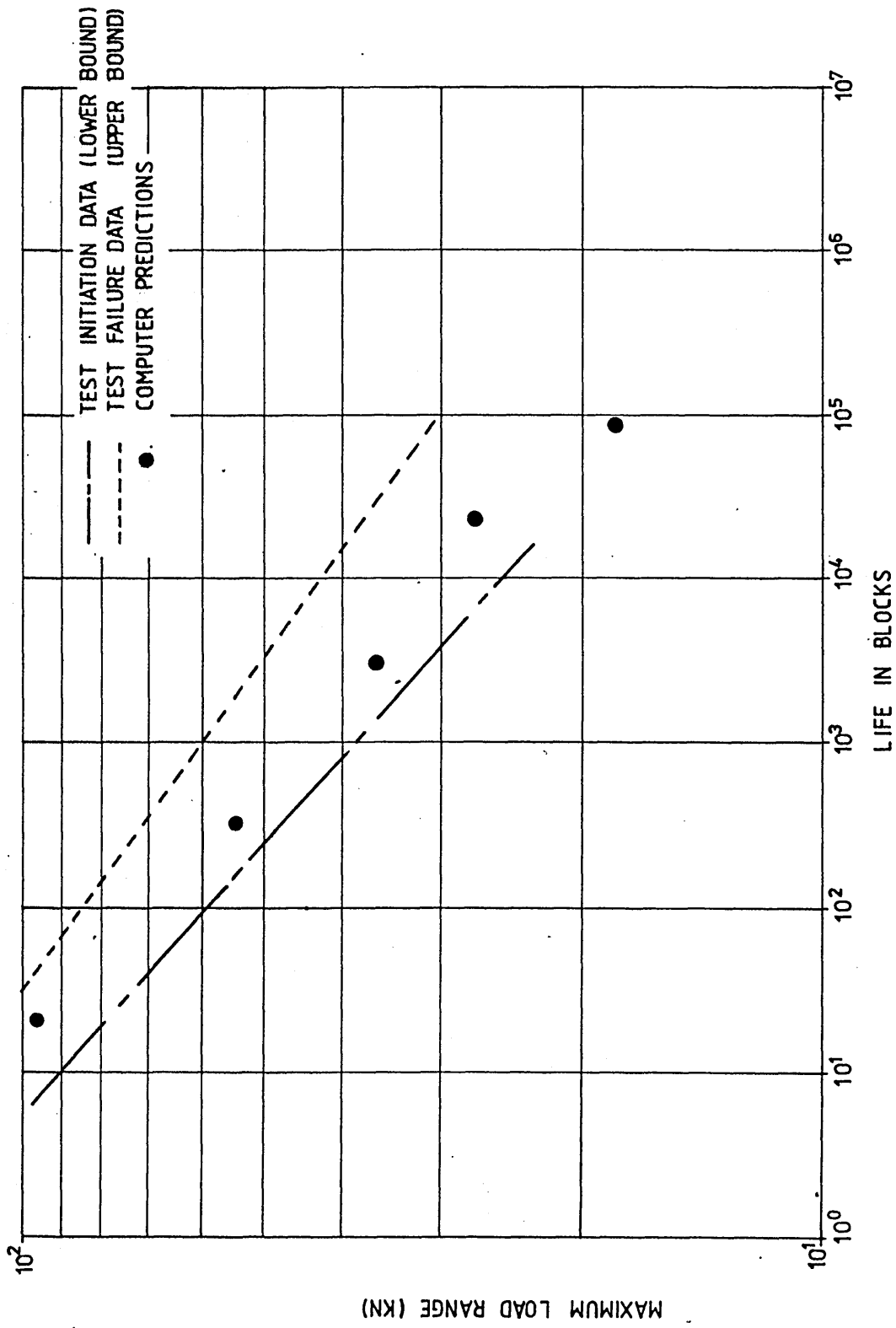


FIG. 70. TEST DATA AND LIFE PREDICTIONS FOR MAN-TEN STEEL AND SUSPENSION HISTORY.

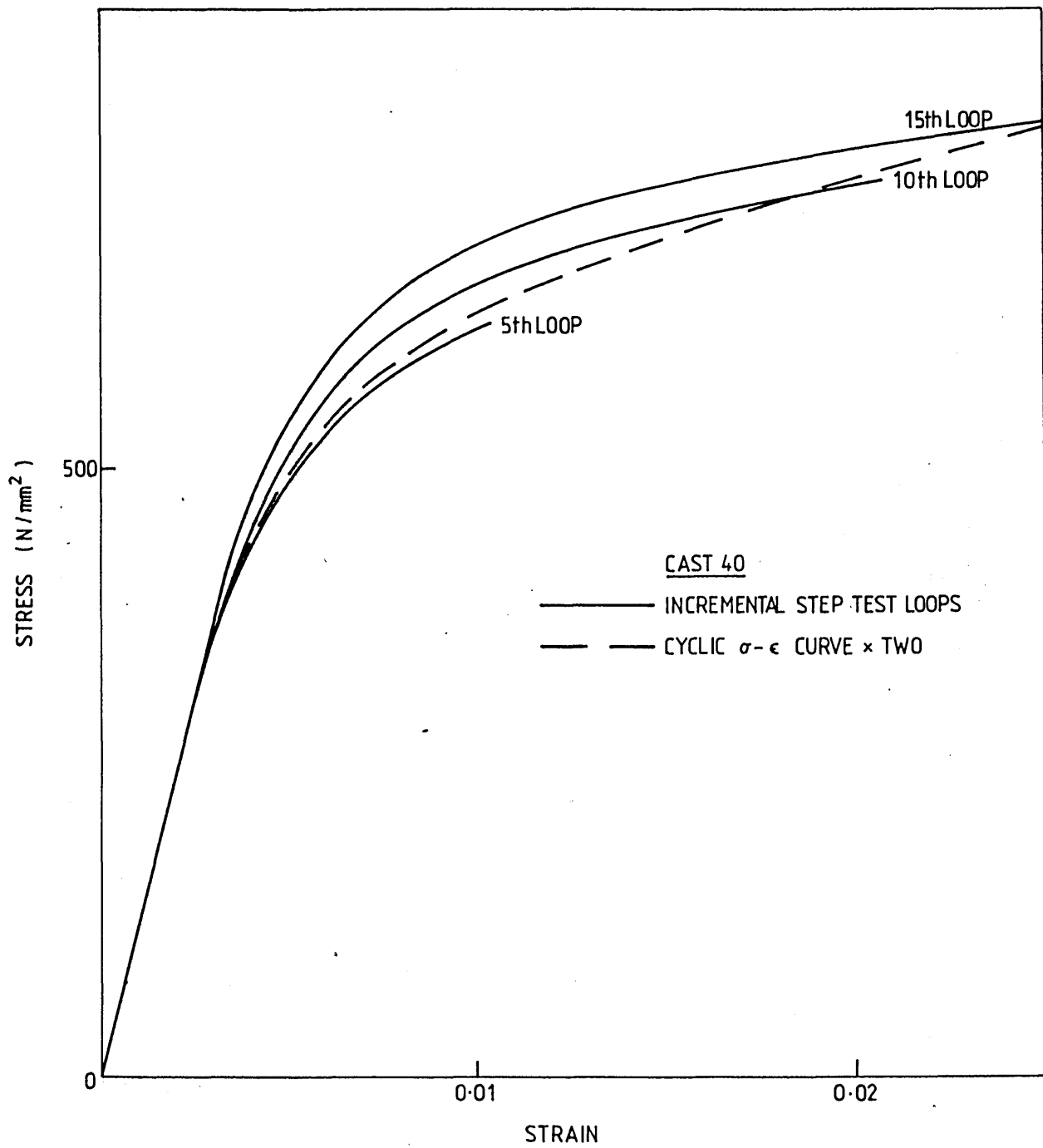
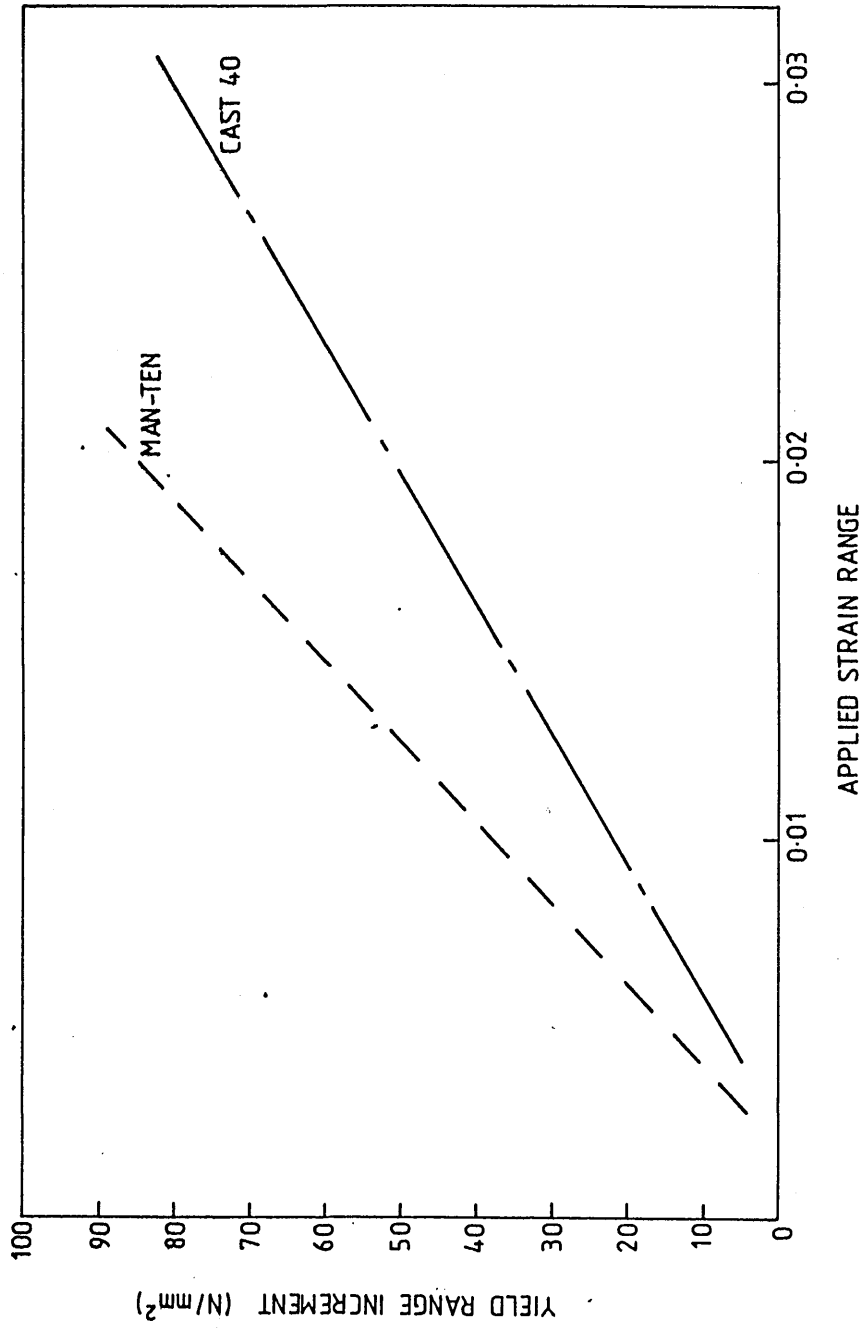


FIG. 71. HYSTERESIS LOOP SHAPES - ACTUAL (I.S. TEST) AND PREDICTED (MASING)



**FIG. 72. VARIATION OF YIELD RANGE INCREMENT WITH APPLIED STRAIN RANGE**

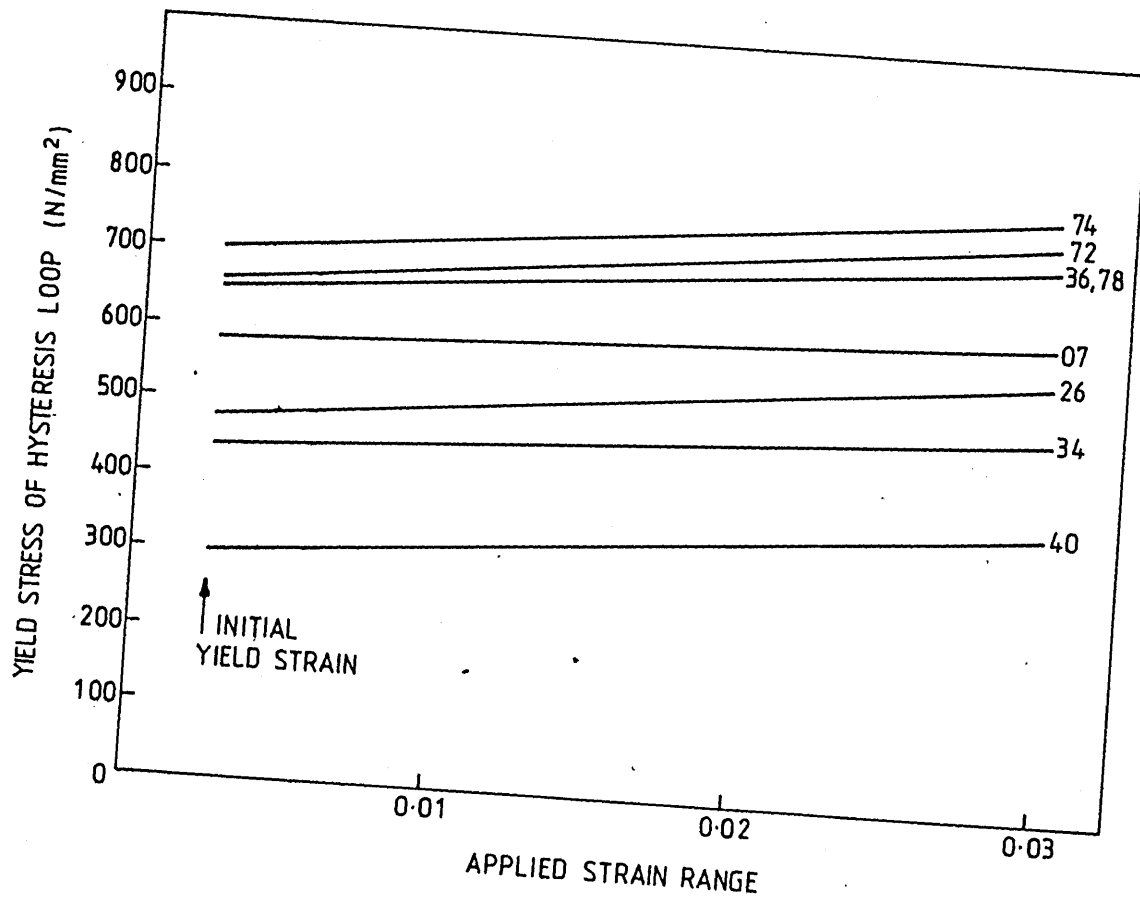


FIG. 73. VARIATION IN YIELD STRESS OF HYSTERESIS LOOPS WITH APPLIED STRAIN RANGE

FATIGUE LIFE PREDICTION ROUTINE (NOM. ELASTICITY)

OPTION	DESCRIPTION	VALUE
1	MODULUS OF ELASTICITY (MPA)	203000.00
2	STRENGTH COEFFICIENT (MPA)	876.00
3	STRAIN HARDENING EXPONENT	0.1790
4	MAX. ABSOLUTE NOMINAL STRESS (MPA)	450.00
5	No. OF MODEL ELEMENTS	200
6	STRESS CONCENTRATION FACTOR	3.00
7	CAL. FACTOR APPLIED TO INPUT HISTORY	0.4497E+00
8	STATIC OFFSET (INPUT UNITS)	0.0000E+00
9	RUN IDENT. 40 S 9	
10	SET UP MATERIAL MODEL	NONE

MAX. NOMINAL STRESS RANGE BUILT IN (NLIM) IS 900.0000

(a)

BASIC FATIGUE DATA

OPTION	DESCRIPTION	VALUE
1	FATIGUE STRENGTH COEFFICIENT (MPA)	876.00
2	FATIGUE DUCTILITY COEFFICIENT	0.9500
3	FATIGUE STRENGTH EXPONENT	-0.1120
4	FATIGUE DUCTILITY EXPONENT	-0.5800
5	ENDURANCE LIMIT (REVERSALS)	1.0000E+07
6	SET UP OK	NONE

(b)

NOMINAL INPUT HISTORY

DATASET IDENTIFICATION	SAESRE
------------------------	--------

(c)

FIG. 74. TYPICAL INPUTS TO LIFE PREDICTION PROGRAMME

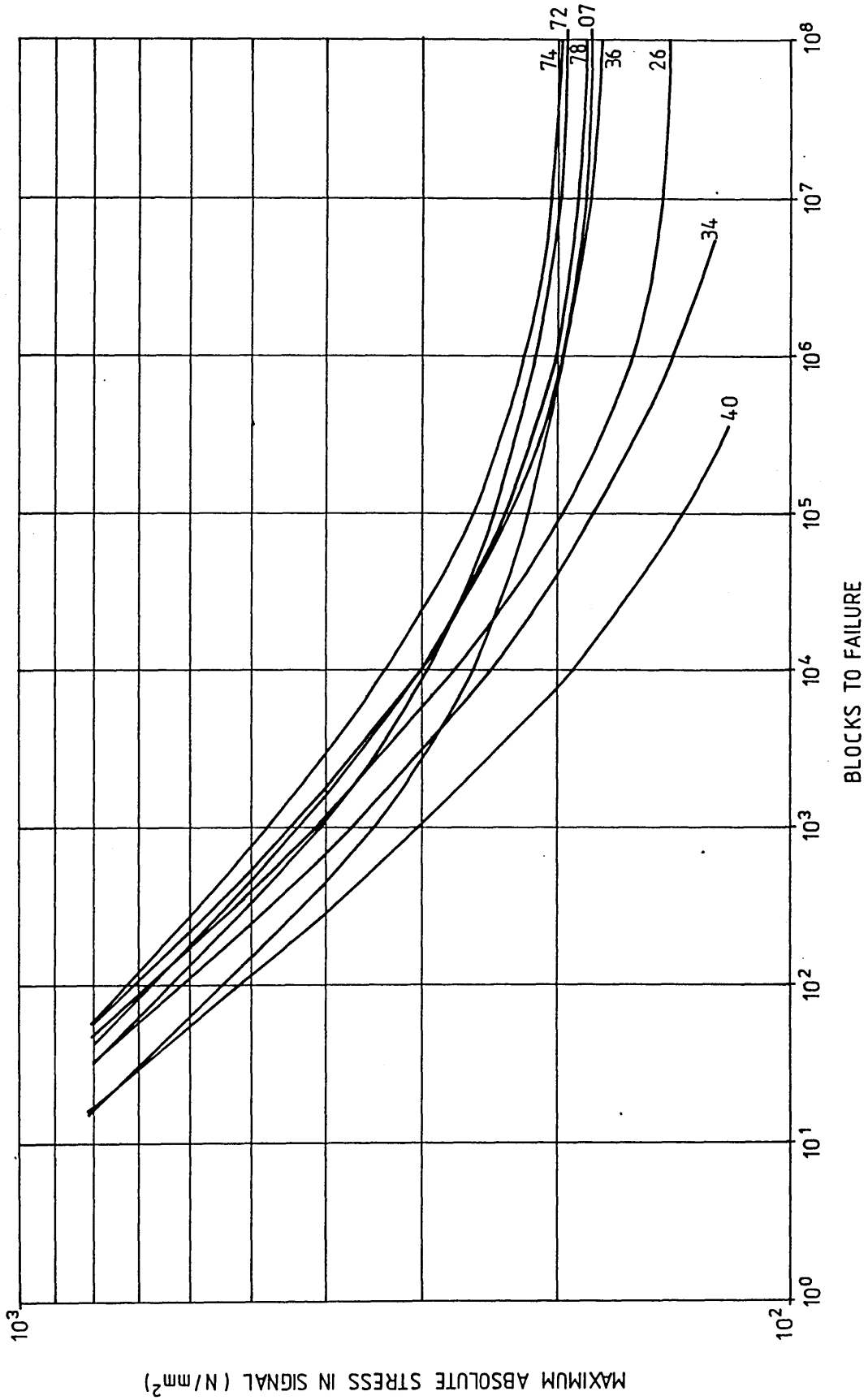
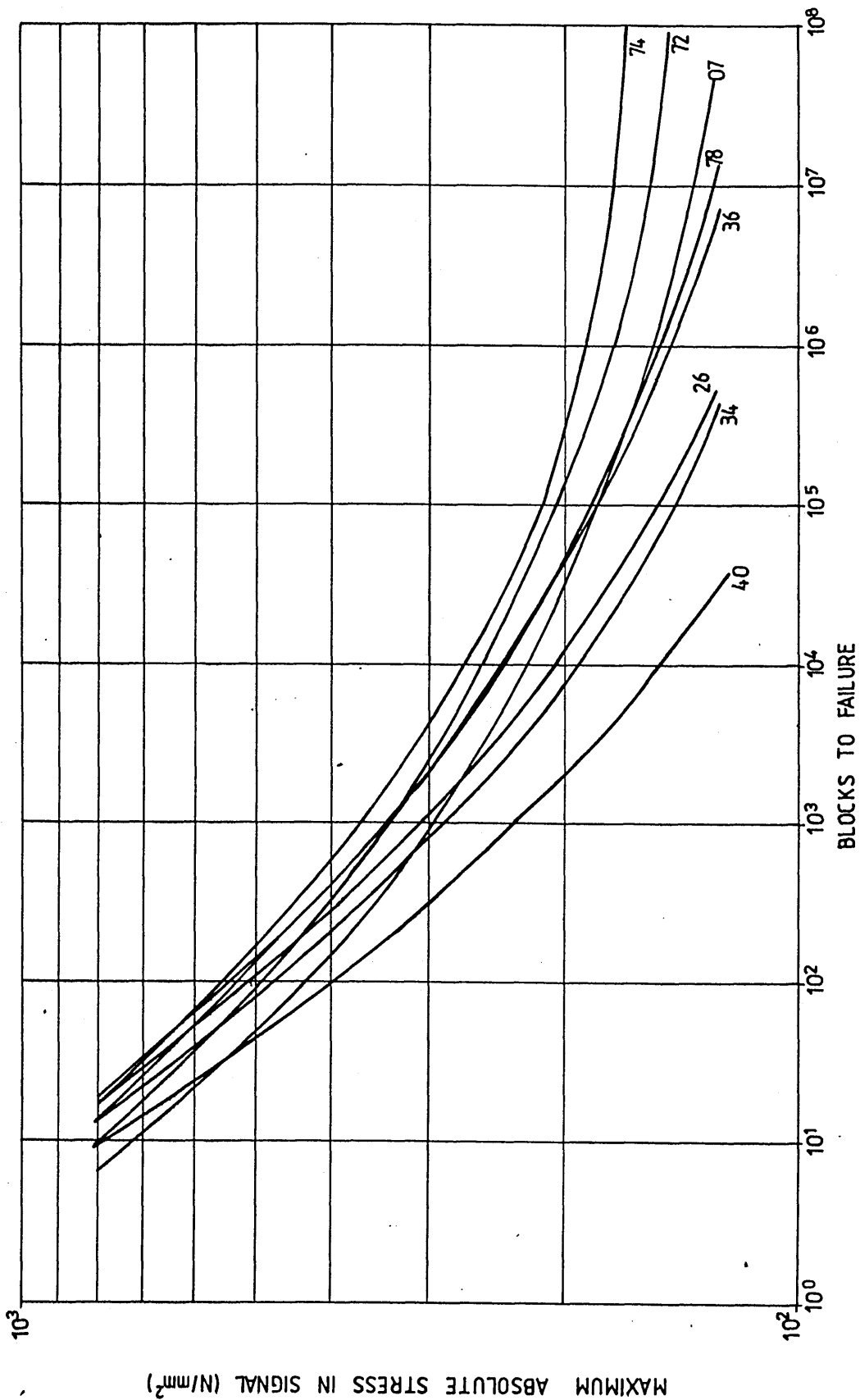


FIG. 75. COMPARISON OF MATERIALS WHEN SUBJECTED TO SUSPENSION HISTORY



**FIG. 76. COMPARISON OF MATERIALS WHEN SUBJECTED TO BRACKET HISTORY**

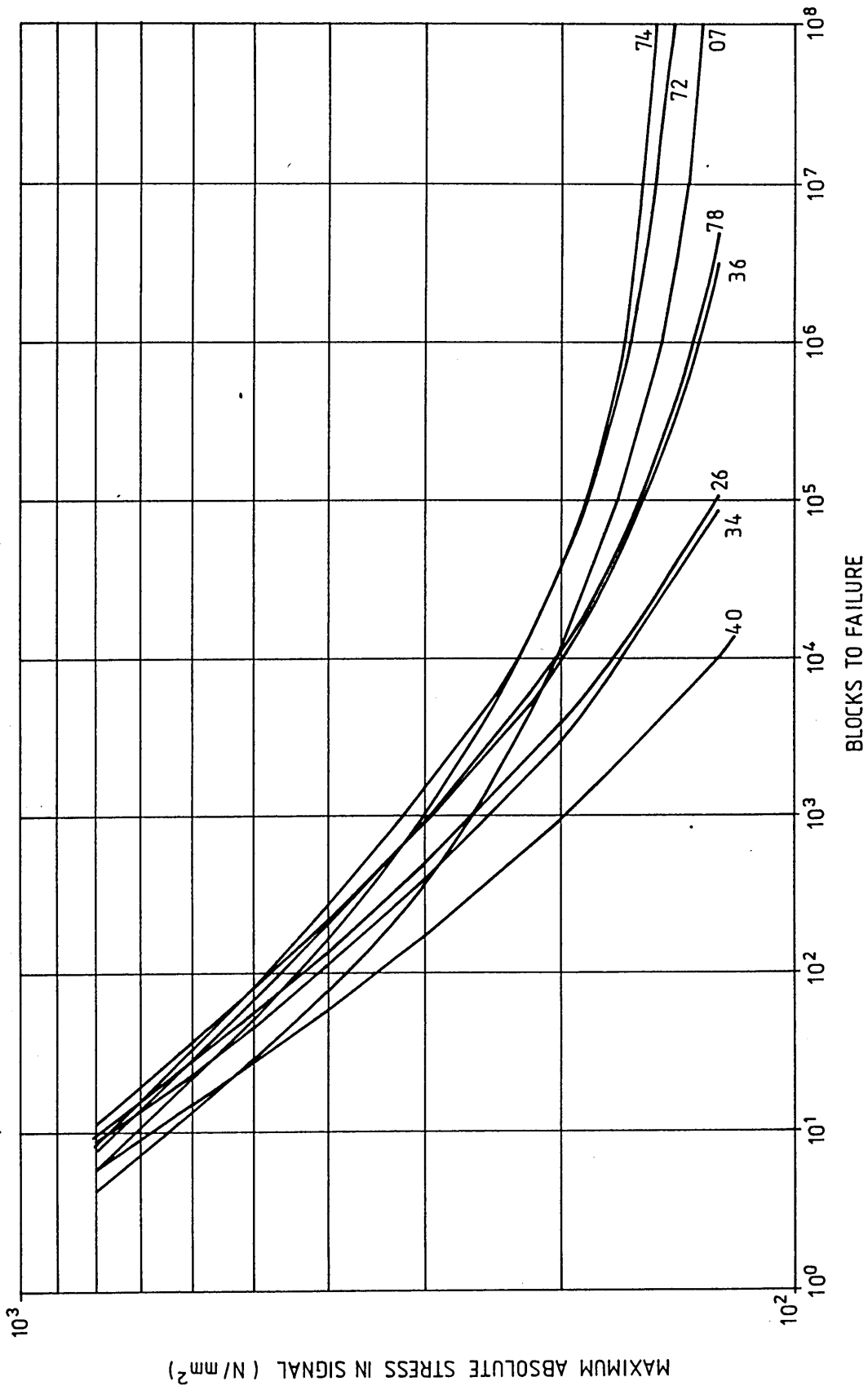


FIG. 77. COMPARISON OF MATERIALS WHEN SUBJECTED TO TRANSMISSION HISTORY

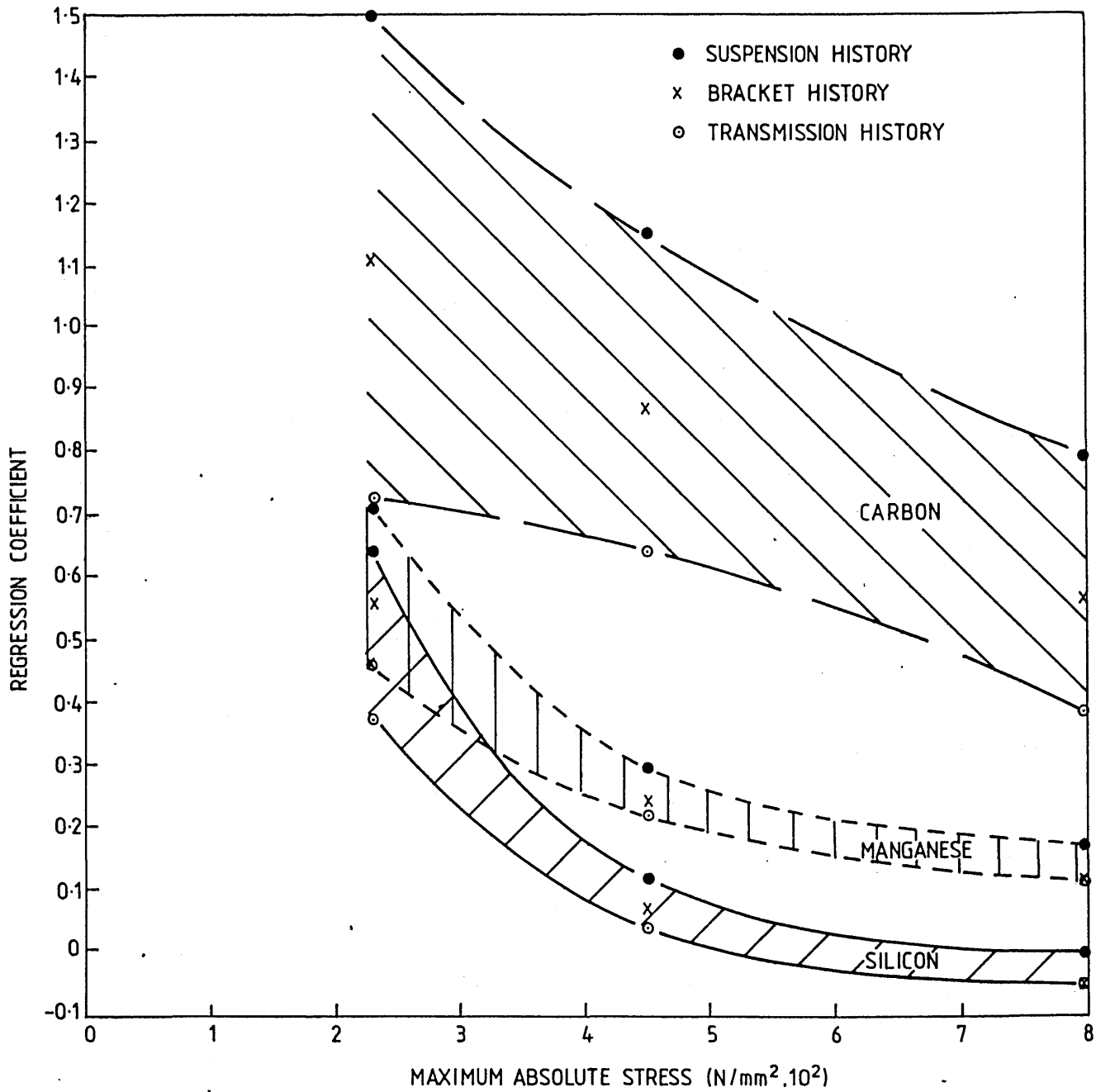


FIG. 78. VARIATIONS IN FATIGUE LIFE WITH COMPOSITION CHANGES,  
SHOWING INFLUENCE OF TYPE AND STRESS LEVEL OF  
RANDOM SIGNAL

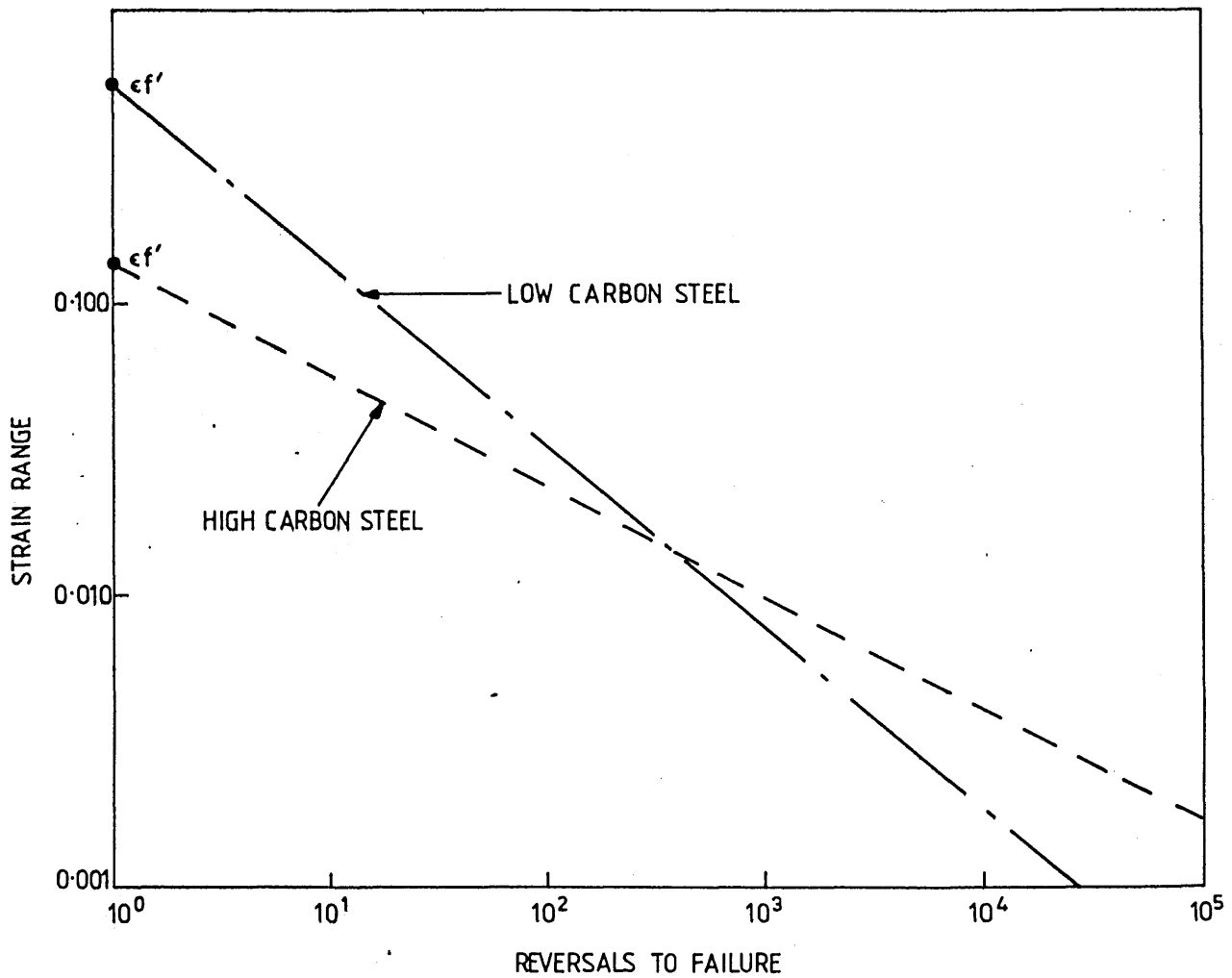
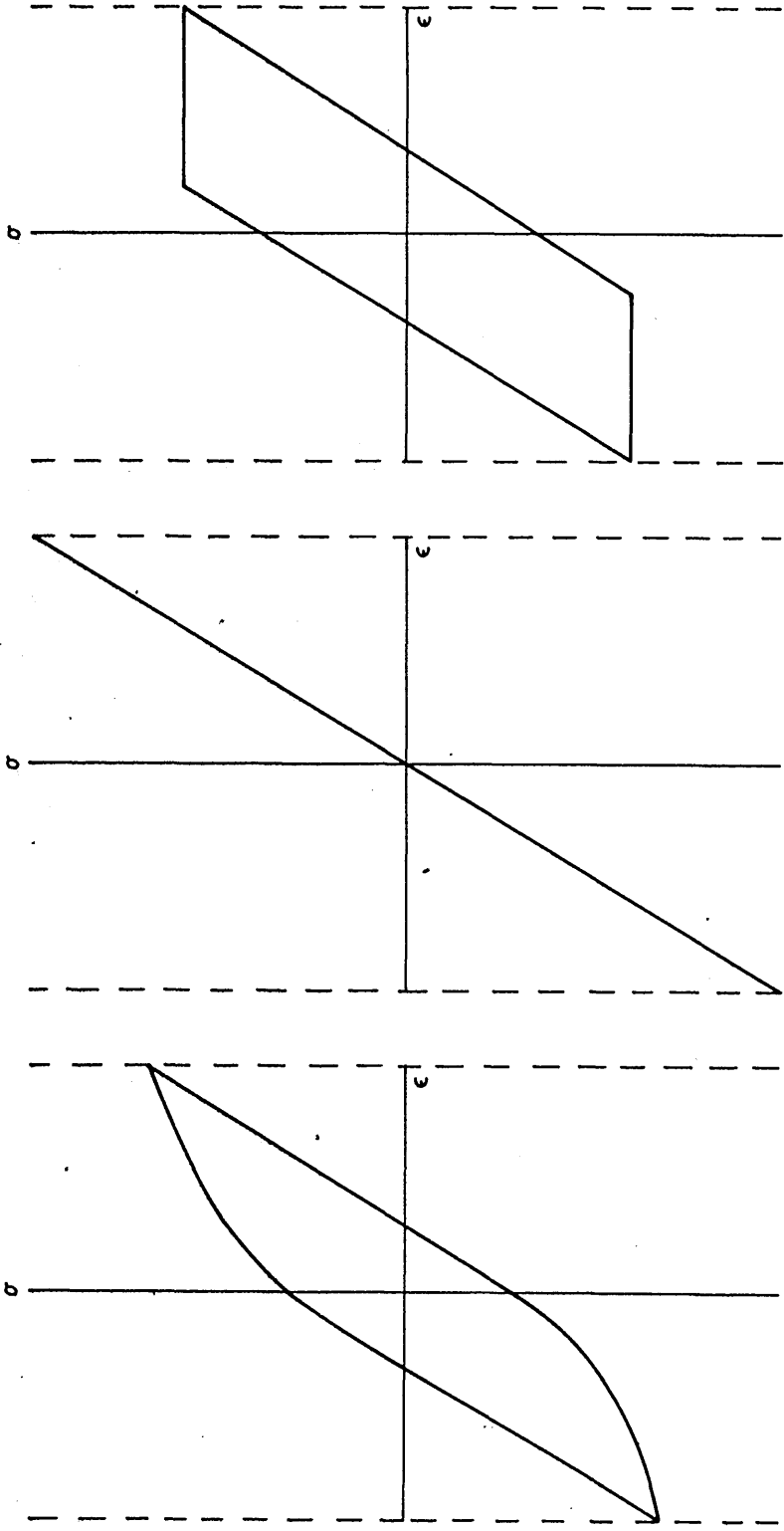


FIG. 79. EFFECT OF INCREASING CARBON CONTENT ON THE FATIGUE DUCTILITY COEFFICIENT AND EXPONENT



a) TYPICAL FERRITE-PEARLITE STEEL      b) ELASTIC BEHAVIOUR      c) ELASTIC-PERFECTLY PLASTIC MATERIAL

FIG. 80. DIAGRAMMATIC REPRESENTATION OF NORMAL AND IDEAL 'FATIGUE RESISTANT' HYSTERESIS LOOPS